NYO - 10205
MITNE - 17

MEASUREMENTS OF THE SPATIAL AND ENERGY DISTRIBUTION OF THERMAL NEUTRONS IN URANIUM, HEAVY WATER LATTICES

by

P.S. Brown, T.J. Thompson, I. Kaplan, A.E. Profio

Contract AT (30-1) 2344
U.S. Atomic Energy Commission

August 20, 1962

Department of Nuclear Engineering
Massachusetts Institute of Technology
Cambridge, Massachusetts

MASSACHUSETTS INSTITUTE OF TECHNOLOGY

DEPARTMENT OF NUCLEAR ENGINEERING

Cambridge 39, Massachusetts

MEASUREMENTS OF THE SPATIAL AND ENERGY DISTRIBUTION OF THERMAL NEUTRONS IN URANIUM, HEAVY WATER LATTICES

by

P. S. Brown, T. J. Thompson, I. Kaplan, A. E. Profio

August 20, 1962

NYO-10205

AEC Research and Development Report

UC-34 Physics

(TID-4500, 17th Edition)

Contract AT(30-1)2344

U.S. Atomic Energy Commission

The contents of this report have been submitted by Mr. Paul S. Brown to the Massachusetts Institute of Technology in partial fulfillment of the requirements for the degree of Doctor of Philosophy.

ABSTRACT

Intracell activity distributions were measured in three natural uranium, heavy water lattices of 1.010 inch diameter, aluminum clad rods on triangular spacings of 4.5 inches, 5.0 inches, and 5.75 inches, respectively, and in a uranium, heavy water lattice of 0.25 inch diameter, 1.03% U^{235}, aluminum-clad rods on a triangular spacing of 1.25 inches. The distributions were measured with bare and cadmium-covered foils of gold, lutetium, and europium. The gold was used as a 1/v absorber to measure the thermal neutron density distribution. Because the activation cross sections of lutetium and europium depart considerably from 1/v behavior, their activation depends strongly on the thermal neutron energy spectrum. Hence, they were used to make integral measurements of the change in the neutron energy spectrum with position in the lattice cell. A method was developed for treating the partial absorption, by cadmium covers, of neutrons at the 0.46 ev europium resonance, and it was found possible to correct the europium activations to energy cutoffs just above and just below the resonance.

The measured activity distributions were compared with those computed with the THERMOS code. In the natural uranium lattices, THERMOS gave excellent agreement with the measured gold activity distributions and very good agreement with the lutetium and europium distributions, indicating that THERMOS gives a very good estimate of the spatial and energy distribution of thermal neutrons in these lattices. In the enriched lattice, THERMOS gave a large overestimate of the activity dip in the fuel for all three detectors. The discrepancy was attributed to a breakdown in the Wigner-Seitz cylindrical cell approximation at small cell radii. However, the measured ratios of lutetium and europium activity to gold activity were in good agreement with the THERMOS values, indicating that THERMOS still gave a good estimate of the degree of spectral hardening.

Neutron temperature calculations were made from the data by using Westcott effective cross sections. The temperature changes so calculated agreed well with those predicted by THERMOS.

Disadvantage factors calculated by the Amouyal-Benoist-Horowitz (ABH) method were in excellent agreement with the measured values in

the natural uranium lattices. The agreement was not as good in the enriched lattice because of an expected breakdown in the ABH method at small cell radii. Values of the thermal utilization obtained from experiment, from THERMOS, and with the ABH method were in excellent agreement for all the lattices studied.

Radial and axial buckling measurements made with lutetium were in excellent agreement with similar measurements made with gold, indicating that the thermal neutron spectrum was uniform throughout the lattice tank. Measurements of intracell gold activity distributions made in off-center cells differed only slightly from those made in the central cell of the lattice, indicating that the radial flux distribution was almost completely separable into a macroscopic J_o and a microscopic cell distribution.

ACKNOWLEDGMENTS

The success of the M. I. T. Lattice Project has been due to the contributions of a number of individuals. The results of this particular report are primarily due to the work of its principal author, Paul Sherman Brown, who has submitted substantially this same report in partial fulfillment for the requirements of the Ph. D. degree at M. I. T. He has been assisted by other students working on the project as well as by those mentioned specifically below.

Over-all direction of the project and its research is shared by Professors I. Kaplan, T. J. Thompson, and Mr. A. E. Profio. Mr. Joseph Barch has been of invaluable assistance in the setting up of experiments and in the design and construction of the facility. Miss Barbara Kelley has been of assistance in the preparation of foils and in many other ways.

Staffs of the M. I. T. Reactor, the Reactor Machine Shop, the Reactor Electronics Shop, and the Radiation Protection Office have provided much assistance and advice during the experimental portion of this work. The secretarial staff of the M. I. T. Reactor and Mrs. M. Bosco have given valuable assistance in the typing of this report.

The authors are indebted to Dr. Henry Honeck, of the Brookhaven National Laboratory, for providing copies of the THERMOS code and considerable advice on its use. Mr. R. Simms has given much assistance in carrying out the THERMOS computations, which were done at the M. I. T. Computation Center.

All of these individuals and groups were essential to the completion of this work.

TABLE OF CONTENTS

TABLE OF CONTENTS (Continued)

TABLE OF CONTENTS (Continued)

LIST OF FIGURES

LIST OF FIGURES (Continued)

LIST OF FIGURES (Continued)

LIST OF FIGURES (Continued)

LIST OF TABLES

LIST OF TABLES (Continued)

CHAPTER I

INTRODUCTION

1.1 THE MIT HEAVY WATER LATTICE RESEARCH PROGRAM

The Nuclear Engineering Department at M.I.T., with the support of the Atomic Energy Commission, is carrying on a research program on the physics of lattices of slightly enriched uranium rods in heavy water. Experimental and theoretical studies are under way on fast fission, epithermal capture, thermal capture, and thermal and epithermal neutron distributions. A subcritical exponential facility, which uses the thermal column of the M.I.T. Reactor (MITR) as a neutron source, is the main experimental tool in the program. Several reports have been published describing the advances that have been made since the start of the program in 1959 (W3), (P1), (P2), (W9), (H3), (M2).

1.2 THERMAL NEUTRON BEHAVIOR IN LATTICE CELLS

This report deals with integral measurements of the spatial and spectral distributions of thermal neutrons within lattice cells. To calculate the relative thermal neutron capture rates in each region of a lattice cell, the variation of the relative neutron flux across the cell must be known. The thermal flux is lower in the fuel than in the moderator because neutron absorption in the fuel is much greater than in the moderator. In addition, since the absorption probability for thermal neutrons is nearly inversely proportional to the velocity, lower energy neutrons are more strongly absorbed than higher energy neutrons, resulting in a "hardening" of the thermal neutron energy spectrum within the fuel. This hardening leads to a decrease in the effective absorption cross section of the fuel and must be taken into account in an accurate calculation of the absorption rate. Measurements of the shape of the thermal neutron density distribution and of the extent of spectral hardening have been made at M.I.T., and will be compared in this report with theoretical calculations of these quantities.

One of the main objectives of measuring or calculating the spatial and spectral distribution of the thermal neutrons is to obtain the thermal utilization f, one of the four factors in the formula

$$k_\infty = \eta \epsilon f p . \qquad (1.1)$$

The thermal utilization is defined as the ratio of the thermal neutron capture rate in the fuel to the total thermal neutron capture rate in the cell. A typical hexagonal cell for fuel rods located in a triangular array is shown in Fig. 4.58b; a lattice would consist of a honeycomb arrangement of such hexagons, each with a fuel rod at its center. In considering k_∞, the cell is considered to be located in an infinite lattice of identical cells. Since measurements of the neutron distributions are made in finite assemblies, the results must be corrected for the effects of neutron leakage out of the assembly.

1.3 VARIOUS EXPERIMENTAL METHODS FOR MEASURING THERMAL CAPTURE

One of the earliest methods for determining the relative thermal neutron capture in each region of a lattice cell is the cadmium ratio method devised by Fermi. It was used at the Metallurgical Laboratory of the Manhattan Project (W1) and in the U.S.S.R. (G2). The theory of the method has been discussed elsewhere (W1). The Fermi method yields a measurement of the fraction of all the thermal neutrons absorbed in the cell which are absorbed in the moderator. In lattices containing only fuel and moderator, all neutron captures occur either in the fuel or in the moderator; thus, the fraction of the neutrons absorbed in the fuel (the thermal utilization) is known by subtraction if the fraction of captures in the moderator has been measured. In lattices containing absorbers other than fuel and moderator, such as cladding, corrections must be made for the absorption in these other materials. The method consists in measuring the bare and epicadmium activity distributions using a detector, say indium foils, in the moderator of a lattice cell. From these distributions, it is possible to determine the ratio, ρ, of the epicadmium to the subcadmium activity at a particular point in the moderator, and $\bar{\phi}_m/\phi_m$, the ratio of the average subcadmium activity in the moderator to the subcadmium activity at the point at which ρ has been

determined. The thermal utilization can then be calculated from the formula (W1)

$$f = 1 - \frac{(1+L^2B^2)\,\bar{\phi}_m b_e \Sigma_a^{mod}}{\rho \phi_m a_s}\,; \qquad (1.2)$$

where a_s is the proportionality constant between the subcadmium activity and the thermal flux, b_e is the proportionality constant between the epicadmium activity and the slowing down density, and a_s and b_e depend upon the counting arrangement, neutron self-shielding, etc. The quantity, $b_e\Sigma_a^{mod}/a_s$, denoted by ρ', can be measured in a calibration experiment. The calibration experiment involves placing a neutron source in an "infinite" amount of moderator, and measuring the activities of bare and cadmium covered foils as functions of distance from the source. The quantity ρ' can then be calculated from the expression (W1):

$$\rho' = \frac{\int_0^\infty A_{th}(\bar{r})\,d\bar{r}}{\int_0^\infty A_{epi}(\bar{r})\,d\bar{r}}\,, \qquad (1.3)$$

and the thermal utilization can be obtained from the formula

$$f = 1 - \frac{(1+L^2B^2)\,\rho'\bar{\phi}_m}{\rho\,\phi_m}\,. \qquad (1.4)$$

The only quantity which remains to be determined in Eq. (1.4) is L^2B^2, which is usually small compared to unity, and for which calculated values of L^2 and B^2 may be used.

Most other measurements of the relative neutron capture rates in the different regions of a cell involve a determination of the ratios of the average neutron fluxes or densities in different regions of the cell. The ratios are usually called disadvantage factors. A method was developed, at the Westinghouse Bettis Laboratory (K4), in which sector foils were used to measure the average thermal flux over each region. The Westinghouse water-moderated lattices consisted of hexagonal cells centered on the fuel rods. Such a hexagonal cell may be broken down into six identical triangles, all with a common vertex at the cell center. The sector foils were cut to the shape and size of one of these triangles.

The part of the foil corresponding to the fuel region was cut away from the triangle and actually placed in the correct position in the fuel element; the part corresponding to the moderator was held by a plastic foil holder in the moderator. The foils were either bare or covered with cadmium, and consisted of an alloy of U^{235}, 10 per cent by weight in aluminum. Because of the odd shape of the foils, the relative response of each foil to the same flux was obtained by determining the natural U^{235} activity in a fixed counting arrangement.

The method used most often for measuring the relative thermal flux in each region of a cell depends on the determination of the intracell neutron density distribution with detector foils or wires. Bare and cadmium covered detectors of 1/v, or nearly 1/v, absorbers are used to map the neutron density in the fuel and in the moderator. Since the measurements are done in finite systems, the intracell ("microscopic") distributions are corrected for the macroscopic J_o, or cosine, distribution. Graphical integration of the subcadmium activations then leads to a value of the average neutron density in each region. The foils most commonly used for such measurements are made of gold, manganese, copper, U^{235}, dysprosium, or indium. The degree of the spectral hardening is measured by using foil materials whose activation depends strongly on the thermal neutron energy spectrum. The activation cross section of such a material deviates strongly from 1/v-dependence. Lutetium, europium, and plutonium are examples of such materials.

The advantage of using a flux mapping method over methods like that used at Bettis is that considerably more information is obtained in an experiment. Not only does the method give information about disadvantage factors, but it also gives experimental activity distributions which can be compared with theoretical calculations of the distributions, and thus provides a method of testing theoretical models.

1.4 THEORETICAL METHODS FOR DETERMINING THERMAL CAPTURE

The solution of the elementary diffusion equation is the simplest method used for the calculation of theoretical thermal flux distributions. Diffusion theory, however, does not account for variations in the angular distribution of neutrons or for anisotropic scattering, and therefore breaks down near boundaries. Consequently, diffusion theory has been

found to underestimate the flux dip into a fuel rod. Diffusion theory may either treat monoenergetic neutrons, in which case it does not account for spectral hardening; or multigroup diffusion theory may be used to get an estimate of the spectral hardening.

An exact description of the behavior of thermal neutrons in a lattice cell is given by the transport equation. But the transport equation is difficult to solve exactly, and approximations to transport theory may lead to disagreement between theory and experiment because of the inadequate treatment of an important parameter. One of the earliest approximations used in solving the transport equation consisted in treating the neutrons as monoenergetic and expanding the flux, source, and scattering cross sections in terms of Legendre polynomials. This method was first used by Placzek (W2). The use of (n+1) Legendre polynomials in the expansion leads to the P_n approximation. Examples of the monoenergetic P_3 treatment in cylindrical cells have been given by Galanin (G1) and by Tait (T1). The effect of the variation of the energy has been considered in multigroup treatments of the P_n approximation, among which references (S3) and (H14) are good examples. Another method for solving the transport equation, especially suited for digital computers, is the S_n method, first developed by Carlson (C1, C2). In this method, the angular dependence of the directional flux is approximated by a series of straight lines and n is the number of straight line segments used in the approximation. Multigroup versions of the S_n approximation have also been developed, such as the Winfrith DSN program (M1).

Methods have also been developed for solving the transport equation numerically. One of the most useful of these is the THERMOS code developed by Honeck (H6, H7, H8). THERMOS is a multigroup code which solves the integral form of the transport equation; it is described more fully in section 3.2. Calculational methods, based on integral transport theory, have also been developed which do not give the shapes of the neutron flux distributions, but do give good estimates of the disadvantage factors and the thermal utilization. These methods do not require the use of computing machines, as do the solutions to the transport equation, but may give results in good agreement with these solutions. The method of Kushneriuk (K2, K3) and that of Amouyal, Benoist, and

Horowitz (A1) are good examples. Both of these methods involve the use of results of integral transport theory in the fuel and diffusion theory in the moderator. Another method, that of Carlvik and Pershagen (C3), which combines certain results from transport theory and experimental results, is also useful.

1.5 EXPERIMENTAL AND THEORETICAL METHODS USED AT M.I.T.

The experimental method used for determining the relative thermal neutron capture rates in the cells of the M.I.T. lattices was that of measuring the intracell neutron distributions as mentioned above. Measurements were made with bare, and cadmium covered, foils of gold, lutetium, and europium. Gold was used as a 1/v absorber to measure the thermal neutron density distributions. The activation of lutetium and europium depends strongly on the shape of the thermal energy spectrum; these materials were used to obtain information about the degree of spectral hardening.

All measured activity distributions were compared with those computed with the THERMOS code, because THERMOS was considered to be the best available theoretical method for computing the spatial and spectral distribution of thermal neutrons in lattice cells. The method of Amouyal, Benoist, and Horowitz was also used to calculate theoretical disadvantage factors and values of the thermal utilization. This method was chosen because it has been found to give good results (A1, T2, H11) and is representative of hand-calculational methods which make use of integral transport theory.

1.6 CONTENTS OF THE REPORT

The experimental facility, the experimental methods, and the measurements that were made are discussed in Chapter II. The theoretical methods used to obtain the activity distributions, disadvantage factors, relative thermal capture rates, and related quantities are discussed in Chapter III; certain analytical methods for deriving information from the experimental data are also given in that chapter. The experimental and theoretical results are discussed and compared in Chapter IV; the results are also compared with those obtained at other laboratories. A summary of the work, the conclusions drawn from the results, and

recommendations for future work are given in Chapter V. The correction factors used to account for various perturbations in the experiments are discussed in Appendices A-E and H. A transmission method for measuring thermal neutron spectra is described in Appendix F. The input data for the THERMOS code are given in Appendix G. The nomenclature is given in Appendix I. The references are given in Appendix J. A comprehensive listing of experimental and theoretical work done in the field of thermal neutron capture and related areas is given in Appendix K.

CHAPTER II

EXPERIMENTAL METHODS

2.1 THE MIT LATTICE FACILITY

Cross sectional drawings of the MIT exponential facility are shown in Figs. 2.1 and 2.2. The facility consists of an exponential tank which is supported above a graphite-lined cavity or "hohlraum." The thermal column of the MITR is used as a source of thermal neutrons which enter the cavity and are reflected upward into the bottom of the exponential tank. The tank, which contains the lattices and the heavy water, is 48 inches in diameter and 67-1/4 inches high.

Four lattices have been studied so far. The first three consisted of 1.010-inch diameter, natural uranium, metal rods on triangular spacings of 4.5 inches, 5.0 inches, and 5.75 inches, respectively. The rods were clad with type 1100 aluminum, 0.028 inch thick. In these lattices, most of the measurements were made in a removable three-rod cluster located at the center of the tank. The fourth lattice consisted of 0.25-inch diameter, 1.03% U^{235}, metal rods on a triangular spacing of 1.25 inches; the rods were clad with type 1100 aluminum, 0.028 inch thick. In this lattice, most of the experiments were done in a removable rod located at the center of the assembly.

The MIT Lattice Facility, together with its peripheral equipment, has been described in detail in an earlier report (H3). The irradiation facilities and the Medical Therapy Room of the MITR were also used for foil irradiations and for calibration experiments.

2.2 THE EXPERIMENTAL PROGRAM

Measurements of the intracell thermal neutron distribution were made with bare and cadmium covered foils of gold, lutetium, and europium. Gold was used as a 1/v absorber to measure the thermal neutron density distribution. Lu^{176}, as shown in Fig. 2.3, has a

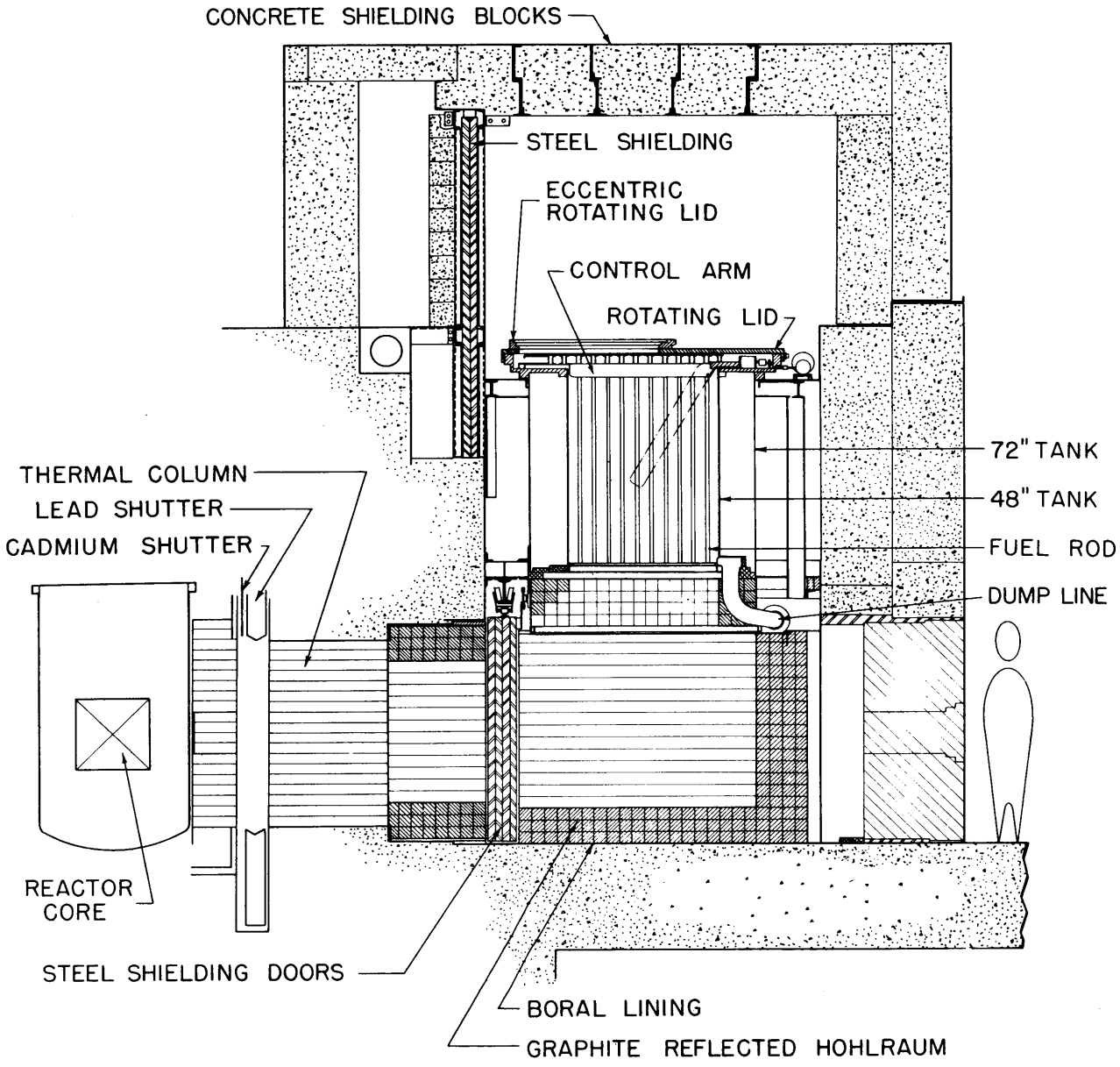

FIG. 2.1 VERTICAL SECTION OF THE SUBCRITICAL ASSEMBLY

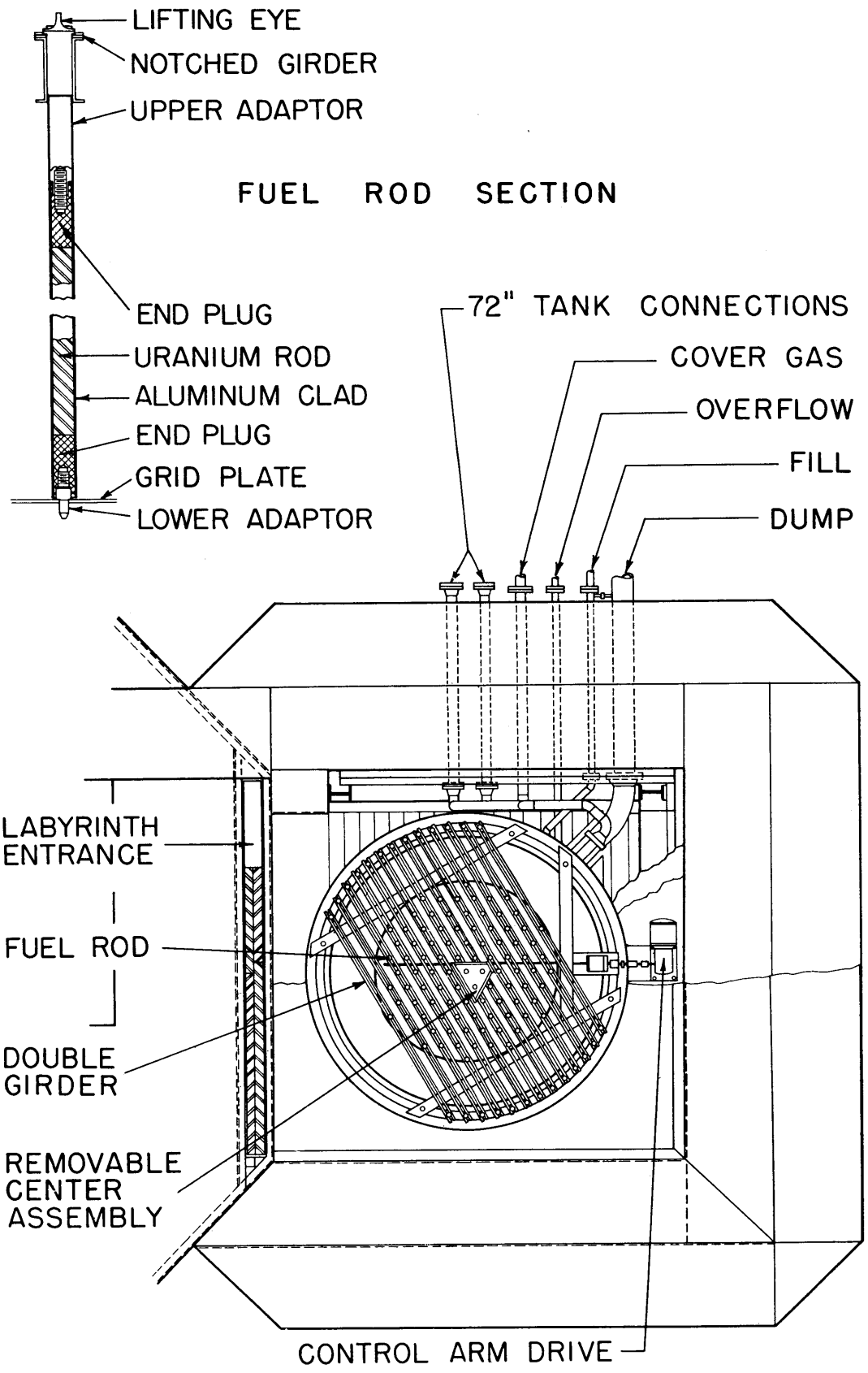

FIG. 2.2 PLAN VIEW OF THE SUBCRITICAL ASSEMBLY

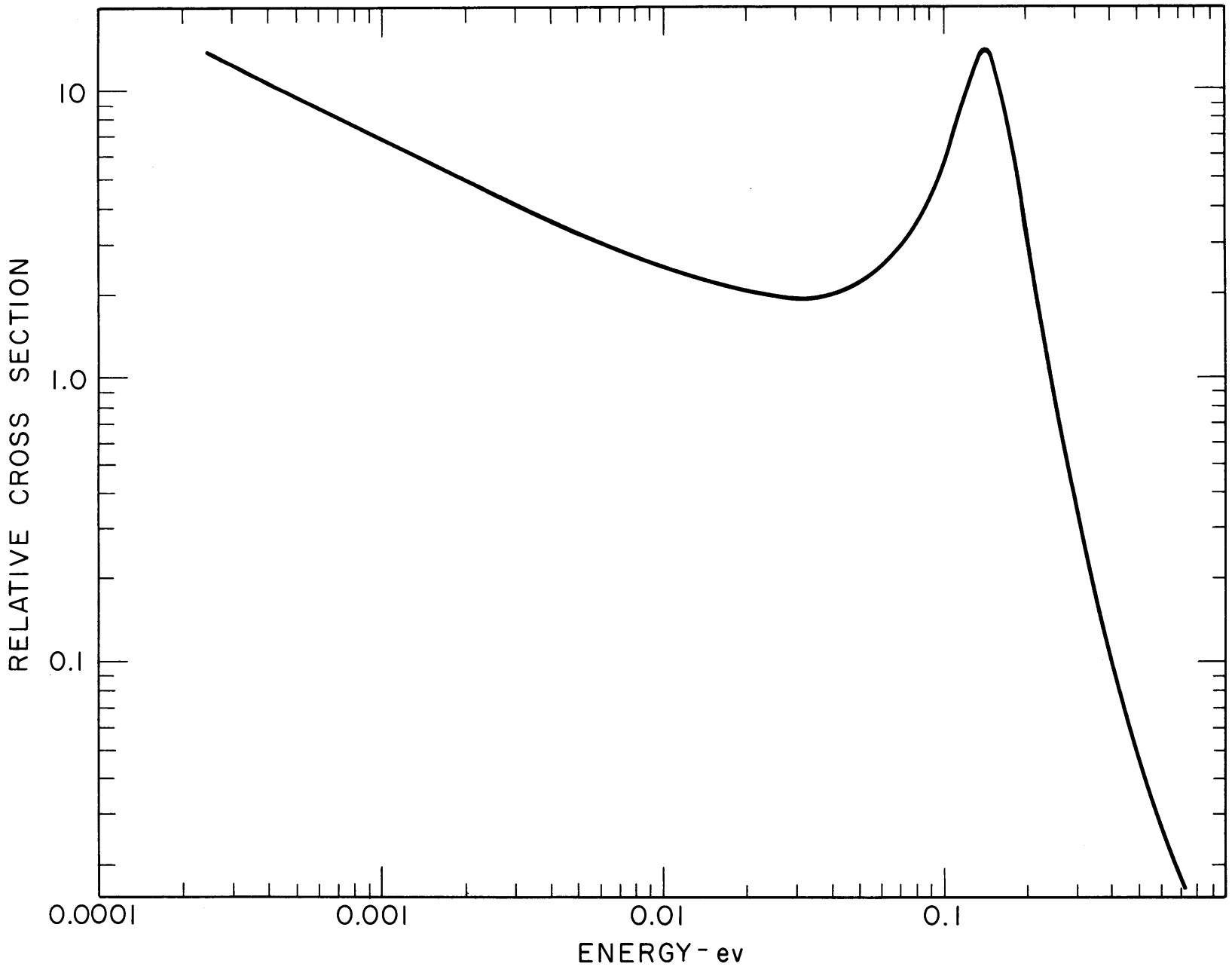

FIG. 2.3 ACTIVATION CROSS SECTION OF Lu^{176}

neutron capture resonance at 0.142 ev, which makes the activation of lutetium sensitive to changes in the shape of the neutron spectrum in the energy region where the 1/E tail joins the thermal distribution. Eu^{151}, as shown in Fig. 2.4, has a thermal neutron absorption cross section, which varies roughly as $1/v^2$, a strong neutron capture resonance at 0.46 ev, and a weaker resonance at 0.321 ev which slightly distorts the shape of the resonance at 0.46 ev. The $1/v^2$ behavior of Eu^{151} means that the absorption cross section varies rapidly in the low energy region of the spectrum and makes the europium activation sensitive to changes in the neutron energy distribution in this region. With the three detectors, lutetium, europium, and gold, it was possible to investigate to some extent, by means of integral measurements, the gross spectral dependence of the intracell, thermal neutron distributions.

2.3 METHODS OF MEASURING THE MICROSCOPIC DISTRIBUTIONS

2.3.1 FOIL FABRICATION PROCEDURES

The gold foils were of high purity, and were about two mils thick. The foils used in the natural uranium lattices were one-eighth inch in diameter; those used in the enriched uranium lattice (1-1/4-inch spacing) were one-thirty-second or one-sixteenth inch in diameter. One-sixteenth inch diameter foils, five mils thick, and consisting of 13.6% by weight of gold in a lead alloy were also used in the 1-1/4 inch lattice; these foils closely matched the absorption and scattering properties of the fuel. All foils were formed with hardened punches and dies machined to close tolerances, and had clean, smooth edges. All gold foils were intercalibrated by weighing them on a high-precision balance. The gold purity was checked several times during the course of the experiments by checking the 2.7 day halflife of Au^{198}.

The lutetium and europium foils were fabricated by spraying a glyptal suspension of the oxides of natural lutetium or europium onto a backing of five mil thick, high-purity aluminum foil. Individual one-eighth inch and one-sixteenth inch diameter foils were then punched out of the sprayed sheet. The one-sixteenth inch foils were used in the enriched lattice, the one-eighth inch foils, in the natural uranium lattices. The foils were intercalibrated for relative γ and β response by measuring the γ activity and the β activity after irradiation in a uniform flux on a rotating foil wheel, located in the lattice tank, with

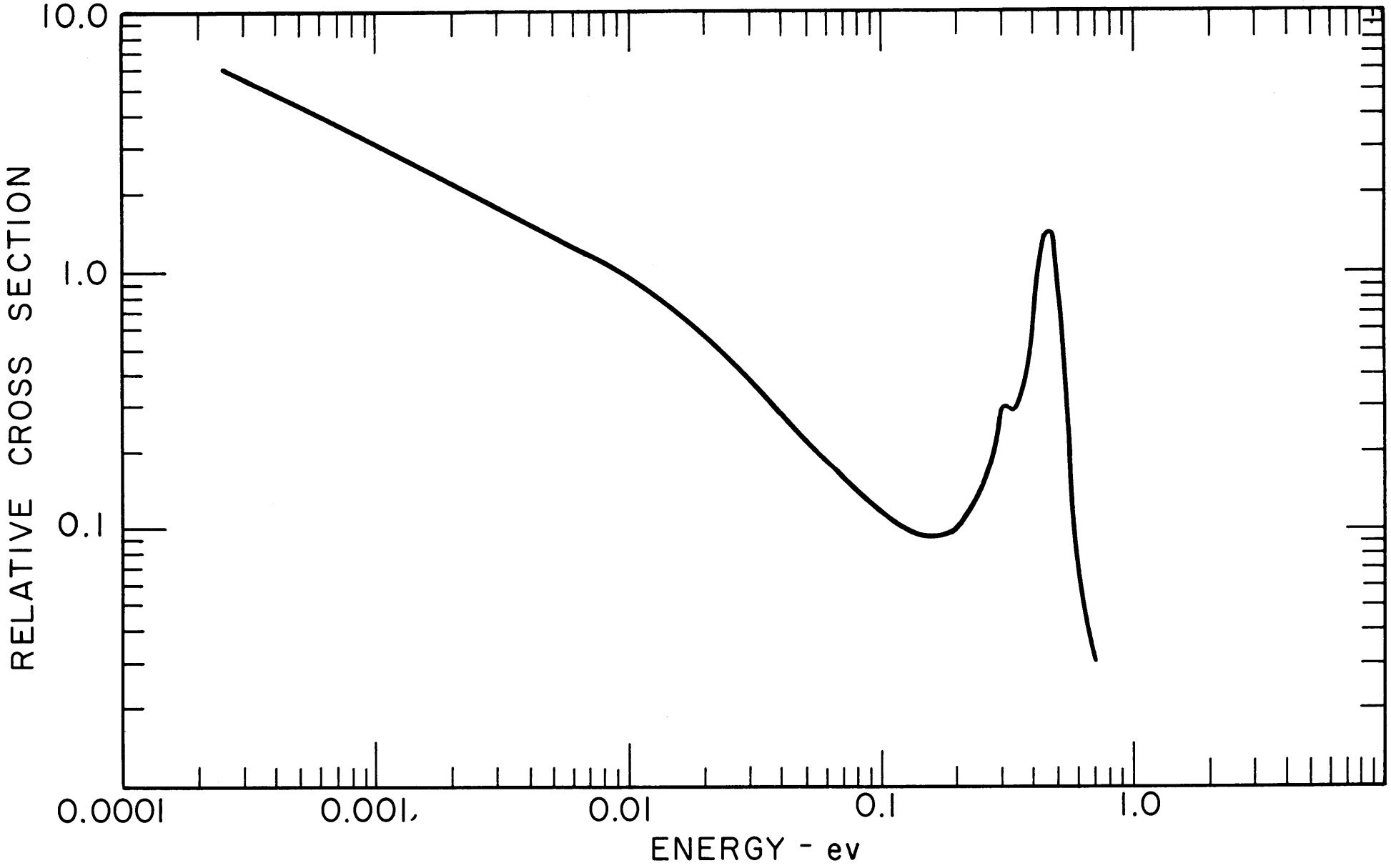

FIG. 2.4 ACTIVATION CROSS SECTION OF Eu^{151}

the latter filled with D_2O. The material purities were tested by halflife measurement and by examining, with a 256 channel TMC analyzer, the gamma and x-ray spectra of the irradiated nuclides. No detectable impurities were found either from the oxide materials, the aluminum, or the glyptal varnish. The lutetium and europium foils were nearly infinitely dilute. The Lu thickness was about 10 mg/cm^2, and the Eu thickness, about 0.2 mg/cm^2; these thicknesses correspond to about 1% of a thermal mean free path. Details of the foil fabrication and calibration procedures are given in Appendix D.

Cadmium foil covers were formed by pressing 0.023 inch thick cadmium sheet into a die, or by machining thicker cadmium foils to the shape desired. The covers were designed in the shape of small pillboxes, a different size for each foil size. The foils fit snugly into the pillboxes, which were capped with a tightly fitting cover. Care was taken to minimize the amount of cadmium in each pillbox and, at the same time, to eliminate all possibilities for thermal neutrons to leak or stream through imperfections in the cover arrangement.

2.3.2 FOIL HOLDERS

The various arrangements for holding foils are shown in Figs. 2.5 - 2.7. Bare and cadmium covered foils in the moderator were placed on type 1100 aluminum foil holders which were strapped to the central rod of the lattice. Aluminum was used instead of plastic, because an experiment showed that plastic holders depressed the thermal flux by as much as 3%, while the effect of thirty mil thick aluminum was only about 0.5%; this experiment is described in Appendix A. The aluminum holders had depressions milled in them for accurate placement of foils. The foils were held in place with a thin strip of mylar tape, which was found to cause a negligible perturbation of the flux. In the natural uranium lattices, the foil holders were thirty mils thick, and a correction was made for the flux perturbation caused by the foil holder. The foil holders used in the enriched uranium lattice did not have to be as rigid as those in the natural uranium lattices, and were only ten mils thick. The foil holders in the moderator extended to the next adjacent rod and to a point midway between the next two adjacent rods, as shown in Fig. 2.5.

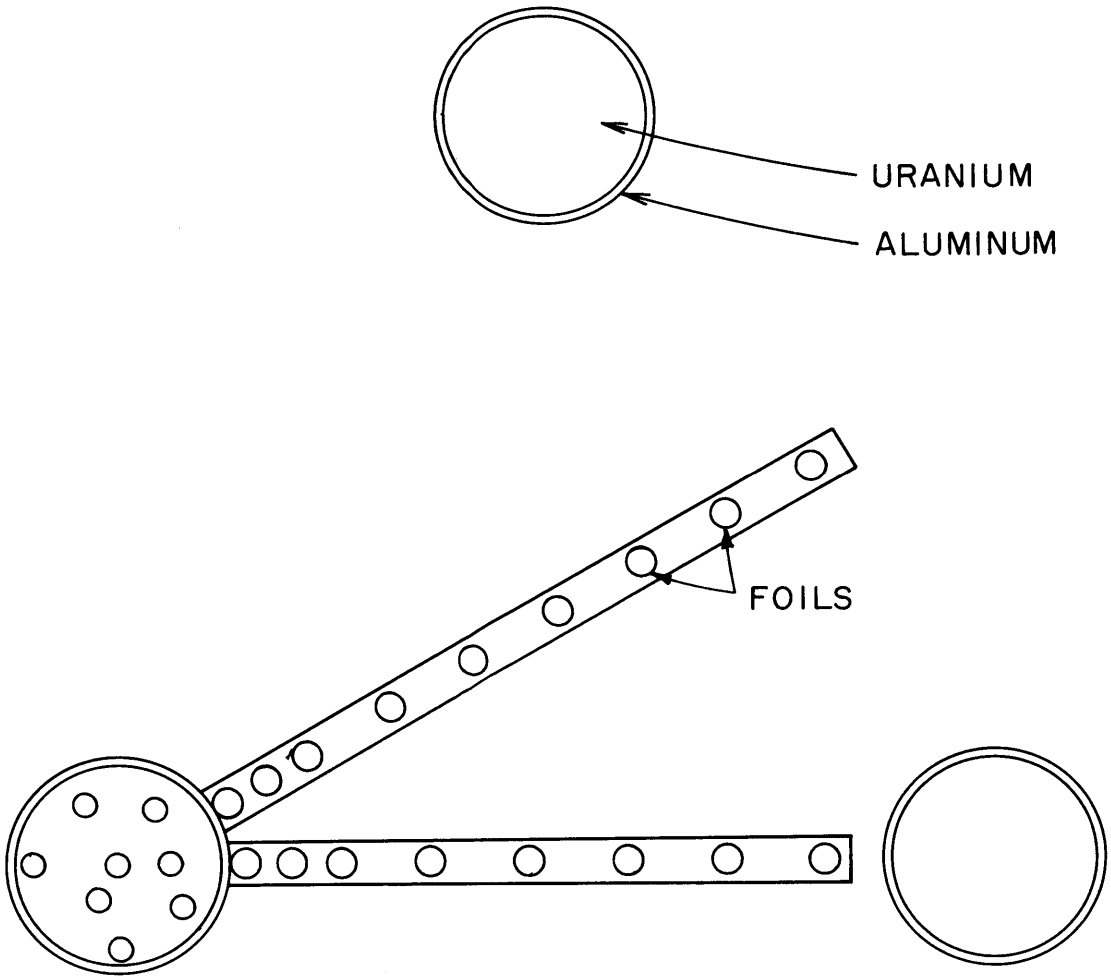

FIG. 2.5 TOP VIEW OF FOIL HOLDER ARRANGEMENT IN THE NATURAL URANIUM LATTICES (NOTE: THE ARRANGEMENT IS SIMILAR IN THE 1.25- IN. LATTICE, IN WHICH THE ONLY DIFFERENCES ARE THE SIZES OF THE CELL REGIONS AND THE SPACING OF THE FOILS)

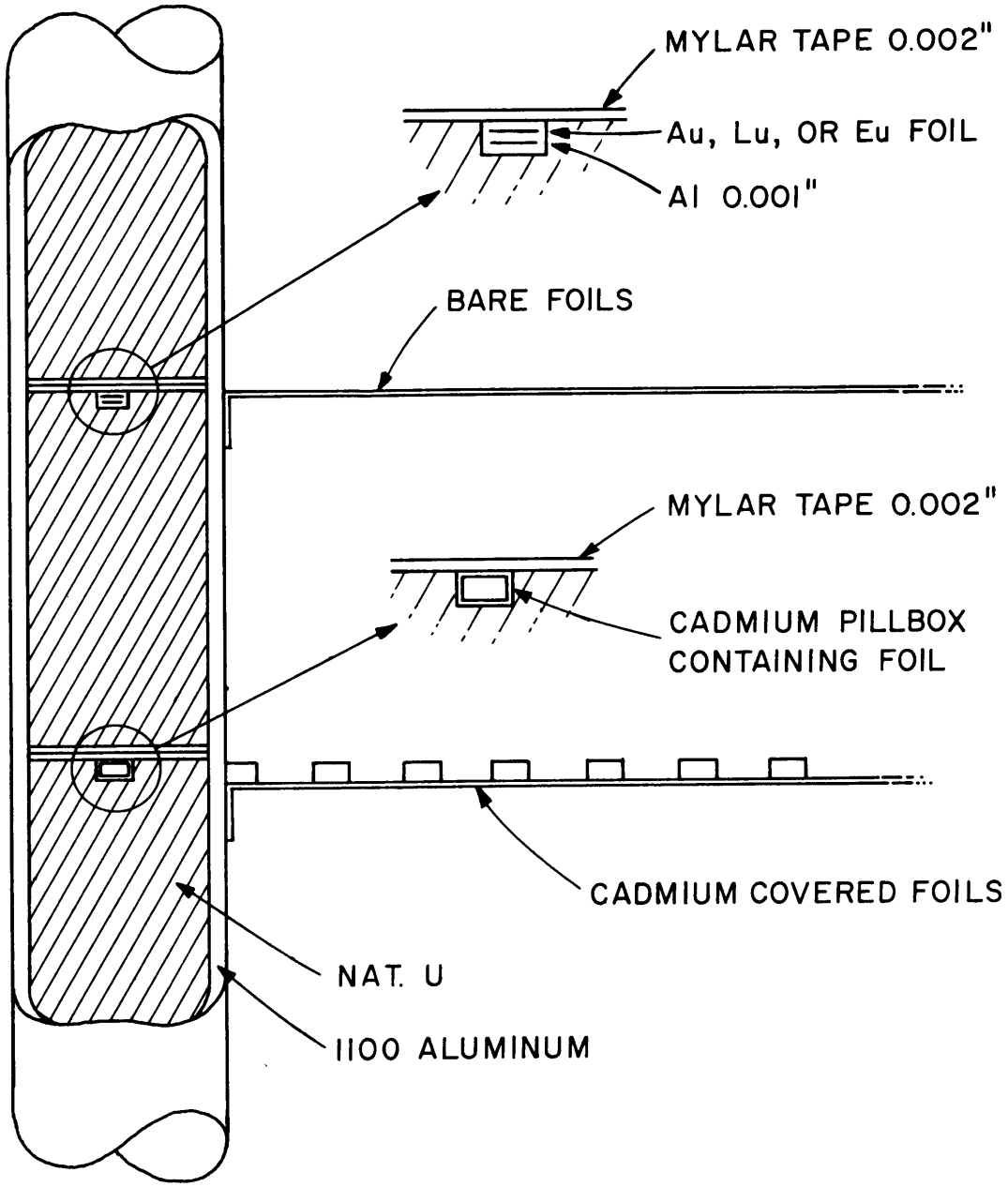

FIG. 2.6 SIDE VIEW OF FOIL HOLDER ARRANGEMENT IN THE NATURAL URANIUM LATTICES

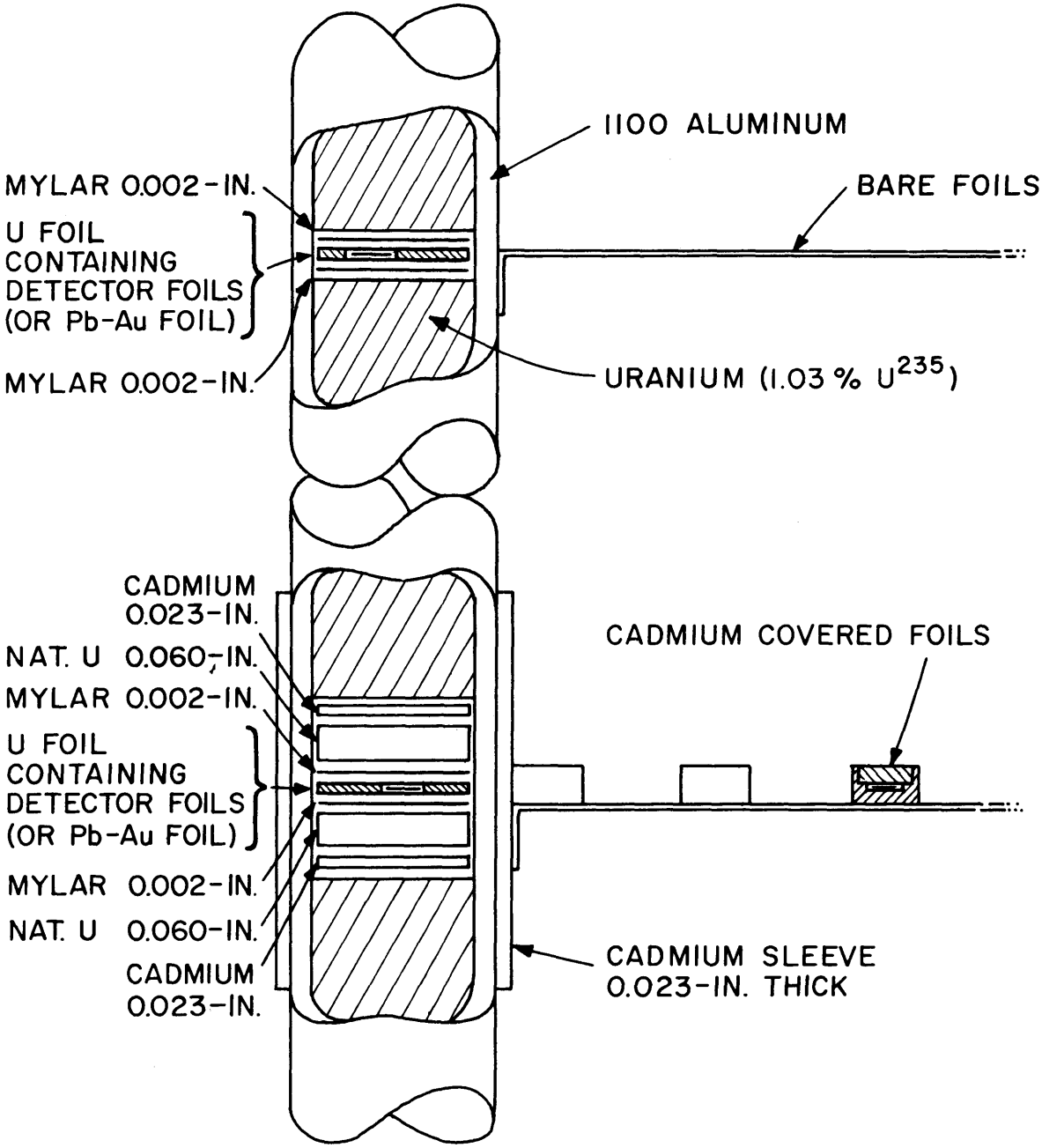

FIG. 2.7 SIDE VIEW OF FOIL HOLDER ARRANGEMENT IN THE 1.25-IN. LATTICE

In the natural uranium lattices, one-eighth inch diameter holes were milled in the ends of two-inch long slugs of uranium. The foils that were placed in these holes were shielded with 2-mil thick aluminum foil or mylar tape to prevent fission product pickup, as shown in Fig. 2.6. Mylar tape was used to prevent the foils from falling out of the holes during handling. The holes were arranged in a spiral pattern, as shown in Fig. 2. 5, to provide maximum spacing between two successive foils. In this way, the foils were not all located in the same region in the fuel, and any positioning errors due to a loose fit of the slug within the fuel element would tend to cancel in the over-all distribution in the fuel. The foils were located at six radial positions. Provision was made for two foils at each of the two outermost positions, since positioning errors in this region might be serious due to a large flux gradient. The uranium slugs were then placed in split fuel elements with the same dimensions as the regular fuel elements. The cadmium covered foils were placed in similar slugs; the holes in these slugs were three-sixteenths of an inch in diameter, large enough to hold the cadmium covers, but fewer in number because of the restrictions of space.

In the lattice of 1. 03% U^{235}, one-quarter inch diameter rods, the foil arrangement in the fuel was similar to that in the natural uranium lattices. But, instead of milling holes in the uranium slugs, holes were punched at the desired locations in one-quarter inch diameter uranium foils. Exact spacing of the holes was achieved through the use of a steel drill jig. The detector foils were placed in these holes. Mylar tape was used to prevent fission product pickup and to keep the foils in place. The foils to be covered with cadmium did not have individual cadmium covers, as in the natural uranium lattices, but were placed in the uranium in the same way as the bare foils. As shown in Fig. 2. 7, the foils to be covered with cadmium were surrounded by a cadmium sleeve, 0. 023 inch thick, attached to the outside of the fuel rod; sixty mils of natural uranium foil were placed above and below the cadmium covered foil to prevent streaming of resonance neutrons through the cadmium, and 0. 023-inch thick cadmium foils were placed above and below these natural uranium shields to complete the cadmium box. The bare detector foils were placed in uranium foils containing 1. 03% U^{235}. Because of the limited supply of 1. 03% U^{235} foil, the cadmium covered detector foils were placed in

natural uranium foils. The use of these natural uranium foils and of the sixty mil thick natural uranium shields mentioned above, instead of 1.03% enriched uranium, probably had a negligible effect on the measurements, since the resonance neutron behavior would be only slightly affected by the small change in the U^{238} concentration. In the case of the lead-gold alloy, single one-quarter inch diameter, lead-gold foils were placed in the rod, and one-sixteenth inch diameter foils were punched out after irradiation.

The cadmium covered foils were irradiated at the same time as the bare foils, but at a different height in the tank, to prevent thermal flux perturbations by the cadmium. An experiment was performed to determine the flux perturbation effect of a cadmium pillbox and is described in Appendix B. It was found that the flux depression due to a cadmium pillbox was not detectable at a distance of 1.5 inches from the pillbox. Hence, cadmium covered foils were always placed at least two inches away from the bare foils. The axial flux distribution in the lattice was measured with bare gold foils and was used to correct for the difference in heights of the bare and cadmium covered foils.

2.3.3 FLUX PERTURBATIONS

The flux perturbations of the foil holders and the cadmium covers have already been discussed in section 2.3.2. The lutetium and europium foils were too dilute to cause any significant flux perturbation. As shown in Appendix C, the only significant perturbation by the gold foils is a self-shielding effect, and the flux depression in the surrounding medium is negligible, also indicating that the disturbance of the flux pattern in the neighborhood of one foil by the presence of another foil was negligible. Section 4.3.1 gives further experimental proof of the insignificance of the flux depression. Since the perturbation was just a self-shielding effect and, since the absorption cross section of gold is so much larger than that of either the uranium or the D_2O, the self-shielding effect should be very nearly the same for all the foils, whether in the fuel or in the moderator, and need not be corrected for in a relative measurement. The self-shielding factor for the two mil thick gold foil is shown in Appendix C to be only about 5%.

2.3.4 COUNTING METHODS

Both gamma and beta counting were used to measure foil activities. A block diagram of the gamma counting system is shown in Fig. 2.8. This system was coupled with a Nuclear Chicago automatic sample changer, Model C-110B, to permit the automatic counting of a large number of foils. A block diagram of the GM beta counting system is shown in Fig. 2.9. This system was coupled with a Baird Atomic automatic sample changer, Model 750.

The gold foils were counted with the gamma counting system. The beta system was not used because, in counting betas, most of the activity comes from the foil surface, making it difficult to correct for the weight of the foil. Furthermore, slight imperfections on the foil surface, such as scratches, increase the surface area of the foil and lead to spurious results. The gold was counted by setting the gamma counting system to straddle the 411 kev Au^{198} gamma ray peak with a window width of 60 kev.

Since the lutetium and europium foils had been intercalibrated on both the gamma and the beta counting systems, both systems were used to measure the activities from which the intracell flux traverses were determined. No significant differences were found in the results obtained by the two methods of counting, although the gamma results seemed to show less scatter. It is possible that distortion of the soft foil surfaces, resulting from handling of the foils, may have had an undesirable effect in beta counting because of the unpredictable attenuation of betas in an uneven surface. The GM results were used in only four out of twenty-five activity distributions, when the gamma results had to be discarded because of difficulties with the counting equipment.

Europium contains 47.77% Eu^{151} with an activation cross section of 1400 barns, giving a Eu^{152} activity with a halflife of 9.2 hours, and 52.23% Eu^{153}, which has an activation cross section of 420 barns. But Eu^{154} has a 16-year halflife, so that the activation of Eu^{153} is negligible compared to that of the Eu^{151}. Since the europium foils were very thin, the resulting activities were not as high as desired. Instead of counting a single gamma or x-ray peak as was done with gold, an integral gamma counting method was used to measure as much activity as possible. The base line of the gamma spectrometer was accordingly set at about 80 kev,

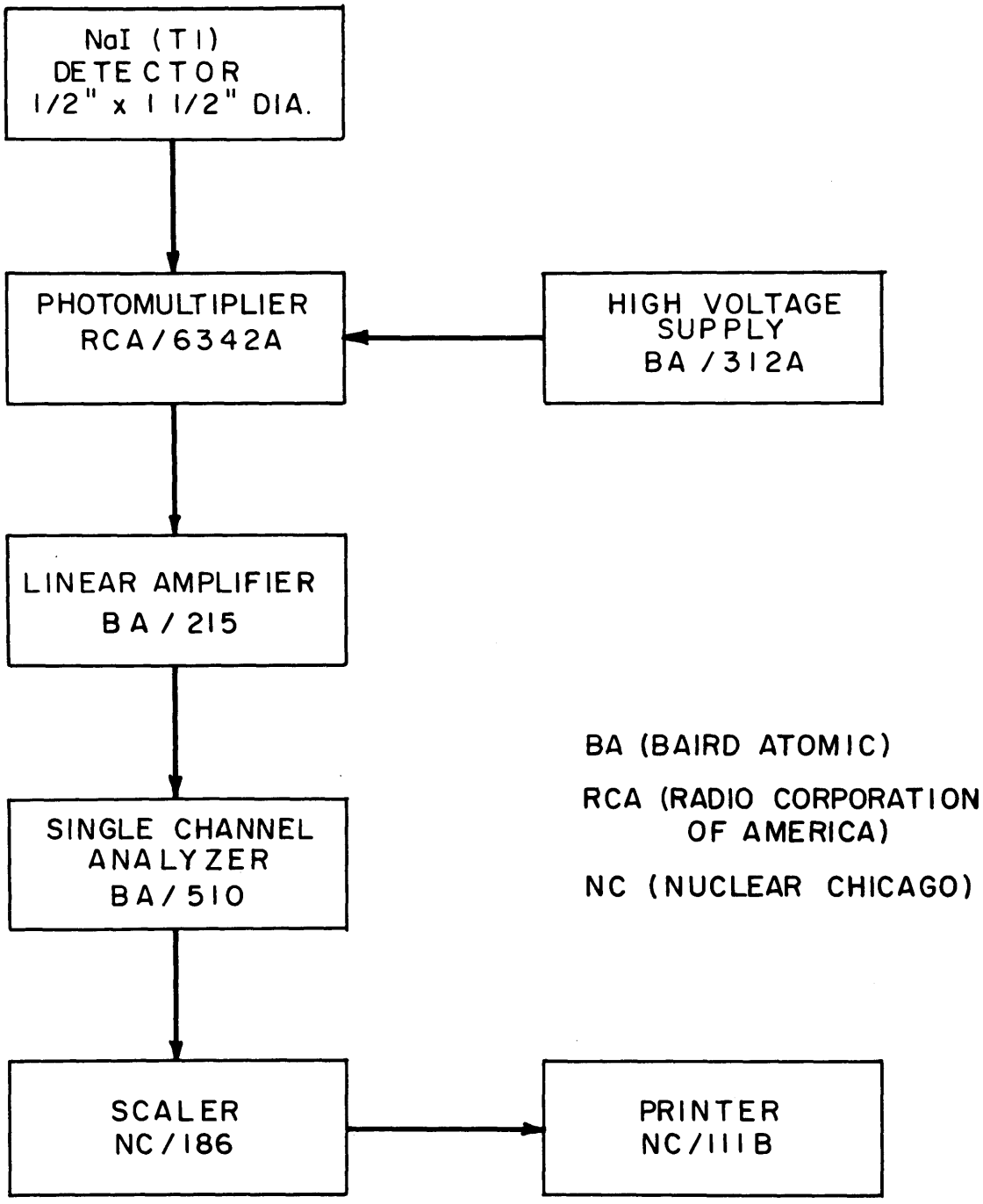

FIG. 2.8 BLOCK DIAGRAM OF GAMMA COUNTING SYSTEM

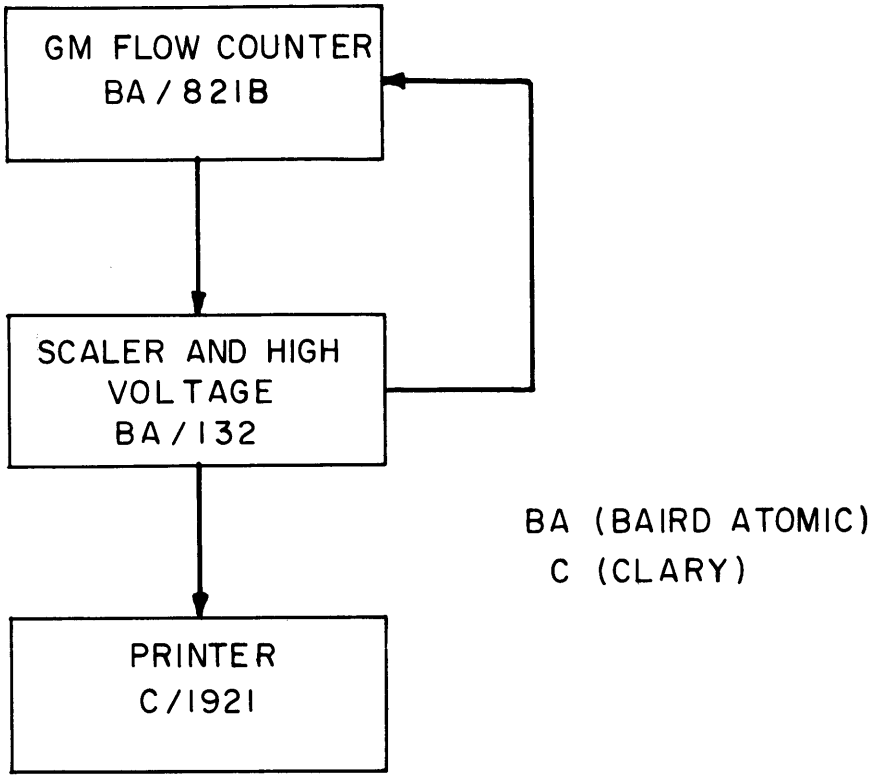

FIG. 29 BLOCK DIAGRAM OF BETA COUNTING SYSTEM

just below the 122 kev gamma peak of Sm^{152}, and an infinite window width was used. The 9.2 hour halflife was checked at this setting and satisfactory values were obtained, within a per cent of the accepted value.

Lutetium consists of 2.6% Lu^{176}, which gives Lu^{177} (6.71 day halflife), and 97.4% Lu^{175}, which gives Lu^{176m} (3.7 hour halflife). It was found that after a cooling period of 48 hours, the Lu^{176m} activity had fallen to less than 0.1% of the Lu^{177} activity. Hence, all lutetium foils were cooled for at least 48 hours before being counted.

Lu^{177} emits several low energy gamma and x rays -- a 57 kev Hf x ray, and 71 kev, 115 kev, 208 kev, 250 kev, and 320 kev gamma rays (H2). The base line of the analyzer was set at about 45 kev, just below the 57 kev Hf x-ray peak. An infinite window width was used. The 6.71 day halflife was checked at this setting. Satisfactory values were obtained, within a per cent of the accepted value.

The scintillation system was recalibrated each time it was used. Periodic checks for drift were made during the counting of each experiment. Because the bare foil activities were at times as low as four times the background, background counts were taken frequently.

2.3.5 EXPERIMENTAL PROCEDURE

The detector foils were first cleaned (the gold, with acetone; the lutetium and europium with water) and then loaded into the foil holders. The fuel foil holders were loaded into a special split fuel element. The remainder of the space in this element was taken by regular fuel slugs. The foils were placed at a height of at least 20 inches from the bottom of the rod because at this height, and above, the cadmium ratio in the lattice tank had been found to be representative of that of the whole lattice. The foil holders in the moderator were strapped to the outside of the special rod, at the same height as the foils inside the rod. Several bare foils were taped with mylar to the surface of the rod to measure the activity in this region of high radial flux gradient. As was mentioned in section 2.3.2, the cadmium covered foils were placed at least two inches away from the bare foils.

With the natural uranium lattices, the central fuel element was part of a three-rod cluster. This cluster was lowered through an airtight

glove box into the exponential tank. In the enriched uranium lattice, a single central rod was lowered through the glove box into the tank. The tank was then filled with heavy water. The experiment was started by opening a series of cadmium and lead shutters at the face of the thermal column; it was terminated by closing the same shutters. The lattice was allowed to cool for several hours after each experiment, the length of the cooling period depending on the length of the irradiation. When radiation levels near the exponential tank became tolerable, the experimental material was removed from the tank. The foil holders were removed in a shielded and ventilated glove box. The foils were removed from the holders, cleaned of any contamination they may have picked up, and placed on special planchets to be counted.

2.3.6 DATA PROCESSING PROCEDURE

The time at which the first foil began to count was denoted as zero time. All foil activities were corrected for the following:

1. Background.
2. Activity decay since zero time.
3. Activity decay during counting.
4. Foil weight or intercalibration.
5. Counter dead time.
6. Foil holder flux perturbations.
7. The macroscopic J_o flux distribution in the exponential tank.
8. Height of foils in the tank.

The activities of the cadmium covered foils were plotted as a function of radius; a smooth curve was drawn through the data, by drawing a straight line through the average of the activities in the moderator (where the epicadmium distribution was flat) and by fitting a line by eye to the distribution in the fuel. The activity at each point was then subtracted from the activity of the bare foils to give the thermal, or subcadmium, activity. As will be described in Chapter IV, the activity of a cadmium covered europium foil was multiplied by a constant before the subtraction. The thermal activity was then plotted as a function of radius; the results of these graphs are shown and discussed in Chapter IV. As was mentioned above, the moderator flux was measured from rod to rod and from rod to moderator. Traverses along these two directions should give the two

extremes of the traverses in all the possible radial directions in the cell. The activity distributions to be discussed in Chapter IV show that, at the cell radius, the rod-to-moderator traverses are, on the average, less than 1% higher than the rod-to-rod traverses for the natural uranium lattices. For the enriched lattice, no difference between the two traverses could be detected. Thus, in drawing a smooth experimental curve through the corrected activities, the rod-to-rod and rod-to-moderator traverses, as far as the cell radius, may be averaged. Beyond the cell radius, the rod-to-rod values should decrease more quickly with increasing radius than the rod-to-moderator values because of the proximity of the neighboring rod. This effect can also be seen in the activity distributions given in Chapter IV.

2.4 SEPARABILITY EXPERIMENTS

A series of experiments was performed to determine whether the thermal neutron temperature was uniform throughout the lattice tank. Radial and axial buckling measurements were made with lutetium foils, and were compared with similar gold traverses which had been made by Dr. P. F. Palmedo (P1). Methods and foil holders developed by Palmedo were used in these experiments. Two off-center microscopic gold traverses were also measured to determine the effects of radial position in the tank. The results of these experiments and of the lutetium buckling experiments are discussed in section 4.2.4.

2.5 TRANSMISSION EXPERIMENT

Several experiments were performed with a new method for obtaining information about the thermal neutron spectrum. This method is based on the transmission of a beam of neutrons through a stack of absorber-detector foils. The transmission curve through the stack is the Laplace transform of a quantity directly related to the spectrum. The methods used were an extension of similar methods developed at the MITR by workers from the Air Force Cambridge Research Center (B3). The transmission experiments are described in Appendix F.

CHAPTER III

THEORETICAL AND ANALYTICAL METHODS

3.1 INTRODUCTION

The theoretical methods used for obtaining spatial and spectral thermal neutron distributions, disadvantage factors, thermal utilization, and other related quantities are treated in this chapter. Analytical methods for deriving certain useful parameters from the experimental data are also discussed.

3.2 THE THERMOS CODE

THERMOS is an integral transport theory code developed by Dr. H. C. Honeck, now of the Brookhaven National Laboratory (H6, H7, H8). The code solves the integral transport equation for the relative neutron density as a function of position and velocity; it treats a cylindrical Wigner-Seitz cell centered on the fuel rod. The cell may be divided up into as many as 20 concentric cylindrical regions, and as many as 30 velocity groups may be used. A detailed discussion of the solution of the integral transport equation will not be given here, but certain aspects of the theory and the assumptions on which it is based will be mentioned because of their possible influence on the theoretical results.

In solving the integral transport equation, THERMOS makes use of two kernels which will be discussed here because of the approximations involved. The first of these kernels is the transport kernel, which relates the flux of neutrons of speed v at position $\bar{r}$ to a unit isotropic source at $\bar{r}'$. In the computation of the transport kernel, a number of possible neutron trajectories in the cell are considered. When one of these trajectories reaches the cell boundary, a reflection condition is imposed there, with the angle of incidence equal to the angle of reflection. This condition implies an infinite lattice with neutrons feeding into each cell at the same rate at which they leave.

As will be discussed in section 4.3.4, the reflection condition at the cell boundary may lead to serious errors if it is necessary to approximate the shape of the cell boundary, as in the Wigner-Seitz cell approximation.

The second kernel is the neutron scattering kernel, which is the probability per second per unit solid angle that a neutron at speed v' will be scattered to a speed v through an angle whose cosine is μ_o. The first approximation is the assumption of isotropic scattering, i.e., the dependence of scattering on μ_o is neglected. To consider anisotropic scattering would greatly complicate the solution of the integral transport equation and would require large amounts of computer time. A first order correction for anisotropic scattering is the multiplication of the scattering cross section by $1 - \bar{\mu}_o$, where $\bar{\mu}_o$ is the average cosine of the scattering angle. The use, or non-use, of such a correction has been investigated and will be discussed in Chapter IV.

The second approximation in the scattering kernel involves the energy transfer. The slowing down of neutrons in hydrogeneous media is greatly affected by several important phenomena. The Wigner-Wilkins (W7) theory treated the moderating atoms in water as forming a free gas of unit mass for hydrogen, and of mass two for deuterium; it also assumed that the scattering cross section is independent of energy. The deuterium (or hydrogen) atoms, however, act as a free gas only when the neutron speed is very high. As the neutrons approach thermal energies, the chemical binding of the moderator atoms in the water molecules renders invalid the assumption of free scattering atoms, and chemical association effects due to nearby molecules also become important. Vibrational and rotational modes in the moderating molecules are then excited by the neutrons being slowed down, and an accurate description of the interactions requires the use of quantum mechanics. Several approximations to the scattering kernel for D_2O have been developed. The first of these is the Brown-St. John kernel (B5), in which the D_2O molecule is treated as a rigid rotator and the scattering cross section varies with energy, but vibrational effects, molecular association effects, inelastic scattering, and interference effects are neglected. The effect of the chemical binding is assumed to increase the mass of deuterium to 3.595 amu, thus decreasing the moderating power. Recently, Honeck (H9) has developed for D_2O a new kernel similar to that derived by Nelkin for H_2O (N1). Honeck treats

the D_2O molecule as a combination of a translator of mass 20, a hindered rotator with mass 4.11, and three vibrational oscillators with masses equal to 14.52 each, and energies at 0.15 ev, 0.35 ev, and 0.35 ev, respectively. Honeck's kernel thus gives a more extensive treatment of the scattering interaction than the Brown-St. John kernel and would be expected to give a more accurate treatment of the thermalization process. The results of a comparison between the THERMOS results based on the two kernels will be given in Chapter IV.

The THERMOS code also computes other useful information. Cross sections of detector materials may be integrated over the computed energy-dependent flux distributions to give spatial activity distributions. Comparison of experimental activity distributions obtained with these same detectors then serves as a good test of the results of the computations. Averages of velocities, fluxes, neutron densities, cross sections, energies, and other useful parameters over the regions of the cell and up to energy limits as high as 0.785 ev may also be calculated from the computed distributions.

3.3 THE NORMALIZATION OF THEORY AND EXPERIMENT

In comparing experimental and THERMOS activity distributions, the two must be normalized in some way. One method involves equating the THERMOS and experimental activities at the cell edge. However, the use in the normalization of just one or two experimental activities at the cell edge may lead to errors because of possible scatter in the data. A more accurate method is to equate the average THERMOS and experimental activities in a small region in the vicinity of the cell edge. In the 1-1/4-inch lattice, the experimental distribution was found to be flat in the vicinity of the cell edge. In addition, no difference was detected between the activities in the rod-to-rod and rod-to-moderator traverses. Hence, the experimental activities in the vicinity of the cell edge were averaged and the THERMOS activity at the cell edge was equated to the average value. In the natural uranium lattices, the distributions were not quite flat near the cell edge. Hence, in a small region in the vicinity of the cell edge, the experimental activity at each point was divided by the THERMOS activity to form a scale factor. All the scale factors in the small region were then averaged to obtain an average

scale factor. In the averaging, the activities in the rod-to-rod and rod-to-moderator traverses were treated as identical for reasons explained in section 2.3.6. The THERMOS distribution was then normalized to the experimental distribution by multiplying the THERMOS distribution by the average scale factor. One advantage of normalizing at the cell edge is that the computed and, as yet, unhardened spectrum there is closest to a Maxwellian, and is least subject to errors in the computation. It is, therefore, this point from which neutron temperature changes in the cell will be computed. A second advantage of normalizing at the cell edge is that the activity distribution there is very nearly flat, and the normalization in a region where the distribution is flat should be more accurate than normalization in a region where the distribution has steep gradients. With such a normalization, the largest differences between theory and experiment occur at the cell center.

There are also some advantages to normalizing theory and experiment at the cell center. First, the activity distribution does not have a steep gradient at the cell center. Second, it is more aesthetically satisfying to normalize at the well-defined cell center rather than at the approximately defined cell edge. However, only one experimental activity is available at the cell center and normalization to just that one activity may be inaccurate because of possible experimental scatter. Hence, an alternate method was used which involves the normalization of the THERMOS and experimental results in the fuel. The experimental activity at each point in the fuel was divided by the THERMOS activity to obtain a scale factor. The scale factors at all the experimental points in the fuel were then averaged to give an average scale factor, as was done at the cell edge. The THERMOS distribution was then multiplied by the average scale factor and was, in this way, normalized to the experimental distribution. Such a method of normalization is less significant than normalization at the center of the rod, but it is more accurate and may be applied consistently to all lattices. With such a normalization, THERMOS may be said to give the correct absorption rate in the fuel if the shapes of the experimental and THERMOS curves are in good agreement; the greatest differences between theory and experiment occur at the cell edge. A disadvantage of such a normalization is that it may emphasize errors in the steep flux gradient present in the outer region of the fuel.

3.4 DISADVANTAGE FACTORS

The thermal utilization, f, may be defined as the fraction of the thermal neutrons absorbed in the cell that are absorbed in the fuel:

$$f = \frac{\text{Thermal neutron absorption rate in the fuel}}{\text{Total thermal neutron absorption rate in the cell}} \tag{3.1}$$

Expressed quantitatively:

$$f = \frac{\int_{\text{fuel}} \int_{v} \sigma_a^{\text{fuel}}(\bar{r}, v)\, N_{\text{fuel}} \phi(\bar{r}, v)\, d\bar{r}\, dv}{\int_{\text{fuel}} \int_{v} \sigma_a^{\text{fuel}}(\bar{r}, v)\, N_{\text{fuel}} \phi(\bar{r}, v)\, d\bar{r}\, dv + \int_{\text{clad}} \int_{v} \sigma_a^{\text{clad}}(\bar{r}, v)\, N_{\text{clad}} \phi(\bar{r}, v)\, d\bar{r}\, dv + \int_{\text{mod}} \int_{v} \sigma_a^{\text{mod}}(\bar{r}, v)\, N_{\text{mod}} \phi(\bar{r}, v)\, d\bar{r}\, dv} , \tag{3.2}$$

where the symbols are defined in Appendix I; all integrations over velocity are up to the cadmium cutoff. If $\bar{\sigma}_a^i$ and $\bar{\phi}_i$ are defined as follows:

$$\bar{\sigma}_a^i = \frac{\int_{\text{region i}} \int_{v} \sigma_a^i(\bar{r}, v)\, \phi(\bar{r}, v)\, d\bar{r}\, dv}{\int_{\text{region i}} \int_{v} \phi(\bar{r}, v)\, d\bar{r}\, dv} , \tag{3.3}$$

$$\bar{\phi}_i = \frac{\int_{\text{region i}} \int_{v} \phi(\bar{r}, v)\, d\bar{r}\, dv}{V_i} , \tag{3.4}$$

then

$$\bar{\sigma}_a^i \bar{\phi}_i V_i = \int_{\text{region i}} \int_{v} \sigma_a^i(\bar{r}, v)\, \phi(\bar{r}, v)\, d\bar{r}\, dv . \tag{3.5}$$

Equation (3.2) may be modified by using Eq. (3.5) and the definition $\Sigma_a^i = N_i \sigma_a^i$:

$$f = \frac{\bar{\Sigma}_a^{fuel} \bar{\phi}_{fuel} V_{fuel}}{\bar{\Sigma}_a^{fuel} \bar{\phi}_{fuel} V_{fuel} + \bar{\Sigma}_a^{clad} \bar{\phi}_{clad} V_{clad} + \bar{\Sigma}_a^{mod} \bar{\phi}_{mod} V_{mod}} \tag{3.6}$$

Equation (3.6) may be written:

$$\frac{1}{f} = 1 + \frac{\bar{\Sigma}_a^{mod} V_{mod} \bar{\phi}_{mod}}{\bar{\Sigma}_a^{fuel} V_{fuel} \bar{\phi}_{fuel}} + \frac{\bar{\Sigma}_a^{clad} V_{clad} \bar{\phi}_{clad}}{\bar{\Sigma}_a^{fuel} V_{fuel} \bar{\phi}_{fuel}} . \tag{3.7}$$

The ratio $\bar{\phi}_{clad}/\bar{\phi}_{fuel}$, defined here as the fuel disadvantage factor, is often denoted by F. The ratio $\bar{\phi}_{mod}/\bar{\phi}_{clad}$, the moderator disadvantage factor, is often denoted by F_m. Then, $\bar{\phi}_{mod}/\bar{\phi}_{fuel}$ may be denoted by FF_m. In a measurement of the thermal utilization, the quantities F and FF_m must be determined. They can be obtained from the experimental activity distributions. These distributions were measured with gold foils and the results are given in Chapter IV. Since gold is a 1/v neutron absorber below the cadmium cutoff, it actually measures neutron density distribution. Equation (3.7) must therefore be expressed in terms of neutron density, which can be done as follows. The average velocity in region i may be defined as

$$\bar{v}_i = \frac{\int_{\text{region i}} \int_v vN(\bar{r}, v)\, d\bar{r}\, dv}{\int_{\text{region i}} \int_v N(\bar{r}, v)\, d\bar{r}\, dv} . \tag{3.8}$$

The average flux $\bar{\phi}_i$ and the average neutron density $\bar{N}_i$ in region i may be defined as

$$\bar{\phi}_i = \frac{\int_{\text{region i}} \int_v vN(\bar{r}, v)\, d\bar{r}\, dv}{\int_{\text{region i}} d\bar{r}} , \tag{3.9}$$

and

$$\bar{N}_i = \frac{\int_{\text{region i}} \int_v N(\bar{r}, v)\, d\bar{r}\, dv}{\int_{\text{region i}} d\bar{r}} . \tag{3.10}$$

From Eqs. (3.8), (3.9), and (3.10), it follows that

$$\bar{v}_i \bar{N}_i = \bar{\phi}_i \tag{3.11}$$

Equation (3.7) then becomes

$$\frac{1}{f} = 1 + \frac{\bar{\Sigma}_a^{mod} \bar{v}_{mod} V_{mod} \bar{N}_{mod}}{\bar{\Sigma}_a^{fuel} \bar{v}_{fuel} V_{fuel} \bar{N}_{fuel}} + \frac{\bar{\Sigma}_a^{clad} \bar{v}_{clad} V_{clad} \bar{N}_{clad}}{\bar{\Sigma}_a^{fuel} \bar{v}_{fuel} V_{fuel} \bar{N}_{fuel}} \tag{3.12}$$

The values of $\bar{N}_i$ are determined from the gold activity distributions. Since most cell materials have very nearly 1/v absorption cross sections, the products of $\bar{\Sigma}_a^i$ and $\bar{v}_i$ should be nearly constant. Although the values of $\bar{v}_i$ will change from region to region because of spectral hardening, the values of $\bar{\Sigma}_a^i \bar{v}_i$ should not change significantly. Hence, if all cross sections in Eq. (3.12) are assumed to correspond to the same spectral distribution (or neutron temperature), the equation used to get an experimental value for f then becomes

$$\frac{1}{f} = 1 + \frac{(\bar{\Sigma} V \bar{N})_{mod}}{(\bar{\Sigma} V \bar{N})_{fuel}} + \frac{(\bar{\Sigma} V \bar{N})_{clad}}{(\bar{\Sigma} V \bar{N})_{fuel}} \tag{3.12a}$$

The only nuclide in the M.I.T. lattices which has a slight non-1/v behavior is U^{235}. The effects of this behavior will be discussed in section 4.2.6.

3.5 TEMPERATURE CALCULATIONS: THE WESTCOTT METHOD

The comparison between THERMOS and experiment, for the gold, lutetium, and europium activity distributions, is the most important consideration in the investigation of the effects of spectral hardening. Another method may be used to extract spectral hardening information from these same activity distributions: temperature calculations based on the Westcott method (W4, W5, W6) of representing effective neutron cross sections. Westcott defines an effective cross section, $\hat{\sigma}$, by means of the expression

$$\hat{\sigma} = \frac{\int_0^\infty N(v)\,\sigma(v)\,v\,dv}{v_o \int_0^\infty N(v)\,dv} . \tag{3.13}$$

Equation (3.13) states that $\hat{\sigma}$ is the effective cross section, which, when multiplied by v_o (2200m/sec) and the total neutron density, gives the expected reaction rate. For N(v), Westcott assumes a Maxwellian distribution with a 1/E tail joining the Maxwellian at an energy of roughly 0.1 ev. A complicated function is used to join the 1/E tail smoothly to the Maxwellian portion of the spectrum. If the integrations in Eq. (3.13) are then carried out, it is found that

$$\hat{\sigma} = \sigma_{2200}(g+rs) , \qquad (3.14)$$

where g expresses the behavior of σ in the Maxwellian region, r is called the "epithermal index" and is very nearly equal to the fraction of the total neutron density in the 1/E tail, and s is a quantity which expresses the behavior of σ in the resonance region and is closely related to the epithermal resonance integral. The factors g and s have been computed by Westcott as functions of neutron temperature and have been tabulated (W4, W5). The factor r must be measured or calculated separately for each case, as shown later in this section. In using the Westcott method, the following limitations must be considered. First, the method is applicable with accuracy only to well-thermalized systems; if the spectrum is not well-thermalized, it may not be possible to represent it simply as a Maxwellian with a 1/E tail. Second, if the spectrum is appreciably hardened, as it is in fuel rods, the thermal region of the spectrum may be approximated only roughly by an equivalent Maxwellian distribution. Third, the g and s factors have been tabulated for infinitely dilute nuclides; for materials which are not infinitely dilute, thermal and epithermal self-shielding corrections must be applied.

With the Westcott notation, the ratio of lutetium activity to gold activity may be represented as:

$$R_{Lu} = \frac{a(g+rs)_{Lu}}{(g+rs)_{Au}} = \frac{\text{Total Lu Activity at } \infty \text{ Dilution}}{\text{Total Au Activity at } \infty \text{ Dilution}} , \qquad (3.15)$$

where a is a constant which depends on the values of σ_{2200}, foil cooling times, and other correction factors; the latter are the same for all of the foils used in a particular measurement of an activity distribution. The value of a can be determined by measuring the activity ratio in a known spectrum, or by assuming that the spectral distribution at a particular

point in the cell is known. In the present study, the spectrum at the cell edge computed with THERMOS is used to determine the effective temperature, which is then combined with the measured values of R_{Lu} at that point to calculate a value for α. All other temperatures in the cell are calculated relative to the cell edge temperature. As will be demonstrated in Chapter IV, the temperature changes from the cell edge to other points in the cell are not sensitive to the value chosen for the cell edge temperature, because of the approximate linear variation with temperature of the Westcott g factors; this method for determining α is consequently adequate for calculating temperature changes.

The value of r at each position in the cell can be determined from a measurement of the cadmium ratio for an infinitely thin gold foil. In all measurements, cadmium ratios were obtained with 0.002 inch (nominal) thick gold foils. Experiments were made to determine the necessary factors to correct these cadmium ratios to values corresponding to infinitely thin foils; these experiments are described in Appendix E. It was found that

$$\frac{(CR-1)_{2\text{-mil}}}{(CR-1)_o} = 3.158 \pm 0.031 \ . \tag{3.16}$$

The value of r can then be determined from the equation (W6):

$$CR_o^{Au} = \frac{(g+rs)_{Au}}{\left[rs + \frac{r}{K_{Cd}}\sqrt{\frac{T}{T_o}}\right]_{Au}} \ , \tag{3.17}$$

where K_{Cd} is a factor correcting for neutron absorption by the cadmium covers and is 2.106 for the M.I.T. experiments (0.023 inch thick cadmium); T is the actual neutron temperature, and T_o is 293.6°K. If the following relation for the s factor of gold (W6) is used,

$$s_{Au} = 17.2\sqrt{\frac{T}{T_o}} \ , \tag{3.18}$$

it is found that

$$r = \frac{g_{Au}}{s_{Au}(1.0275\ CR_o - 1)} \ . \tag{3.19}$$

The value of r can then be determined from Eqs. (3.16) and (3.19) if the neutron temperature is known and if the cadmium ratio for a 0.002-inch thick gold foil has been measured.

If Eq. (3.19) is substituted into Eq. (3.15), it is found that

$$R_{Lu} = \frac{a(g+rs)_{Lu}}{\left[\frac{1.0275CR_o}{1.0275CR_o-1}\right] g_{Au}} = \frac{\text{Total Lu Activity at } \infty \text{ Dilution}}{\text{Total Au Activity at } \infty \text{ Dilution}} \tag{3.20}$$

The total lutetium activity in the M.I.T. experiments is measured directly, since the lutetium foils used are nearly infinitely dilute (less than 1% of a thermal mean free path in thickness). Measurements of the lutetium cadmium ratios were consistent with those to be expected from the Westcott g and s factors, indicating that the lutetium foils were indeed close to infinite dilution.

It is more difficult to obtain the total gold activity to be used in Eq. (3.20) because the gold foils are far from infinitely dilute. The total gold activity at infinite dilution can be obtained, however, by using Eq. (3.16). The two quantities measured for gold are the thermal and epicadmium activities for 0.002-inch thick foils, $A_{th}^{0.002}$ and $A_{epi}^{0.002}$. By definition,

$$(CR-1)_{0.002} = \frac{A_{th}^{0.002}}{A_{epi}^{0.002}}, \tag{3.21}$$

and

$$(CR-1)_o = \frac{A_{th}^{o}}{A_{epi}^{o}}. \tag{3.22}$$

As discussed in Appendix C, the only perturbation by the 0.002-inch thick gold foil on the thermal activity is a self-shielding effect. If $A_{th}^{0.002}$ is divided by the self-shielding factor for a 0.002-inch thick foil, which is 0.946 in this case, and Eq. (3.16) is used, it is found that the total gold activity at infinite dilution is

$$A_{Au}^{o} = \frac{1}{0.946}\left(A_{th}^{0.002} + 3.158\, A_{epi}^{0.002}\right). \tag{3.23}$$

Combining Eqs. (3.23) and (3.20) gives

$$\frac{0.946\, A_{Lu}^{Total}}{\left(A_{th}^{0.002} + 3.158\, A_{epi}^{0.002}\right)_{Au}} = R_{Lu} = \frac{a(g+rs)_{Lu}}{\left[\frac{1.0275\, CR_o}{1.0275\, CR_o - 1}\right]_{Au} g_{Au}} . \tag{3.24}$$

Equations (3.16), (3.19), and (3.24) and the Westcott tables make possible the calculation, by trial and error, of temperature changes, from the experimentally determined gold and lutetium activity distributions. As described above, the value of a is determined by using the temperature computed with THERMOS at the cell edge and the gold and lutetium activities at that point.

A somewhat different procedure must be used for the europium activations. The Westcott s factors for europium are open to question because of uncertainties in the measurement of the epithermal europium resonance integral. As will be explained in Chapter IV, europium has a resonance at 0.46 ev, which is very close to the commonly accepted cadmium cutoff energy; the cadmium covers only partially absorb the neutrons at 0.46 ev, and there is considerable uncertainty as to what fraction of the epicadmium resonance integral is due to europium resonances at energies higher than 0.46 ev, and what fraction is due to the 0.46 ev resonance. A method has been outlined in Chapter IV, which permits corrections to be made experimentally for the partial absorption of the 0.46 ev neutrons. As described there, the europium activities can be corrected to thermal cutoff energies, both below and above the europium resonance, at 0.194 ev and 0.785 ev, respectively. As will be explained in the remainder of this section, only the activity below 0.194 ev will be used to determine the temperature changes based on the europium activation.

According to the Westcott notation, the g factor for a nuclide, like Eu^{151}, is given by Eq. (3.26):

$$g = \frac{4}{\sqrt{\pi}\sigma_o v_o} \int_0^\infty M(v)\, \sigma(v)\, v\, dv , \tag{3.25}$$

where

$$M(v) = \frac{v^2}{v_t^3} e^{-\left(\frac{v}{v_t}\right)^2}, \quad \text{with } v_t = v_o \sqrt{\frac{T}{T_o}}, \tag{3.26}$$

is a Maxwellian distribution and the other symbols have their usual meanings. Equation (3.25) shows that the g factor for europium depends only on the Maxwellian portion of the spectrum. The Maxwellian neutron densities in the lattices studied at M.I.T. rapidly approach negligible values at 0.194 ev, the lower europium energy cutoff. Thus, the integral in Eq. (3.25) includes mainly the contribution of the europium cross section which lies below 0.194 ev; below this energy, the europium cross section behaves approximately as $1/v^2$ and is strongly temperature-dependent. The contribution just above 0.194 ev adds a very small amount to the g factor, which would lead to a slight overestimate of the activity below 0.194 ev. If the spectrum were a pure Maxwellian, the europium g factor would thus be sufficient to predict the activity below 0.194 ev. Figure 4.39 shows two THERMOS spectra typical of the M.I.T. lattices. The presence of a 1/E tail increases the neutron flux between 0.1 and 0.2 ev, the transition region between the Maxwellian and the 1/E tail. Thus, to use only the g factor to calculate europium activity below 0.194 ev would lead to an underestimate of this activity. This effect would be balanced in part by the slight overestimate in activity mentioned above. The neutron density in Fig. 4.39 is seen to drop very rapidly in the region of 0.1 to 0.2 ev; the Eu^{151} cross section in this same region is, furthermore, very small compared to its values at lower energies. The contribution to the europium activity below 0.194 ev in this region should, therefore, be only a small fraction of the total contribution. The net result of such an underestimate in the predicted europium activity leads to an underestimate in the europium g factor obtained from a measured activity. This, in turn, leads to an overestimate in the thermal neutron temperature; this overestimate occurs for all foil positions in the lattice cell. Even though the temperature at each point may be too high, when temperature differences are calculated, part of the error should cancel.

The errors due to the above approximations seem to be small, and, in fact, should cancel one another in the calculation of temperature changes. In view of the other approximations of the Westcott notation, and considering that a calculation using the Westcott s factors might also involve some error, it seems justifiable to use the g factor method outlined above to treat the europium activations. The equation for the ratio of europium to gold activity is then given by:

$$R_{Eu} = \frac{0.946\, A_{Eu}^{sub-0.194\ ev}}{\left[A_{th}^{0.002} + 3.158 A_{epi}^{0.002} \right]_{Au}} = \frac{{}^{ag}_{Eu}}{\left[\frac{1.0275\, CR_o}{1.0275\, CR_o - 1} \right]_{Au} g_{Au}} . \tag{3.27}$$

Equation (3.27) differs from Eq. (3.24) only in the absence of an rs term for europium.

3.6 THE AMOUYAL-BENOIST-HOROWITZ METHOD

Amouyal, Benoist, and Horowitz (ABH) (A1) have developed a method for computing thermal flux disadvantage factors and the thermal utilization in lattice cells. The method assumes that diffusion theory is applicable a few mean free paths away from the rod, in the moderator, and uses some results from integral transport theory for the fuel. The method may break down if the moderator region is only one or two mean free paths thick. A detailed discussion of the theory of this method is given in reference (A1), which treats the case of an unclad fuel rod in a moderating medium. Theys (T2) has extended the method to include the presence of cladding. It has been reported (A1) that the method gives results as good as those obtained from a P_3 or a P_5 computation.

The ABH method will be used to calculate the values of $\bar{\phi}_{mod}/\bar{\phi}_{fuel}$, and $\phi_{fuel\ surf}/\bar{\phi}_{fuel}$. Since the ABH method treats monoenergetic neutrons, it does not take into account spectral hardening. The hardened cross sections computed with THERMOS will be used in the calculations to account for this hardening. The natural uranium lattices consist of cells, in which the rod spacing is about 5 mean free paths; the ABH method is expected to give good results for these lattices. In the 1-1/4-inch lattice, the cell radius is less than a mean free path, and agreement between the ABH method and experiment may not be as good for this lattice.

CHAPTER IV

RESULTS

4.1 INTRODUCTION

This chapter has two purposes. First, the measured activity distributions will be given and compared with the theoretical distributions computed with the THERMOS code; they will also be compared with the results of the analytical calculations outlined in Chapter III. Second, the experimental and theoretical neutron density and spectral distributions will be used to calculate quantities useful in the design of heavy water-moderated reactor cores. These quantities include: disadvantage factors, thermal utilization, effective neutron temperature, and effective cross sections of nuclides present in the lattices measured at M. I. T., and of nuclides commonly used as neutron activation detectors.

4.2 NATURAL URANIUM LATTICES

The results of the measurements on the natural uranium lattices will be discussed first. Since these lattices had large physical dimensions: 1.010 inch diameter rods and spacings of 4.5 inches, 5.0 inches, and 5.75 inches, respectively, it was possible to make accurate measurements of the activity distributions. Thus, these lattices served as a testing ground for experimental methods and for the comparision of theory and experiment.

4.2.1 GOLD ACTIVITY DISTRIBUTIONS

The results of the experimental and theoretical gold activity distributions in the natural uranium lattices are shown in Figs. 4.1 to 4.7. In each lattice, two sets of measurements were made with each kind of detecting foil to insure reproducibility of the results. One of the gold experiments in the 5.0-inch spacing lattice was discarded because the foil holders in the moderator were found to have come loose

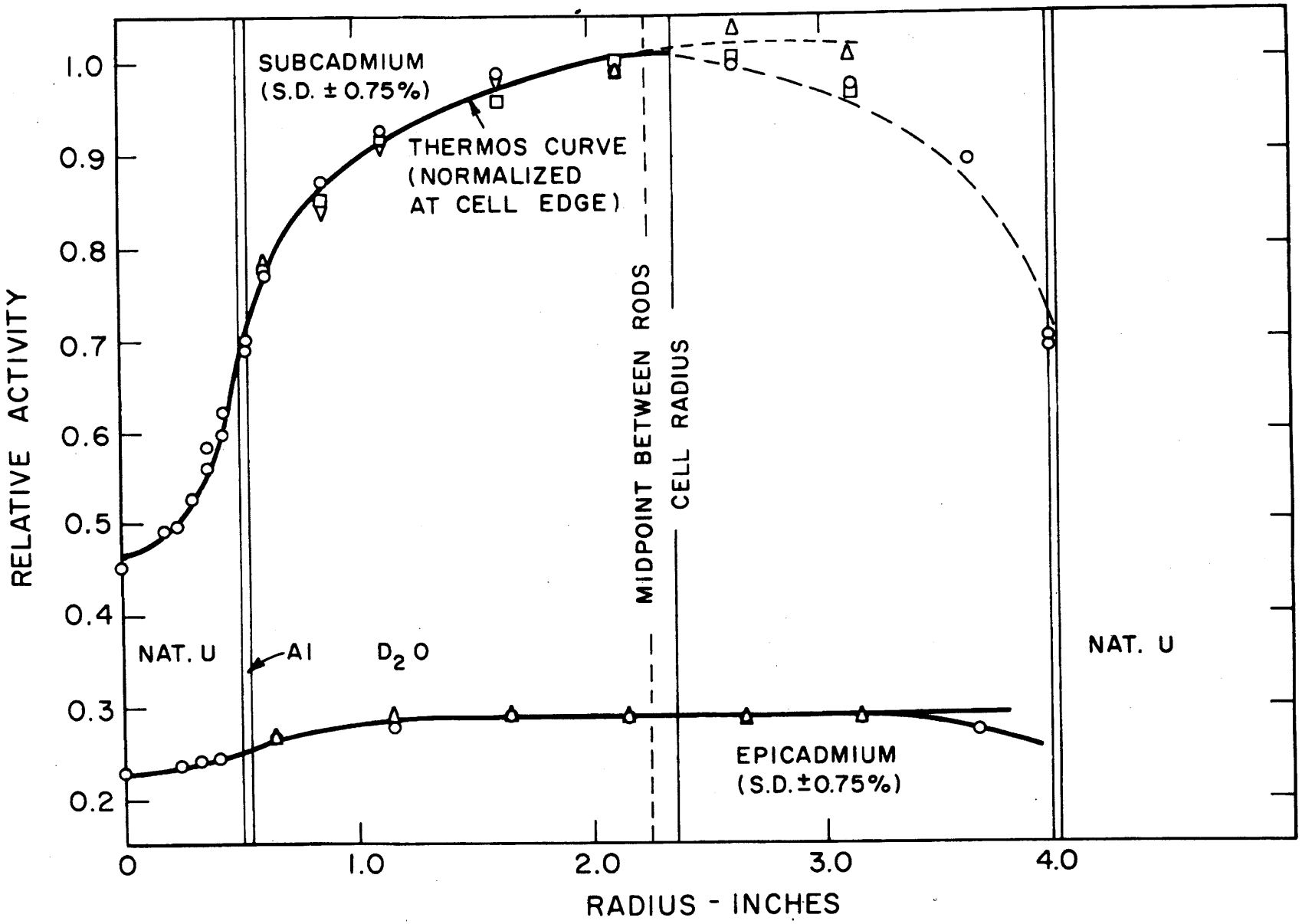

FIG. 4.1 GOLD ACTIVITY DISTRIBUTION NO. 1, 1.010-IN. DIA. NAT. U RODS ON A 4.5-IN. TRIANGULAR SPACING

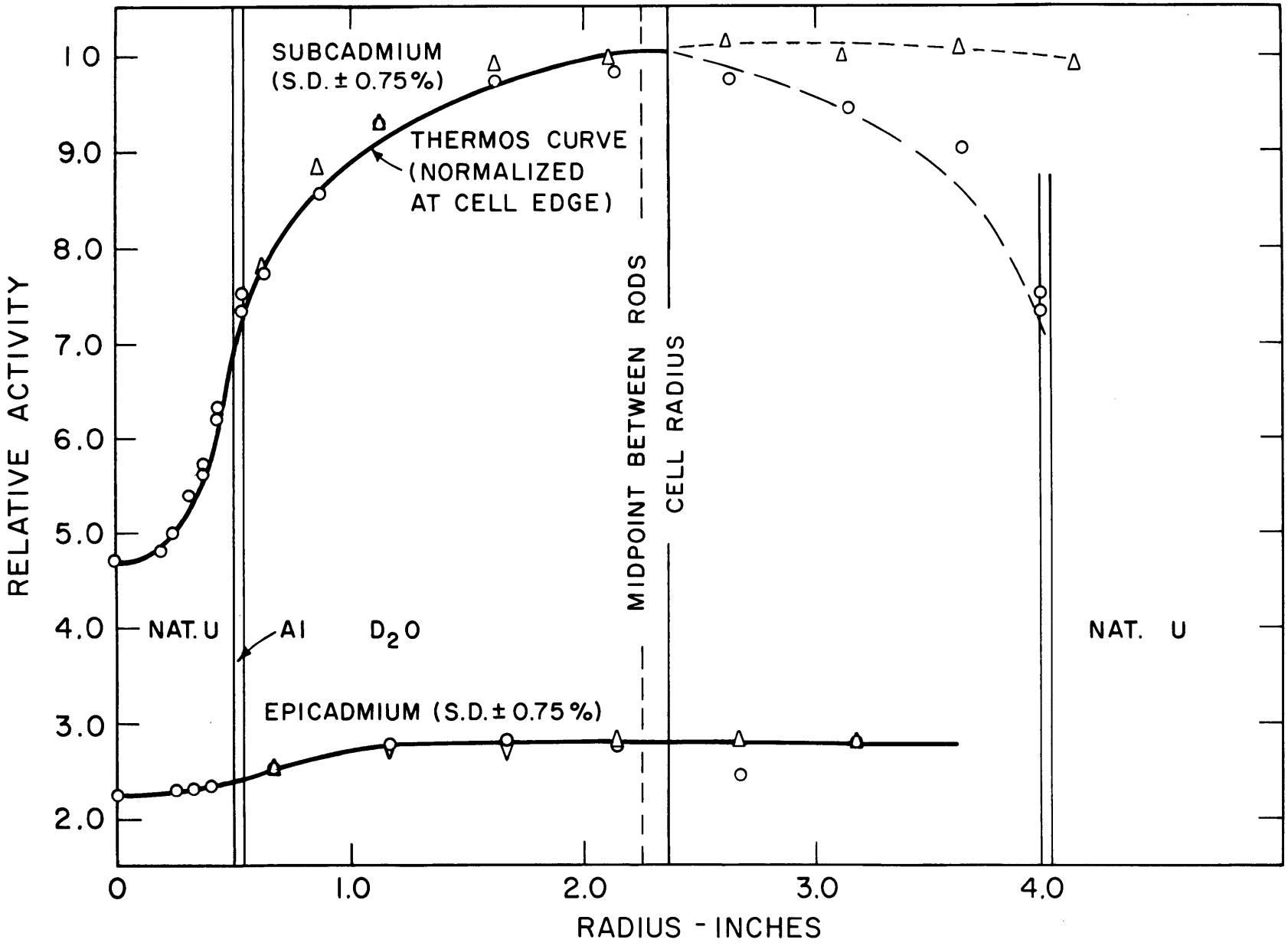

FIG. 4.2 GOLD ACTIVITY DISTRIBUTION NO. 2, 1.010-IN. DIA. NAT. U RODS ON A 4.5-IN. TRIANGULAR SPACING

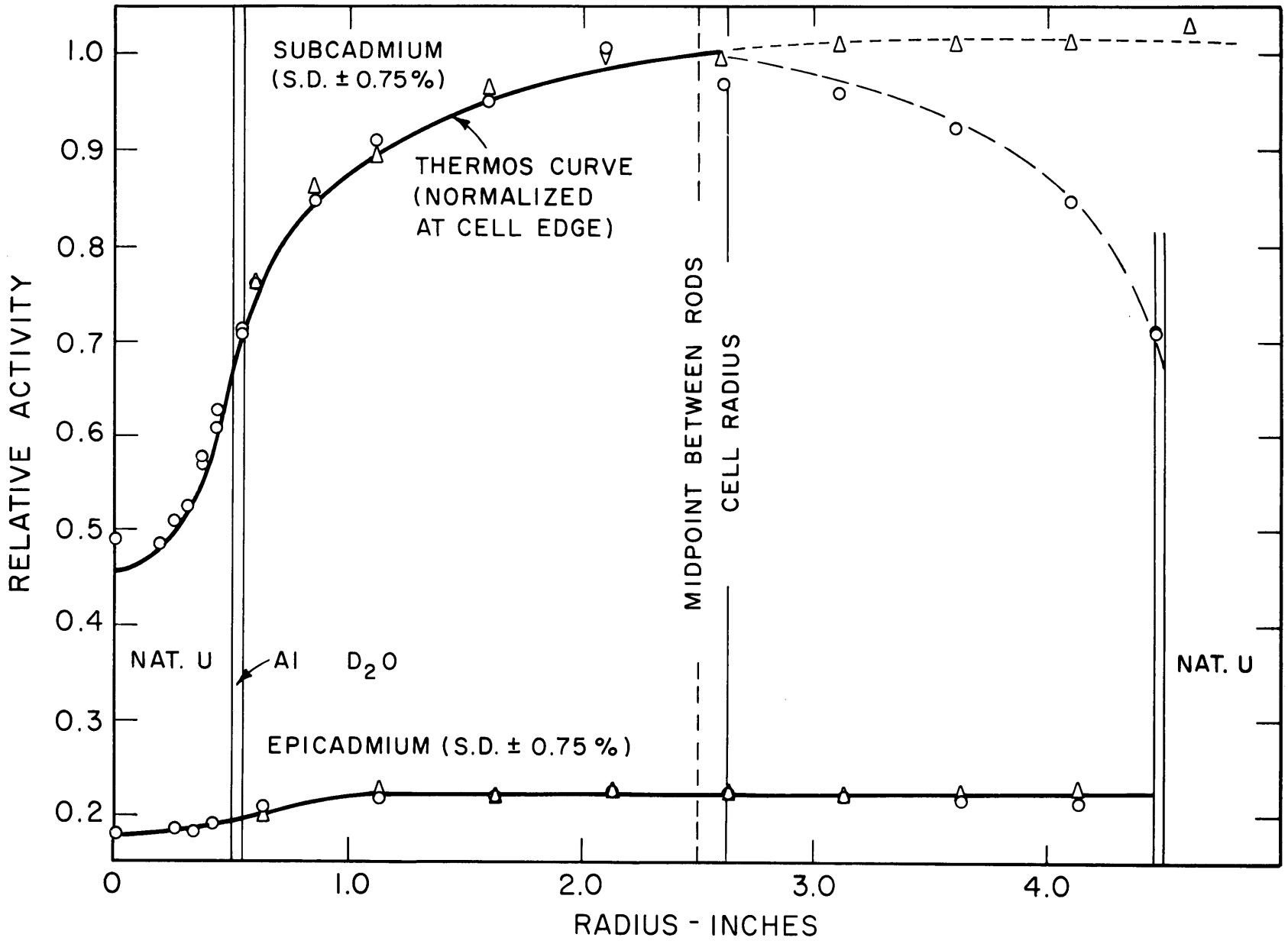

FIG. 4.3 GOLD ACTIVITY DISTRIBUTION, 1.010-IN. DIA. NAT. U RODS ON A 5.0-IN. TRIANGULAR SPACING

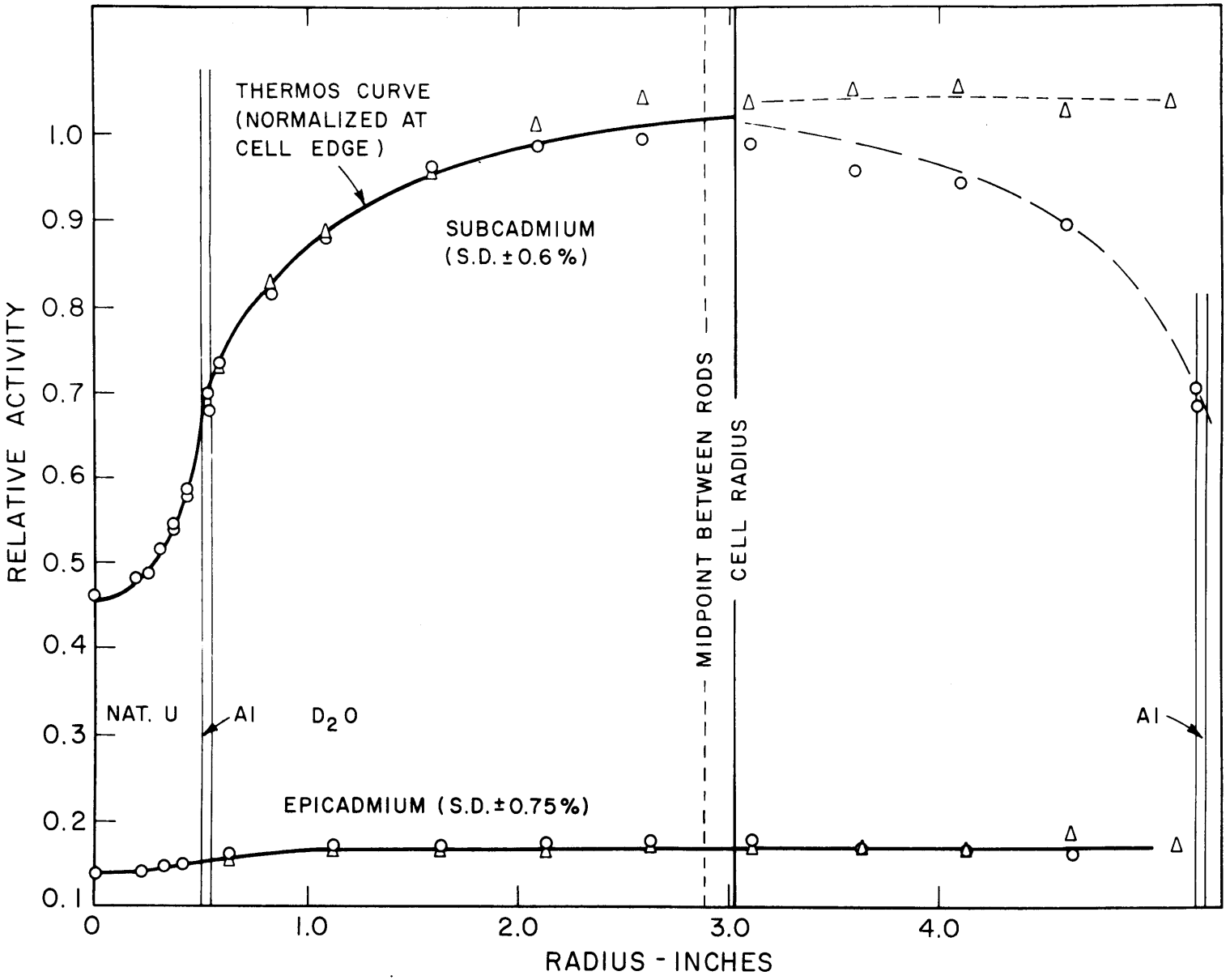

FIG. 4.4 GOLD ACTIVITY DISTRIBUTION NO.1, 1.010-IN. DIA. NAT. U RODS ON A 5.75-IN. TRIANGULAR SPACING

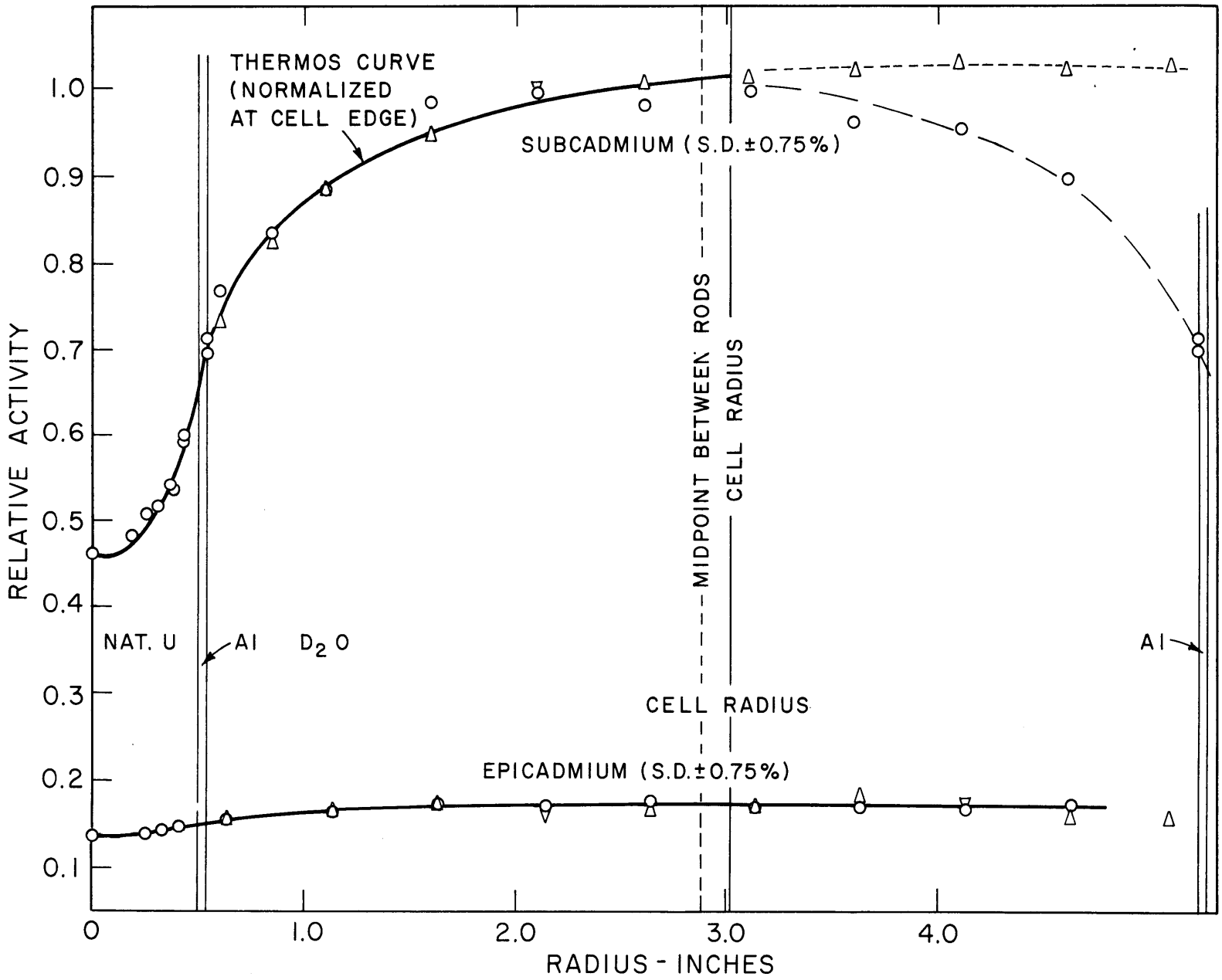

FIG.4.5 GOLD ACTIVITY DISTRIBUTION NO.2, 1.010-IN. DIA. NAT. U RODS ON A 5.75-IN. TRIANGULAR SPACING

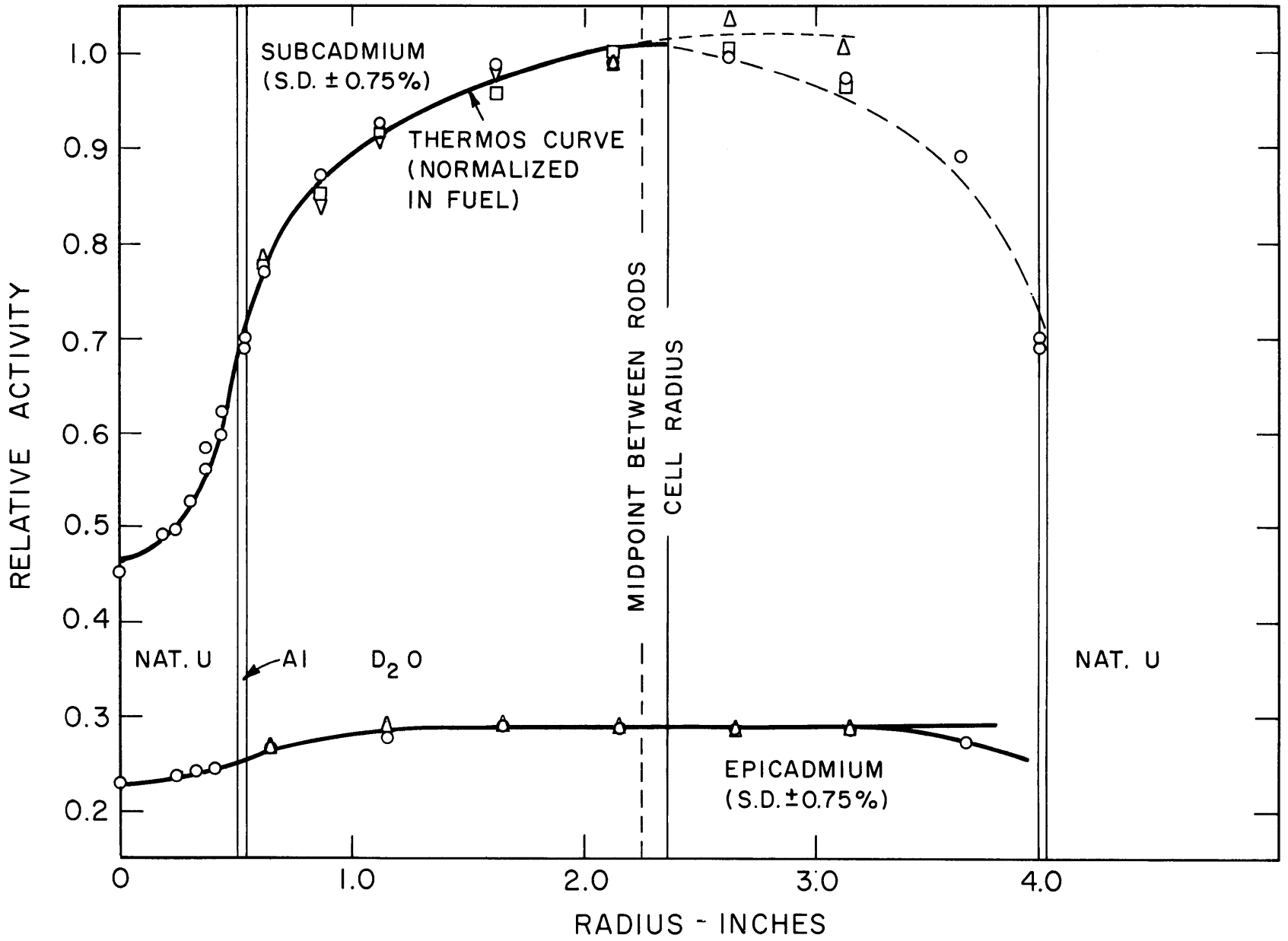

FIG. 4.6 GOLD ACTIVITY DISTRIBUTION NO. 1, 1.010-IN. DIA. NAT. U RODS ON A 4.5-IN. TRIANGULAR SPACING

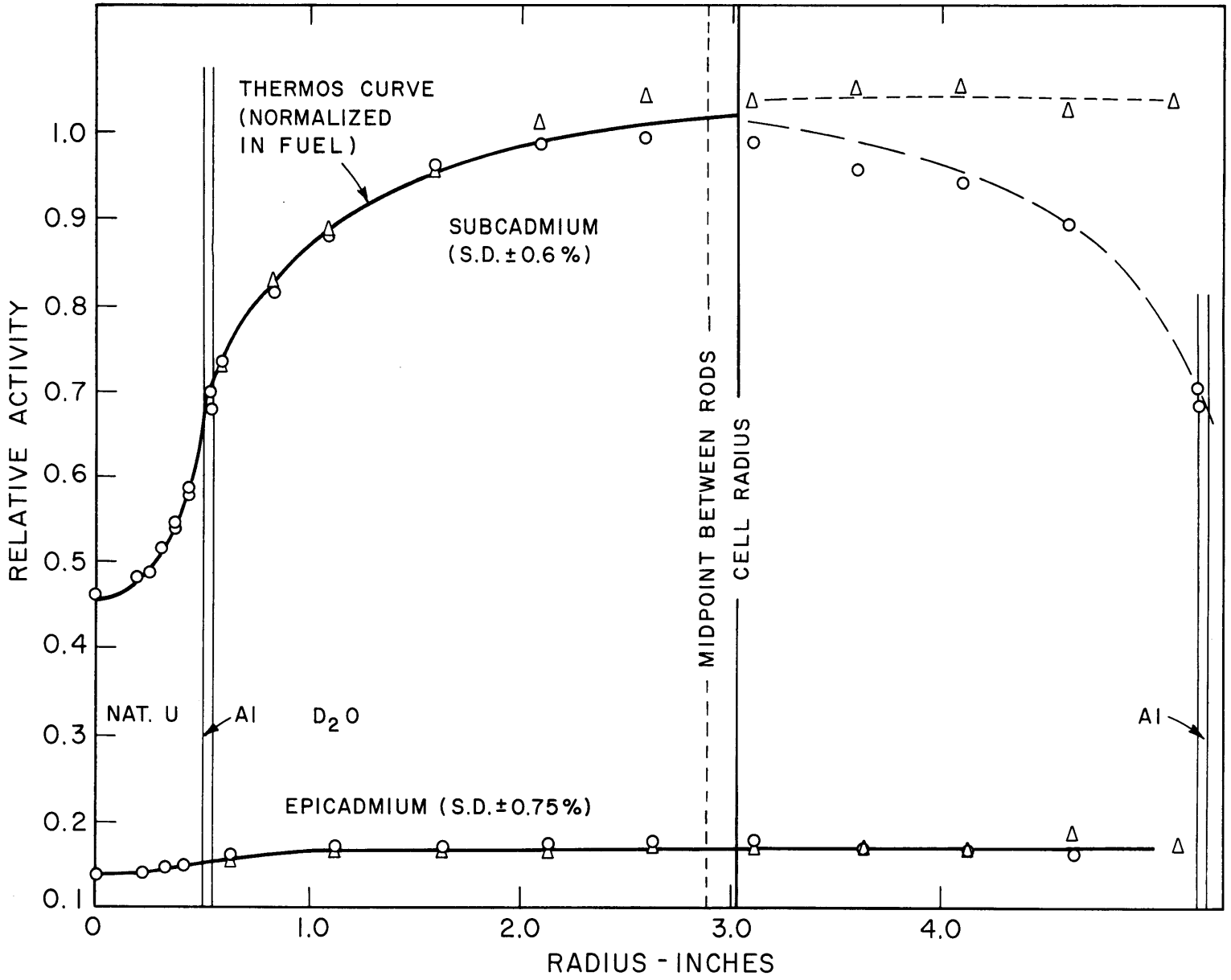

FIG. 4.7 GOLD ACTIVITY DISTRIBUTION NO.1, 1.010-IN. DIA. NAT. U RODS ON A 5.75-IN. TRIANGULAR SPACING

during the experiment. Since the other gold measurement in this lattice gave the same sort of agreement between theory and experiment as the gold measurements in the 4.5-inch and 5.75-inch lattices, the results of this single gold experiment were considered sufficient. The results for the 4.5-inch and 5.75-inch lattices demonstrate the reproducibility of the measurements within the estimated statistical uncertainties and the scatter of the data.

Two curves are shown in each of the figures: the upper curve is the subcadmium distribution; the lower, the epicadmium distribution. The explanation of the symbols used in all figures showing activity distributions is given in Table 4.1. The subcadmium distribution is to be compared with that computed with the THERMOS code. THERMOS has thirty energy mesh points (or edit points) which can be used as upper integration limits (or energy cutoffs) in the activity distributions. For gold and lutetium, the usual cadmium cutoff is at about 0.4 ev, but the exact location of this cutoff depends on the thickness of the cadmium filters. Variation of the THERMOS cutoff energy from 0.415 ev to 0.633 ev produced changes in the dip of the activity in the fuel of less than 0.05% for the lutetium, and less than 0.5% for the gold. Hence, the THERMOS cutoff energy of 0.415 ev was used as the thermal cutoff energy in the lutetium and gold activity distributions. The europium energy cutoffs were treated differently, as will be explained in section 4.2.3.

TABLE 4.1

Standard Legend for All Activity* Distributions

○	Rod-to-rod traverse.
Δ	Rod-to-moderator traverse.
——	THERMOS curve for subcadmium traverse in central cell; also, a smooth curve drawn through the epicadmium traverse.
– – –	Reflection of THERMOS curve to cell centered at the first off-center rod.
- - -	Smooth curve drawn (by eye) through the rod-to-moderator traverse.

*Any changes from the notation in this table will be indicated when they arise.

In Figs. 4.1 to 4.5, the curves computed with THERMOS are normalized to the experimental results at the cell edge. The experimental and theoretical curves agree very well in the moderator and in the fuel; the greatest percentage difference between the two curves (other than experimental scatter) seems to occur at the center of the fuel rod and is less than about one per cent. In some of the curves, the experimental activities lie slightly higher than the THERMOS curve at radii of from one to two inches, indicating that experiment may give a slightly steeper gradient near the surface of the fuel than is predicted by THERMOS. This may be due partly to experimental scatter. However, the activities in this region are almost twice those in the fuel; an activity which differs from the theoretical curve by 0.01 units of relative activity would be about two per cent off in the fuel but only about one per cent off in the moderator. Hence, even though the differences between theory and experiment may look larger in the moderator than in the fuel, the percentage differences in the moderator are still only of the order of one per cent.

In Figs. 4.6 and 4.7, the results of Figs. 4.1 and 4.4 have been normalized in the fuel (by the method outlined in section 3.3). With such a normalization, the THERMOS curves were shifted by less than 0.2% from their location with normalization at the cell edge. Thus, as far as the eye can tell, Fig. 4.1 is identical to Fig. 4.6 and Fig. 4.4 is identical to Fig. 4.7.

The epicadmium activity distributions for the gold, and also for the lutetium and europium, were flat in the moderator and dipped very slightly in the fuel, as can be seen from the figures. This result verifies the assumption usually made that the slowing-down density is flat in the moderator.

The THERMOS calculations for Figs. 4.1 to 4.7 were made with Honeck's kernel (H9) for D_2O. Similar calculations (S2) with a Brown-St. John kernel showed an increase of less than 0.2% in the flux dip in the fuel over that obtained with Honeck's kernel. Others (H10) have also found that the computed activity distributions for various assemblies are not sensitive to refinements in the neutron scattering models used in the thermalization calculations.

As mentioned in section 3.2, one of the major theoretical approximations in THERMOS is the assumption of isotropic scattering. To correct for anisotropic scattering effects, the scattering cross section for D in D_2O in all cases has been multiplied by $(1-\bar{\mu}_o)$, where $\bar{\mu}_o$ is given by 2/3A with A, the Brown-St. John effective mass for D in D_2O, taken to be 3.595. THERMOS calculations (S2) on the three natural uranium lattices show that the flux dip in the fuel is about 2% higher if no $\bar{\mu}_o$ correction is applied to the scattering cross section than if such a correction is made. Thus, if the $\bar{\mu}_o$ correction is not made, the agreement between theory and experiment is slightly less satisfactory. It seems justifiable, therefore, to make the $\bar{\mu}_o$ correction in all the calculations. Similar results were obtained for the effects on the lutetium and europium distributions of varying the scattering kernel and of applying the $\bar{\mu}_o$ correction. More will be said about these effects later in this chapter, during the discussion of the lutetium and europium results, in particular with regard to the effects of these corrections on the spectral distributions.

In view of the excellent agreement between THERMOS and experiment for the gold distributions in the natural uranium lattices, it is evident that THERMOS makes possible an accurate calculation of the intracell thermal neutron density distribution in these particular lattices. The prediction by THERMOS of the intracell spectral distributions will be discussed in the next sections of this chapter.

4.2.2 LUTETIUM ACTIVITY DISTRIBUTIONS

The results for the lutetium activity distributions measured in the natural uranium lattices are shown in Figs. 4.8 to 4.16. In Figs. 4.8 to 4.14, the THERMOS results are normalized to experiment at the cell edge. In Figs. 4.15 and 4.16, the data of Figs. 4.8 and 4.14 are normalized in the fuel rod. The reproducibility of the experimental results is within the estimated statistical uncertainty and the scatter of the data.

The agreement between THERMOS and experiment is not quite as good as that for gold. With normalization at the cell edge, the "best" curve through the lutetium data points in the fuel is, on the average, higher than the THERMOS curve at the cell center by 4.9% for the 4.5-inch lattice, 2.2% for the 5.0-inch lattice, and 2.4% for the 5.75-inch

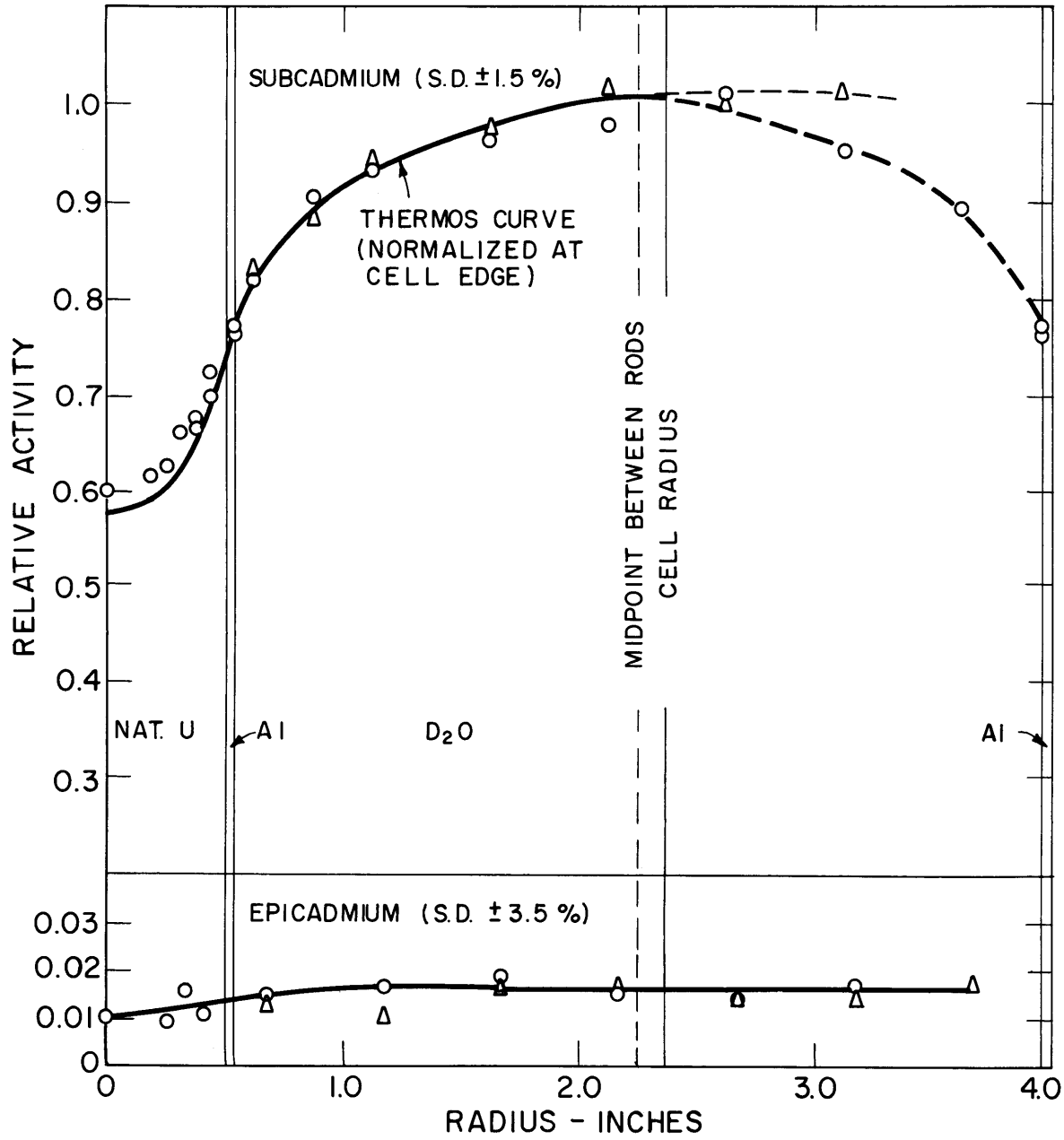

FIG. 4.8 LUTETIUM ACTIVITY DISTRIBUTION NO. 1, 1.010 - IN. DIA. NAT. U RODS ON A 4.5 - IN. TRIANGULAR SPACING

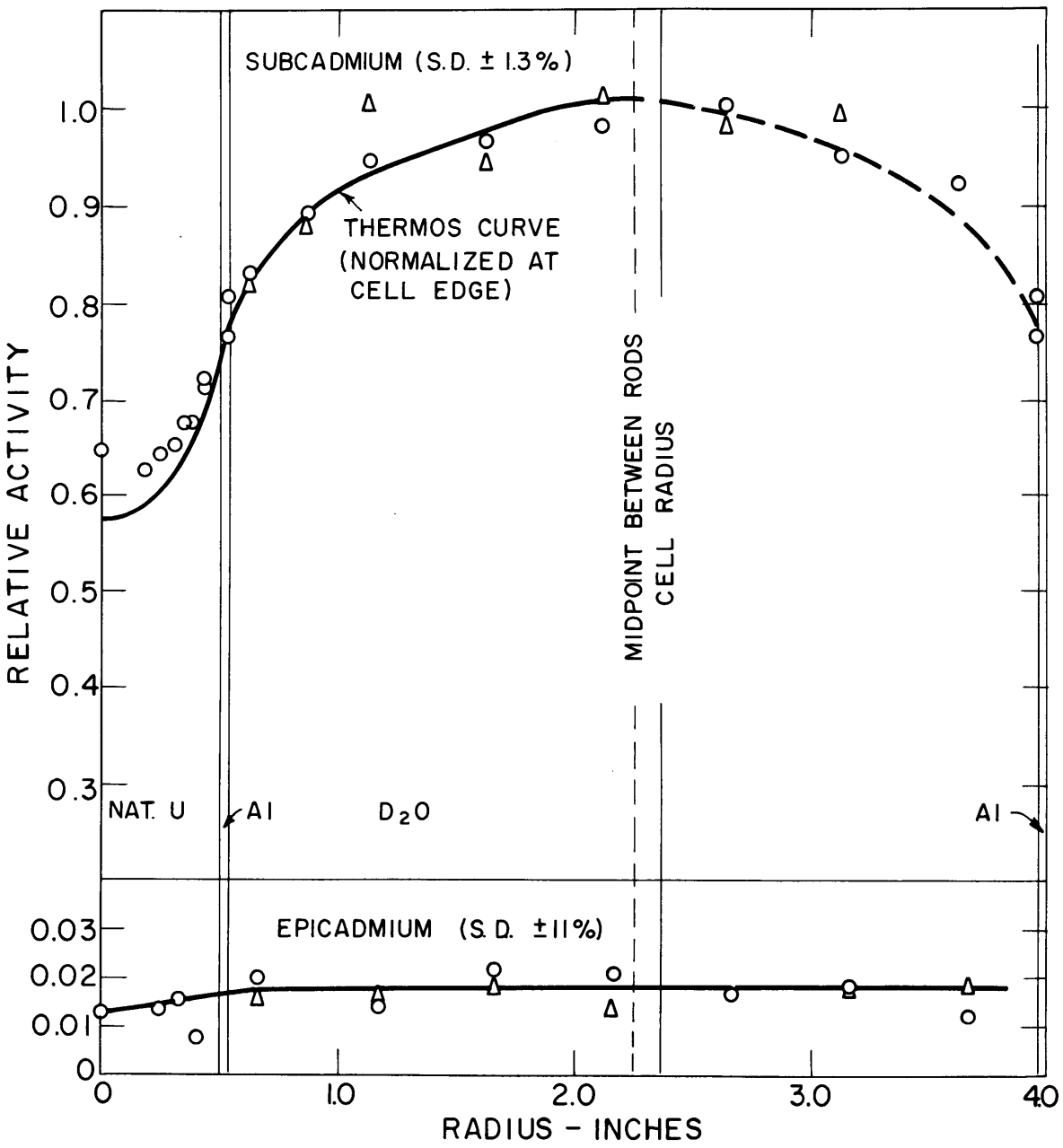

FIG. 4.9 LUTETIUM ACTIVITY DISTRIBUTION NO. 2, 1.010 - IN. DIA. NAT. U RODS ON A 4.5 - IN. TRIANGULAR SPACING

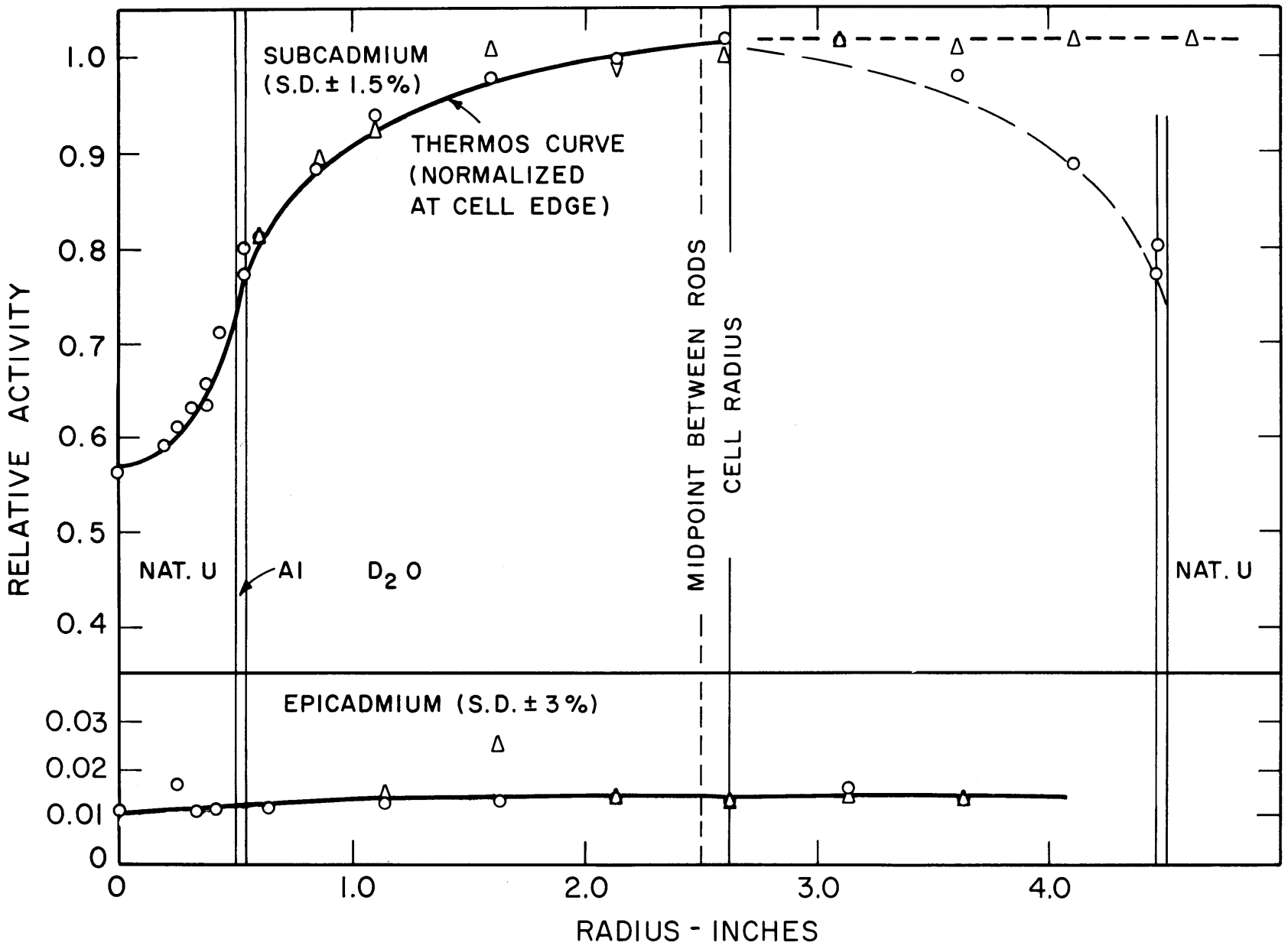

FIG. 4.10 LUTETIUM ACTIVITY DISTRIBUTION NO. 1, 1.010-IN. DIA. NAT. U RODS ON A 5.0-IN. TRIANGULAR SPACING

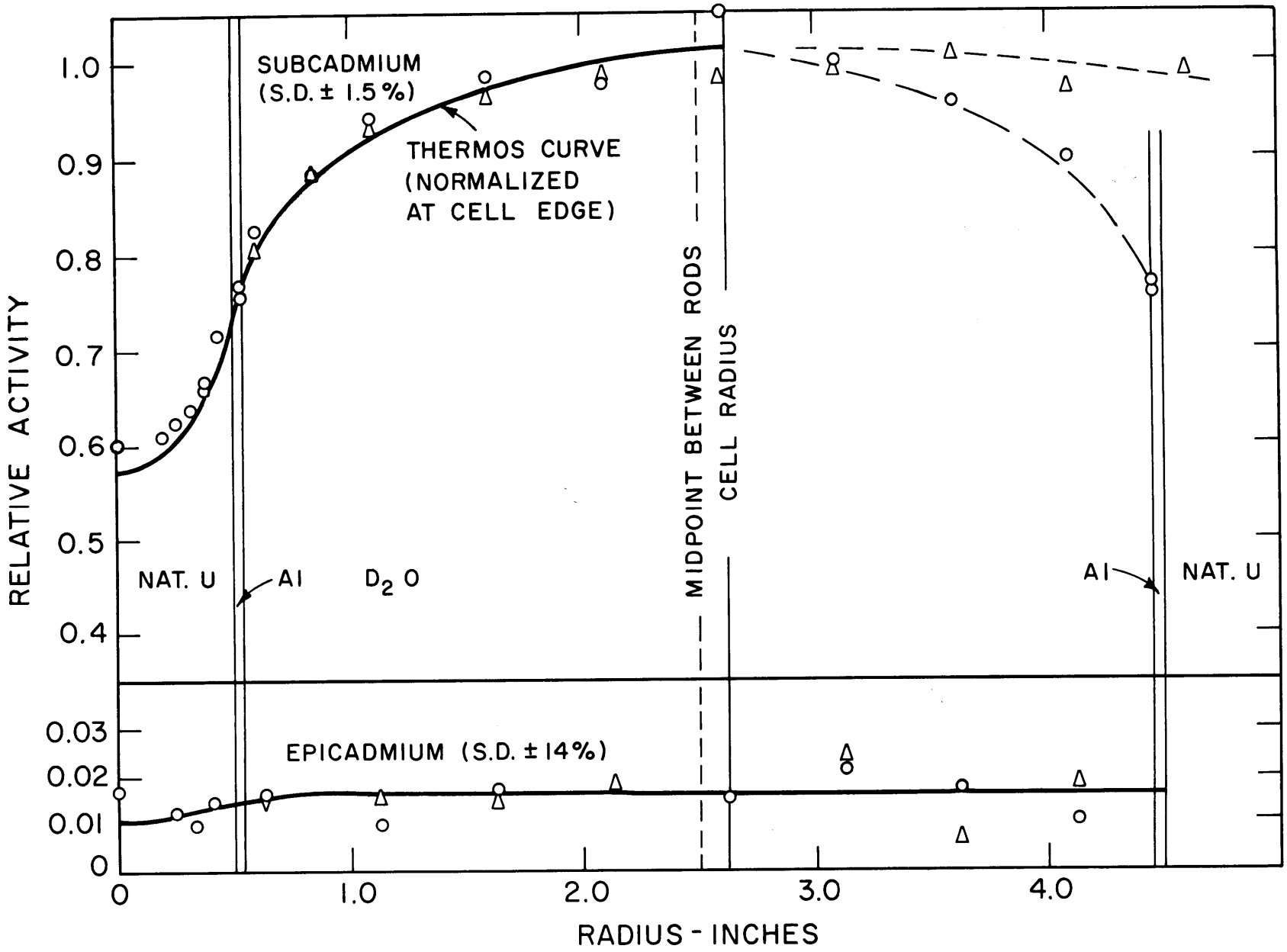

FIG. 4.11 LUTETIUM ACTIVITY DISTRIBUTION NO. 2, 1.010-IN. DIA. NAT. U RODS ON A 5.0-IN. TRIANGULAR SPACING

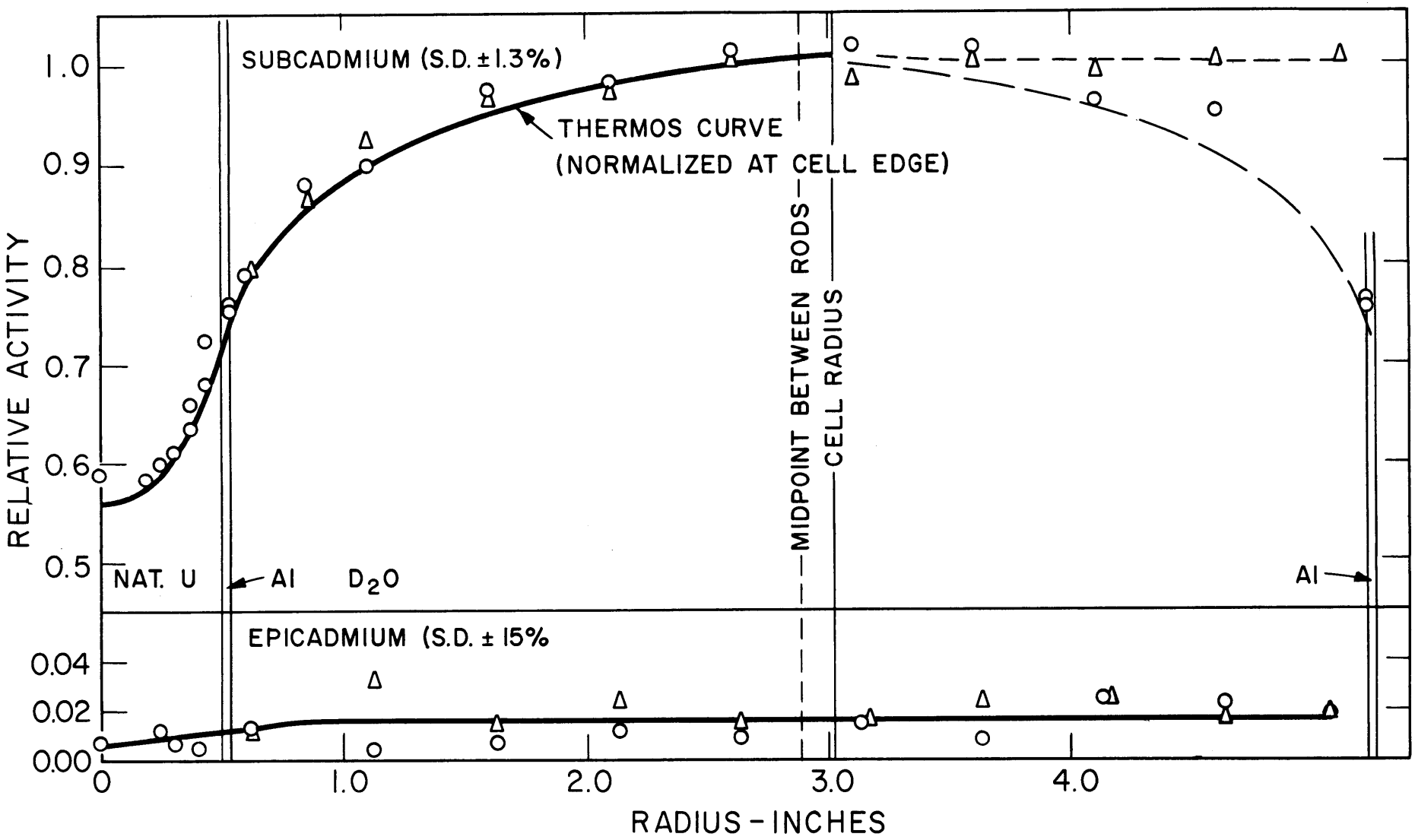

FIG. 4.12 LUTETIUM ACTIVITY DISTRIBUTION NO. 1, 1.010-IN. DIA. NAT. U RODS ON A 5.75-IN. TRIANGULAR SPACING

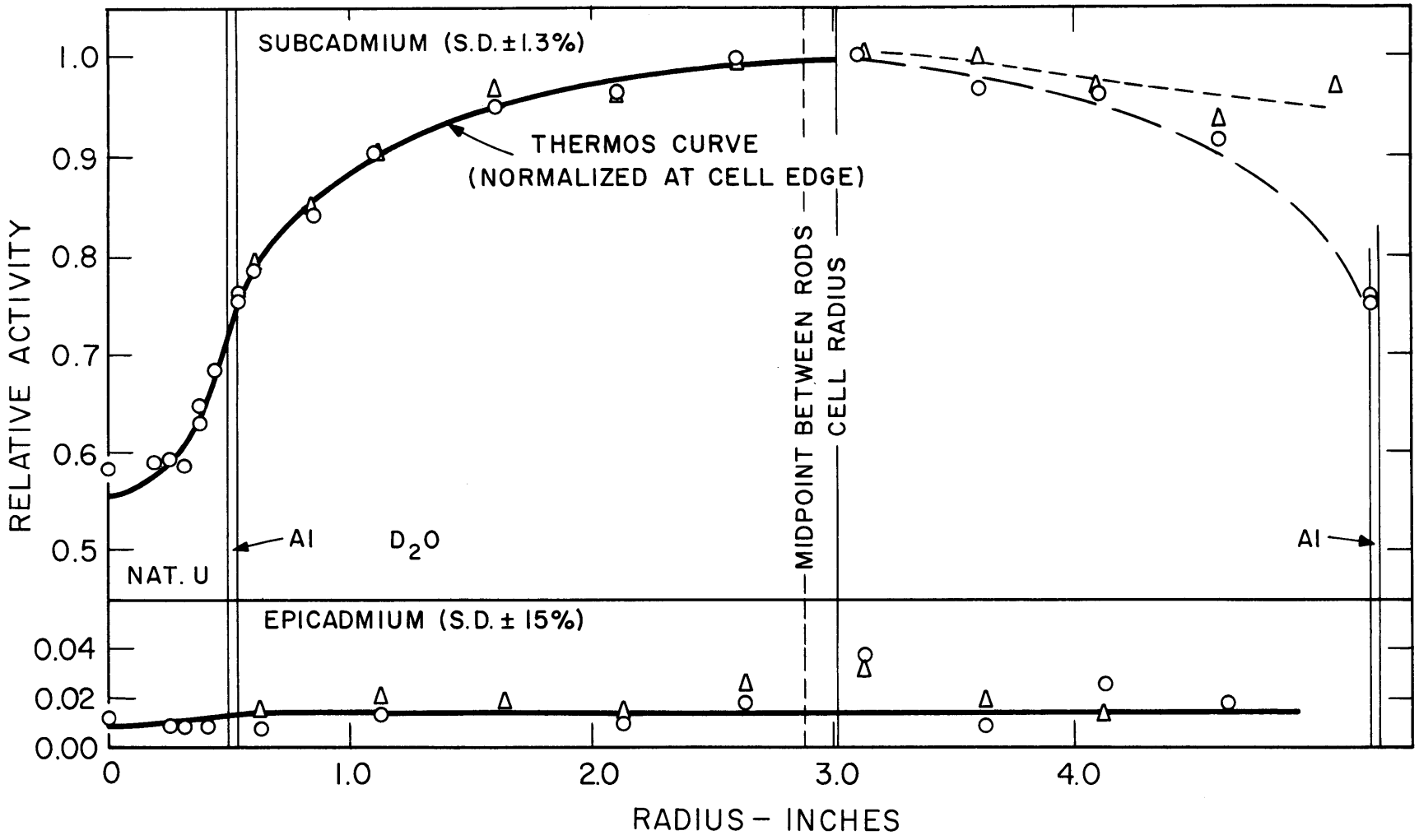

FIG. 4.13 LUTETIUM ACTIVITY DISTRIBUTION NO 2, 1.010-IN. DIA. NAT. U RODS ON A 5.75-IN. TRIANGULAR SPACING

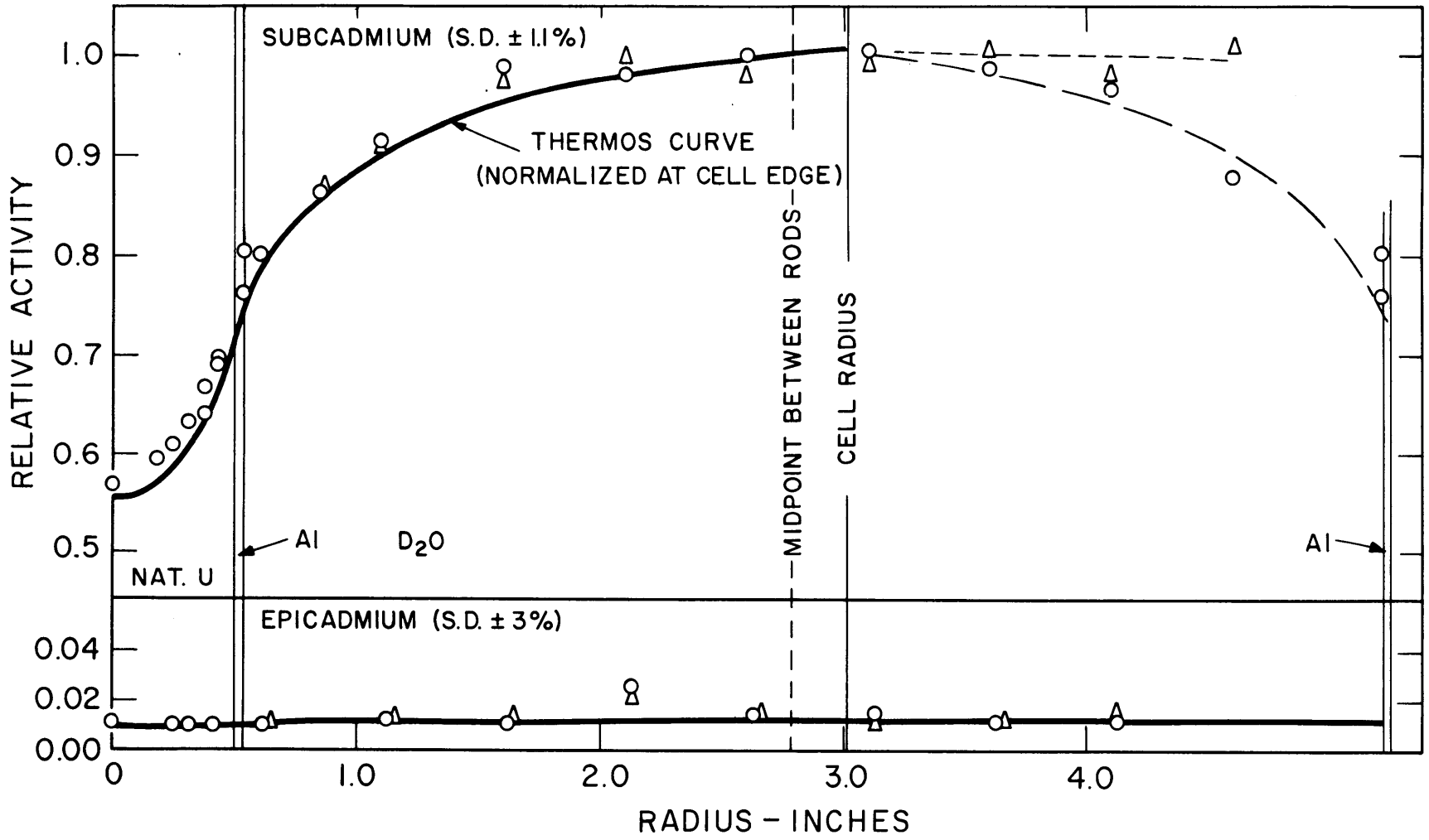

FIG. 4.14 LUTETIUM ACTIVITY DISTRIBUTION NO. 3, 1.010-IN. DIA. NAT. U RODS ON A 5.75-IN. TRIANGULAR SPACING

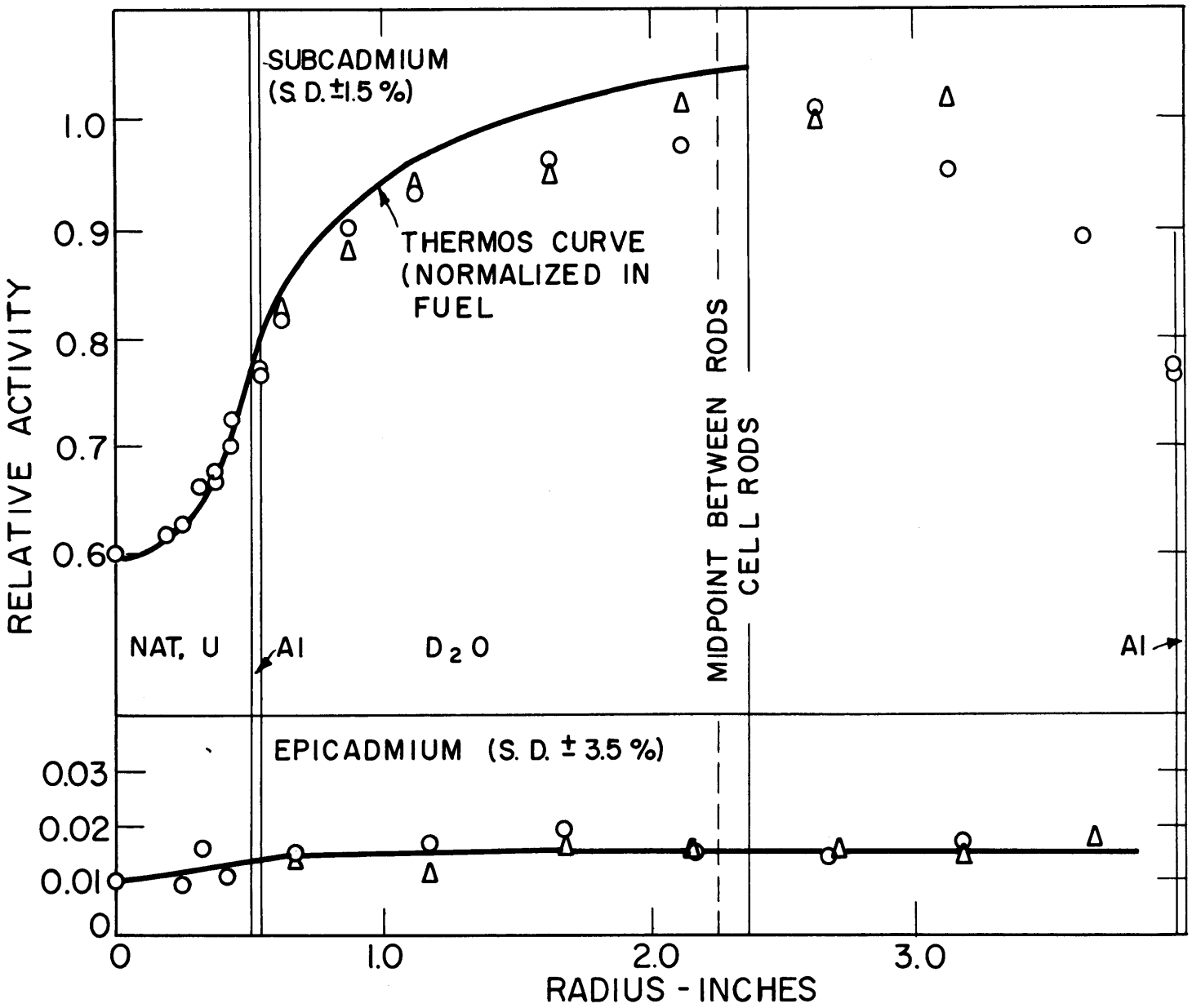

FIG. 4.15 LUTETIUM ACTIVITY DISTRIBUTION NO.1, 1.010 IN. DIA. NAT. U RODS ON A 4.5-IN. TRIANGULAR SPACING

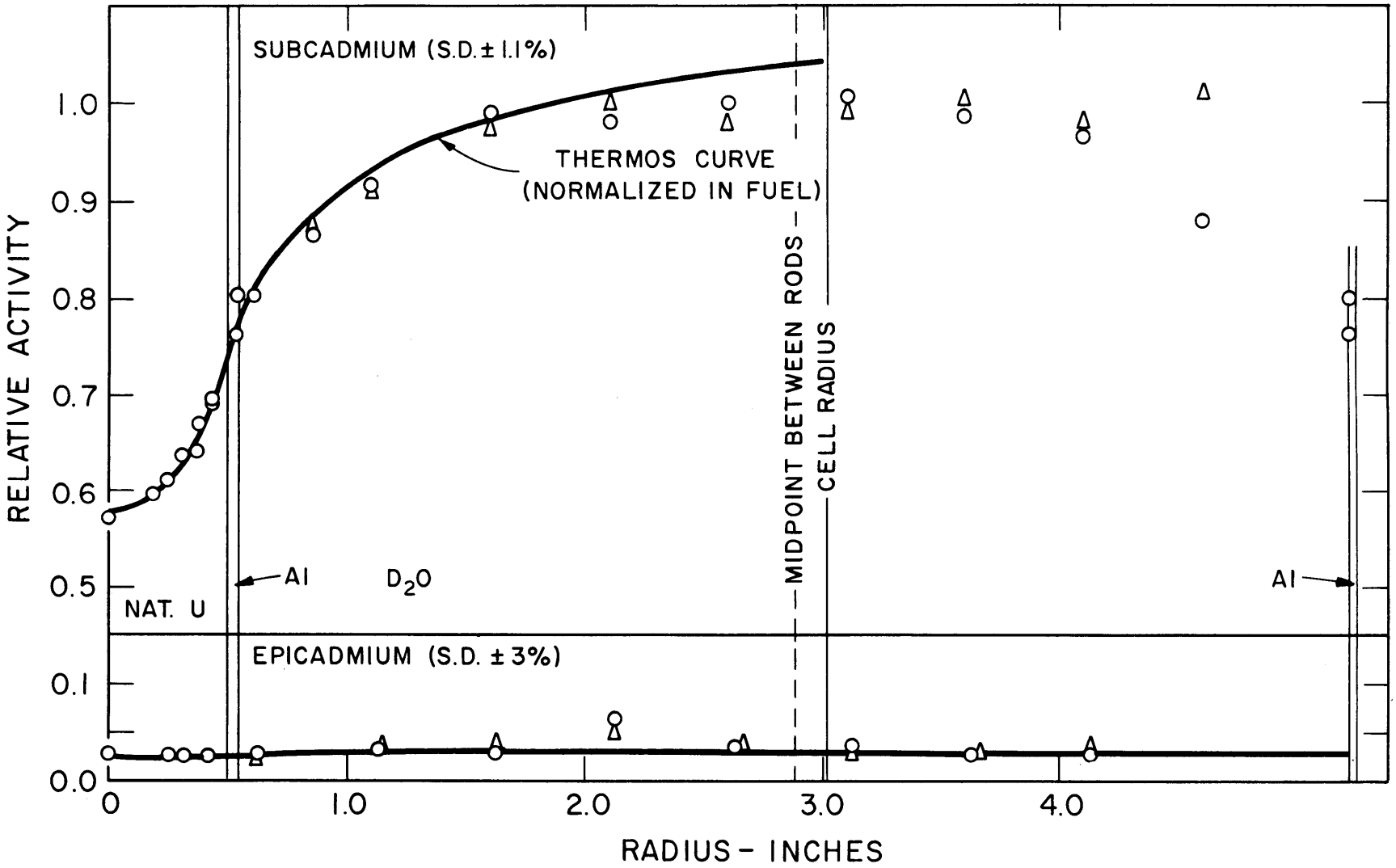

FIG. 4.16 LUTETIUM ACTIVITY DISTRIBUTION NO. 3, 1.010-IN. DIA. NAT. U RODS ON A 5.75-IN. TRIANGULAR SPACING

lattice. By "best" curve in the fuel is meant a curve which has the same shape as the THERMOS curve and which gives the best visual fit to the fuel rod data, together with its experimental scatter. The discrepancy between theory and experiment is greater in the tightest lattice than in the two lattices with the wider spacings. This discrepancy may be due to a fault in the physical basis of THERMOS, or it may be caused by uncertainties in the lutetium cross sections. In the latter case, it could come about in the following way. The tighter the lattice spacing, the greater is the fraction of neutrons in the 1/E tail. The activity response of lutetium depends strongly on the resonance at 0.142 ev, which is located in an energy region where a large 1/E tail markedly increases the neutron density. Because of such an increase, any errors in the theoretical curves due to uncertainties in the lutetium resonance cross section might be magnified. This effect might explain the increase in difference between theory and experiment, in going from the 5.75-inch to the 4.5-inch lattice. The lutetium distributions were first computed with cross sections taken from the latest edition of BNL-325 (H13); they were then repeated with more recent cross section data (R2). In the later calculations, the differences, at the rod center, between THERMOS and experiment were decreased by about 2%. Further improvements in the values of the lutetium cross section may affect the theoretical results still more.

With normalization in the fuel, as shown in Figs. 4.15 and 4.16, it is evident that the shape of the lutetium activity distribution in the fuel is given well by THERMOS. But, the THERMOS curve lies higher than the experimental distribution in the moderator. (In this case and in all others, the normalization is such that the percentage differences between theory and experiment at the cell edge are about the same as the percentage differences at the cell center when normalization is at the cell edge.) Most of the spectral hardening is due to absorption of thermal neutrons as they penetrate into the fuel rod. The agreement between THERMOS and experiment for the lutetium activity distribution in the fuel indicates that THERMOS gives a good estimate of this hardening effect.

Although the agreement between THERMOS and the experimental lutetium data is not quite as good as that for gold, the quantity most indicative of the amount of spectral hardening, the change in the ratio

of lutetium to gold activation from cell edge to rod center, does give reasonably good agreement between theory and experiment. Table 4.2 shows the experimental results for the ratio of thermal lutetium activity to thermal gold activity at the cell center. This ratio is normalized to unity at the cell edge.

TABLE 4.2

Values of the Ratio of Lutetium to Gold Activity at the Cell Center

Lattice Spacing (inches)	4.5	5.0	5.75
THERMOS	1.239	1.241	1.244
Experiment	1.294 ± 0.020	1.256 ± 0.021	1.264 ± 0.019

In Fig. 4.17, typical results for lutetium and gold in the 4.5-inch lattice are plotted together in the same graph, both normalized to THERMOS at the cell edge. This figure shows that the measured activity distribution of lutetium has a considerably smaller dip in the fuel than that of the gold. The difference between the dips in the distributions computed with THERMOS is not as great, indicating that the amount of spectral hardening is possibly greater than that computed with THERMOS.

The effect of the scattering kernel on the theoretical distribution of the lutetium activation has been examined by comparing the distribution based on the Honeck and Brown-St. John kernels. As was found with gold, the effect of the change in kernel was negligible: the activity dips in the rod computed with the Honeck kernel were smaller than those computed with the Brown-St. John kernel by only 0.25%. The use of a $\bar{\mu}_o$ correction for anisotropic scattering gave results similar to those for gold. Calculations (S2) have also shown that, at each radial point, the computed spectral distribution (the neutron density as a function of velocity) is insensitive to the change in kernel and to the use or non-use of a $\bar{\mu}_o$ correction.

At present, the discrepancy between theory and experiment in the case of lutetium cannot be explained. The excellent agreement obtained for gold makes it appear likely that the absorption cross section of lutetium is at fault, as has been discussed above. Moreover, it should be pointed out that the observed disagreement is small, as compared with the results usually obtained in such experiments.

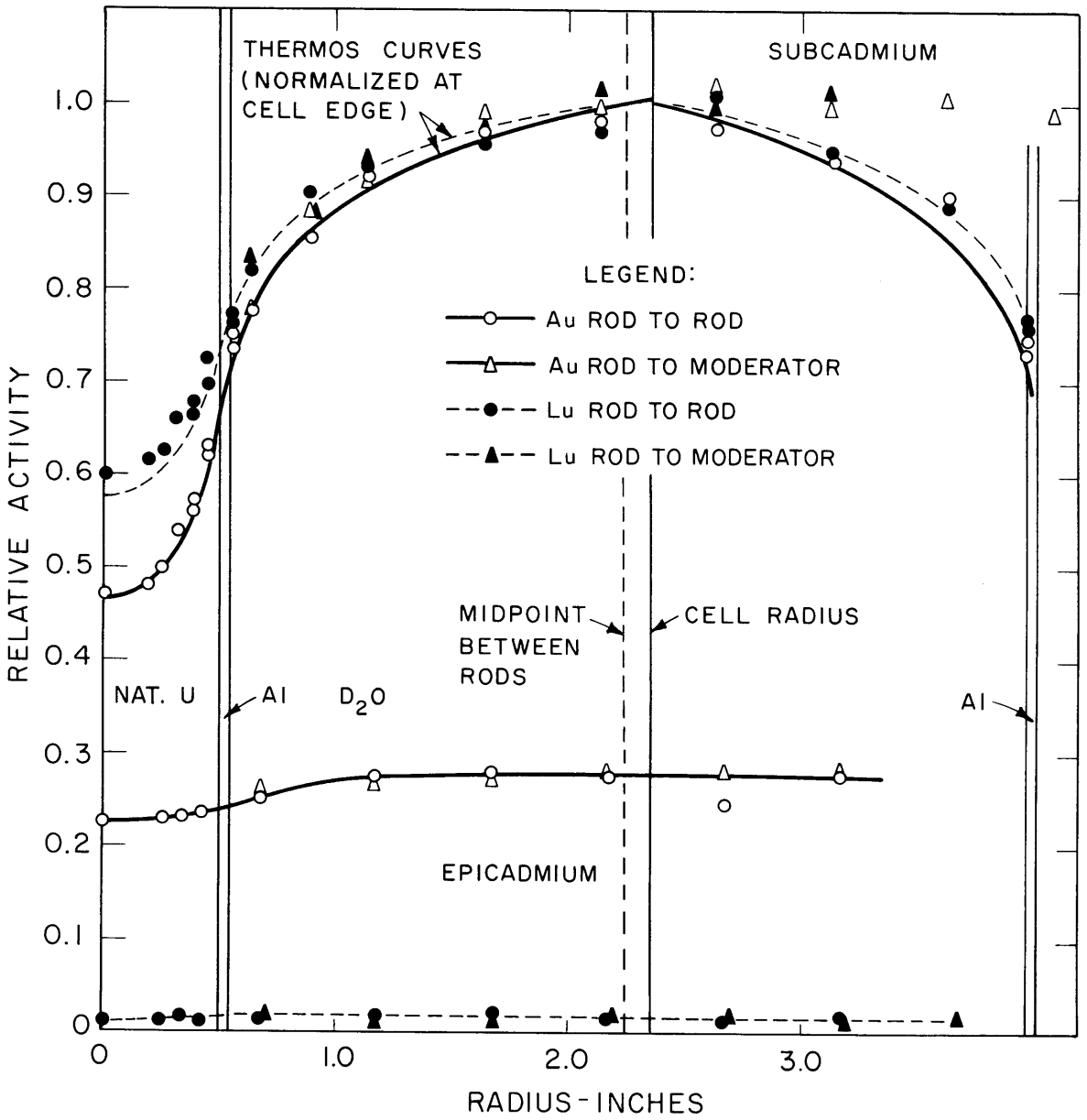

FIG. 4.17 COMPARISON OF GOLD AND LUTETIUM ACTIVITY DISTRIBUTIONS, 1.010-IN. DIA. NAT. U RODS ON A 4.5-IN. TRIANGULAR SPACING

4.2.3 EUROPIUM ACTIVITY DISTRIBUTIONS

The activity distributions for europium involved additional problems because of the presence of the europium resonance at 0.46 ev, which is practically at the cadmium cutoff (usually taken to be between 0.4 to 0.5 ev). When the activity of the cadmium-covered europium foils is subtracted from the total europium activity, there is some question as to where the thermal cutoff should be taken, because of the partial absorption by cadmium of neutrons with energies in the range of the europium resonance. If the 0.023-inch thick cadmium covers could be made "infinitely thin" so that they would not absorb these resonance neutrons, but would still cut out all thermal neutrons below the 0.46 ev resonance, the problem would disappear. The procedure described below essentially carries out this idealized situation in a practical manner.

The method used in these experiments was to measure the activity of cadmium-covered europium foils as a function of the thickness of the cadmium filter. It is assumed here that the cadmium covers were thick enough to cut out all neutrons below the europium resonance. The thinnest cadmium cover used was ten mils thick; at smaller thicknesses, the neutrons below the europium resonance would have leaked through the cadmium in large numbers. The results of this measurement are shown in Fig. 4.18. The activity was found to decrease rapidly with increasing cadmium thickness, approaching a constant value for large cadmium thickness. (One of the activities in Fig. 4.18 is especially low for some unknown reason and was assumed to be in error.) Since the cadmium cross section becomes relatively small (< 10 barns) at energies above 0.46 ev, it was assumed that the constant activity was due to absorption in the europium resonances at energies higher than 0.46 ev. This constant activity was then subtracted from all of the activity values in Fig. 4.18, and the resulting activities were again plotted against cadmium thickness, in Fig. 4.19. The europium activity values now represent only the absorptions at the 0.46 ev resonance. The attenuation of the isotropic neutron flux by the cadmium covers can be described by an exponential integral of the second kind, $E_2(\Sigma_{Cd}x)$, (see Appendix H), where Σ_{Cd} is the macroscopic cadmium cross section, and x is the cadmium thickness. Such a function was fitted to the

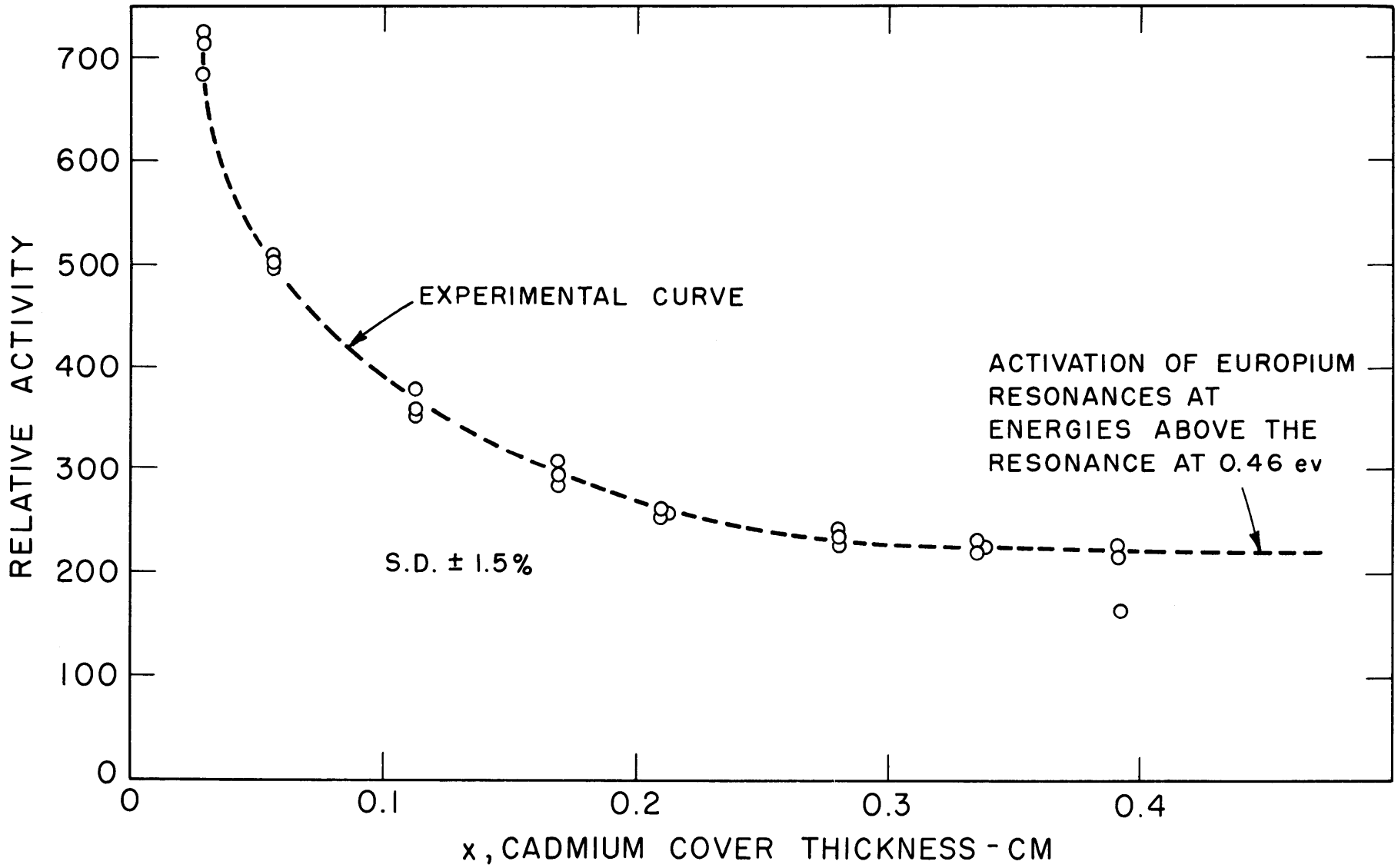

FIG. 4.18 ACTIVITY OF CADMIUM COVERED EUROPIUM FOILS AS A FUNCTION OF THE THICKNESS OF THE CADMIUM

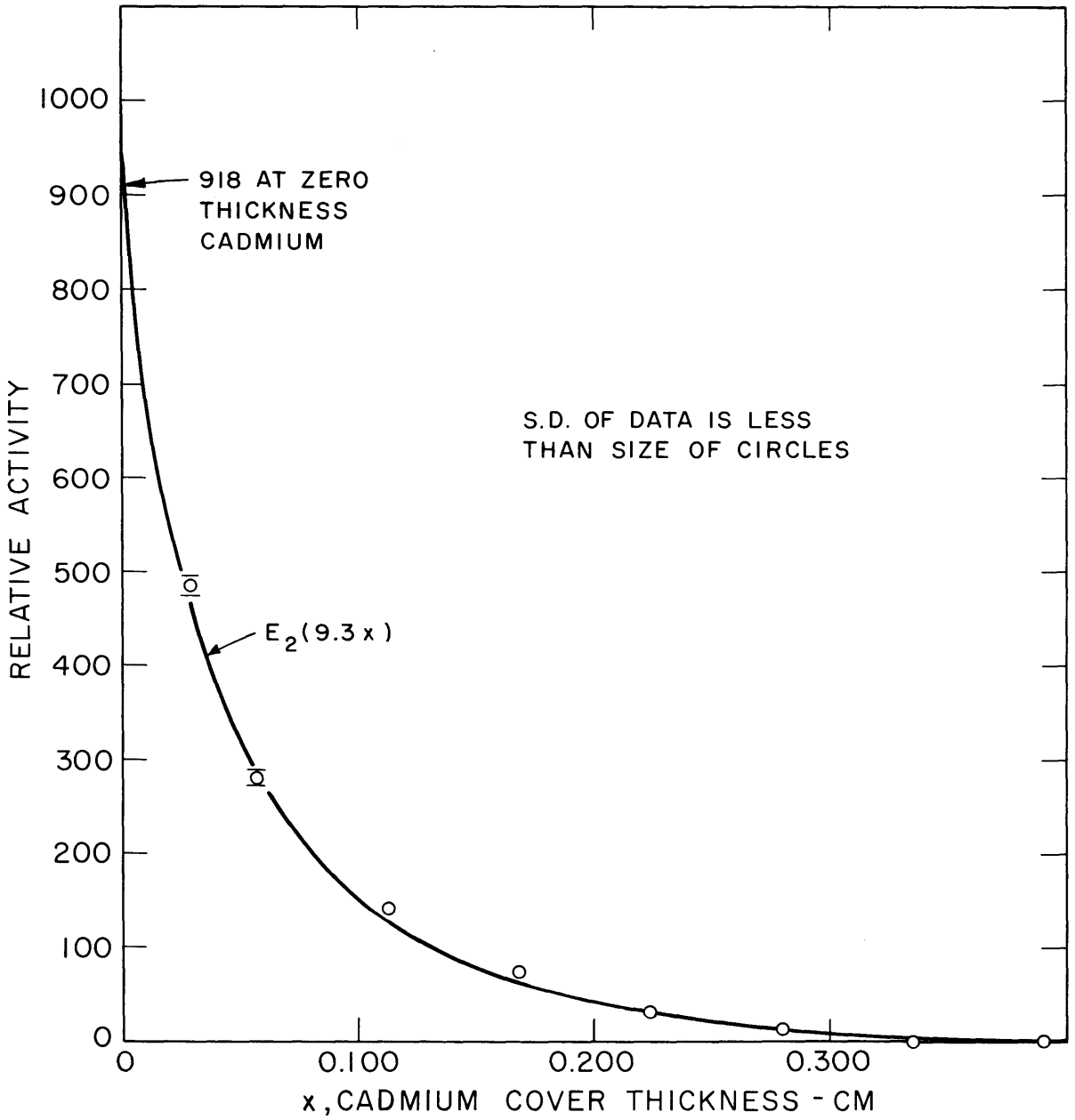

FIG. 4.19 EUROPIUM ACTIVITY AT 0.46 ev AS A FUNCTION OF THICKNESS OF CADMIUM COVERS

corrected activities as shown in Fig. 4.19. The value of Σ_{Cd} which gave the best fit, 9.3 cm^{-1}, is close to the actual value of Σ_{Cd} (H13) at 0.46 ev, 8.9 cm^{-1}. By using the fitted function $E_2(\Sigma_{Cd}x)$, it was possible to extrapolate the activity of cadmium-covered europium foils to zero thickness of cadmium.

The use of the constant activity and the extrapolated activity made it possible to correct the europium plots to values of the cutoff energy both below and above the 0.46 ev resonance. The upper cutoff was taken at 0.785 ev, which is the upper limit of the neutron energy in the THERMOS code and also corresponds roughly to the upper limit of the europium resonance (see Fig. 2.4). To get the activity at the upper energy cutoff, the activities for the europium foils covered with 0.023 inches of cadmium were multiplied by the ratio of the constant activity (from Fig. 4.18) to the activity (in Fig. 4.18) at 0.023 inches (0.058 cm) of cadmium. The value found for this ratio is 0.439. The product of 0.439 and the cadmium-covered activity in the flux plots was then subtracted from the bare europium activity to get the total thermal activity up to a cutoff energy of 0.785 ev. The results for the three natural uranium lattices are shown, normalized to THERMOS at the cell edge, in Figs. 4.20 to 4.25. The results of Fig. 4.21 were replotted in Fig. 4.26, where normalization is at the center of the cell. In Figs. 4.20 to 4.25, the experimental activity at the rod center is, on the average, 3.9% higher than THERMOS. There does not seem to be any trend in this deviation from THERMOS as the lattice spacing varies. Figure 4.26, where normalization is in the fuel rod, shows that the agreement between THERMOS and experiment is very good in the fuel rod; but the THERMOS curve is slightly higher than the measured distribution in the moderator.

The lower cutoff was taken as 0.194 ev, for reasons which will become clear in the following discussion. The europium activity at 0.46 ev and zero thickness of cadmium is obtained from Fig. 4.19. Addition to this activity of the extrapolated constant activity (due to all higher europium resonances) shown in Fig. 4.18 gives the total europium activity for energies greater than about 0.2 ev, the energy at which the 0.46 ev europium resonance begins to take shape (see Fig. 2.4). The ratio of the europium activity above 0.2 ev to the activity for a foil

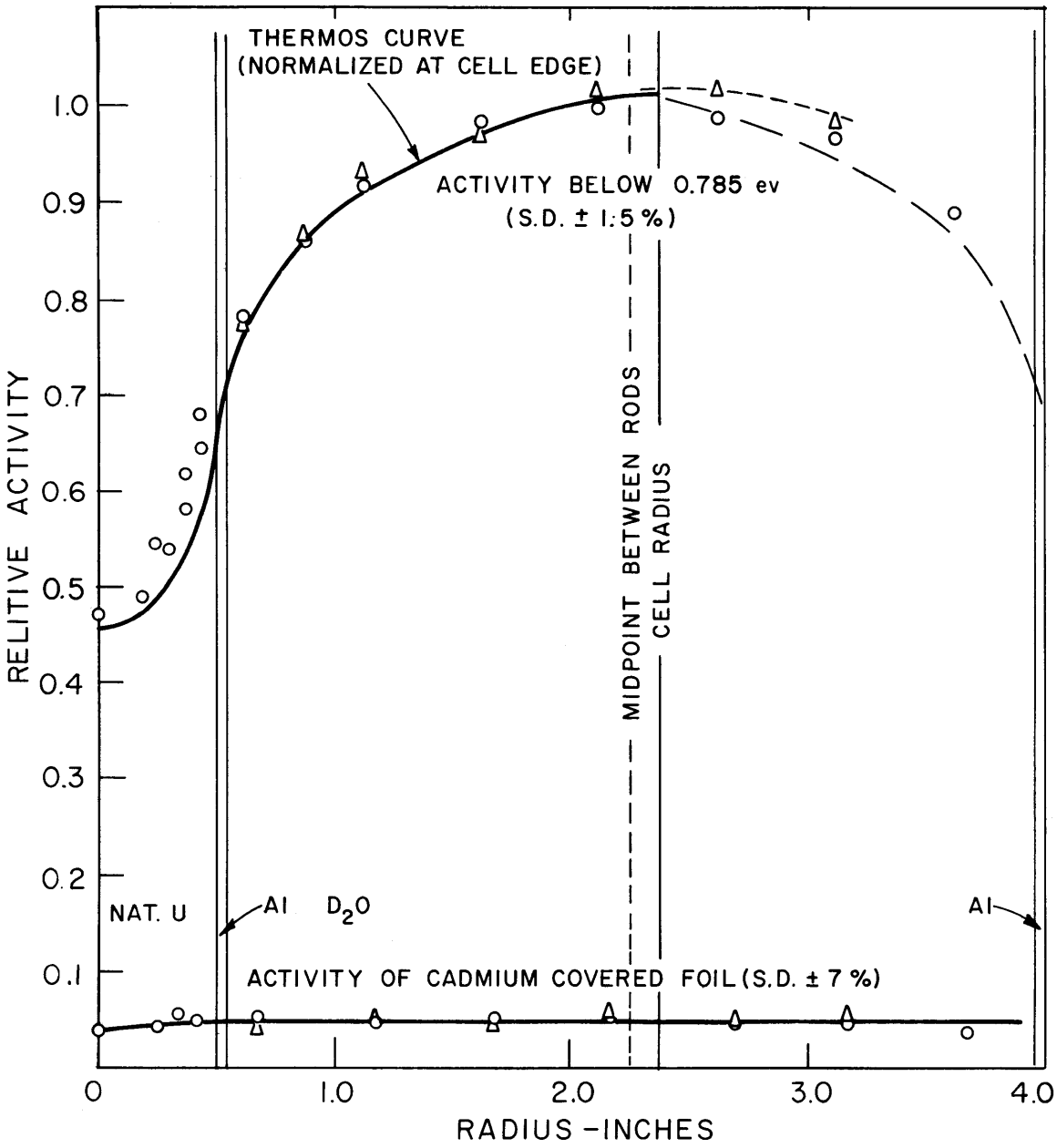

FIG. 4.20 EUROPIUM ACTIVITY DISTRIBUTION NO. 1a, 1.010- IN. DIA. NAT. U RODS ON A 4.5-IN. TRIANGULAR SPACING

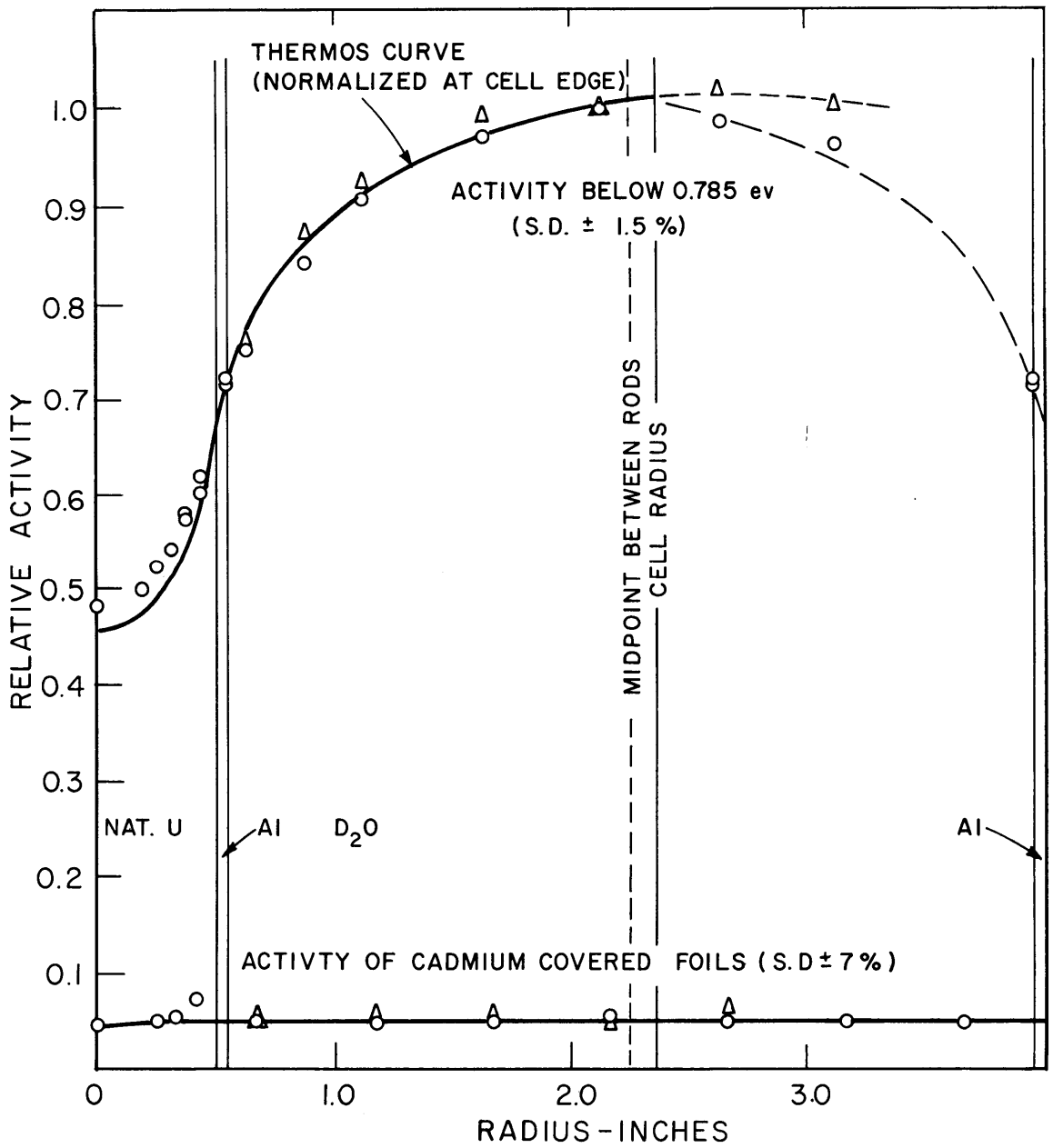

FIG. 4.21 EUROPIUM ACTIVITY DISTRIBUTION NO. 2c, 1.010-IN. DIA. NAT. U RODS ON A 4.5-IN. TRIANGULAR SPACING

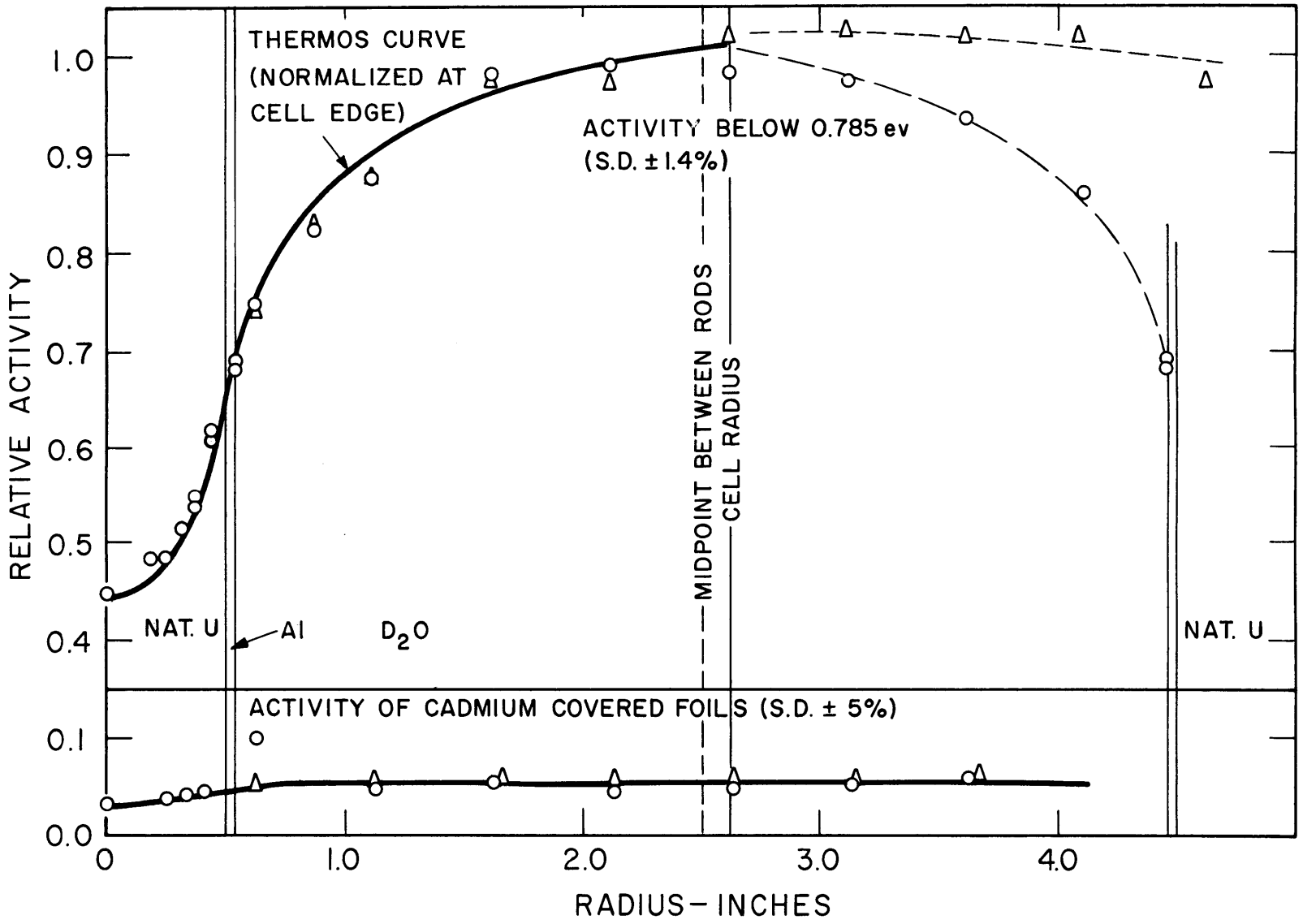

FIG. 4.22 EUROPIUM ACTIVITY DISTRIBUTION NO. 1a, 1.010-IN. DIA. NAT. U RODS ON A 5.0-IN. TRIANGULAR SPACING

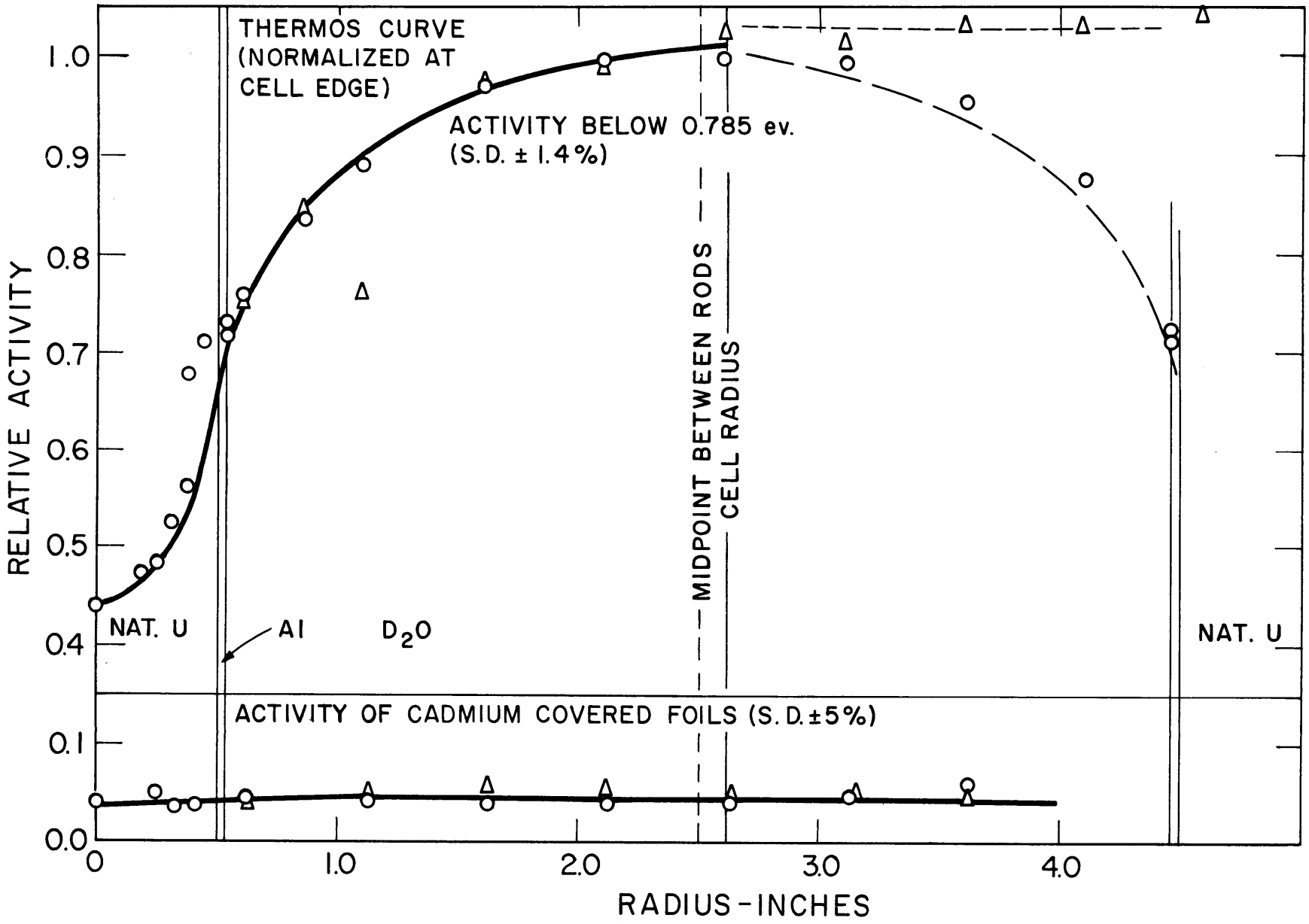

FIG. 4.23 EUROPIUM ACTIVITY DISTRIBUTION NO. 2a, 1.010-IN. DIA. NAT. U RODS ON A 5.0-IN. TRIANGULAR SPACING

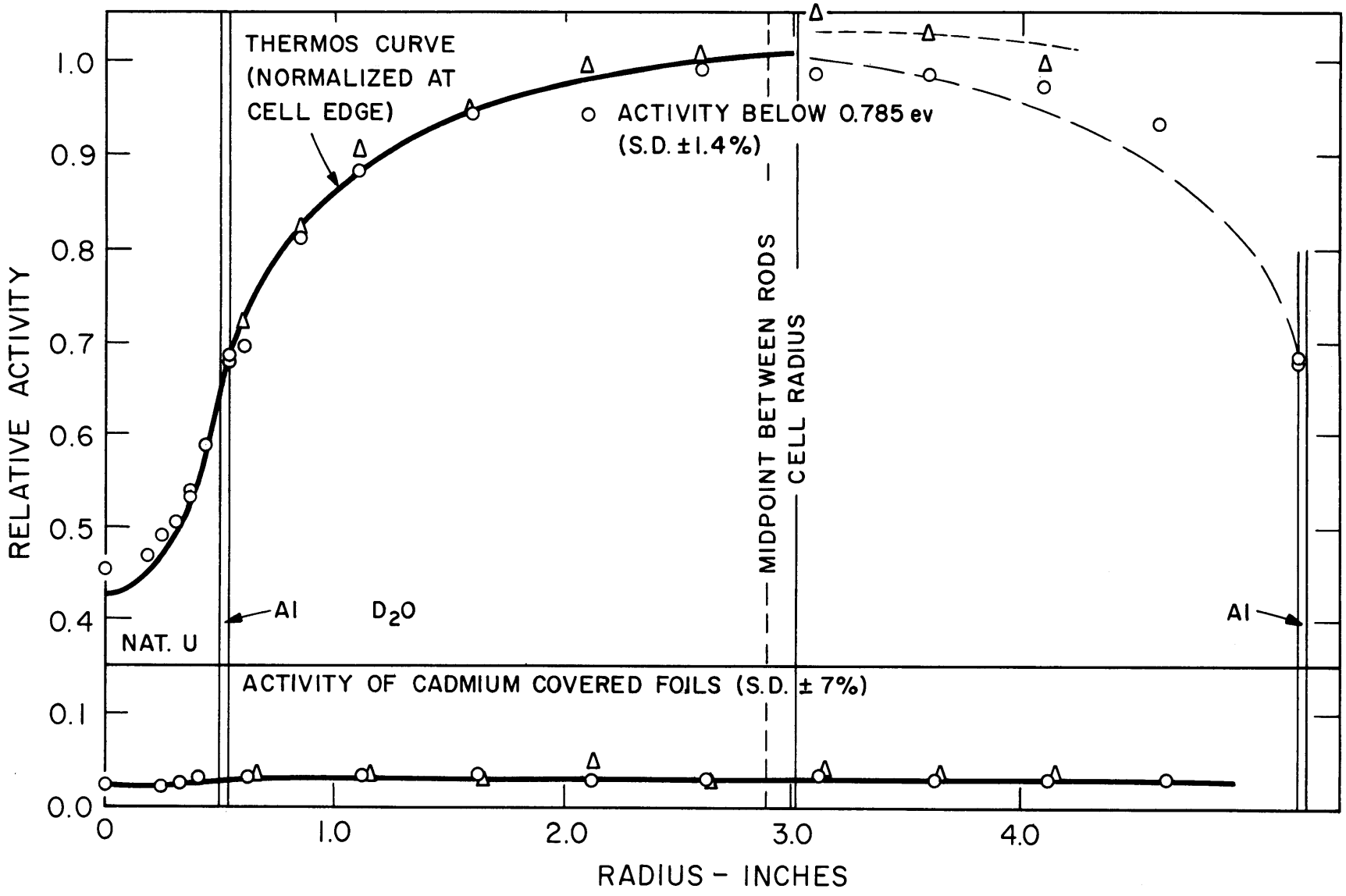

FIG. 424 EUROPIUM ACTIVITY DISTRIBUTION NO. 1a, 1.010-IN. DIA. NAT. U RODS ON A 5.75-IN. TRIANGULAR SPACING

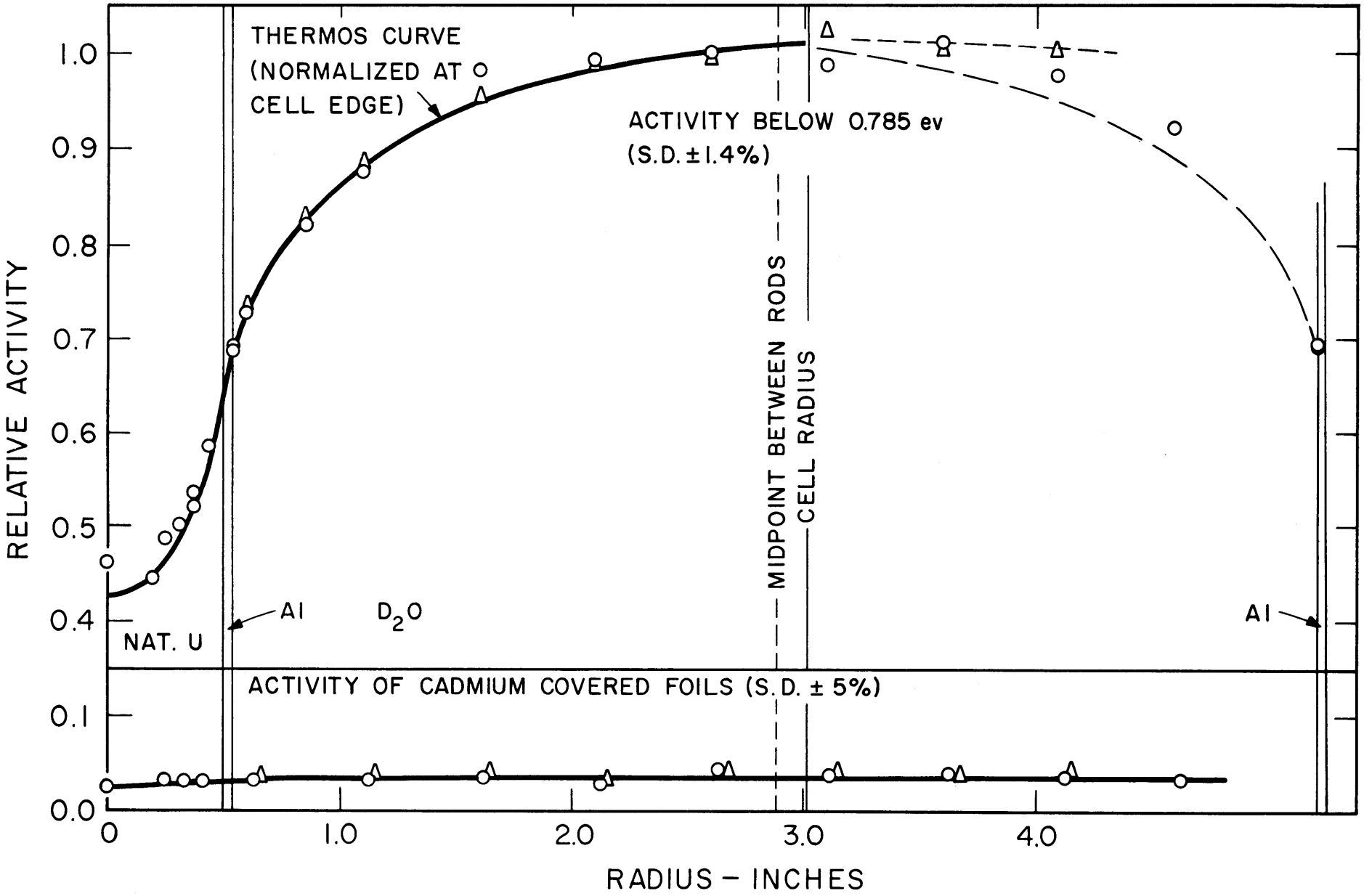

FIG. 4.25 EUROPIUM ACTIVITY DISTRIBUTION NO. 2a, 1.010-IN. DIA. NAT. U RODS ON A 5.75-IN. TRIANGULAR SPACING

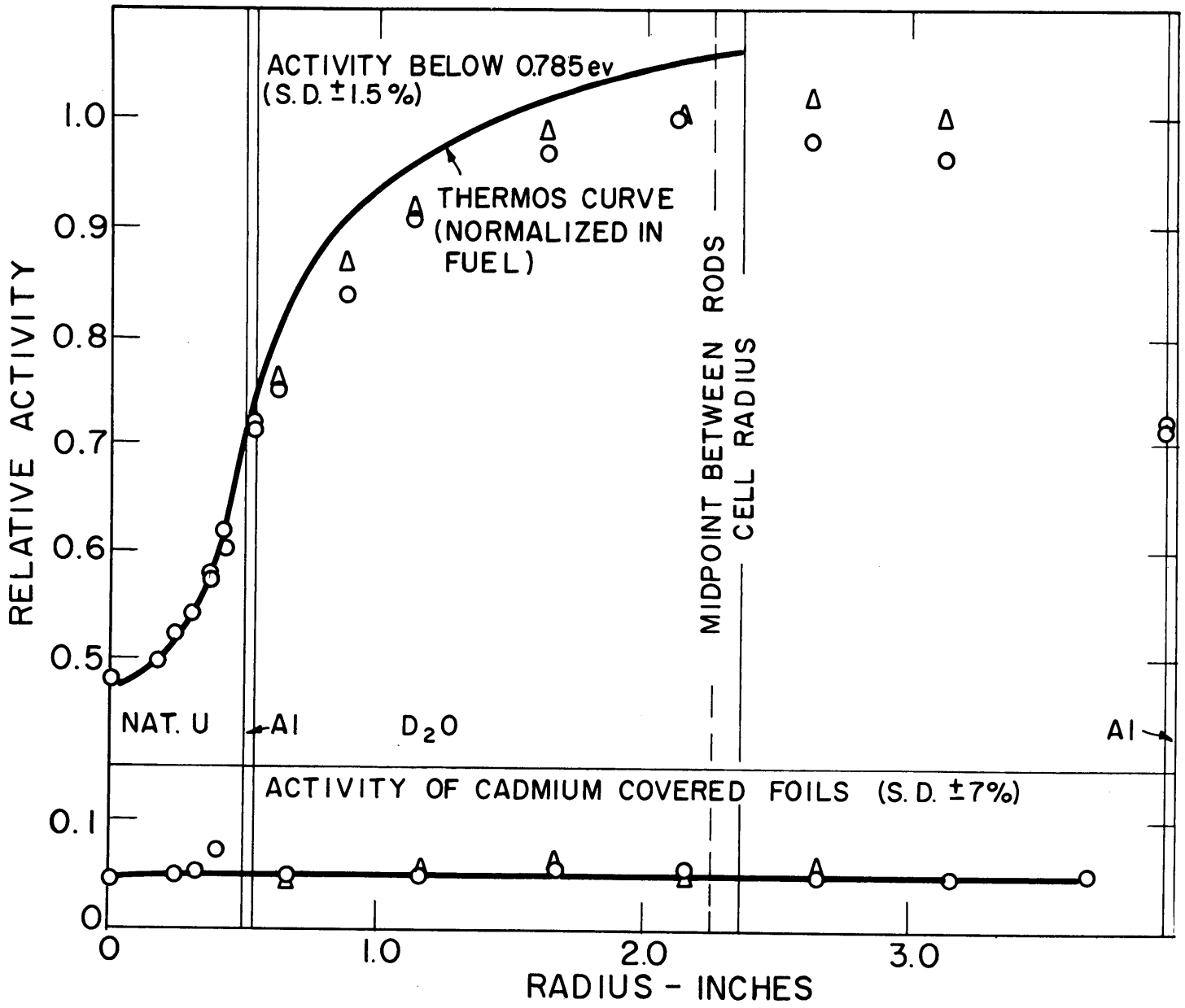

FIG. 4.26 EUROPIUM ACTIVITY DISTRIBUTION NO. 2a, 1.010-IN. DIA. NAT. U RODS ON A 4.5-IN. TRIANGULAR SPACING

covered with 0.023 inch of cadmium (Fig. 4.18) is 2.246. The product of 2.246 and the activity of the cadmium-covered foils found in the lattice flux plots is then subtracted from the bare europium activity to get the thermal activity up to about 0.2 ev. The energy cutoff point in THERMOS closest to 0.2 ev is 0.194 ev which was, therefore, chosen for the lower europium cutoff. The results for this cutoff energy are shown, normalized to THERMOS at the cell edge in Figs. 4.27 to 4.32. The results of Fig. 4.29 are replotted, normalized in the fuel, in Fig. 4.33. With normalization at the cell edge, the experimental activities at the rod center are, on the average, 4.7% higher than THERMOS; there does not seem to be any trend with lattice pitch. Figure 4.33, where normalization is in the fuel, shows that the agreement is good in the fuel, and that THERMOS is higher than experiment in the moderator. Several other THERMOS energy cutoff points, ranging in energy from 0.141 ev to 0.279 ev, were used to check the effect of the energy cutoff on the theoretical activity distribution; these variations affected the activity dip in the fuel by less than ±1.0%, and showed that 0.194 ev was a reasonable choice for a lower energy cutoff.

The europium distributions computed for both cutoff energies were not significantly affected by changing from a Brown-St. John kernel to a Honeck kernel. The effects of not using the anisotropic scattering correction were similar to those found with gold and lutetium.

The disagreement between THERMOS and experiment seems to be slightly greater for europium (for both cutoffs) than for lutetium. It should be pointed out, however, that if the activities of the cadmium-covered europium foils are just subtracted from the bare foils, as was done with the lutetium and the gold, there is considerable uncertainty as to which energy cutoff should be used. If a cadmium cutoff of 0.415 ev is used, the discrepancy between THERMOS and experiment is about three times as great as it is when the activity of the cadmium covered foils is corrected for partial absorption by the cadmium and cutoff energies of 0.194 and 0.785 ev are used. If a cadmium cutoff of 0.511 ev is used, the agreement between theory and experiment is very good; this agreement is, however, fortuitous, and has no definite physical basis. On the other hand, the physical bases for using the europium cutoffs at 0.194 ev and 0.785 ev seem to be valid, for reasons already given in this section.

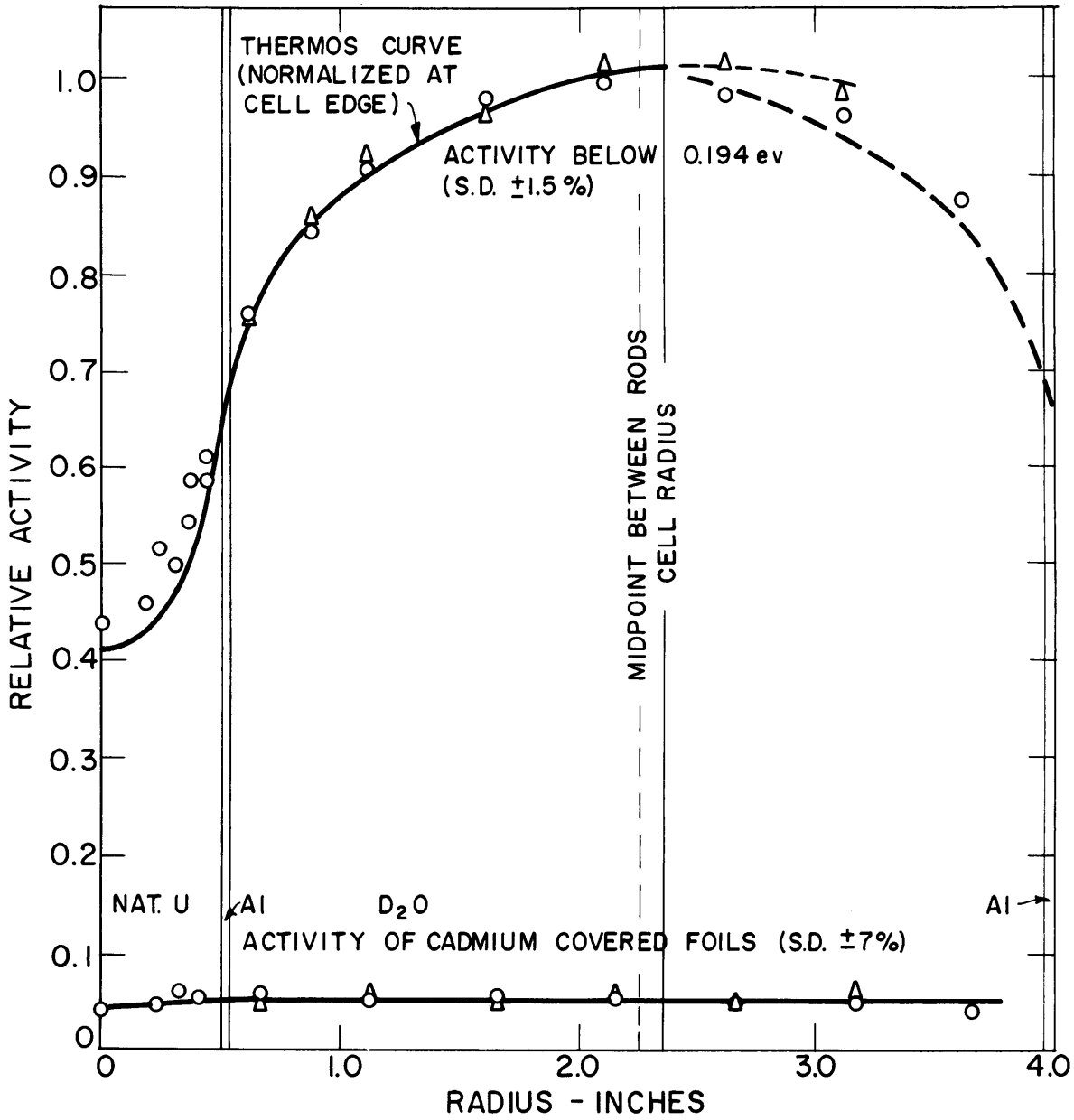

FIG. 4.27 EUROPIUM ACTIVITY DISTRIBUTION NO. 1b, 1.010-IN.DIA. NAT. U RODS ON A 4.5-IN. TRIANGULAR SPACING

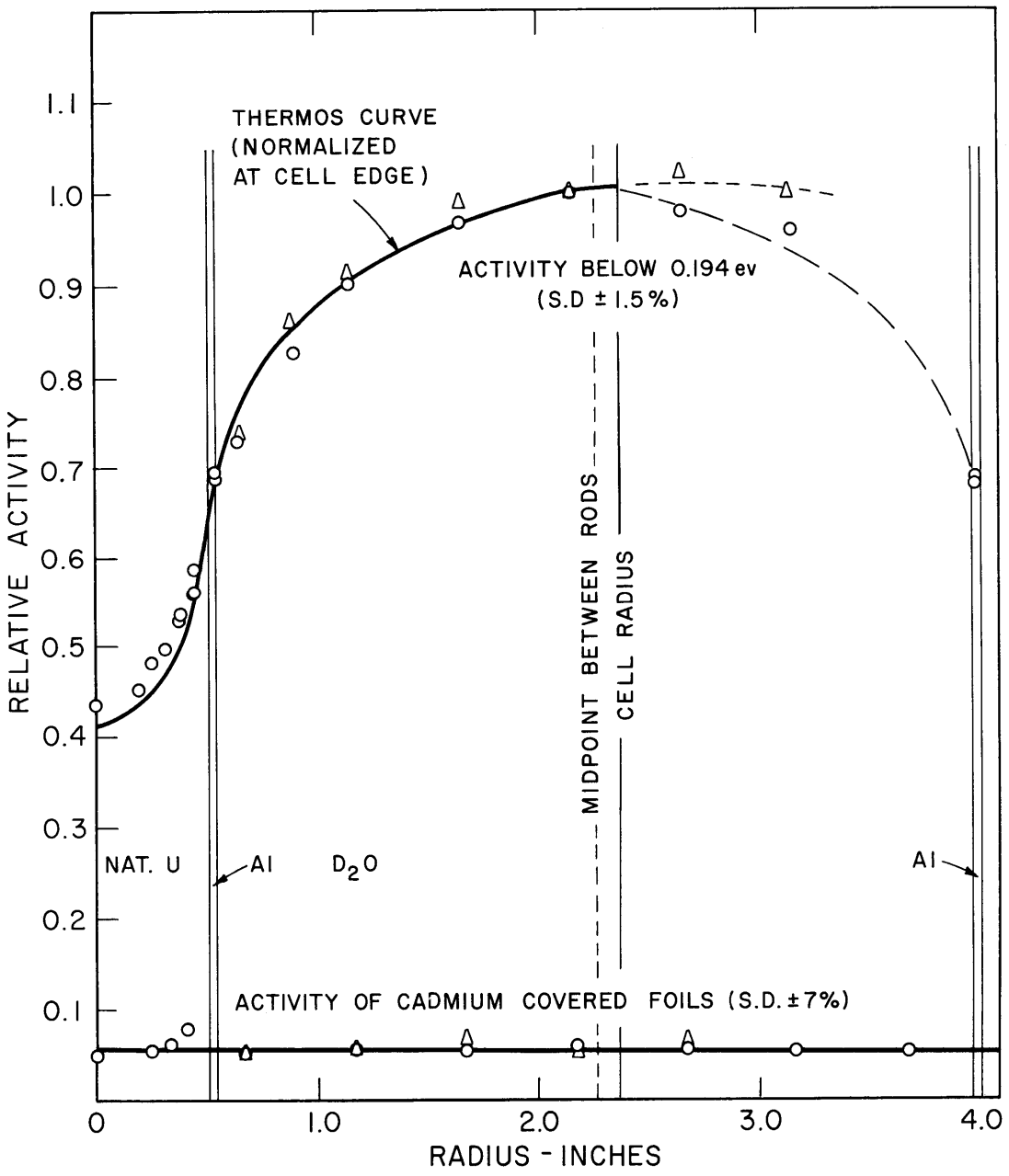

FIG. 4.28 EUROPIUM ACTIVITY DISTRIBUTION NO. 2b, 1.010-IN. DIA. NAT. U RODS ON A 4.5-IN. TRIANGULAR SPACING

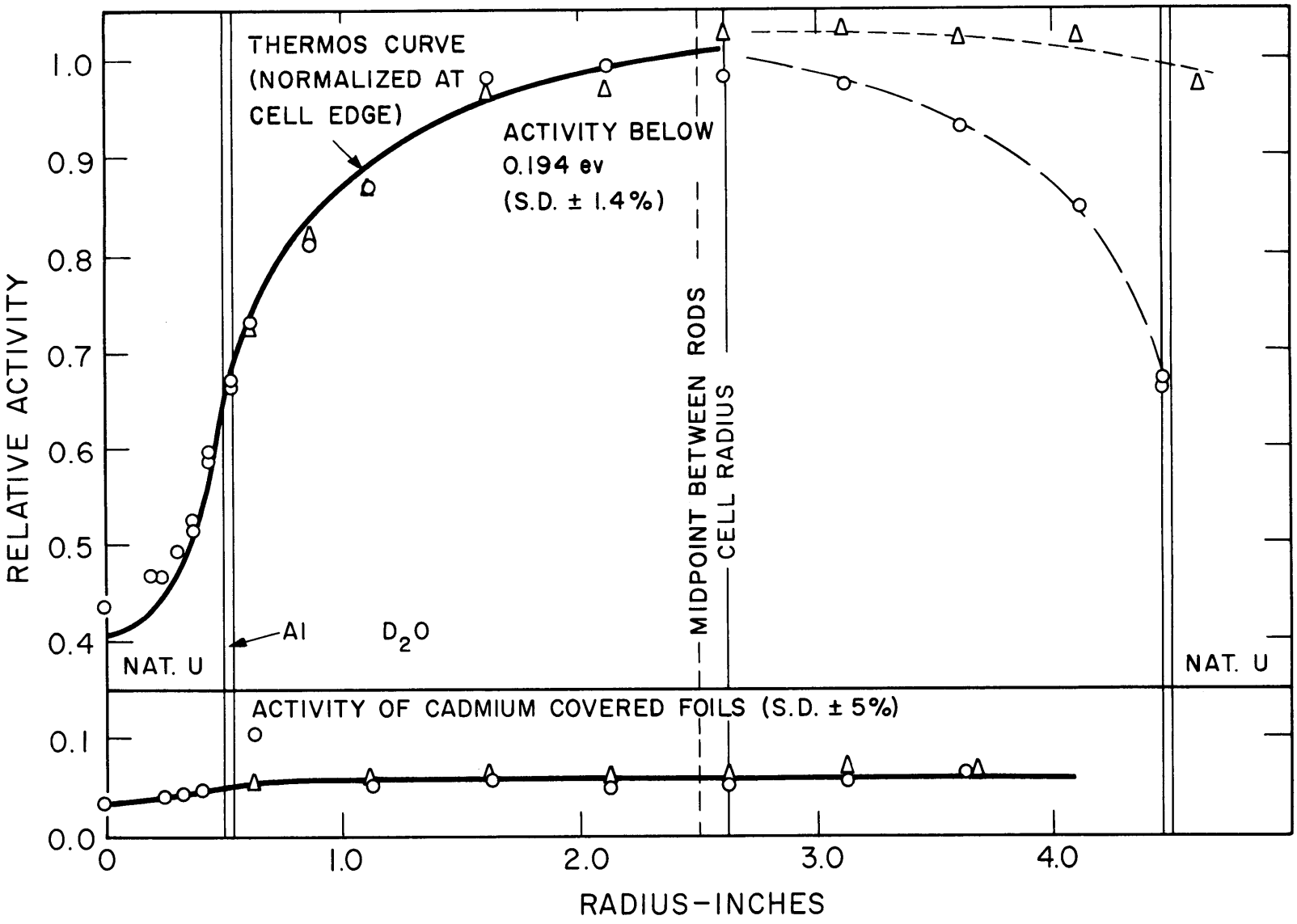

FIG. 4.29 EUROPIUM ACTIVITY DISTRIBUTION NO. 1b, 1.010-IN. DIA. NAT. U RODS ON A 5.0-IN. TRIANGULAR SPACING

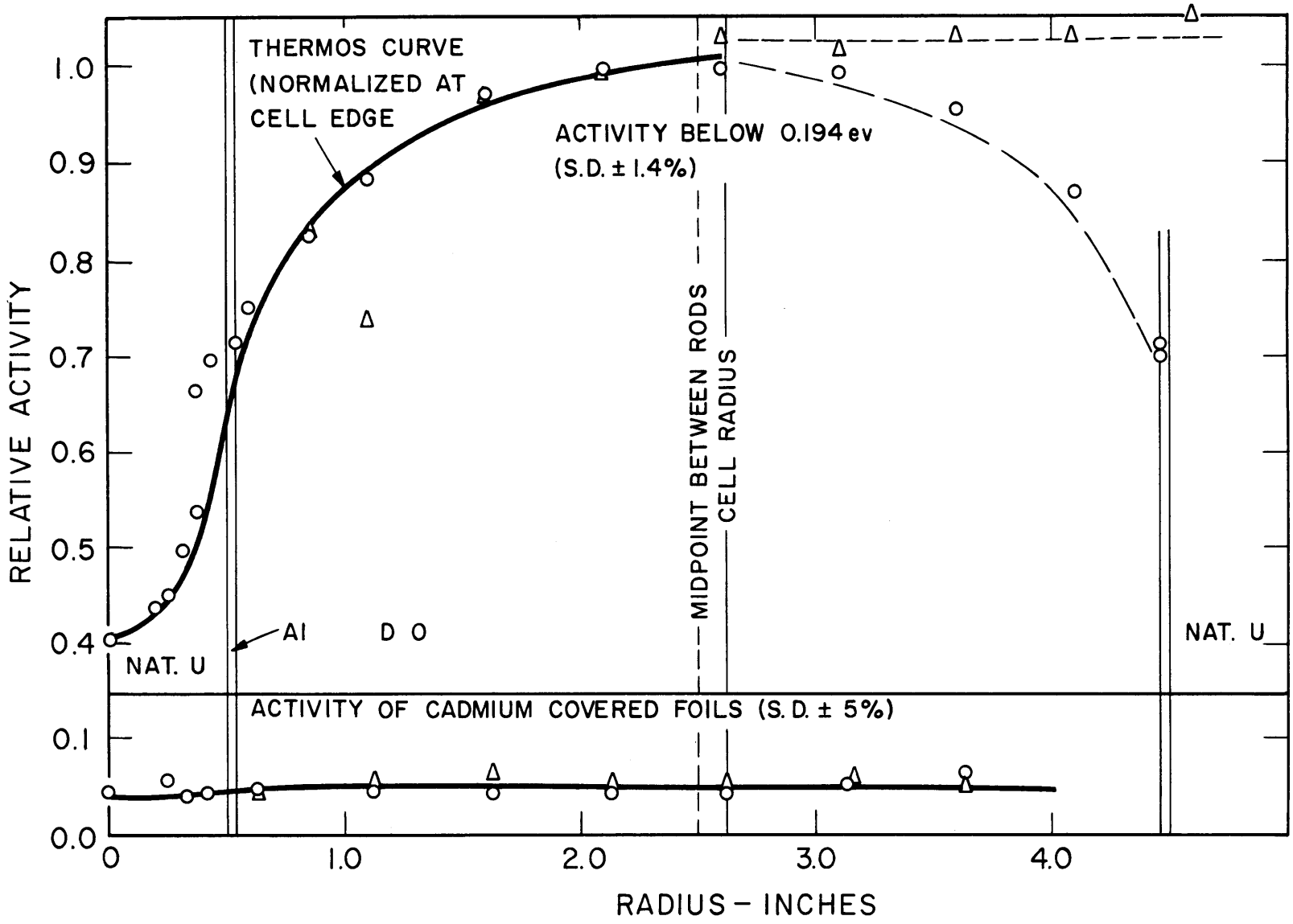

FIG. 4.30 EUROPIUM ACTIVITY DISTRIBUTION NO. 2b, 1.010-IN. DIA. NAT. U RODS ON A 5.0-IN TRIANGULAR SPACING

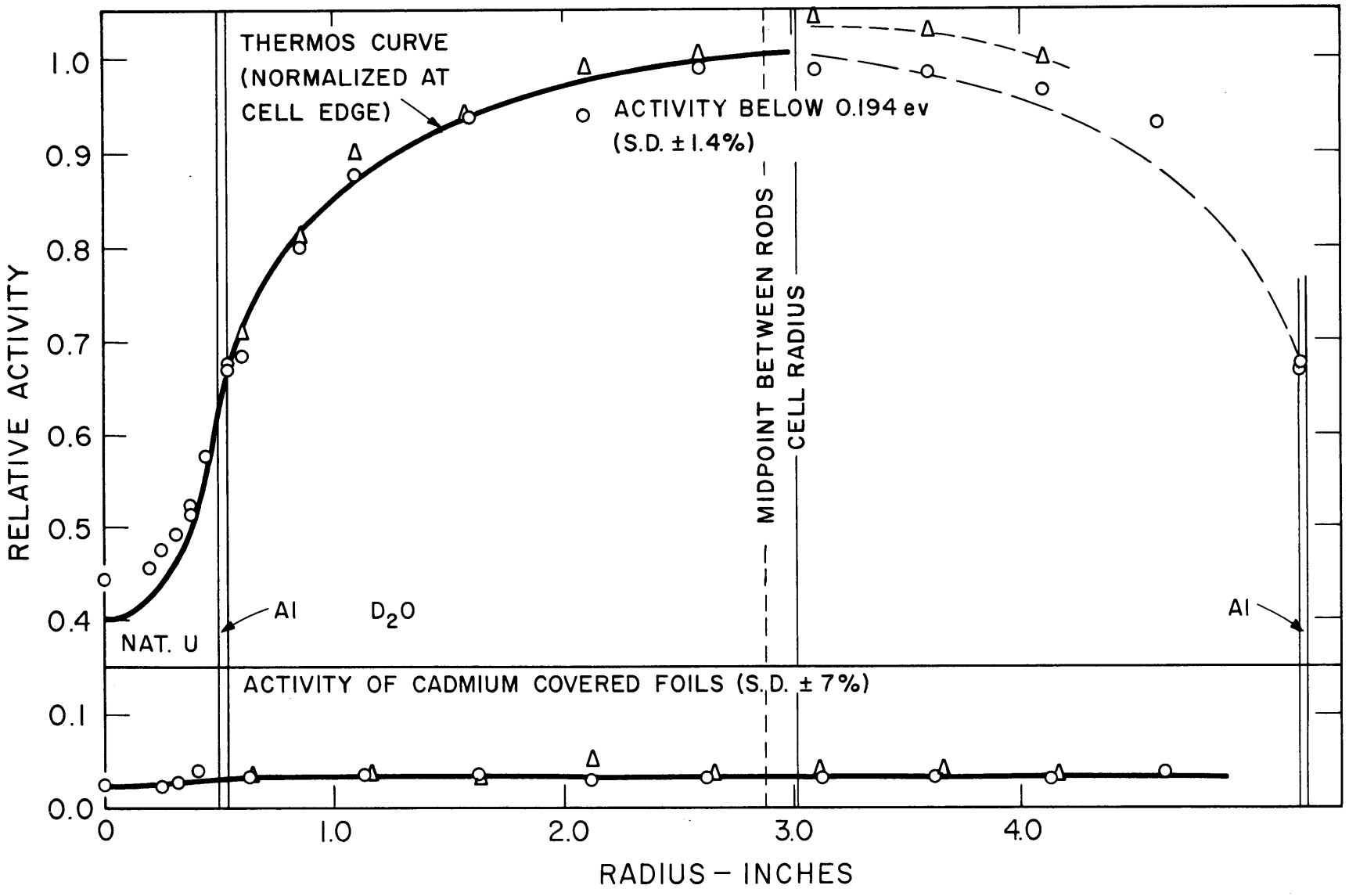

FIG. 4.31 EUROPIUM ACTIVITY DISTRIBUTION NO. 1b, 1.010-IN. DIA. NAT. U RODS ON A 5.75-IN. TRIANGULAR SPACING

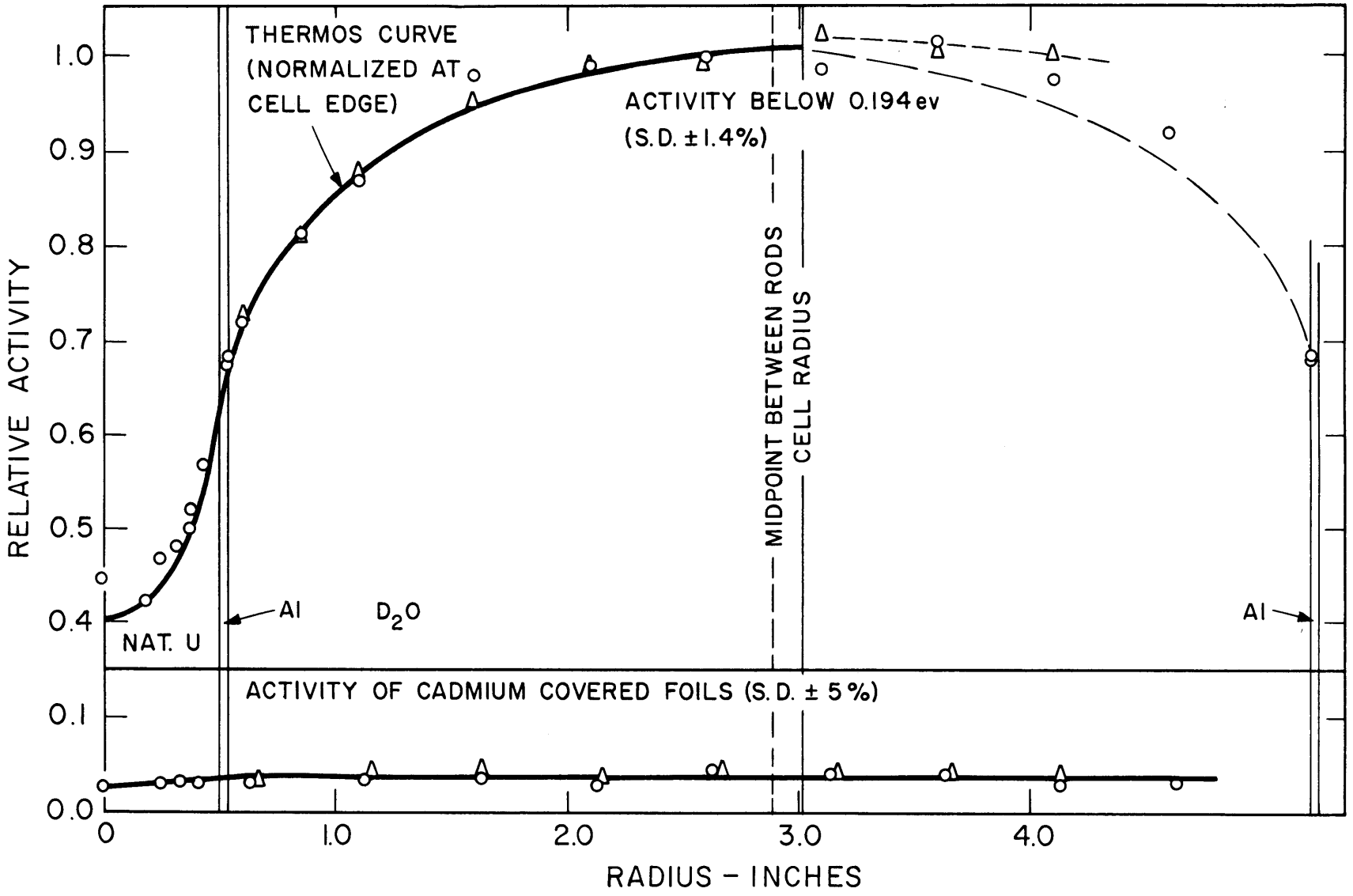

FIG. 4.32 EUROPIUM ACTIVITY DISTRIBUTION NO. 2b, 1.010-IN. DIA. NAT. U RODS ON A 5.75-IN. TRIANGULAR SPACING

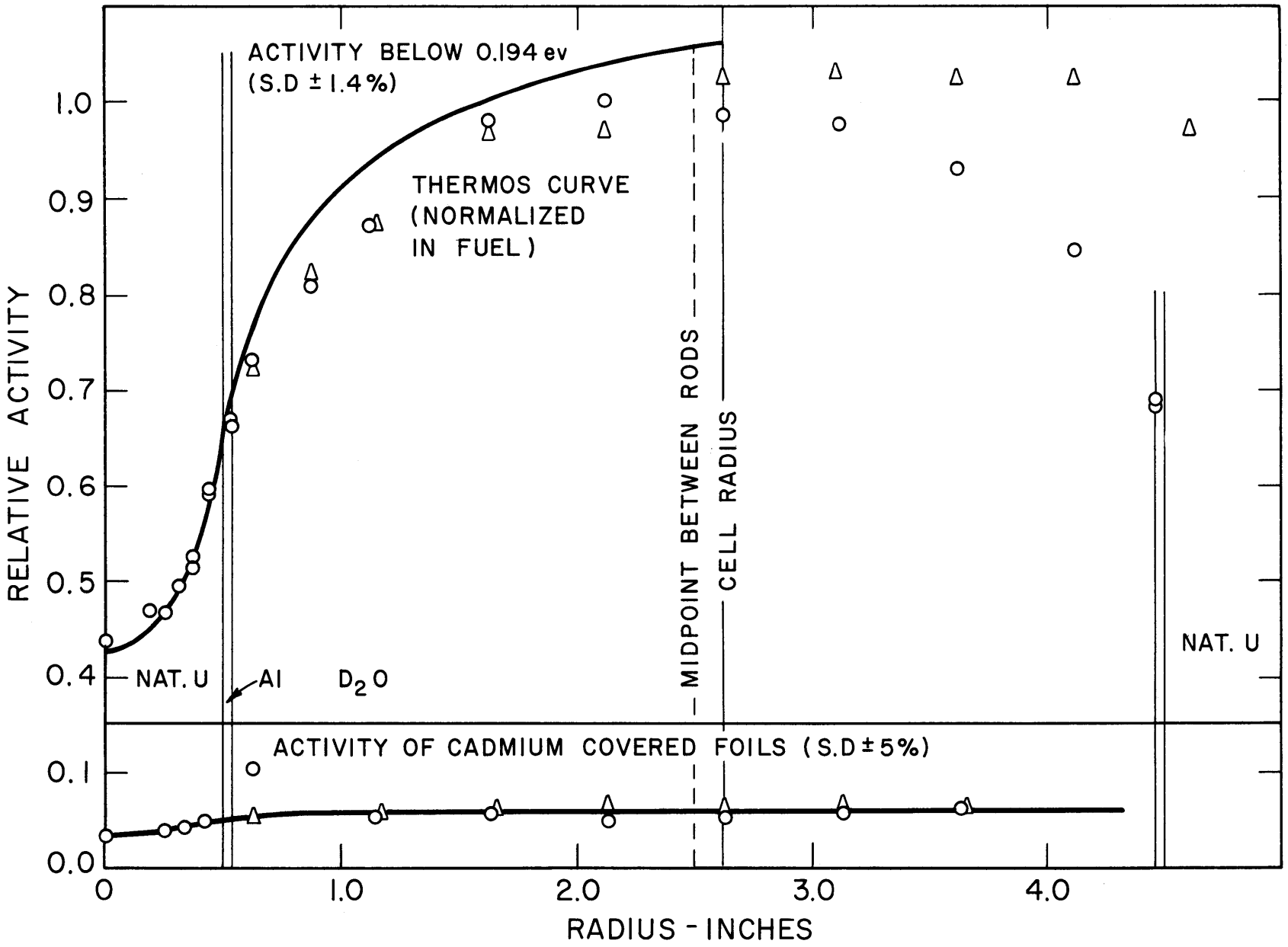

FIG. 4.33 EUROPIUM ACTIVITY DISTRIBUTION NO. 1b, 1.010-IN. DIA. NAT. U FOILS ON A 5.0-IN. TRIANGULAR SPACING

The existing discrepancies may have several causes. First, the europium cross section data may not be quite correct. Second, and perhaps more important, the model described in Appendix H to fit the data of Fig. 4.19 to an exponential integral of the second kind, may be too simple. The cadmium covers have been idealized into slabs, for which the function $E_2(\Sigma_{Cd}x)$ is suitable, and a one-velocity model has been used in the $E_2(\Sigma_{Cd}x)$ fit. A more rigorous treatment would involve a complicated integration over the actual foil and cover arrangement and over the energy-dependent europium and cadmium cross sections. The simplicity of the model seems to be justified, however, by the fact that the activity of the cadmium covered europium foils is less than 10% of the total activity, and the model is used to apply a correction to this relatively small activity.

Attempts were also made to use samarium instead of cadmium filters, because the samarium cross section is similar to that for cadmium and has a lower effective cutoff (H13, H5) (about 0.2 ev lower than that of cadmium), which lies below the 0.46 ev europium resonance. However, the samarium could not be obtained in soft metallic foil, and sufficiently thin covers could not be made by compressing the brittle crystalline form of the metal, because of mechanical difficulties. Attempts to melt the crystals into homogeneous metal gave a substance too brittle for rolling into foils. Thick samarium foils caused perturbations of the same magnitude as did cadmium. Samarium also has resonances which could interfere with the epithermal europium resonances; these samarium resonances made questionable any transmission experiment similar to that made with cadmium. The apparent success of the cadmium transmission technique made it seem unnecessary to pursue the possibility of samarium covers any further. If thin enough samarium covers could be obtained, however, they might prove useful in europium flux plots.

4.2.4 DEPENDENCE OF MEASUREMENTS ON POSITION IN LATTICE FLUX

The gold, lutetium, and europium measurements described in sections 4.2.1 to 4.2.3 were all made in the central cell of the lattice and at heights of two to three feet above the bottom of the tank. Several experiments were performed to insure that measurements made in this

location were representative of measurements made anywhere in the lattice tank. The results follow.

Other work at M.I.T. (P1, W3) has shown that axial and radial macroscopic flux traverses made with bare gold, cadmium covered gold, and cadmium covered U^{238} foils all had the same shape at heights between 1 and 4-1/2 feet. These measurements show that the thermal and epithermal distributions have the same shapes sufficiently far from the source. Axial and radial macroscopic lutetium measurements were made in the present study, in the 5.75-inch lattice, and the results are shown in Figs. 4.34 and 4.35; the results were the same as those obtained with the other detectors, mentioned above. It is, therefore, reasonable to assume that the effective thermal neutron temperature also does not change in lattice regions sufficiently far from the source. Traverses made with lutetium, gold, and uranium foils disagreed at heights above 4-1/2 feet, where a complicated reflector effect due to structural material at the top of the tank disturbs the equilibrium lattice spectrum (P1).

Experiments were also performed to determine whether the radial flux distribution was separable into a macroscopic J_o distribution and a microscopic distribution computed by THERMOS for an infinite lattice. Experimenters in Sweden have reported non-separability effects in uranium-D_2O lattices (W8). The method used at M.I.T. consisted in making intracell traverses, in the 5.75-inch lattice, in cells centered two rods and three rods off center, respectively, as shown in Fig. 4.36. Each intracell activation has been divided by the appropriate J_o factor corresponding to the radial location of the foil. The results are shown in Figs. 4.37 and 4.38, in which the THERMOS results are normalized to experiment in the fuel. Figure 4.37 shows the distribution for the cell two rods off center; the experimental distribution is very well fit by THERMOS except for small differences in the moderator. These differences are slightly greater in Fig. 4.38, which shows the distribution for the cell three rods off center. In Fig. 4.38, the rod-to-moderator traverse is especially low, indicating a possible reflector effect at the edge of the tank.

Two conclusions may be drawn from the off-center microscopic gold traverses. First, the agreement between THERMOS and experiment

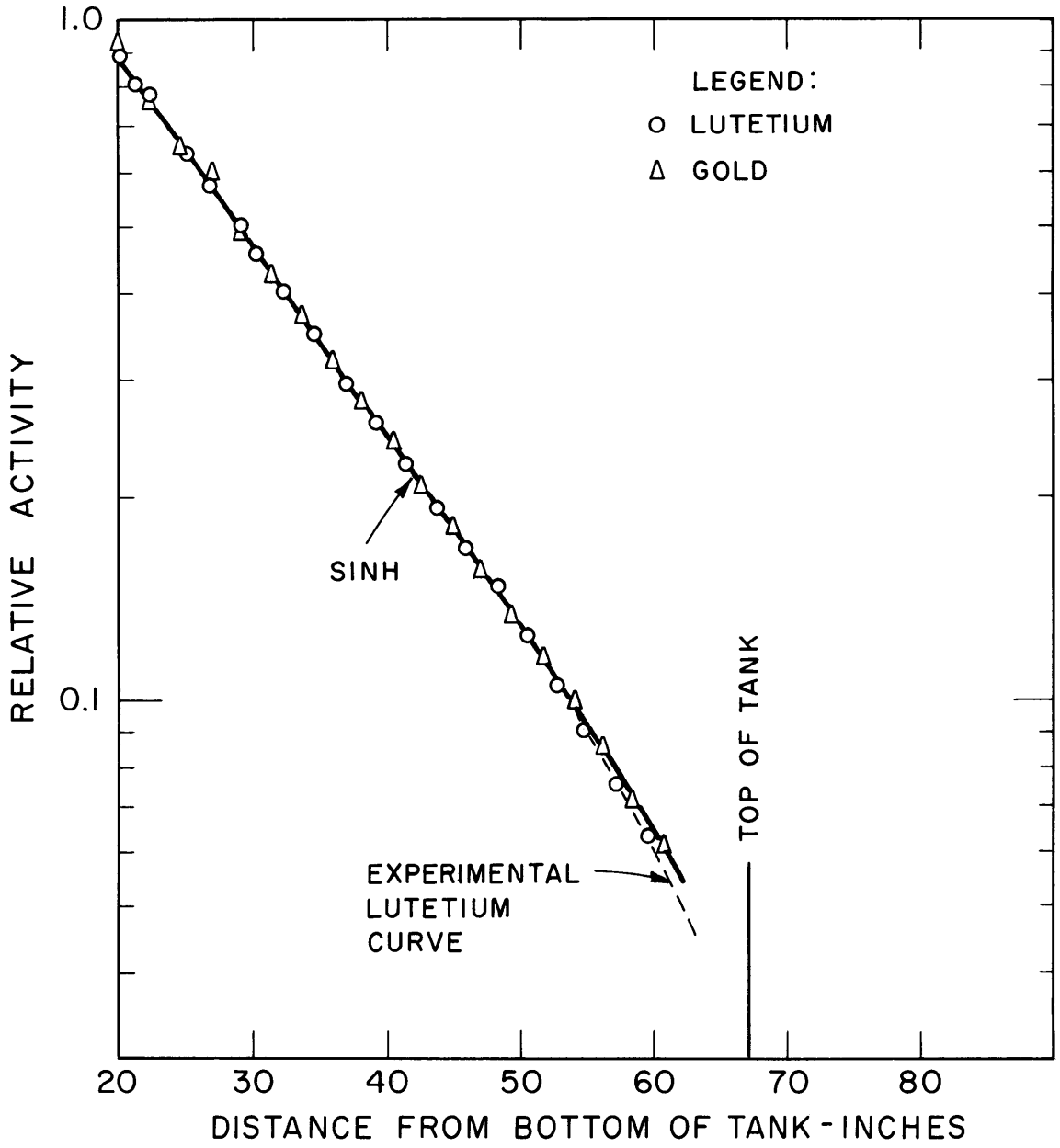

FIG. 4.34 COMPARISON OF GOLD AND LUTETIUM AXIAL TRAVERSES (5.75-IN. LATTICE)

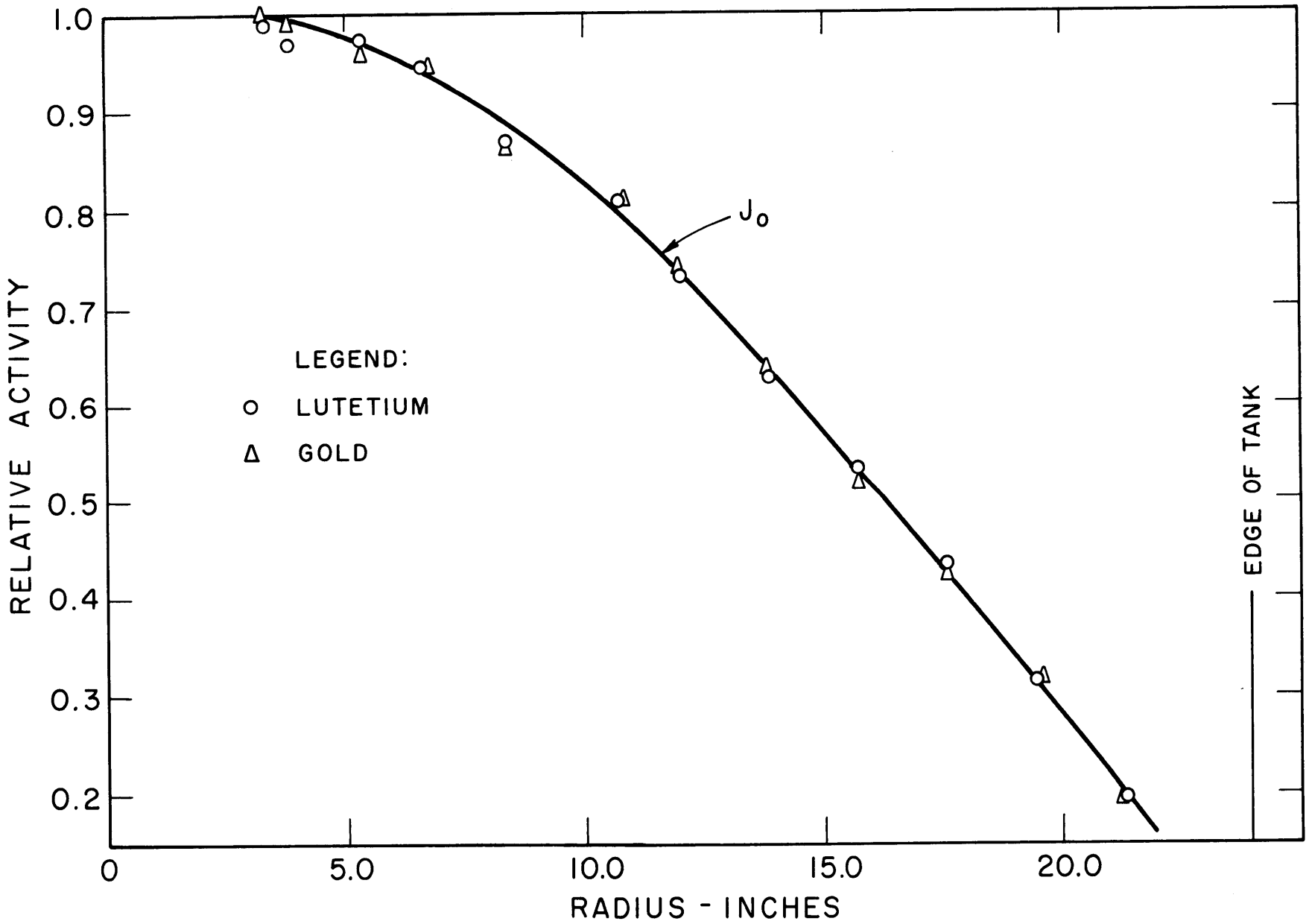

FIG. 4.35 COMPARISON OF GOLD AND LUTETIUM RADIAL TRAVERSES (5.75-IN. LATTICE)

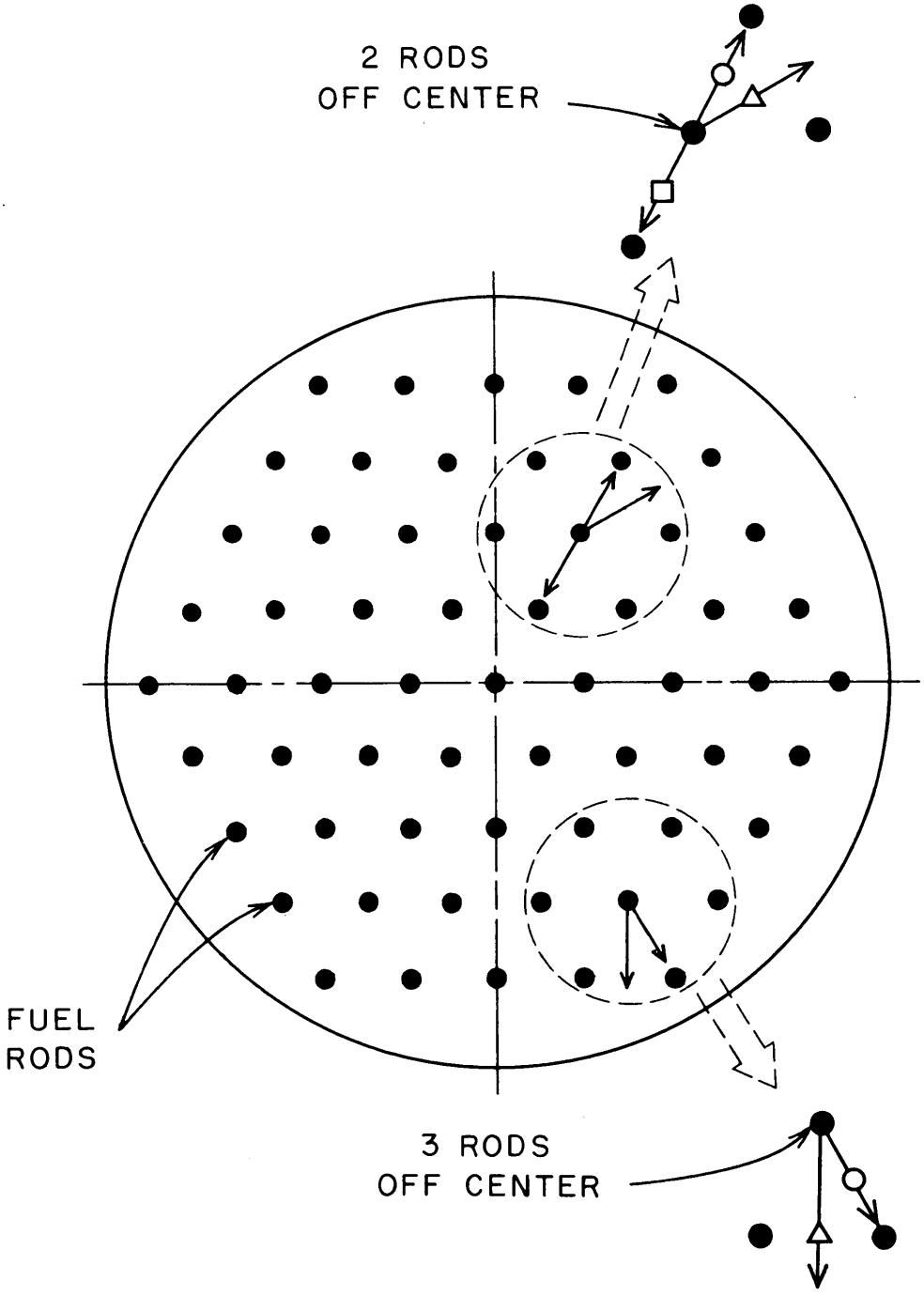

FIG. 4.36 LOCATIONS AND DIRECTIONS OF TRAVERSES IN MEASUREMENTS OF OFF-CENTER GOLD MICROSCOPIC DISTRIBUTIONS

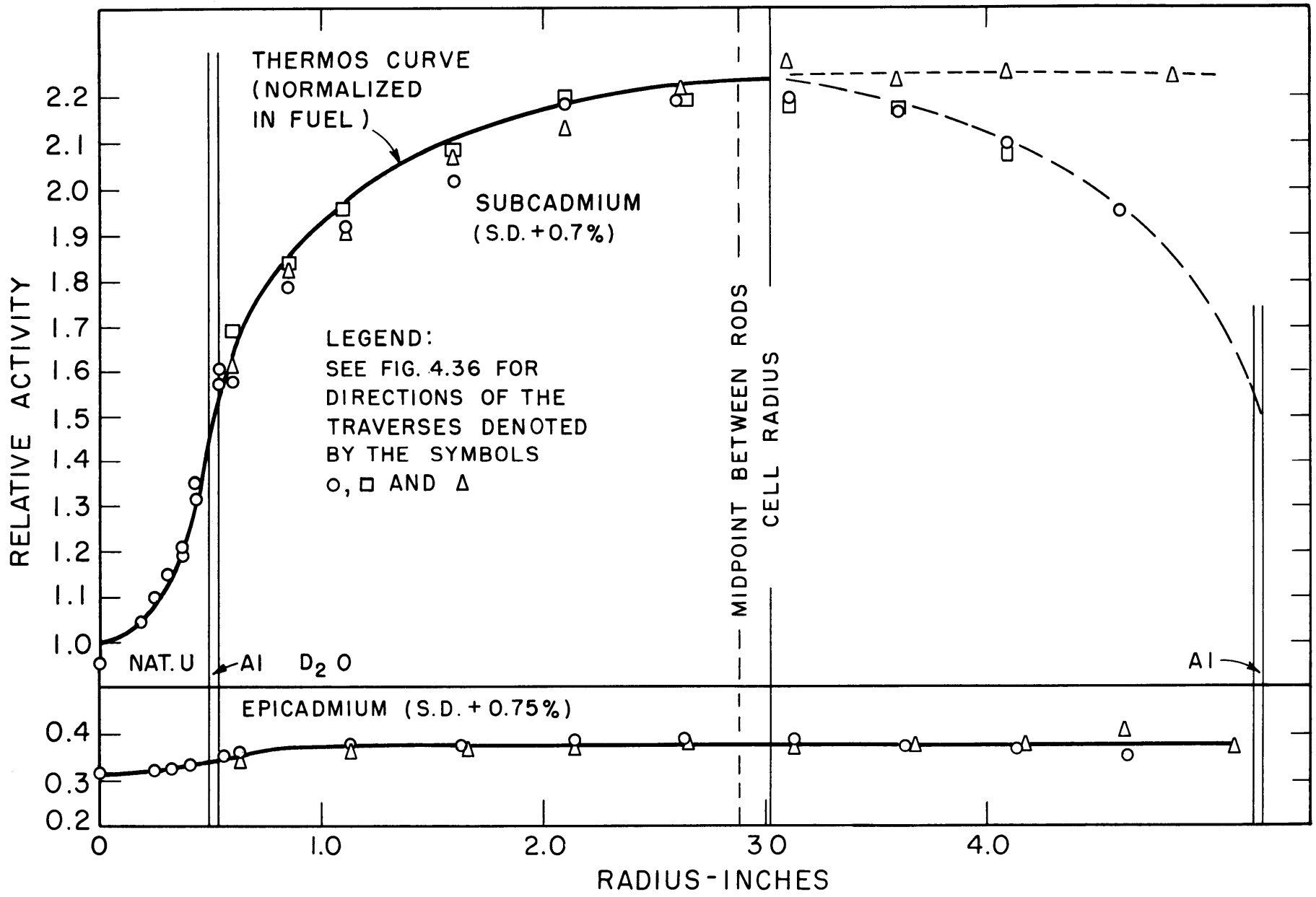

FIG. 4.37 GOLD ACTIVITY DISTRIBUTION IN A CELL 2 RODS OFF-CENTER, 1.010-IN. DIA. NAT. U RODS ON A 5.75-IN. TRIANGULAR SPACING

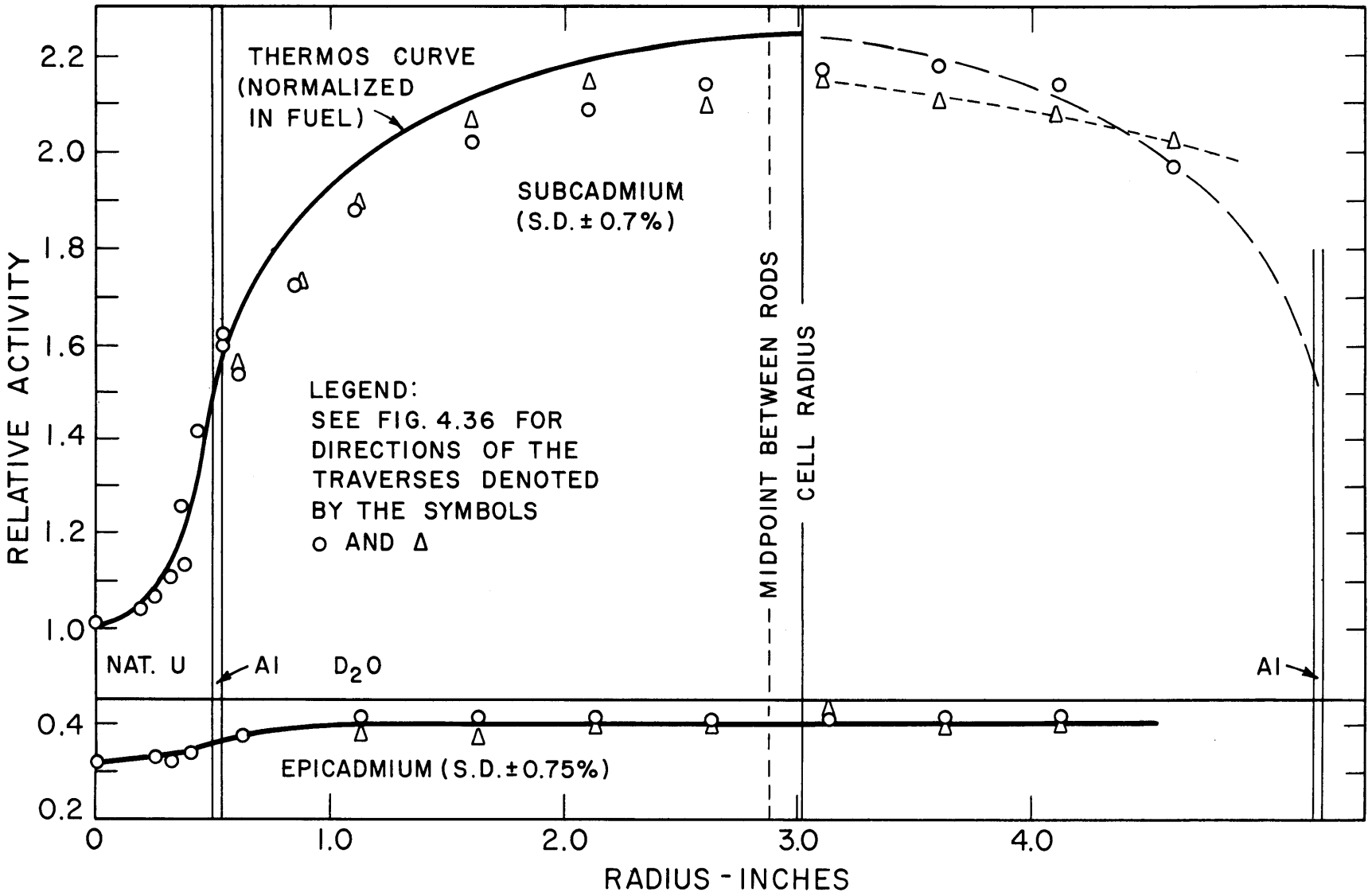

FIG. 4.38 GOLD ACTIVITY DISTRIBUTION IN A CELL 3 RODS OFF CENTER, 1.010-IN. DIA. NAT. U RODS ON A 5.75-IN. TRIANGULAR SPACING

improves in going from cells at the tank edge to the center cell. Second, even at the tank edge, the disagreement is small, and the resulting disadvantage factors are not significantly affected. A similar experiment was performed at North American Aviation, Inc. (C4), where an intracell flux distribution was measured in a cell located 6.7 inches from the wall of a 4-foot diameter tank. The lattice consisted of 1.0-inch diameter, slightly enriched uranium rods in D_2O. The microscopic distribution in the outer cell was only "slightly distorted" from that measured in the central cell. The NAA and MIT lattice and tank sizes are very similar, so that the separability effects found in the two systems would be expected to agree, and they apparently do.

4.2.5 NEUTRON TEMPERATURE CALCULATIONS

In this section, the results of the temperature calculations based on the Westcott method discussed in section 3.5 will be given. As pointed out in section 3.5, all temperatures in the cell are calculated relative to the temperature at the cell edge. The latter can be obtained in two ways.

First, THERMOS computes the value of the average velocity of the spectrum at all radial mesh points in the cell. This average velocity can be computed up to any desired THERMOS cutoff energy. Since the Westcott method assumes a Maxwellian thermal neutron distribution with a 1/E tail, it is desirable to relate the computed average velocity in some way to a Maxwellian temperature. Accordingly, a Maxwellian temperature with the same average velocity as that computed by THERMOS is assigned to the cell edge. Inspection of a typical THERMOS spectral distribution, Fig. 4.39, shows that the 1/E tail seems to join the Maxwellian portion of the spectrum in the neighborhood of 0.2 to 0.25 ev. Furthermore, if there were no tail, the Maxwellian distribution would approach negligible values at approximately these same energies. The average velocity used in obtaining a temperature at the cell edge is, therefore, taken as the average velocity of all neutrons below a 0.232 ev cutoff. Temperatures at other radial mesh points can be determined in the same manner.

The second method for obtaining a temperature at the cell edge is to fit a Maxwellian to the computed spectral distribution, N(v). In a Maxwellian distribution,

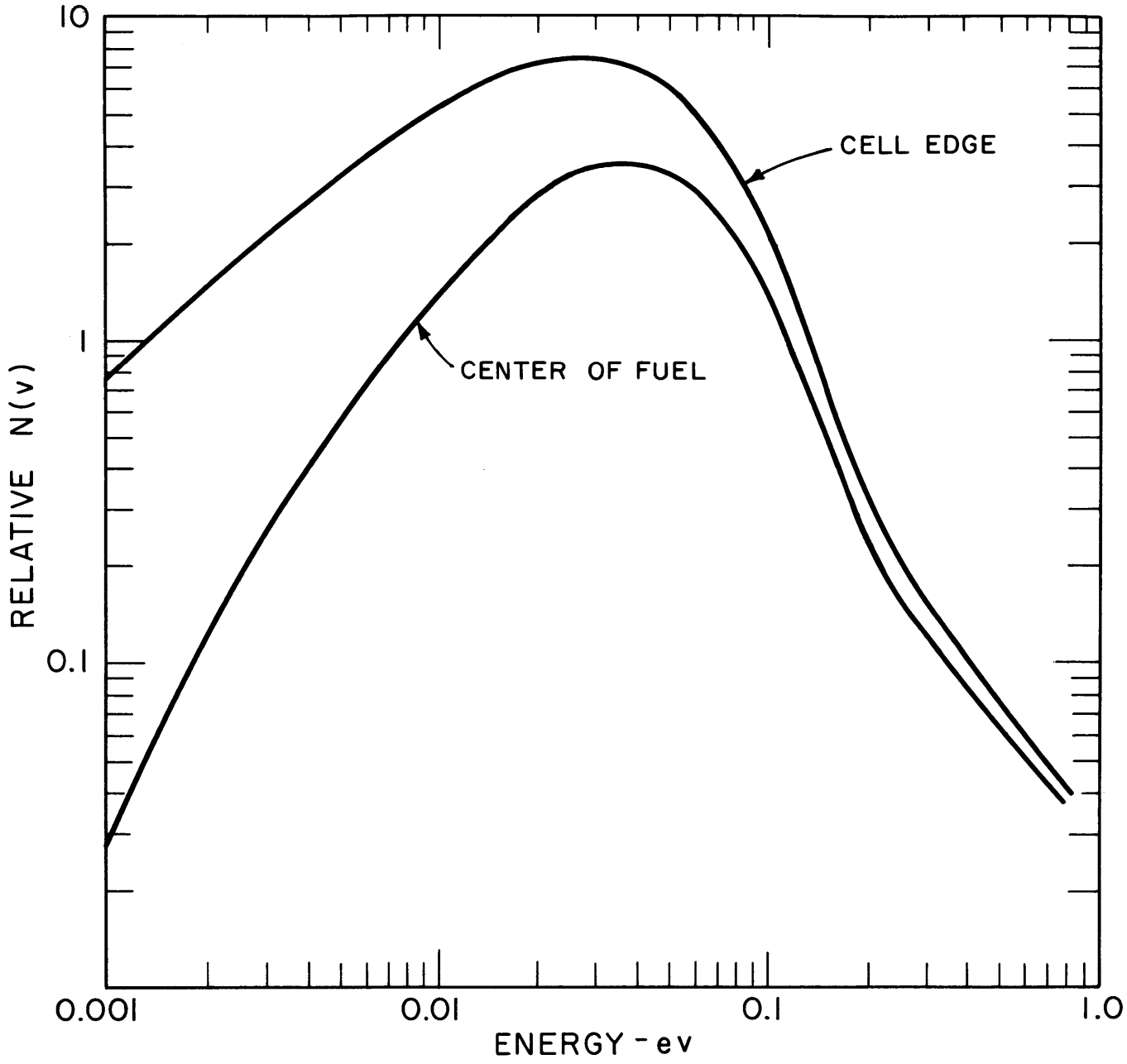

FIG. 4.39 TYPICAL SPECTRA COMPUTED WITH THERMOS (4.5-IN. LATTICE)

$$N(v) = K v^2 e^{-\frac{v^2}{v_o^2}}, \qquad (4.1)$$

where N(v) is the neutron density per unit velocity, K is a constant, v is the velocity, and v_o is the most probable velocity. Since the energy E is proportional to v^2, Eq. (4.1) may be written as

$$\ln \frac{N(v)}{E} = \text{constant} - \frac{1}{E_o} . \qquad (4.2)$$

A semilogarithmic graph of N(v)/E against E should give a straight line of slope $-1/E_o$, where E_o is the energy corresponding to v_o and is 0.025 ev for a Maxwellian spectrum at room temperature. Such a plot is shown in Fig. 4.40, where the cell edge spectrum of Fig. 4.39 is plotted in this way. The graph is linear up to about 0.06 ev, where non-linear effects due to the transition into the 1/E region appear. The straight line up to 0.06 ev is long enough to permit an estimate of E_o.

A semilog plot to obtain a Maxwellian effective temperature is reliable only in the moderator. An example of such a plot at the center of the fuel is shown in Fig. 4.41. Because of the large amount of spectral hardening, the low energy end of the semilog plot is strongly depleted. A straight line does fit part of the semilog spectrum, but, because the Maxwellian nature of the spectrum has been destroyed, the value of E_o obtained from the slope of the straight line is meaningless. It is only in the moderator that a straight line can be fitted to the semilogarithmic plot, down to very low neutron energies.

The cell edge temperatures for the natural uranium lattices computed by the $\bar{v}$ and semilog methods are compared in Table 4.3. The effective temperatures as calculated by the $\bar{v}$ method are somewhat higher than those computed by the semilog method. The reason for this is that in the $\bar{v}$ method, the low energy end of the 1/E tail increases the computed average velocity and leads to a higher calculated temperature. The semilog method does not include this effect because the straight line is fit only to the Maxwellian portion. As the lattice spacing increases, and with it the amount of moderation by the D_2O, the 1/E tail contribution becomes smaller; then, as Table 4.3 shows, the temperatures calculated by the two methods approach each other.

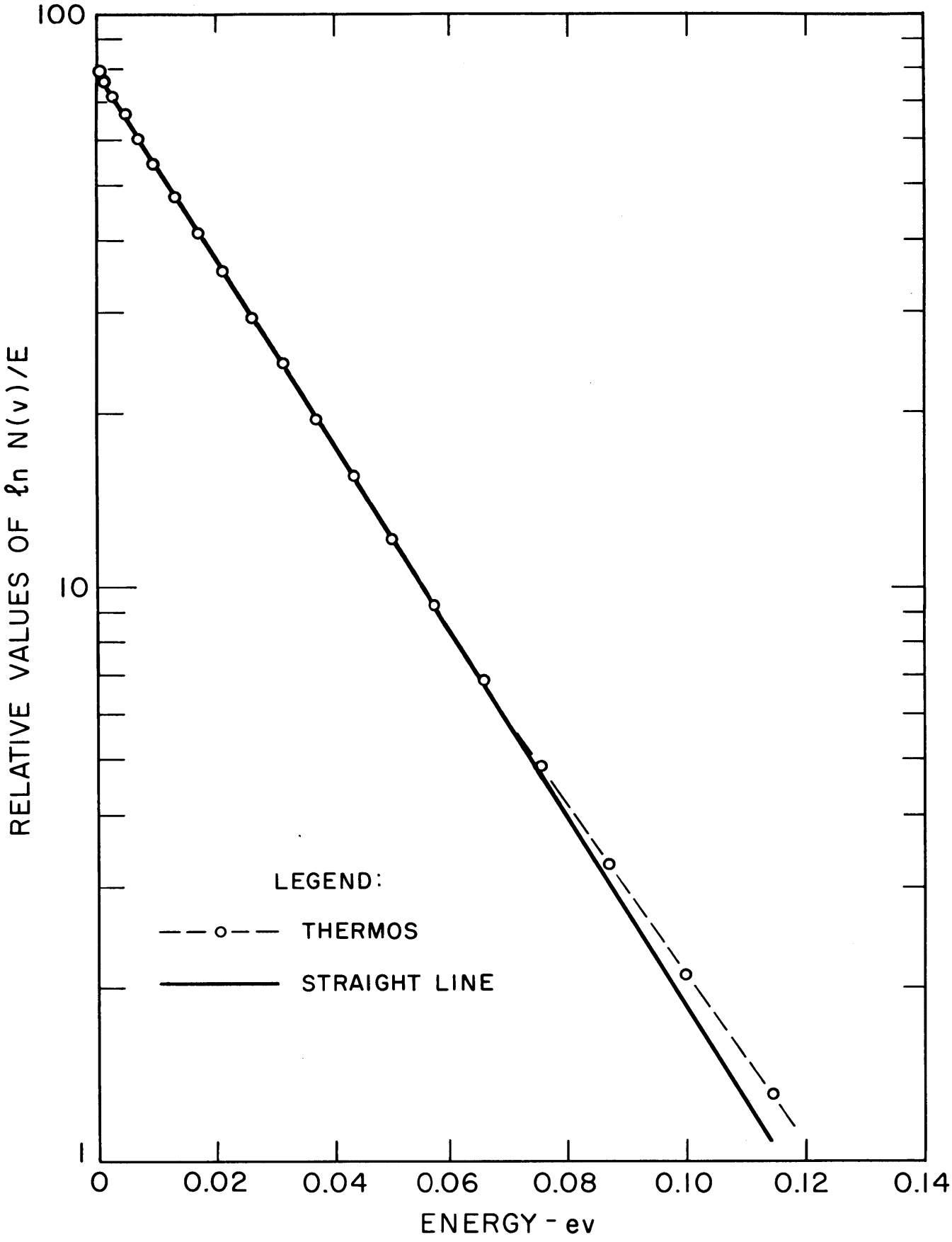

FIG. 4.40 TYPICAL PLOT OF ℓn N(v)/E vs. ENERGY AT CELL EDGE (4.5 - IN. LATTICE)

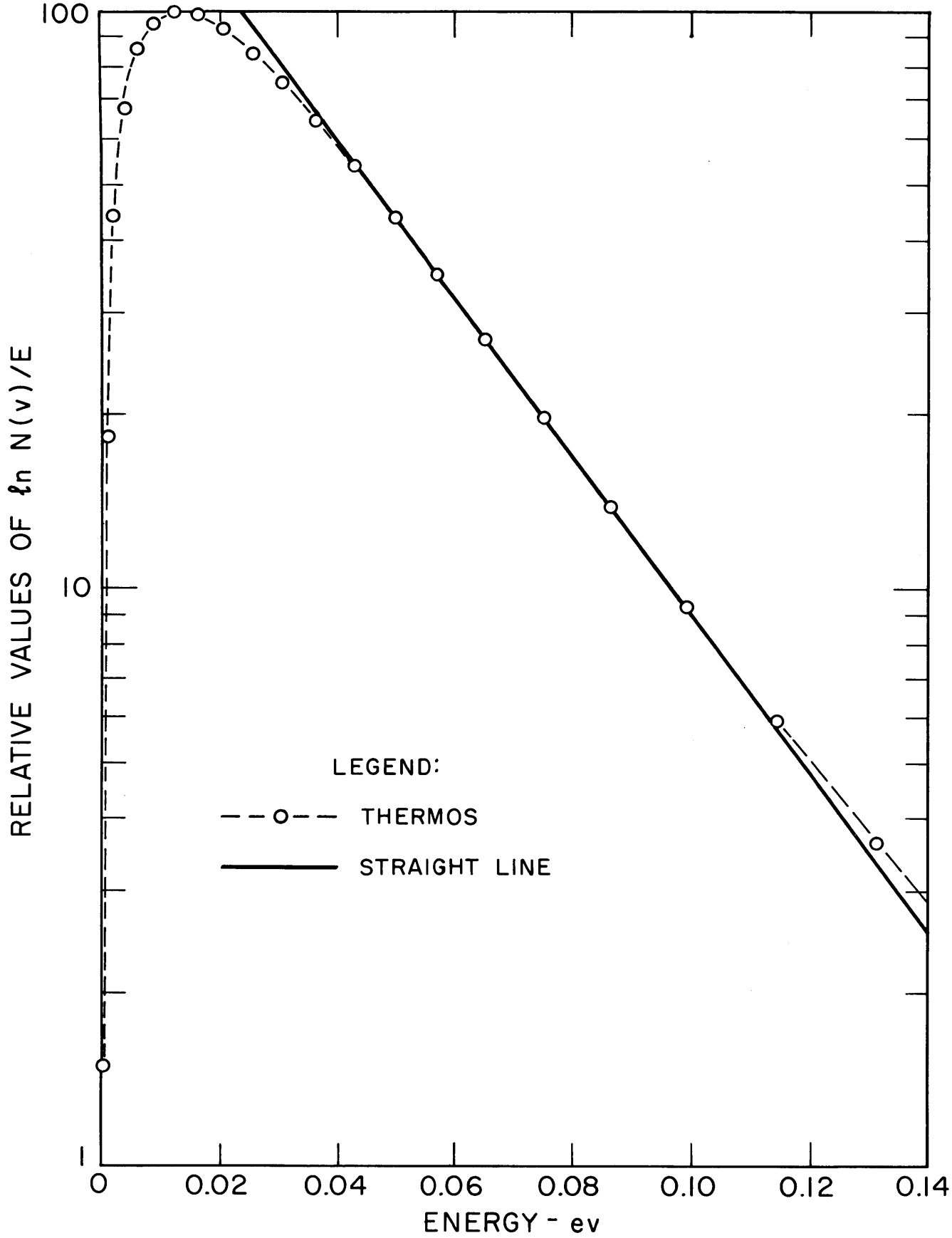

FIG. 4.41 TYPICAL PLOT OF ℓn N(v)/E vs. ENERGY AT CENTER OF FUEL (4.5-IN. LATTICE)

TABLE 4.3

Comparison of Cell Edge Temperatures Obtained by the $\bar{v}$ and Semilog Methods

Lattice Spacing (inches)	$\bar{v}$ Method	Semilog Method
4.5	59.3° C	40.5° C
5.0	51.1	36.2
5.75	42.8	31.7

Temperature changes from cell edge to rod surface and rod center have been calculated from the lutetium, europium, and gold data. Temperatures obtained with both the $\bar{v}$ and semilog method have been used at the cell edge, giving two sets of temperature changes. The temperature changes from the cell edge to other points in the cell should be independent of the magnitude of the cell edge temperature, if this temperature does not vary too much. In Tables 4.4 and 4.5 are shown the temperature changes from cell edge to cell center for the semilog and v methods, respectively. The columns entitled $\Delta T_{THERMOS}$ are the theoretical temperature changes based upon the $\bar{v}$ method.

TABLE 4.4

Temperature Changes, Cell Edge to Cell Center, Semilog Fit to Cell Edge Spectrum

Lattice Spacing (inches)	$\Delta T_{THERMOS}$	ΔT_{Lu}	ΔT_{Eu}	$T_{Cell\ Edge}$
4.5	100.0° C	98.0 ± 9.6° C	87.0 ± 30° C	40.5° C
5.0	98.1	78.2 ± 9.5	98.7 ± 34	36.2
5.75	96.5	71.8 ± 8.1	80.1 ± 27.2	31.7

TABLE 4.5

Temperature Changes, Cell Edge to Cell Center,
$\bar{\nu}$ Fit to Cell Edge Spectrum

Lattice Spacing (inches)	$\Delta T_{THERMOS}$	ΔT_{Lu}	ΔT_{Eu}	$T_{Cell\ Edge}$
4.5	100.0° C	105.8 ± 10.8° C	93.3 ± 33.7° C	59.3° C
5.0	98.1	83.0 ± 10.2	104.2 ± 37.2	51.1
5.75	96.5	75.3 ± 8.5	83.3 ± 28.9	42.8

It is evident that the temperature changes in the two tables are almost the same, within the experimental uncertainties. The lutetium and europium temperature changes agree within the experimental uncertainties, but the europium temperature changes have much greater uncertainties than those for lutetium. The g factors for these nuclides have been determined to about 2.5%. Since the g factor for europium varies with temperature much more slowly than that for lutetium, a 2.5% uncertainty in the g factor leads to a much larger uncertainty in the temperature. The 2.5% uncertainty may, however, be somewhat large in view of the good agreement of the europium and THERMOS results.

The lutetium temperature changes agree with those given by THERMOS for the 4.5-inch lattices, but differ significantly from the latter at the larger lattice spacings. The calculations in these tables were made with the latest edition of the Westcott cross sections (AECL-1101) (W4). Earlier calculations made with an earlier edition (AECL-670) (W5) gave better agreement. The lack of agreement between the two editions of Westcott and the THERMOS calculations is probably due to uncertainties in the lutetium cross section and, especially, to the approximations of the Westcott method. The Westcott method is based on the arbitrary choice of a Maxwellian with a 1/E tail always joining at approximately the same energy. Computed THERMOS spectra show that the joining point cannot be defined so simply, and that the thermal spectrum cannot always be represented by a Maxwellian distribution because of hardening effects. In spite of the approximations, however, the Westcott method does give results for well-moderated lattices which do not differ too much from THERMOS to be without use. Horowitz and

Tretiakoff (H12) have developed a method for defining effective cross sections which should be an improvement over Westcott's method. A thermalization operator based on the heavy gas model is used to characterize the spectrum rather than a Maxwellian distribution with a 1/E tail. Horowitz and Tretiakoff have also treated the effects of heterogeneity and hardening. Instead of using the concept of neutron temperature, they have tried to characterize the neutron distribution "by means of a small number of parameters, each of them directly related to a definite physical property of the lattice." Up to now, they have published cross sections for U^{235} and Pu^{239}.

In Tables 4.6 and 4.7 are shown the temperature changes from cell edge to rod surface (surface of cladding) for semilog and $\bar{v}$ fits to the cell edge temperatures, respectively.

TABLE 4.6

Temperature Changes, Cell Edge to Rod Surface,
Semilog Fit to Cell Edge Spectrum

Lattice Spacing (inches)	$\Delta T_{THERMOS}$	ΔT_{Lu}	ΔT_{Eu}	$T_{Cell\ Edge}$
4.5	38.0 ± 5.0° C	31.0 ± 7.0° C	15.8 ± 23.7° C	40.5° C
5.0	38.0 ± 5.0	27.8 ± 7.9	31.0 ± 28.3	36.2
5.75	38.0 ± 5.0	27.7 ± 5.6	29.8 ± 23.3	31.7

TABLE 4.7

Temperature Changes, Cell Edge to Rod Surface,
$\bar{v}$ Fit to Cell Edge Spectrum

Lattice Spacing (inches)	$\Delta T_{THERMOS}$	ΔT_{Lu}	ΔT_{Eu}	$T_{Cell\ Edge}$
4.5	38.0 ± 5.0° C	33.5 ± 8.0° C	16.8 ± 24.8° C	59.3° C
5.0	38.0 ± 5.0	29.4 ± 8.3	32.0 ± 28.0	51.1
5.75	38.0 ± 5.0	28.7 ± 7.4	31.0 ± 24.0	42.8

The uncertainty assigned to the THERMOS temperature change in Tables 4.6 and 4.7 is due to the lack of a THERMOS mesh point at the cladding surface and the need to interpolate between the cladding temperature and the temperature at the first mesh point in the moderator where the temperature gradient is steep. For the most part, the discussion concerning the results in Tables 4.4 and 4.5 also applies to the results of Tables 4.6 and 4.7.

In computing the Westcott effective temperatures, it was necessary to compute the r factors. The values for these r factors are shown in Tables 4.8 and 4.9, for the semilog and $\bar{v}$ fits to the cell edge temperature, respectively.

TABLE 4.8

Values of the r Factor, Semilog Fit to Cell Edge Spectrum

Lattice Spacing (inches)	Cell Edge	Rod Surface	Rod Center
4.5	0.0479 ± 0.0021	0.0556 ± 0.0029	0.0714 ± 0.0031
5.0	0.0377 ± 0.0017	0.0452 ± 0.0020	0.0586 ± 0.0026
5.75	0.0290 ± 0.0013	0.0355 ± 0.0015	0.0463 ± 0.0020

TABLE 4.9

Values of the r Factor, $\bar{v}$ Fit to the Cell Edge Spectrum

Lattice Spacing (inches)	Cell Edge	Rod Surface	Rod Center
4.5	0.0464 ± 0.0020	0.0541 ± 0.0023	0.0693 ± 0.0030
5.0	0.0369 ± 0.0016	0.0442 ± 0.0020	0.0572 ± 0.0025
5.75	0.0285 ± 0.0012	0.0349 ± 0.0015	0.0455 ± 0.0020

The r factors in Tables 4.8 and 4.9 are the same within the experimental uncertainties. The largest contribution to this uncertainty is a 4% uncertainty in the value of the gold resonance integral.

4.2.6 COMPARISON OF THE AMOUYAL-BENOIST-HOROWITZ METHOD AND THERMOS

The Amouyal-Benoist-Horowitz (ABH) method was used to compute the values of $\phi_a/\bar{\phi}_f$, the ratio of the flux at the fuel rod surface to the average flux in the fuel, and the values of $\bar{\phi}_m/\bar{\phi}_f$ (also denoted by FF_m), the ratio of the average flux in the moderator to the average flux in the fuel. In the calculations, the effects of spectral hardening in the fuel were accounted for by using the average hardened cross sections computed with the THERMOS code for each region of the cell. The ABH method is one of the better single velocity methods used to calculate disadvantage factors. It is difficult, however, to compare the calculations made by this method directly with experiment, because experiments with 1/v-absorbers measure neutron densities and the ABH method deals with neutron fluxes. An experimentally measured neutron density must be multiplied by the average velocity to convert it to a neutron flux. To do this, it is necessary to know the degree of spectral hardening, which causes the average velocity to vary significantly from the moderator to the fuel. Since the neutron density distributions measured with gold in the natural uranium lattices agree with those computed with THERMOS, the flux disadvantage factors computed with THERMOS will be compared with those obtained by the ABH method. This procedure is equivalent to comparing the ABH disadvantage factors with those obtained from the experimental neutron densities transformed into fluxes by multiplication with the appropriate values of $\bar{v}$.

In Tables 4.10 and 4.11 are listed values of $\bar{\phi}_m/\bar{\phi}_f$ and $\phi_a/\bar{\phi}_f$ as computed by THERMOS and the ABH method with THERMOS-averaged cross sections.

TABLE 4.10

Values of $\bar{\phi}_m/\bar{\phi}_f$ for the Natural Uranium Lattices

Lattice Spacing (inches)	ABH	THERMOS
4.5	1.546	1.570
5.0	1.580	1.594
5.75	1.623	1.625

TABLE 4.11

Values of $\phi_a/\bar{\phi}_f$ for the Natural Uranium Lattices

Lattice Spacing (inches)	ABH	THERMOS
4.5	1.146	1.158
5.0	1.149	1.160
5.75	1.152	1.163

The disadvantage factors calculated by the two methods are in excellent agreement. The agreement between the THERMOS and the ABH values for $\bar{\phi}_m/\bar{\phi}_f$ seems to improve slightly as the lattice spacing increases. This may be due to the fact that, in the ABH method, the moderator flux, which is based on diffusion theory, is only approximate at distances less than a mean free path from the rod; at distances greater than a mean free path, the flux may be accurately represented by diffusion theory. Thus, the larger the moderator region, the larger will be the region to which diffusion theory is applicable, and the better will be the results of the ABH treatment. Since THERMOS does not calculate a flux at the rod surface, graphical interpolation between the adjacent mesh points in the fuel and cladding has been necessary to get a value for ϕ_a. Since this is a region of high flux gradient, inaccuracy in this interpolation may be the reason for the 1.0% difference between the results for the two methods in Table 4.11.

The results of this section show, for the natural uranium lattices measured at M.I.T., that the ABH method could be a useful tool for the calculation of disadvantage factors, provided that a good table of effective hardened cross sections is available, an example of which will be presented in the next section. Honeck (H11) has also found that the ABH method gives very good agreement with experiment for uranium, water lattices. Theys (T2) has applied the method to uranium lattices moderated by water, heavy water, and graphite, respectively. The ABH method gave excellent agreement with experiment for the values of $\phi_a/\bar{\phi}_f$ for all of the moderators. The agreement between the ABH method and experiment for the values of FF_m was very good for the water and heavy water lattices, but not as good for the graphite lattices. The reason for the disagreement in the case

of graphite is not clear; it may be due to the lack of sufficiently detailed, published, experimental results.

4.2.7 COMPARISON WITH OTHER RESULTS

Measurements of intracell neutron distributions and disadvantage factors have been made, at other laboratories, in heavy water-moderated lattices of 1.0-inch diameter natural uranium rods. In this section, the results obtained at M.I.T. will be compared with earlier results.

Measurements of intracell neutron distributions were made at the North American Aviation Company (NAA) in a heavy water-moderated exponential assembly (H4, W10, B2, C4). The lattices contained natural uranium rods, 1.0-inch in diameter, and clad with aluminum, 0.1 cm thick, in square arrays with spacings of 3.625 inches, 4.5 inches, 4.9 inches, 7.5 inches, 9.0 inches, and 12.0 inches, respectively. The detectors used were: gold, lead-indium, dysprosium, manganese, and europium. The measured NAA activity distributions have been compared (H7, H8)with those computed with THERMOS. With normalization at the cell edge, the theoretical neutron density distributions deviated less than 4% from the experimental results. The agreement between theory and experiment was considered to be good, although the statistical accuracy of the measurements was about 2% and the scatter of the results was as much as 10%. The experimental distributions of europium activity agreed well with those computed with THERMOS. The epicadmium europium activity was multiplied by a factor of 1.4 to correct for the effects of the europium resonance at 0.46 ev (B2, H4). This factor is different from that (2.246) used in the present experiments; the source of the NAA value is not clear from the available literature.

The ratio of the neutron density at the fuel surface to the average neutron density in the fuel was found to be 1.198 ± 0.018, for one-inch rods, in the NAA experiments. No change in this ratio was observed as the rod spacing was changed, and the above value is the average of the ratios measured in all the lattices at NAA. The results of some measurements made at the Argonne National Laboratory (ANL) on 1.0-inch diameter uranium rods in heavy water have also been reported (C4). A value of 1.192 was found for the ratio of the neutron density at the fuel surface to the average neutron density in the rod. The average value for

the three natural uranium lattices studied at M.I.T. is 1.225 ± 0.010, only 2.2% higher than that of NAA. The results at M.I.T., NAA, and ANL are, therefore, all in good agreement.

The experimental values of the ratio of the average neutron density in the fuel, found at NAA and M.I.T., are shown in Fig. 4.42. The M.I.T. values lie about 3.5% higher than those obtained at NAA. In view of the experimental uncertainties, the agreement between the two is good. The fact that this ratio and the ratio mentioned in the preceding paragraph are both lower in the NAA lattices, seems to be due to a greater neutron density in the fuel of the NAA lattices. (This may be due to fission product contamination of the foils in the fuel at NAA. It is not clear from the available literature whether or not NAA used catcher foils to protect the detectors.) It seems unlikely that the observed differences are due to the use of a triangular array at M.I.T., and a square array at NAA.

4.2.8 NATURAL URANIUM LATTICES: TABULATION OF SOME USEFUL PARAMETERS

In this section, some useful parameters will be tabulated which have been calculated from the experimental and theoretical distributions in the natural uranium lattices. The parameters are: values of disadvantage factors and of the thermal utilization, temperature distributions, effective cross sections of the lattice materials, and effective cross sections of some detectors used in measuring neutron distributions.

Theoretical values of flux disadvantage factors were given in section 4.2.5. However, since gold activation measures the neutron density, neutron density disadvantage factors were obtained from the experimental gold activity distributions. These disadvantage factors were obtained by graphical integration of the gold distributions over the volume of each cell region. The results of these integrations, together with the neutron density disadvantage factors computed with THERMOS, are listed in Table 4.12. The experimental and theoretical disadvantage factors agree. The experimental values of $\bar{N}_{clad}/\bar{N}_{fuel}$ are all slightly smaller than the THERMOS values. This result may by due to the lack of experimental data in the clad; without an experimental activity in the cladding, there is some uncertainty in the flux shape between the outer fuel region and the inner moderator region.

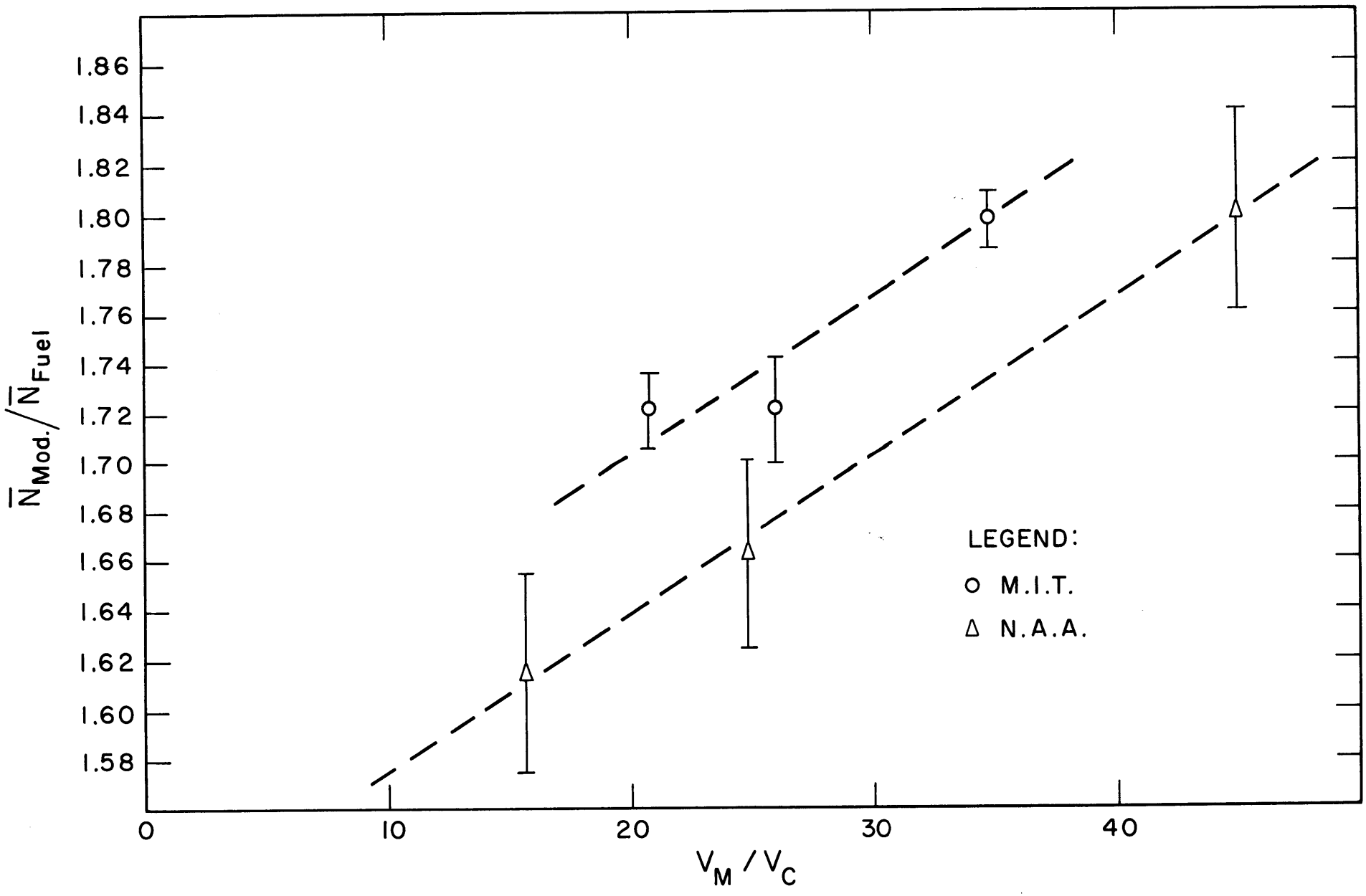

FIG. 4.42 COMPARISON OF M.I.T. AND N.A.A. VALUES OF $\bar{N}_{Mod}/\bar{N}_{Fuel}$

TABLE 4.12

Thermal Neutron Density Disadvantage Factors for the Natural Uranium Lattices

Cell Spacing (inches)	$\frac{V_{mod}}{V_{fuel}}$	$\frac{\bar{N}_{mod}}{\bar{N}_{fuel}}$		$\frac{\bar{N}_{clad}}{\bar{N}_{fuel}}$	
		Experiment	THERMOS	Experiment	THERMOS
4.5	20.8	1.720±0.017	1.734	1.254±0.015	1.266
5.0	26.0	1.721±0.022	1.760	1.248±0.019	1.268
5.75	34.7	1.796±0.012	1.795	1.247±0.011	1.271

As was discussed in section 3.4, the thermal utilization can be calculated from the experimentally determined neutron density disadvantage factors; no account need be taken of spectral hardening since all absorption cross sections, except that of U^{235}, vary as 1/v, and the absorption cross section of U^{235} varies very nearly as 1/v. All the cross sections must, however, be evaluated at the same temperature. Calculations, with THERMOS, for uranium show that the product $\bar{\Sigma}\bar{v}$ changes by less than 1.0% from the moderator to the fuel. Thus, for all practical purposes, U^{235} may also be treated as a 1/v absorber. Equation (3.12a) was, therefore, used to determine the experimental values of the thermal utilization, with the values of $\bar{\Sigma}$ taken at 0.025 ev:

$$\frac{1}{f} = 1 + \frac{(\bar{\Sigma}V\bar{N})_{mod}}{(\bar{\Sigma}V\bar{N})_{fuel}} + \frac{(\bar{\Sigma}V\bar{N})_{clad}}{(\bar{\Sigma}V\bar{N})_{fuel}} \quad . \tag{3.12a}$$

The THERMOS values of f were computed from the THERMOS results for the absorption rates in each region. The ABH values of f were calculated using THERMOS hardened cross sections. The values obtained for f are shown in Table 4.13. The experimental and theoretical values of f are in excellent agreement. The major contribution to the uncertainties in both the theoretical and experimental values is a 22% uncertainty in the heavy water absorption cross section. The uncertainties in f are small because the values of f are close to unity.

TABLE 4.13

Thermal Utilization Values for the Natural Uranium Lattices (99.773% D_2O)

Lattice Spacing (inches)	$\frac{V_{mod}}{V_{fuel}}$	Experiment	THERMOS	ABH
4.5	20.8	0.9855 ± 0.0006	0.9849 ± 0.0006	0.9851 ± 0.0006
5.0	26.0	0.9836 ± 0.0007	0.9828 ± 0.0007	0.9830 ± 0.0007
5.75	34.7	0.9799 ± 0.0010	0.9792 ± 0.0010	0.9793 ± 0.0010

The degree of spectral hardening from moderator to fuel is a quantity of special interest, but it is difficult to describe this effect by a single physically significant number. Although the meaning of effective neutron temperature is questionable because of the non-Maxwellian behavior of the hardened spectrum, this concept has often been used. The change in the average subcadmium absorption cross section of a 1/v absorber, is a more useful idea operationally. Since many nuclides occurring in nature have a 1/v neutron capture cross section in the thermal energy region, the change in absorption cross section is indicative of how neutron absorption by cell materials varies with position in the cell. In Fig. 4.43 are plotted values of the THERMOS-averaged subcadmium (0.415 ev energy cutoff) cross sections of a 1/v absorber for the three natural uranium lattices. Figure 4.44 shows plots of neutron temperature as a function of cell position for the same three lattices; the temperatures at each point have been calculated by the $\bar{v}$ method described in section 4.2.5. Both of these figures illustrate the importance of the spectral hardening and the necessity of taking it into account in cell calculations.

In Table 4.14 are listed the values of the THERMOS-averaged subcadmium absorption cross sections of the cell materials; these cross sections have been averaged over the space of each region and up to an energy of 0.415 ev. The heavy water consists of 99.773% D_2O and 0.227% H_2O, by weight.

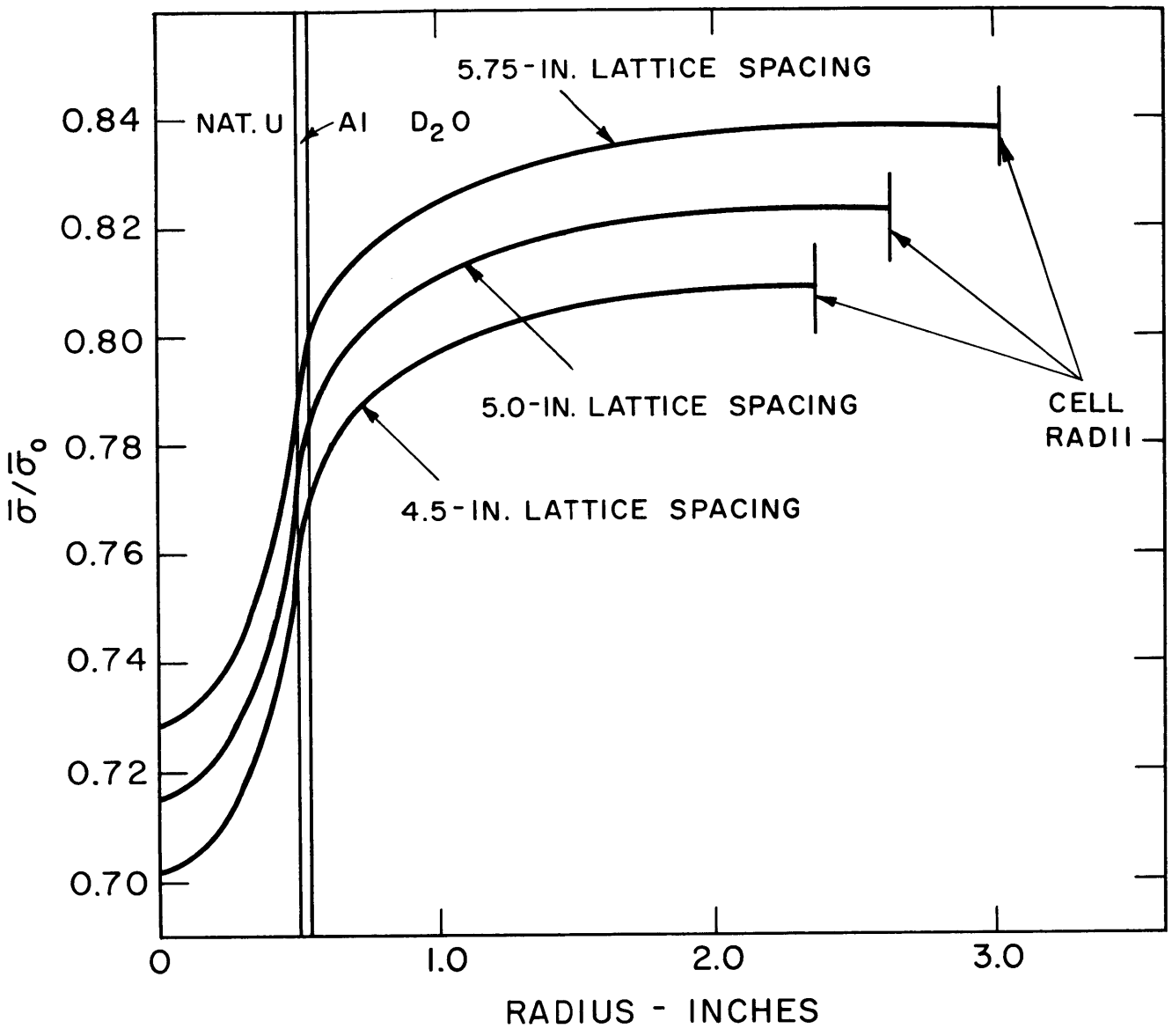

FIG. 4.43 AVERAGE CROSS SECTION OF A I/V ABSORBER, 1.010-IN. DIA. NAT. U RODS ON THREE TRIANGULAR SPACINGS

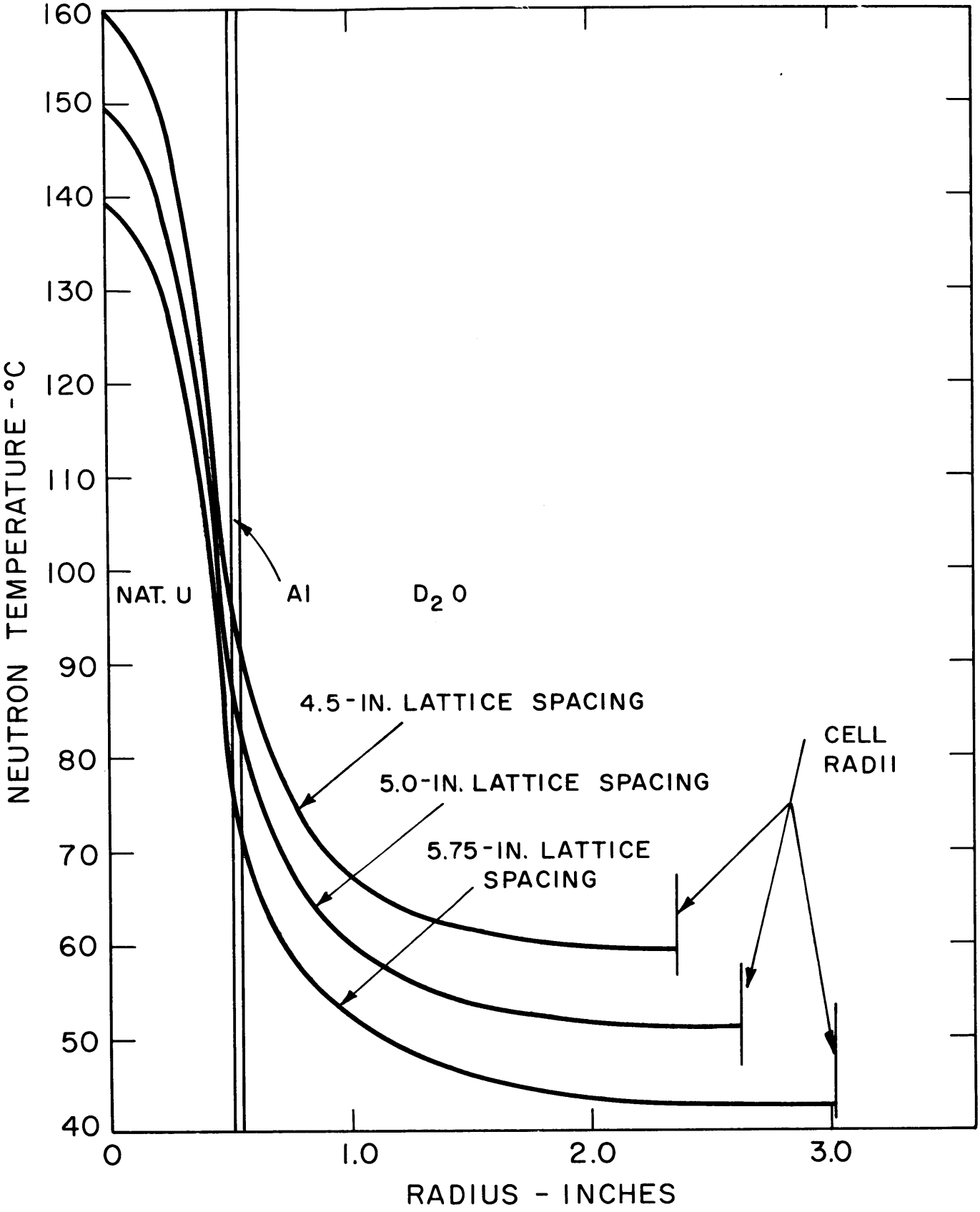

FIG. 4.44 NEUTRON TEMPERATURE DISTRIBUTIONS, 1.010-IN. DIA. NAT. U RODS ON THREE TRIANGULAR SPACINGS

TABLE 4.14

Average Subcadmium Absorption Cross Sections (in cm^{-1}) of Cell Materials in the Natural Uranium Lattices

Cell Spacing (inches)	$\frac{V_{mod}}{V_{fuel}}$	$\bar{\Sigma}(U^{235})$	$\bar{\Sigma}(U^{238})$	$\bar{\Sigma}(D_2O)$	$\bar{\Sigma}(Al)$
4.5	20.8	0.1633	0.09395	$(6.42)10^{-5}$	0.01063
5.0	26.0	0.1665	0.09567	$(6.54)10^{-5}$	0.01082
5.75	34.7	0.1699	0.09750	$(6.67)10^{-5}$	0.01103

In Table 4.15 are listed THERMOS-averaged values of subcadmium activation cross sections of detectors commonly used in lattice measurements. The cross sections have been averaged over space and up to an energy of 0.415 ev. The activation cross sections of Pu^{239}, U^{235}, and U^{233} are equivalent to the fission cross sections of these nuclides. All cross sections in this table are based on the latest BNL-325 (H13) 2200 m/sec. cross sections, which are listed in the last line of the table. Europium-151 has been included in this table but, because of the 0.46 ev resonance, the values for europium are probably not very useful. In Table 4.16 are listed europium cross sections which have been averaged over energy up to 0.194 ev and 0.785 ev, corresponding to the two cutoff energies discussed earlier in this chapter.

TABLE 4.15

Average Subcadmium Activation Cross Sections (barns)
of Nuclides Commonly Used to Measure Activity
Distributions, Natural Uranium Lattices

Cell Spacing (inches)	$\frac{V_M}{V_U}$	$\bar{\sigma}(Au)$	$\bar{\sigma}(Lu^{176})$	$\bar{\sigma}(Eu^{151})$	$\bar{\sigma}(Dy^{164})$	$\bar{\sigma}(Pu^{239})$	$\bar{\sigma}(U^{235})$	$\bar{\sigma}(U^{233})$
			Fuel					
4.5	21.0	72.0	7037	5009	575	716	405	381
5.0	26.4	73.3	6963	5100	587	703	413	387
5.75	35.6	74.7	6885	5195	599	689	422	395
			Moderator					
4.5	21.0	79.5	6690	5863	637	737	453	420
5.0	26.4	80.9	6610	5987	650	728	462	427
5.75	35.6	82.5	6520	6120	664	719	472	435
σ(2200 m/sec) - Latest BNL-325 values:		98.8	4000	7800	800	742	582	525

TABLE 4.16

Average Cross Sections (barns) of Eu^{151} in the Natural Uranium Lattices

Cell Spacing (inches)	Cutoff Energy 0.194 ev	Cutoff Energy 0.785 ev
	FUEL	
4.5	5106	5279
5.0	5188	5319
5.75	5271	5363
	MODERATOR	
4.5	5996	6032
5.0	6104	6121
5.75	6218	6220

4.3 THE LATTICE OF 0.25-INCH DIAMETER, SLIGHTLY ENRICHED URANIUM RODS WITH A SPACING OF 1.25 INCHES

A program is now underway at M.I.T. to study the physics of heavy water lattices of 0.25-inch diameter rods with U^{235} concentrations of 1.03 and 1.15 per cent, respectively. A study of the first lattice, consisting of 1.03 per cent U^{235} rods with a triangular spacing of 1.25 inches, has just been completed. Because the unit lattice cell is so different in physical dimensions from those of the natural lattices studied, the first measurements on them served to produce useful information about various parameters, and also to test the methods for measuring these parameters. The results of these measurements, together with an evaluation of the theoretical and experimental methods used, will be discussed in this section.

4.3.1 GOLD ACTIVITY DISTRIBUTIONS

Three kinds of gold foils were used to measure the gold activity distribution in the 1.25-inch lattice: one-sixteenth inch diameter pure gold foils, one-thirty-second inch diameter pure gold foils, and one-sixteenth inch diameter foils containing 13.6 weight per cent gold in lead. The one-thirty-second inch foils were used to obtain a more detailed mapping of the flux inside the rod, and to determine the effects, if any, of flux

depression by the larger one-sixteenth inch foils. The lead-gold foils closely matched the absorption and scattering properties of the fuel rod and were also used to determine the flux perturbation effects of the pure gold foils.

The experimental and theoretical results for the one-sixteenth inch gold, the one-thirty-second inch gold, and the lead-gold foils are shown in Figs. 4.45, 4.46, and 4.47, respectively. In Figs. 4.45, 4.46, and 4.47, several experimental activities are plotted at each radial position. For purposes of comparing the results of these three figures, in each figure all the activities at each radial position have been averaged and the average values for each of the three types of gold foils have been normalized to one another on the same graph in Fig. 4.48. Figure 4.48 shows that all three detectors give the same results within the experimental uncertainties.

In Figs. 4.45 to 4.48, the THERMOS results have been normalized to experiment both in the rod and at the cell edge. When the normalization is in the fuel, the theoretical and experimental results agree well in the rod; and the THERMOS code predicts the neutron distribution in the fuel accurately. However, the agreement in the moderator is poor. With normalization at the cell edge, the experimental curve in Fig. 4.48 is 13.2% higher than the THERMOS prediction at the cell center. The reasons for this large discrepancy will be discussed in section 4.3.4.

The activity distributions of the cadmium covered foils are flat in the moderator and dip slightly in the fuel. The activities of the lead-gold foils, however, dip appreciably more in the fuel than those of the pure gold foils. This result is to be expected in view of the discussion in Appendix E from which it may be seen that the value of $\frac{(CR-1)_{Pb\text{-}Au}}{(CR-1)_{0.002}}$, denoted here by the symbol, RC, should be a constant independent of the absolute value of the cadmium ratio. The value of RC derived from Fig. E.1 is 0.541 ± 0.009. The values of RC obtained from Figs. 4.45 and 4.47 are 0.565 ± 0.014 at the cell edge, and 0.601 ± 0.021 at the cell center. The value at the cell edge is in good agreement with the expected value (0.541), within the experimental uncertainties, but it is about 10% higher than the expected value at the cell center. This result could be due to a greater dip, in the fuel, of the epicadmium activity of the lead gold foils than

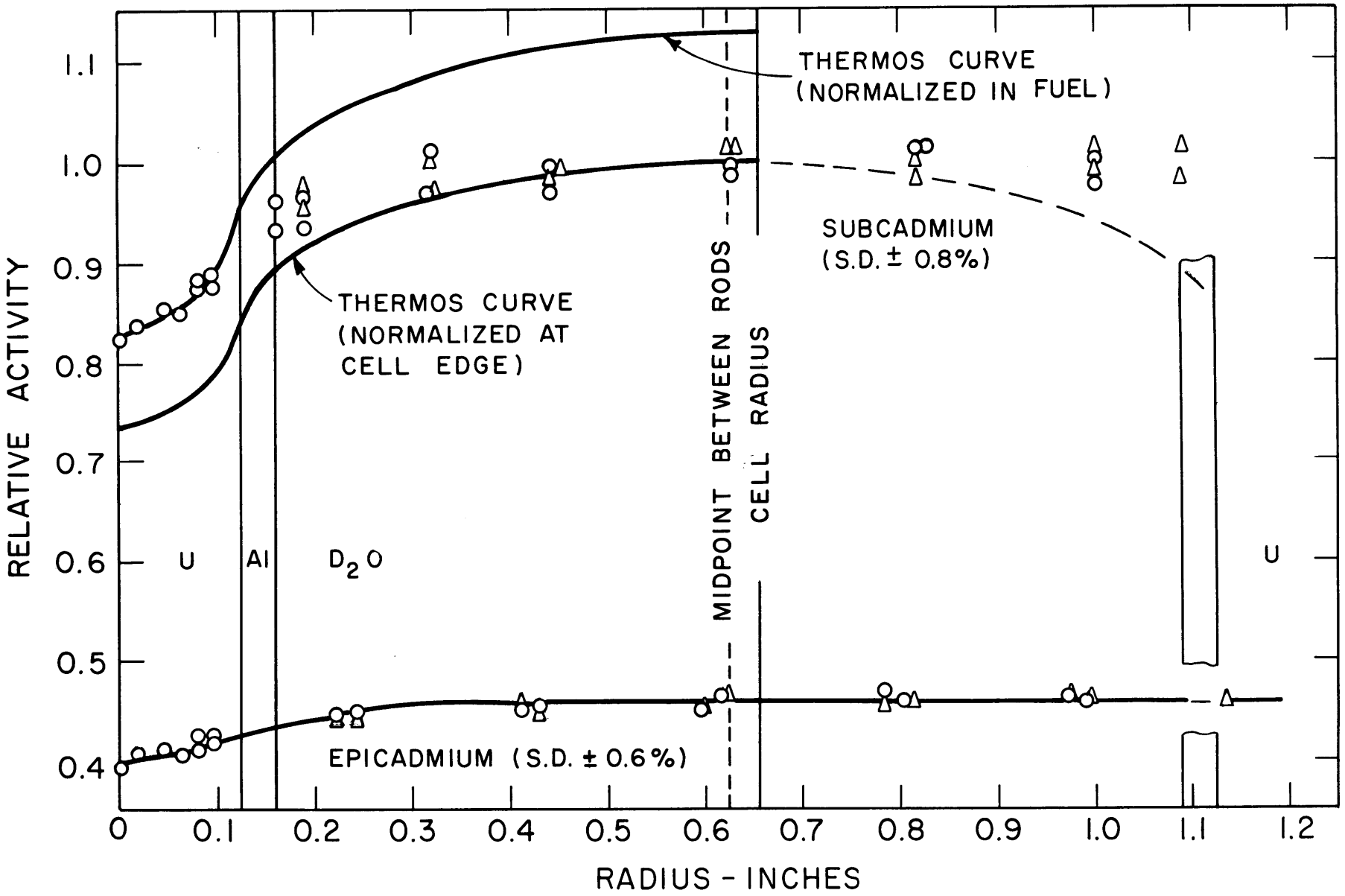

FIG.4.45 GOLD ACTIVITY DISTRIBUTION (1/16-IN. DIA. FOILS), 0.250-IN. DIA. RODS OF 1.03% U^{235} ON A 1.25-IN. TRIANGULAR SPACING

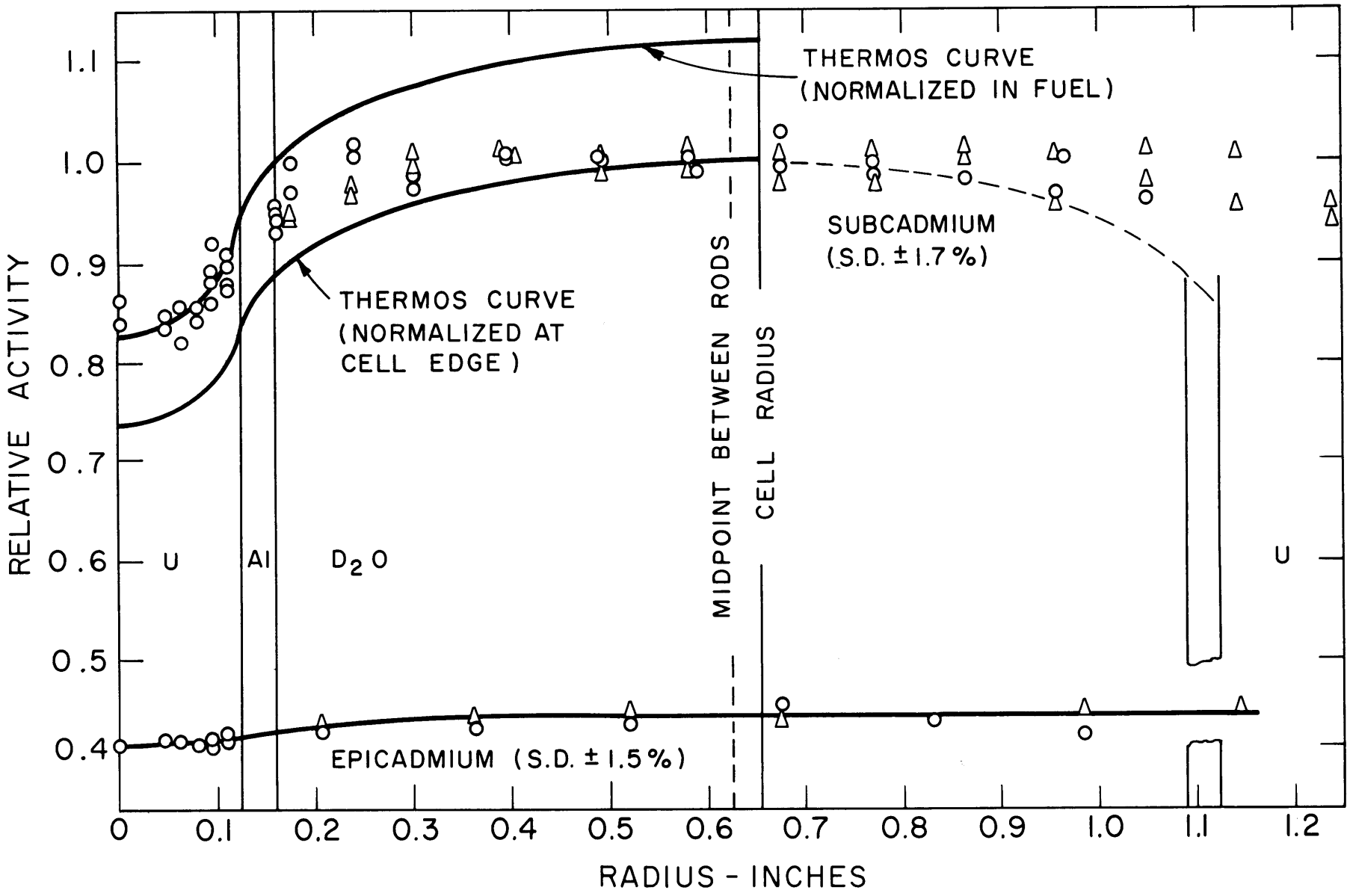

FIG. 4.46 GOLD ACTIVITY DISTRIBUTION (1/32-IN. DIA. FOILS), 0.250-IN. DIA. RODS OF 1.03% U^{235} ON A 1.25-IN. TRIANGULAR SPACING

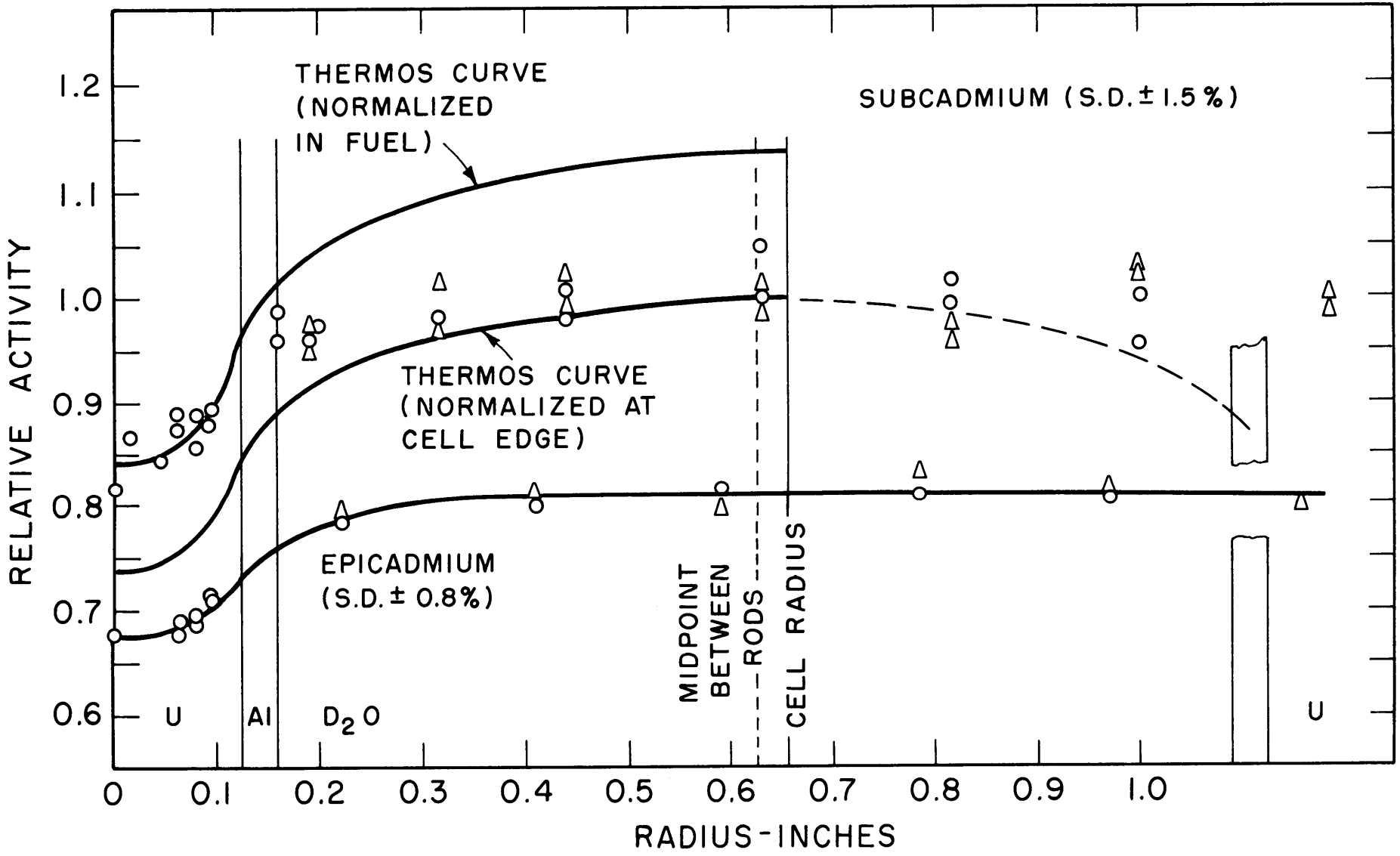

FIG. 4.47 GOLD ACTIVITY DISTRIBUTION (1/16-IN. DIA. Pb-Au FOILS), 0.250-IN. DIA. RODS OF 1.03% U^{235} ON A 1.25-IN. TRIANGULAR SPACING.

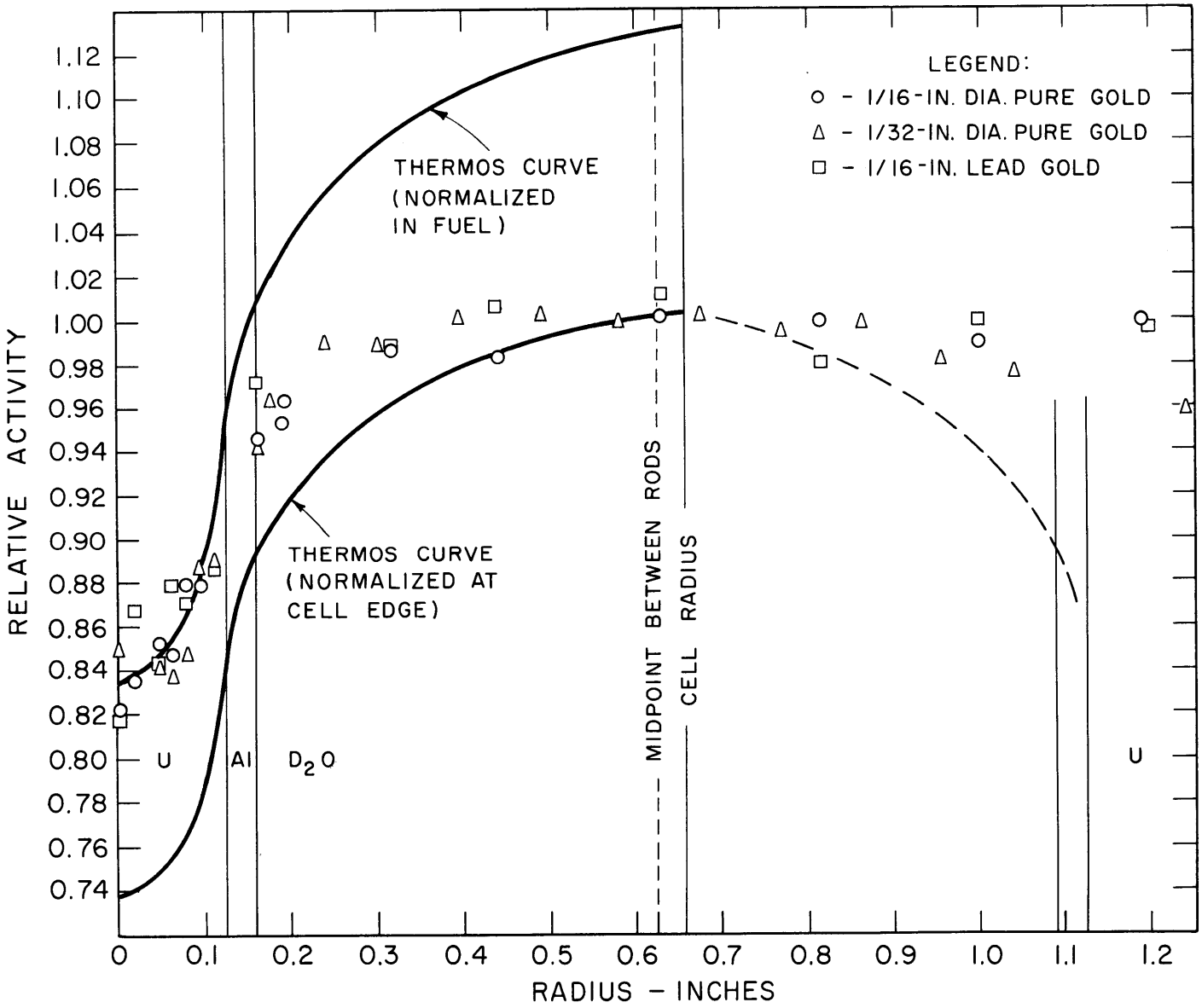

FIG. 4.48 SUBCADMIUM ACTIVITY DISTRIBUTION - COMPARISON OF 1/16 - IN. DIA. PURE GOLD, 1/32-IN. DIA. PURE GOLD, AND 1/16 - IN. DIA. Pb-Au, 0.25-IN. DIA. RODS OF 1.03% U^{235} ON A 1.25-IN. TRIANGULAR SPACING.

would be expected from requiring the value of RC to be constant. Such an increased dip may be due to a depression of the resonance flux by the relatively large amount of gold in the one-quarter inch diameter lead-gold foil located in the fuel. No similar thermal flux depression occurs, because the thermal absorption cross section of the lead-gold alloy matches that of the fuel. Since the resonance flux depression would be the same in both the bare and the cadmium-covered lead-gold foils that were exposed in the experiment, the thermal activity resulting from the subtraction of the epicadmium activity from the bare activity should be unaffected by the resonance flux depression.

Since the three kinds of gold detectors all gave the same thermal neutron distributions, it may be concluded that the effects of external thermal flux depression by the foils were small. Calculations show that the only significant foil perturbation is a self-shielding effect which depends on the difference between the absorption cross sections of the foil and the surrounding medium (see Appendix C). Since the absorption cross section of pure gold is much greater than that of either the uranium or the moderator, the self-shielding effect is very nearly the same in both media, and no correction need be applied in a relative measurement. Because the lead-gold foils match the absorption cross section of the uranium, the self-shielding effect in the fuel was negligible; but a correction of about 2% had to be applied to the foils in the moderator. The only other possible perturbation might arise from the replacement of fuel by nonfissionable foil material. The results do not, however, show such an effect, probably because only a very small amount of fuel material was displaced. The lead-gold foils, therefore, do not seem to offer any advantages over the pure gold foils for neutron density measurements. In fact, the lead-gold data have a somewhat greater scatter than do the pure gold data, because of lower activities and possibly because of slight inhomogeneities in the alloy. In addition, the epicadmium lead-gold activities are greater than those for pure gold because of the increased value of the gold resonance integral (a dilution effect). Hence, the thermal activities have a higher uncertainty owing to the subtraction of the greater epicadmium activity. The data for the one-thirty-second inch gold foils also have considerably more scatter than do those for the one-sixteenth inch foils, because of smaller activities and relatively greater uncertainty

in foil weight. The one-thirty-second inch foils could be weighed only to about one per cent because they were so light; it is recommended that such small foils be intercalibrated in the future in a uniform flux on a rotating foil wheel. Because the one-sixteenth inch foils are so much easier to handle and give less experimental scatter than the one-thirty-second inch foils, they are to be recommended for future measurements of activity distributions. They do not give as detailed a measurement of the distribution as the one-thirty-second inch foils, but the dip in the rod is so small that enough detail is obtained with the larger foils.

4.3.2 LUTETIUM ACTIVITY DISTRIBUTIONS

The lutetium activity distributions were measured with one-sixteenth inch diameter foils. The first lutetium measurements are shown in Fig. 4.49. The second measurements, done by Mr. E. Sefchovich (S1) are shown in Fig. 4.50. For purposes of comparing the results of Figs. 4.49 and 4.50, the activities at each radial position have been averaged for each measurement, and the averages have been plotted normalized to each other in Fig. 4.51, as was done for the gold distributions in Fig. 4.48. Within the scatter of the data, the two sets of measurements agree. The THERMOS results have been normalized to experiment, in Figs. 4.49 to 4.51, both at the cell edge and in the fuel.

The lutetium results show considerably more scatter than do the gold results. This is probably due to the low foil activity, which was only about four or five times the background of the counter. In Fig. 4.51, where the average activities at each radial position are plotted, most of the scatter is eliminated. Normalization in the fuel shows that there is good agreement between theory and experiment for the activity distribution in the fuel. With normalization at the cell edge, the experimental curve is about 12.8% higher than the THERMOS curve at the rod center. Future lutetium measurements will be made with foils containing a higher percentage of lutetium, which should improve the statistical accuracy. The lutetium foils will not be "infinitely thin" (see Appendix D), and the resulting foil perturbations may offer new problems.

The discrepancy between THERMOS and experiment will be discussed in section 4.3.4.

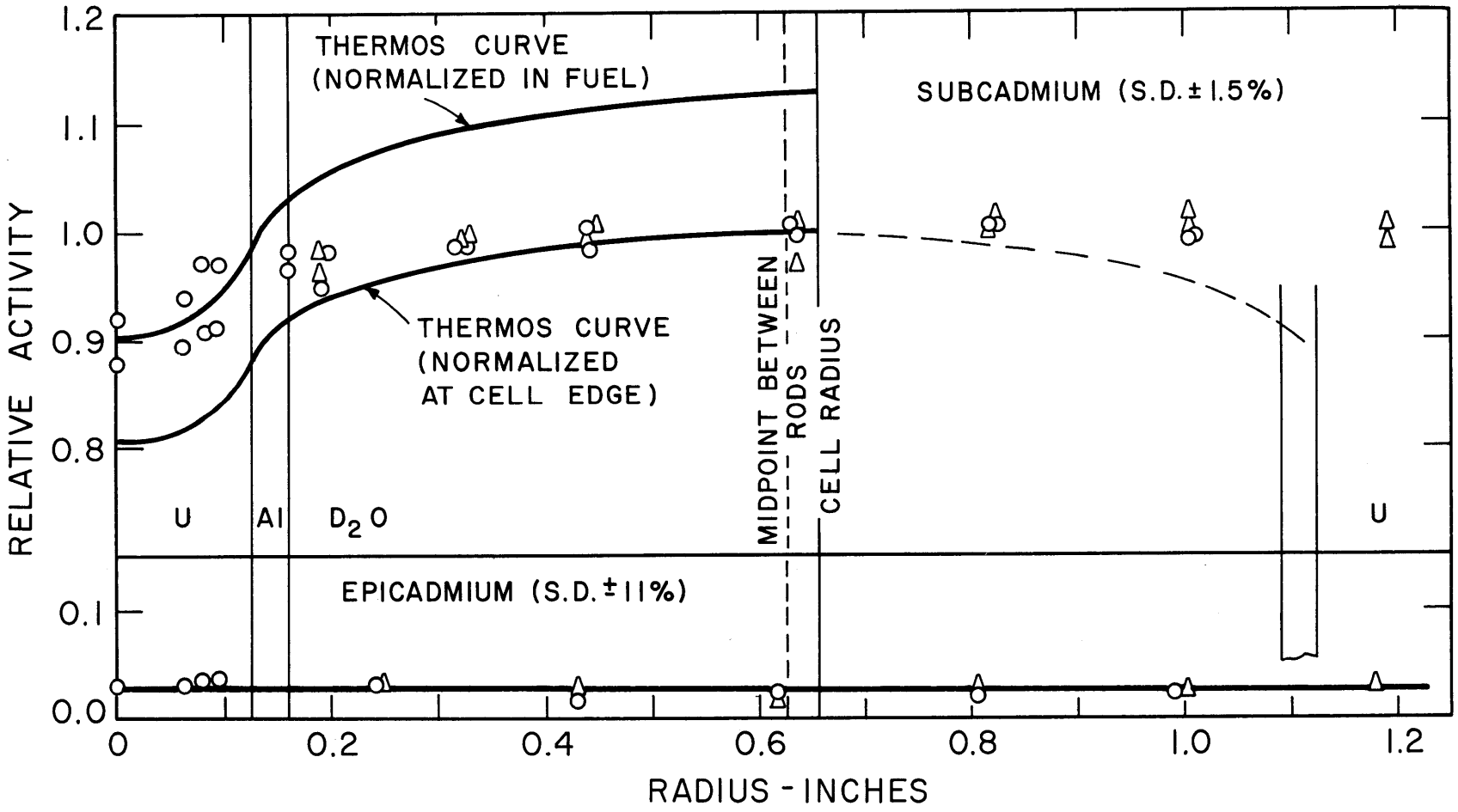

FIG. 4.49 LUTETIUM ACTIVITY DISTRIBUTION NO. 1, 0.25-IN. DIA. RODS OF 1.03% U^{235} ON A 1.25-IN. TRIANGULAR SPACING

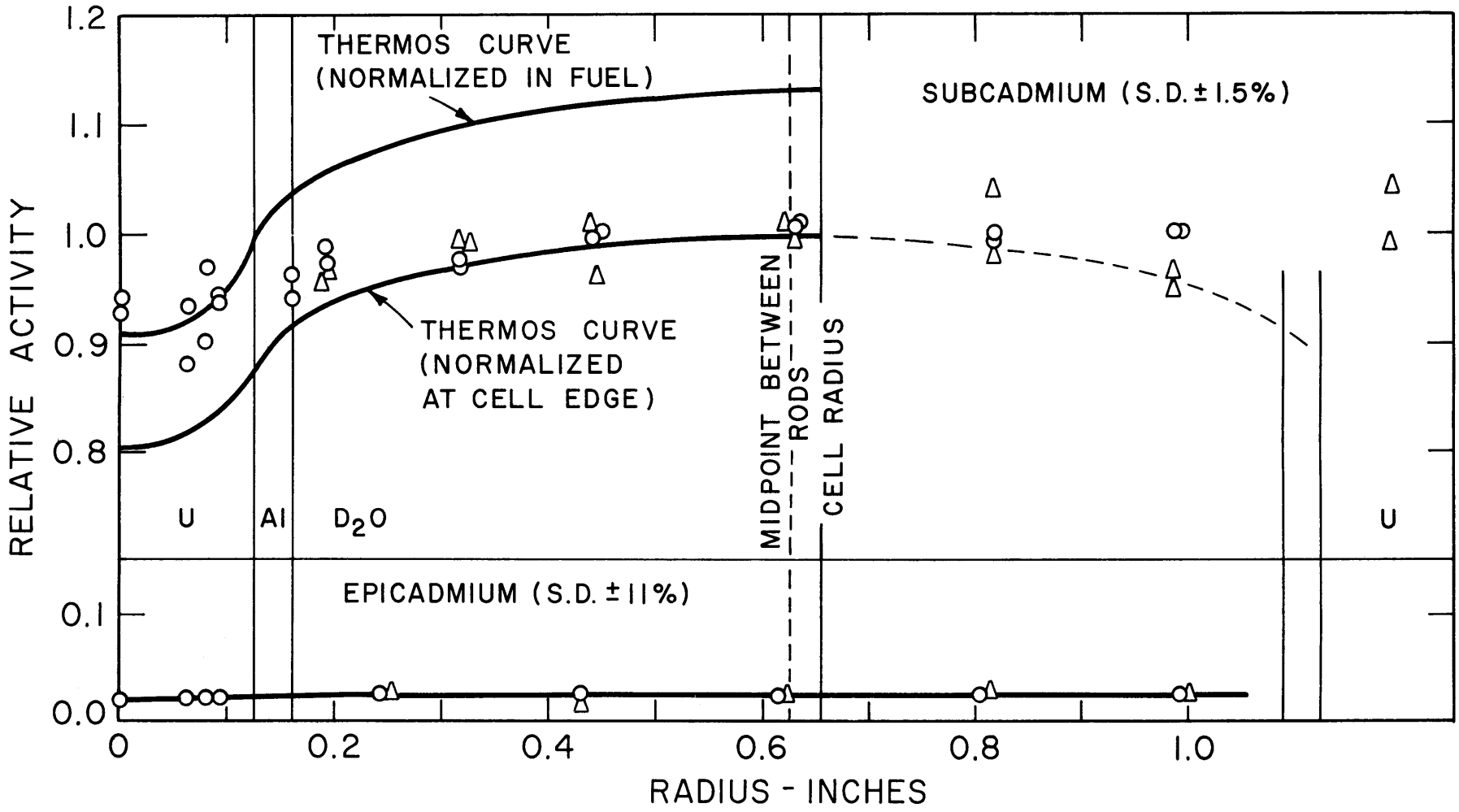

FIG. 4.50 LUTETIUM ACTIVITY DISTRIBUTION NO.2 (DONE BY SEFCHOVICH[SI]), 0.25-IN. DIA. RODS OF 1.03% U^{235} ON A 1.25-IN. TRIANGULAR SPACING

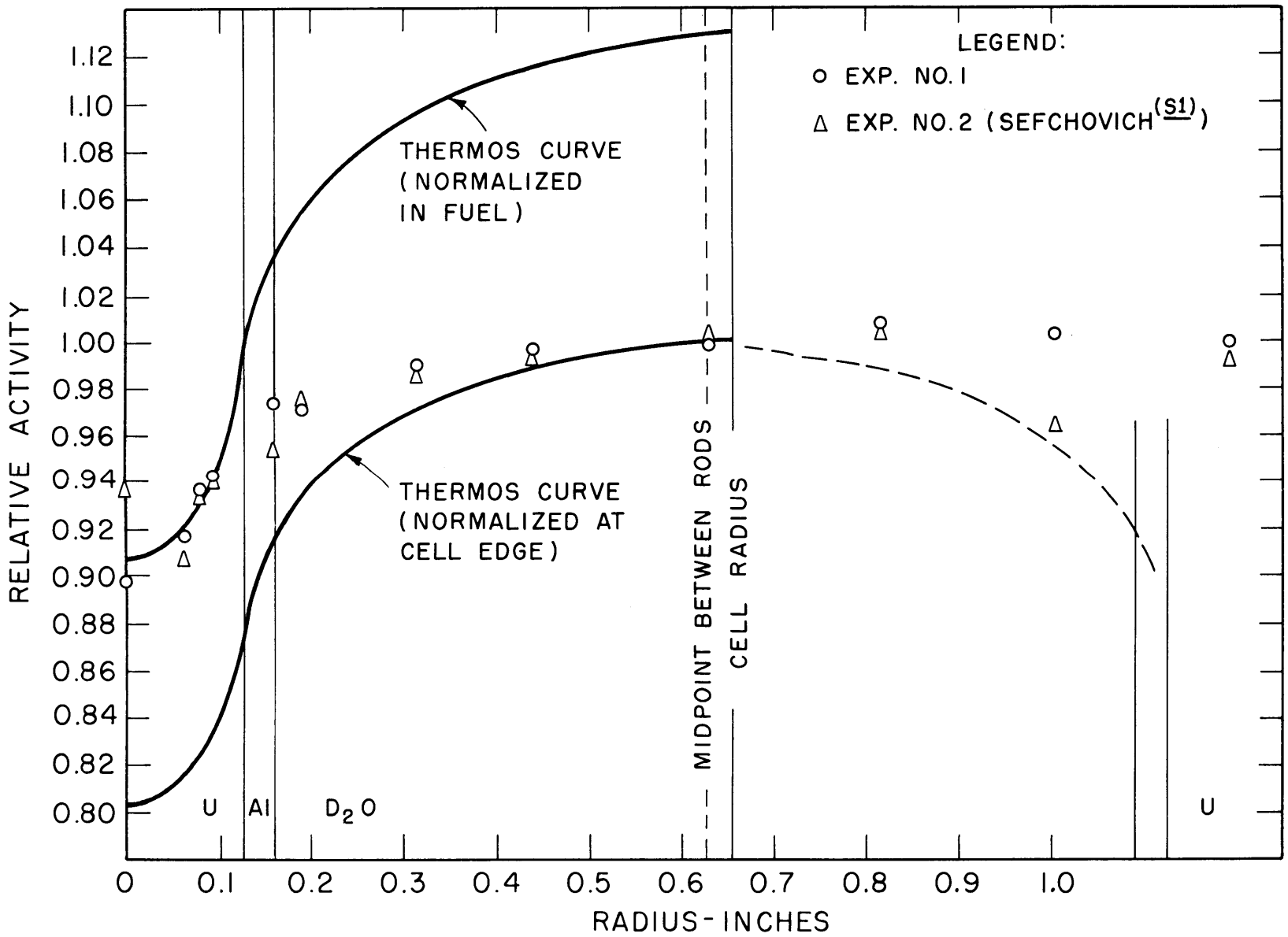

FIG. 4.51 SUBCADMIUM LUTETIUM ACTIVITY DISTRIBUTION-COMPARISON OF EXPERIMENTS NO.1 AND NO.2, 0.25-IN. DIA. RODS OF 1.03% U^{235} ON A 1.25-IN. TRIANGULAR SPACING

4.3.3 EUROPIUM ACTIVITY DISTRIBUTIONS

The europium activity distributions were made with one-sixteenth inch diameter foils. Two sets of europium measurements were made, the second by Mr. H. Kim (K1). Sets Nos. 1 and 2, with a cutoff energy of 0.785 ev, are shown in Figs. 4.52 and 4.53. The activities shown in Figs. 4.52 and 4.53 were averaged and normalized in the same way as the gold activities (Fig. 4.48), and are compared in Fig. 4.54. The results obtained with a cutoff energy of 0.194 ev, are shown in Figs. 4.55 and 4.56; the averaged activities of the two measurements are compared in Fig. 4.57. In all of these figures, the distributions computed with THERMOS have been normalized to experiment at the cell edge and in the fuel. Normalization in the fuel again shows that the activity distribution in the fuel computed with THERMOS agrees well with the experimental results. With a cutoff energy of 0.785 ev and normalization at the cell edge, the experimental curve is about 14.4% higher than the THERMOS curve at the center of the cell. With a cutoff energy of 0.194 ev, the experimental curve is about 17.5% higher than the THERMOS curve at the cell center. These discrepancies will be discussed in the next section.

4.3.4 DISAGREEMENT BETWEEN THEORY AND EXPERIMENT -- THE CYLINDRICAL CELL EFFECT

Before discussing the possible reasons for the large differences between the THERMOS and experimental distributions observed in the 1.25-inch lattice, several important points concerning the results should be mentioned.

1. The extent of the disagreement is approximately the same for gold (13.2%), lutetium (12.8%), and europium (14.4% and 17.5%). The activity ratios of lutetium or europium to gold are predicted by THERMOS to within a few per cent, indicating that THERMOS gives a good estimate of the degree of spectral hardening (or is consistently in error).

2. The neutron distribution in the fuel rod is, in all cases, very well fit by THERMOS. This result suggests that any errors in the theory may be due to some phenomenon in the treatment of the moderator region. The ability of THERMOS to predict correctly the extent of spectral hardening points to the same conclusion; since the hardening is almost entirely

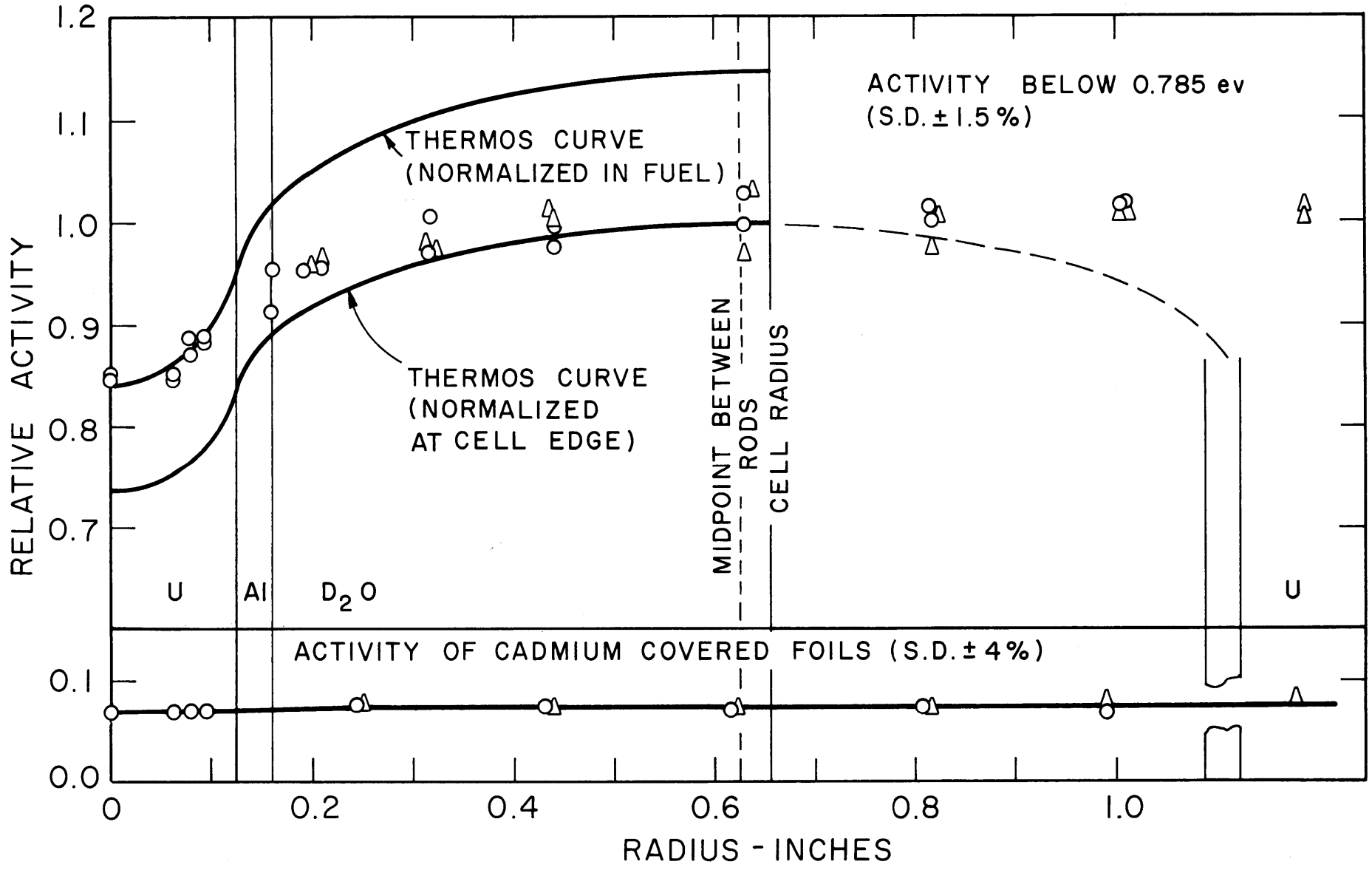

FIG. 4.52 EUROPIUM ACTIVITY DISTRIBUTION NO. 1a, 0.25-IN. DIA. RODS OF 1.03% U^{235} ON A 1.25-IN. TRIANGULAR SPACING

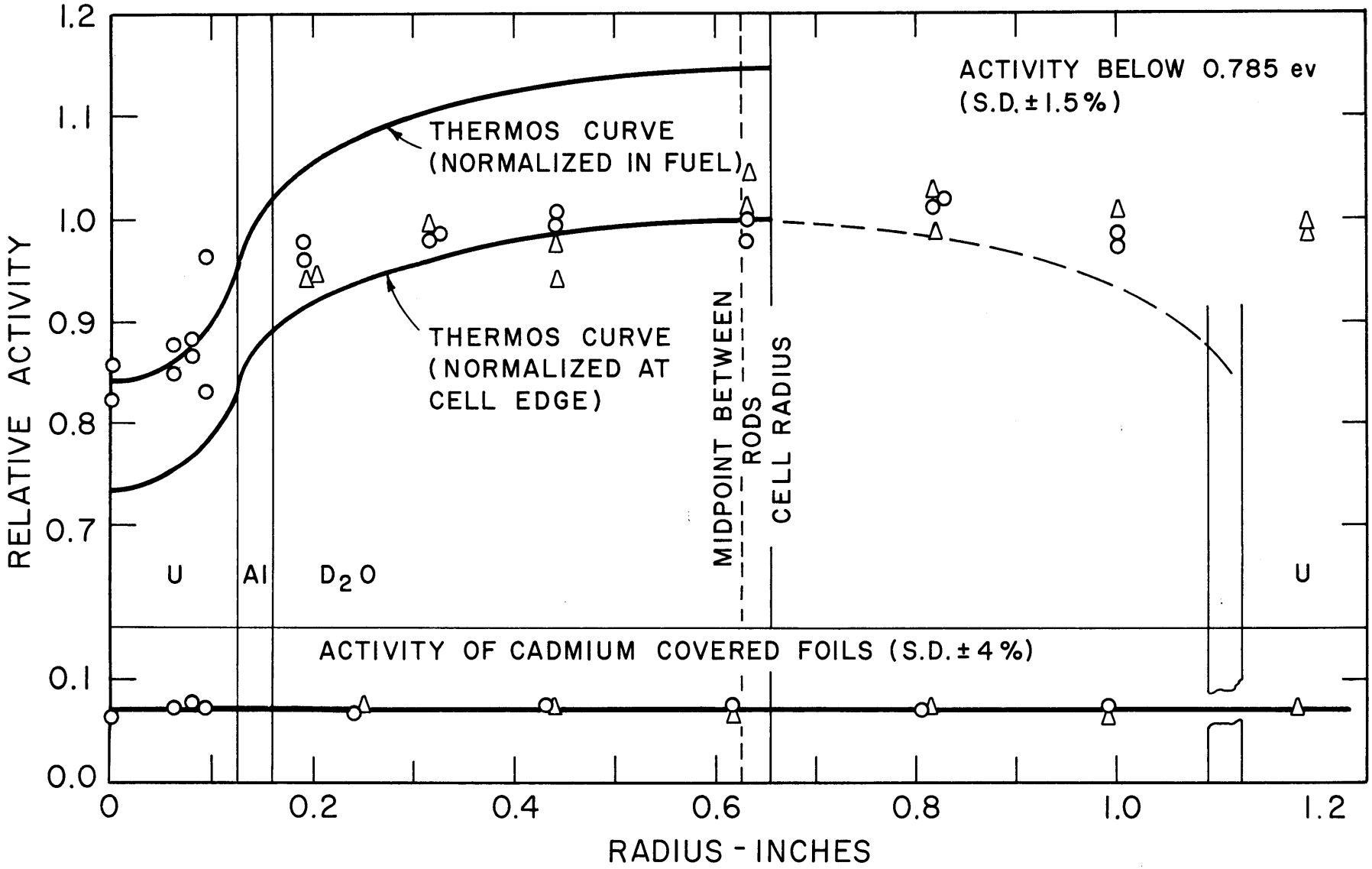

FIG. 4.53 EUROPIUM ACTIVITY DISTRIBUTION NO. 2a (DONE BY KIM (KI)), 0.25-IN. DIA. RODS OF 1.03% U^{235} ON A 1.25-IN. TRIANGULAR SPACING

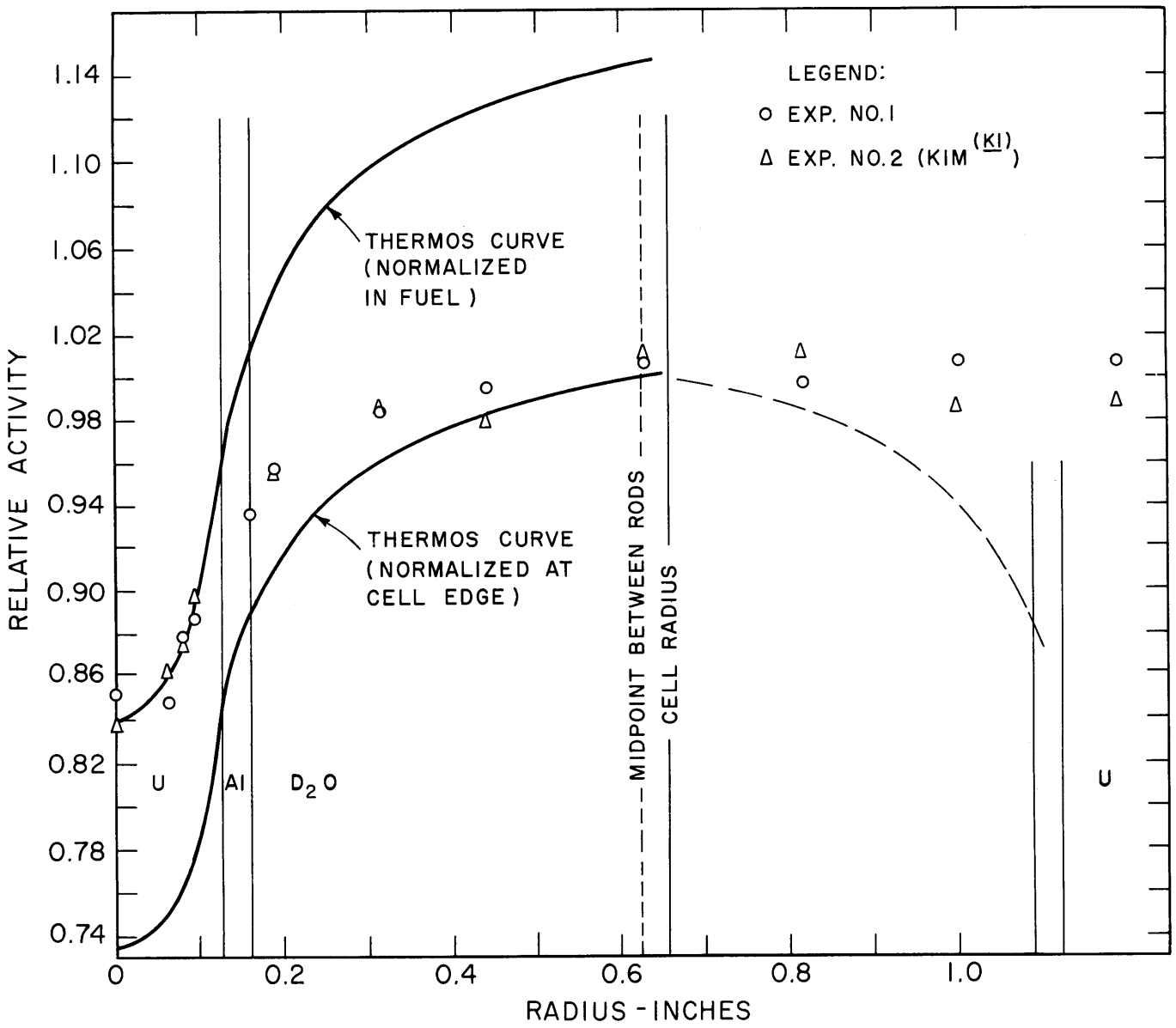

FIG. 4.54 DISTRIBUTION OF EUROPIUM ACTIVITIES BELOW 0.785 ev – COMPARISON OF EXPERIMENTS NO.1 AND NO. 2, 0.25-IN. DIA. RODS OF 1.03 % U^{235} ON A 1.25-IN. TRIANGULAR SPACING

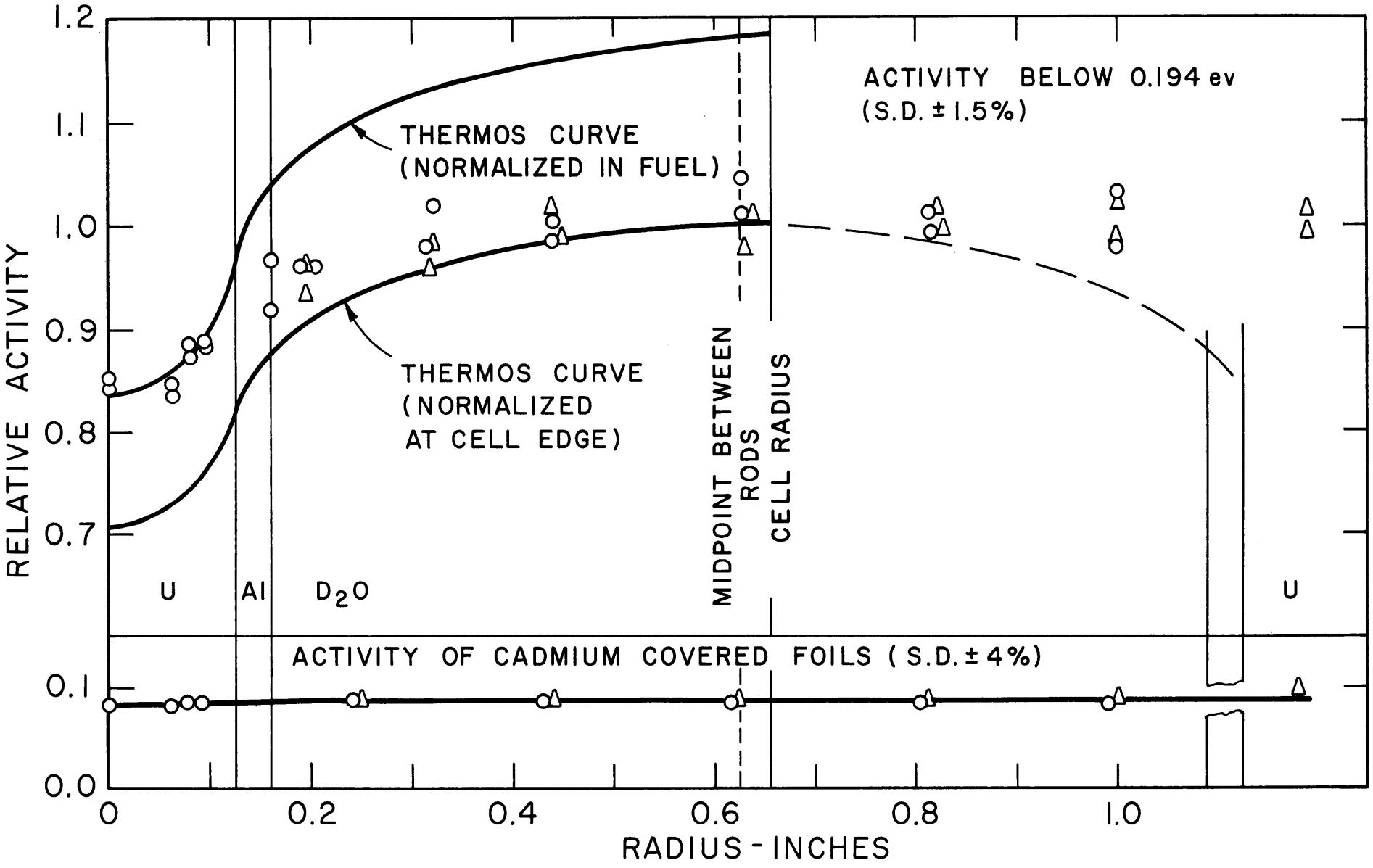

FIG. 4.55 EUROPIUM ACTIVITY DISTRIBUTION NO. 1b, 0.25-IN. DIA. RODS OF 1.03% U^{235} ON A 1.25-IN. TRIANGULAR SPACING

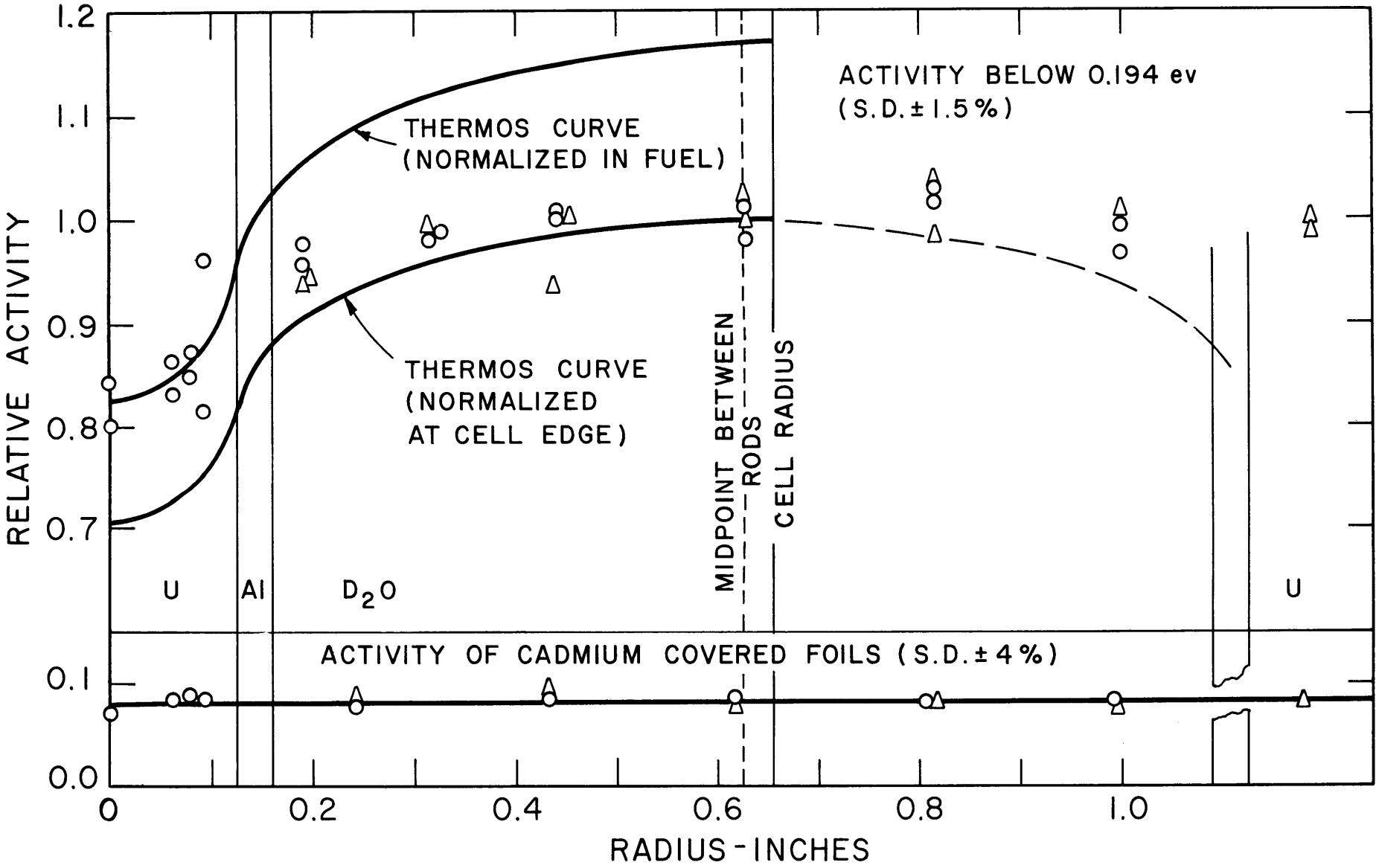

FIG. 4.56 EUROPIUM ACTIVITY DISTRIBUTION NO. 2b (DONE BY KIM (KI)), 0.25-IN. DIA. RODS OF 1.03% U^{235} ON A 1.25-IN. TRIANGULAR SPACING

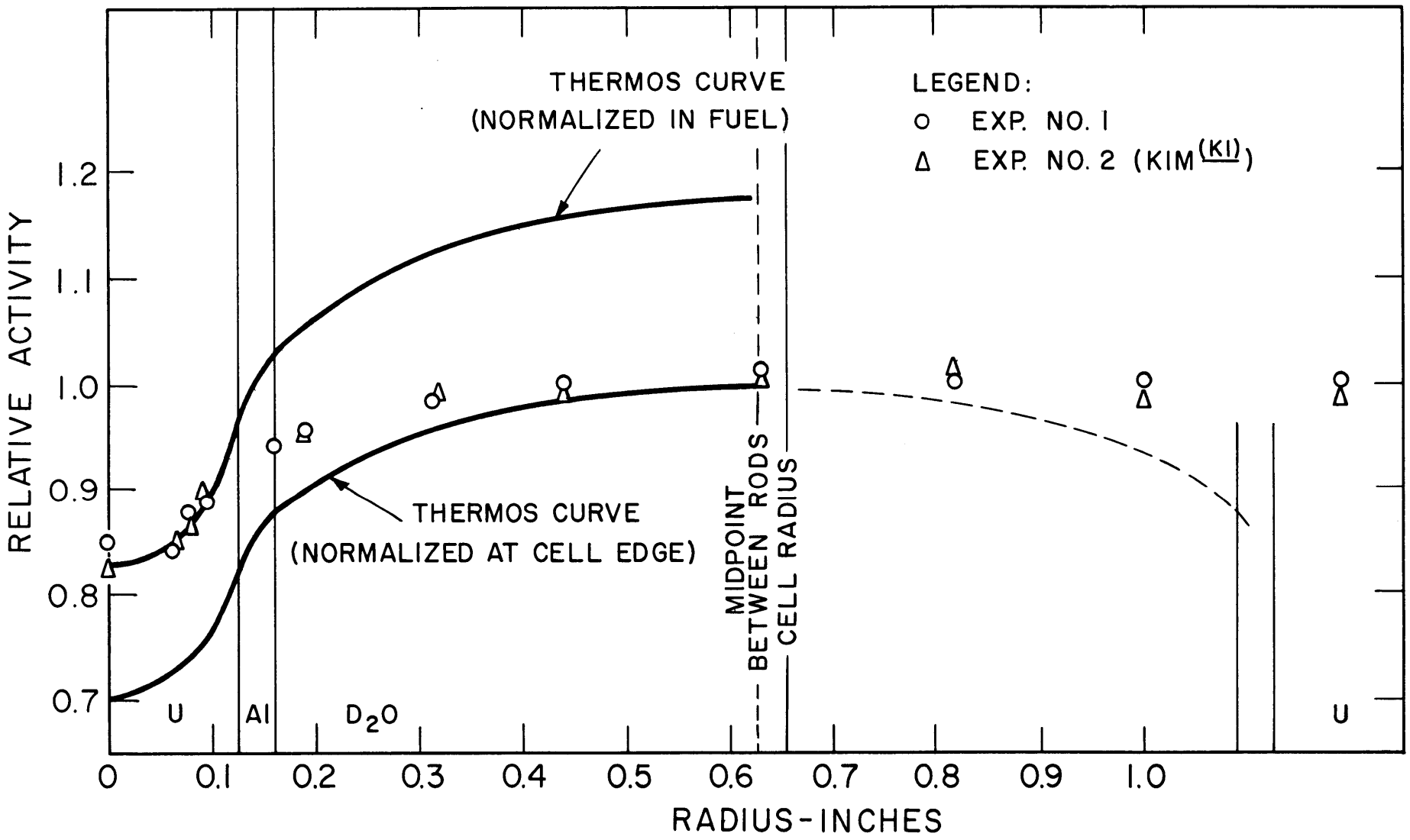

FIG. 4.57 DISTRIBUTION OF EUROPIUM ACTIVITIES BELOW 0.194 ev- COMPARISON OF EXPERIMENTS NO. 1 AND NO. 2, 0.25-IN. DIA. RODS OF 1.03% U^{235} ON A 1.25-IN. TRIANGULAR SPACING

due to absorption in the fuel, it is almost independent of what happens in the moderator.

3. The THERMOS results presented in sections 4.3.1 through 4.3.3 were all computed with the Honeck kernel, and with a $\bar{\mu}_o$ correction applied to account for anisotropic scattering. Calculations made by Mr. R. Simms (S2) with other kernels (mass-2, and Brown-St. John) and without a correction for anisotropic scattering produced insignificant changes in the theoretical distributions. Thus, it seems that neither anisotropic scattering effects nor the details of the energy exchange kernels are the causes of the disagreement between theory and experiment.

4. The possibility exists that the experimental data may be in error; but, as pointed out above, three different methods for measuring the gold distributions all gave the same results. It is possible that the epicadmium distribution measurements may be in error because of perturbations of the large cadmium sleeve surrounding the fuel rod. But the epicadmium activity of lutetium foils is less than 3% of the total lutetium activity and any errors in the measured epicadmium distribution would have a negligible effect on the thermal neutron distribution. Thus, for lutetium, at least, possible errors in the epicadmium distribution do not explain the observed disagreement. Since THERMOS predicts the ratio of lutetium to gold activities satisfactorily, it is probable that errors in the epicadmium distribution do not seriously affect the gold measurements. In the case of europium, the epicadmium activity is less than 10% of the total activity and, as in the case of lutetium, it is unlikely that errors in the measured epicadmium distribution have any serious effect.

All the information presented in items 1 - 4 above indicates that the disagreement between THERMOS and experiment is probably caused by some factor involving the total neutron density rather than the energy spectrum. The experimental results for the natural uranium lattices agreed very well with those predicted by THERMOS, much better than the results for the 1.25-inch lattice. The most notable difference between the lattice of 1.010-inch diameter rods and the lattice of 0.25-inch diameter rods is the difference in the cell dimensions. The mean free path for neutrons in heavy water is approximately one inch (2.4 cm). The rod spacings in the natural uranium lattices were about five mean free paths; the rod spacing in the enriched lattice is about one mean free path.

When cell dimensions are in the neighborhood of one mean free path, considerable caution must be exercised in cell calculations. Calculations on cylindrical and slab cells about one mean free path in size have been made by Thie (T3) who applied the Monte Carlo method to the actual (non-cylindricalized) cell shape. With the Monte Carlo calculations as a standard, he then used the S_n, ABH, P_3 and P_1 methods. The ABH calculations gave fairly good agreement with the Monte Carlo calculations for both cylinders and slabs. The S_n method gave better agreement than the P_3 and P_1 methods for the slabs, as would be expected, since the S_n method gives a more accurate solution to the transport equation. But, for the cylindricalized cells, the P_3 and P_1 calculations and the ABH method gave better agreement than the supposedly more accurate S_n method. Thus, Thie found that the use of higher order transport theory for cylindrical cells about a mean free path in size, may lead to incorrect results, depending on the methods used. More will be said about this later.

Honeck (H11) has noticed a similar cylindricalization effect in the case of slightly enriched uranium rods in water lattices, in which the rod spacing was about one mean free path. He has developed a two-dimensional THERMOS code which does not cylindricalize the cell boundary, but maintains the actual boundary, whether it is a square or hexagon. He has found that the cylindrical cell approximation leads to greater disadvantage factors than experiment (the same effect seen in the 1.25-inch lattice) because of the boundary conditions at the cell edge. The two-dimensional THERMOS calculations give good agreement with experiment. He also found that the ABH method gives good agreement with experiment, from large cells down to small cells.

As explained in Chapter III, when THERMOS calculates the transport kernel for a neutron being transported from one part of the cell to another, the code follows the neutron along various possible paths in the cell. A reflection condition is imposed at the cell boundary, with the angle of rebound of a neutron colliding with the boundary equal to the angle of incidence. As Fig. 4.58a shows, there are certain paths in the moderator from which a neutron cannot possibly be reflected into

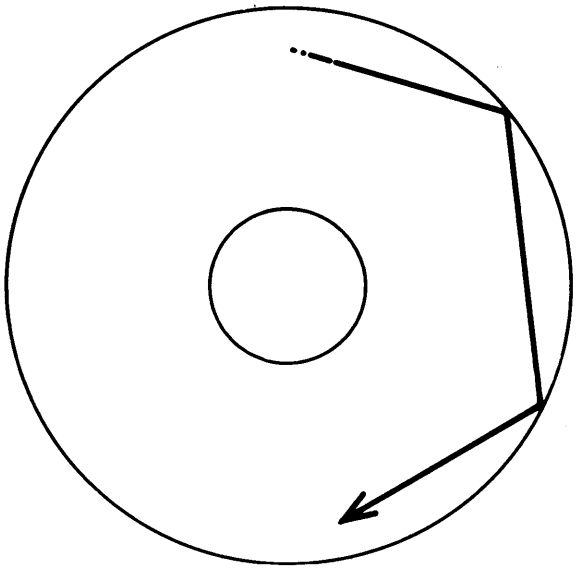

FIG. 4.58a TYPICAL NEUTRON PATH
IN A CYLINDRICAL CELL

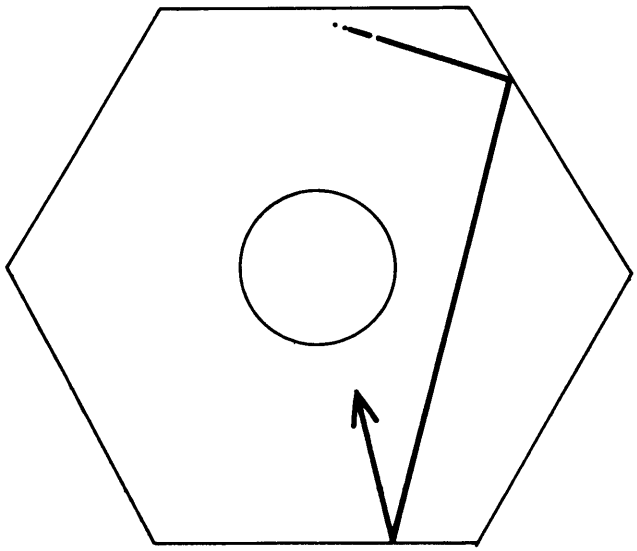

FIG. 4.58b TYPICAL NEUTRON PATH
IN A HEXAGONAL CELL

the fuel region by the circular boundary. These neutrons remain in the moderator and increase the flux there. Figure 4.58b shows the same path in a cell with a hexagonal boundary; now, this path can bring the neutron into the fuel. Such reflections increase the number of neutrons in the fuel relative to those in the moderator, and reduce the calculated disadvantage factor. This effect, however, is noticeable only at small (in mean free paths) cell sizes. The larger the cell, the larger is the moderator region and the smaller is the effect of cylindricalization. This comes about because THERMOS follows a neutron for only five mean free paths along each of the possible trajectories in the cell. The trajectory shown in Fig. 4.58b does carry the neutron toward the fuel, but if the cell is almost five mean free paths in diameter, the neutron might never reach the fuel. Since the natural uranium lattice cells were about five mean free paths in diameter, the cylindrical cell effect in these lattices should be much smaller than in the 1.25-inch lattice. In fact, Honeck has found that the one-dimensional version of THERMOS gives good agreement with experimental neutron distributions in water-moderated lattices when the rod spacing is several mean free paths. Work at M.I.T. by Dr. J. Peak (P2) confirms that, as the cell spacing increases from one to several mean free paths, the agreement with THERMOS improves. He measured gold activity distributions in a miniature lattice assembly containing mixtures of D_2O and H_2O and lattices of 0.25-inch diameter, 1.15% U^{235} rods with triangular spacings of 0.880 inches, 1.128 inches, and 1.340 inches, respectively. It was found that increasing the cell radius by increasing the rod spacing (or by increasing the concentration of H_2O in the moderator mixtures) led to better agreement between the experimental and the THERMOS distributions. In a lattice containing 80.2% D_2O, the disagreement with THERMOS was about 10% at the cell edge (with normalization at the center of the fuel rod) for a spacing of 0.880-inch, and less than 2% for a spacing of 1.340 inches. Since the S_n method involves the use of a reflecting boundary condition similar to that in THERMOS, it is likely that the discrepancies that Thie noticed are also due to the cylindrical cell effect. Thie also found that the prediction of the S_n method improved with an increase in the cell radius. Since the ABH, P_1, and P_3 calculations used by Thie do not use a reflecting boundary condition, these

methods gave better results in small cylindrical cells than the usually more accurate S_n calculations.

At present, the two-dimensional version of THERMOS is not ready for distribution. Unfortunately, it takes as much as twenty minutes of machine time on the IBM 7090 computer to run a two-dimensional problem. It is hoped that, in the near future, such calculations will be made for the lattices measured at M. I. T.

4. 3. 5 AMOUYAL-BENOIST-HOROWITZ CALCULATIONS -- 1. 25-INCH LATTICE

In section 4. 2. 6, it was found that calculations with the ABH method gave disadvantage factors that were in excellent agreement with those calculated with THERMOS, and that the disadvantage factors calculated with THERMOS were in excellent agreement with those measured. However, as Amouyal, Benoist, and Horowitz state in their paper (A1), care must be taken in applying their method to cases in which the cell radius is less than a mean free path. Since the ABH method involves the use of diffusion theory in the moderator, and since diffusion theory breaks down within a mean free path of the cell edge, an ABH calculation for the 1. 25-inch lattice might be subject to some error. Amouyal, Benoist, and Horowitz state, however, that for D_2O their method may sometimes be applicable when the moderator region is less than a mean free path wide. Since THERMOS seems to give a good estimate of the spectral hardening for the 1. 25-inch lattice, an ABH calculation for this lattice was performed with average absorption cross sections computed with THERMOS. Before comparing the ABH method (which calculates flux disadvantage factors) with the experimental disadvantage factors (measured in terms of neutron density), the experimental disadvantage factors must be converted to flux disadvantage factors. The experimental disadvantage factors for the 1. 25-inch lattice are shown in Table 4. 17. (The neutron density disadvantage factors computed with THERMOS are also shown in this table for comparison.) The experimental neutron density disadvantage factors in Table 4. 17 are converted to flux disadvantage factors by multiplying the neutron densities in each region by the average subcadmium neutron velocity for that region, as computed by THERMOS.

TABLE 4.17

Neutron Density Disadvantage Factors
for the 1.25-inch Lattice

	THERMOS	Experiment
$\frac{\bar{N}_{mod}}{\bar{N}_{fuel}}$	1.262	1.138 ± 0.011
$\frac{\bar{N}_{clad}}{\bar{N}_{fuel}}$	1.124	1.073 ± 0.016
$\frac{\bar{N}_{fuel\ surf}}{\bar{N}_{fuel}}$	1.099	1.059 ± 0.016

Table 4.18 gives the results for the flux disadvantage factors computed by THERMOS, calculated with the ABH method (with THERMOS-averaged cross sections), and obtained from the experimental results, respectively.

TABLE 4.18

Flux Disadvantage Factors for the 1.25-inch Lattice

	THERMOS	ABH	Experiment
$\frac{\bar{\phi}_{mod}}{\bar{\phi}_{fuel}}$	1.2086	1.1388	1.090 ± 0.011
$\frac{\bar{\phi}_{a}}{\bar{\phi}_{fuel}}$	1.0759	1.0332	1.033 ± 0.015

The ABH method gives much better agreement with experiment than THERMOS for the moderator disadvantage factor. The agreement between the ABH calculation and experiment for the ratio of the flux at the fuel rod surface to the average flux in the fuel is excellent. This result indicates that the disagreement in the moderator disadvantage factor may be due to too high an estimate of the moderator flux by the ABH method, and may be a good example of the breakdown of the ABH method for cell radii of less than a mean free path.

4.3.6 TEMPERATURE CALCULATIONS -- 1.25-INCH LATTICE

Temperature calculations were made for the measured activity distributions in the 1.25-inch lattice. As was done with the natural uranium lattices, the cell edge temperature was obtained by both the semilog and $\bar{v}$ methods. The results of these calculations for the temperature changes between the cell edge and the rod center are shown in Tables 4.19 and 4.20. The temperature changes obtained with THERMOS are based on $\bar{v}$ fits to the THERMOS spectra at the cell edge and at the rod center.

TABLE 4.19

Temperature Changes from the Cell Edge to the Rod Center for the 1.25-inch Lattice, $\bar{v}$ Fit to Cell Edge Spectrum

Cell Edge Temperature	ΔT_{Lu}	ΔT_{Eu}	$\Delta T_{THERMOS}$
82.7° C	34.5 ± 11.1° C	9.7 ± 30.5° C	40.0° C

TABLE 4.20

Temperature Changes from the Cell Edge to the Rod Center for the 1.25-inch Lattice, Semilog Fit to Cell Edge Spectrum

Cell Edge Temperature	T_{Lu}	T_{Eu}	$T_{THERMOS}$
59.4° C	33.3 ± 10.0° C	9.2 ± 28.5° C	40.0° C

The temperature changes found from the lutetium data are in good agreement with those obtained from THERMOS. The temperature changes computed from the europium data are inconclusive because of the large uncertainties involved. Europium is not a sensitive enough spectral indicator for such small temperature changes. The results in Tables 4.19 and 4.20 are very close, indicating that the temperature changes across the cell are practically independent of the actual temperature at the cell edge. Temperature changes from the cell edge to the rod surface have not been given because they are smaller than the uncertainties involved.

The values of the r factors computed for the 1.25-inch lattice are shown in Table 4.21.

TABLE 4.21

Values of the r Factor, 1.25-inch Lattice

Cell Edge Temperature (°C)	$r_{\text{cell edge}}$	$r_{\text{rod center}}$
82.7	0.07062 ± 0.0030	0.07300 ± 0.0031
59.4	0.07295 ± 0.0031	0.07528 ± 0.0032

The r factors change only slightly from the cell edge to the rod center, owing to the small decreases, in the fuel, of both the thermal and resonance fluxes, as compared to the decreases in the natural uranium lattices.

4.3.7 THE 1.25-INCH LATTICE: TABULATION OF SOME USEFUL PARAMETERS

The thermal utilization for the 1.25-inch lattice was obtained in the same way as in the natural uranium lattices. Table 4.22 lists the experimental, ABH, and THERMOS values of f, respectively; absorption cross sections obtained from THERMOS were used in the ABH calculation.

TABLE 4.22

Values of the Thermal Utilization in the 1.25-inch Lattice

Experiment	ABH	THERMOS
0.9760 ± 0.0006	0.9766 ± 0.0006	0.9738 ± 0.0006

$$\frac{V_{\text{mod}}}{V_{\text{fuel}}} = 25.9$$

The uncertainties in Table 4.22 are due primarily to uncertainties in the deuterium and aluminum cross sections. It should be noted that the absorption in the aluminum is more than three times as great as the absorption in the heavy water. The ABH method gives a value of f that agrees almost exactly with the experimental value, while THERMOS

gives a value which is low by only 0.2%. Even though the theoretical disadvantage factors are in considerable disagreement with experiment, the theoretical values of f are sufficiently accurate. This would be true only in a heavy water system, however, since other moderators, e.g., H_2O, may have considerably higher absorption cross sections and may give f values much smaller than unity.

Figures 4.59 and 4.60 show graphs of the average subcadmium absorption cross section of a 1/v absorber, and of the thermal neutron temperature, respectively. These distributions have been computed with the THERMOS code, and may be in some error because of the cylindrical cell effect. Because of this effect, the number of neutrons reaching the fuel is underestimated, and the calculated hardening may be smaller than the hardening that actually occurs. But, since the ratios of lutetium and europium activities to gold activity were well estimated by THERMOS for the 1.25-inch lattice, the effects of cylindricalization on the extent of spectral hardening would be expected to be small. Figures 4.59 and 4.60 indicate that the degree of spectral hardening is much smaller in the fuel of the 1.25-inch lattice than it was in the natural uranium lattices.

The values of the absorption cross sections of the cell materials computed with THERMOS and averaged over the energies below the cadmium cutoff are given in Table 4.23; these cross sections have also been averaged over space. The heavy water contains 99.773% D_2O by weight.

TABLE 4.23

Effective Absorption Cross Sections (in cm^{-1}) of the Cell Materials in the 1.25-inch Lattice

$\bar{\Sigma}(U^{235})$	$\bar{\Sigma}(U^{238})$	$\bar{\Sigma}(D_2O)$	$\bar{\Sigma}(Al)$
0.2392	0.09467	6.156×10^{-5}	0.01048

In Table 4.24 are listed THERMOS values of average subcadmium activation cross sections of detectors commonly used in lattice measurements. The activation cross sections of Pu^{239}, U^{235}, and U^{233} are equivalent to the fission cross sections of these nuclides. All of the cross

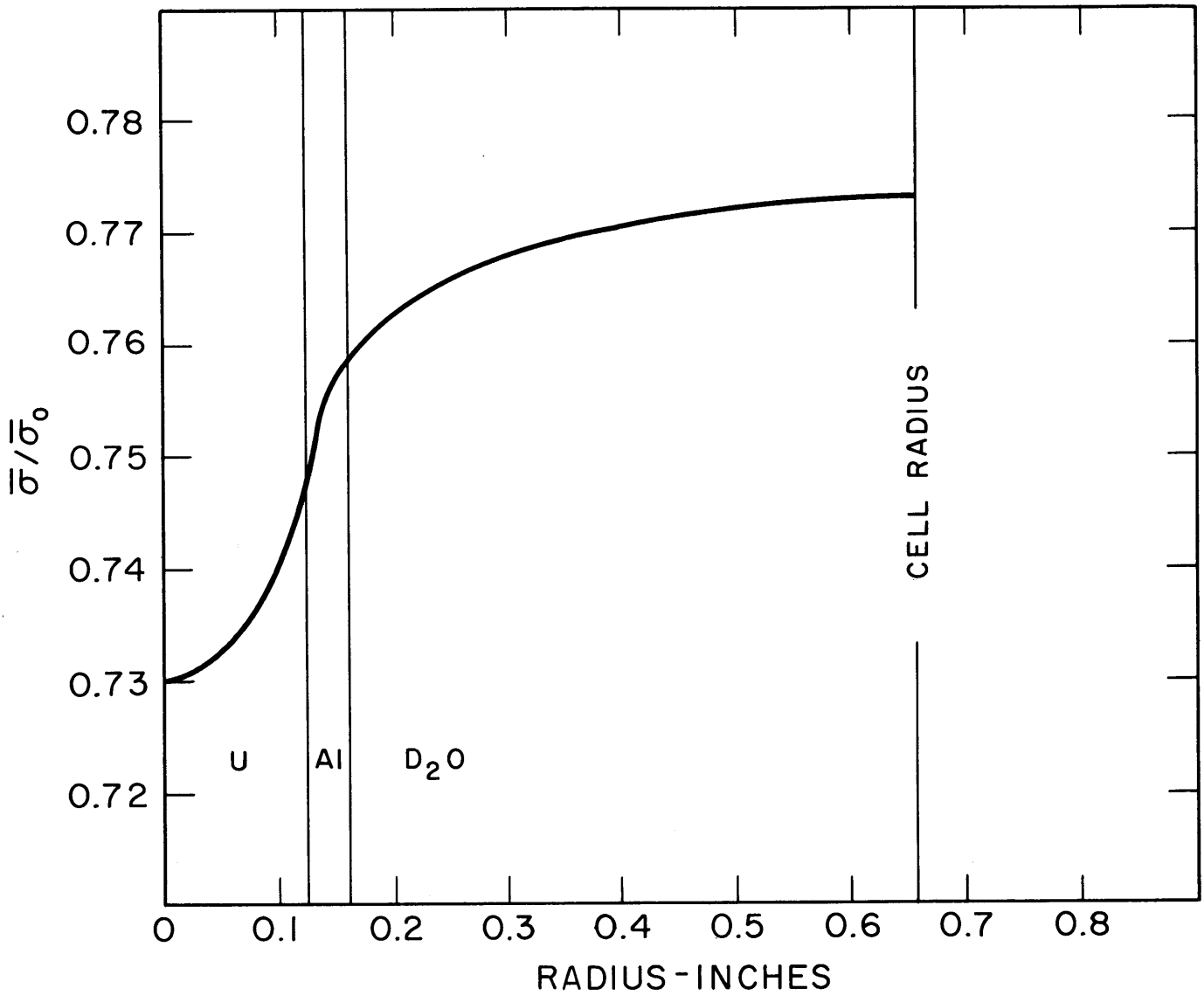

FIG. 4.59 AVERAGE CROSS SECTION OF A 1/V ABSORBER, 0.25-IN. DIA. RODS OF 1.03% U^{235} ON A 1.25-IN. TRIANGULAR SPACING

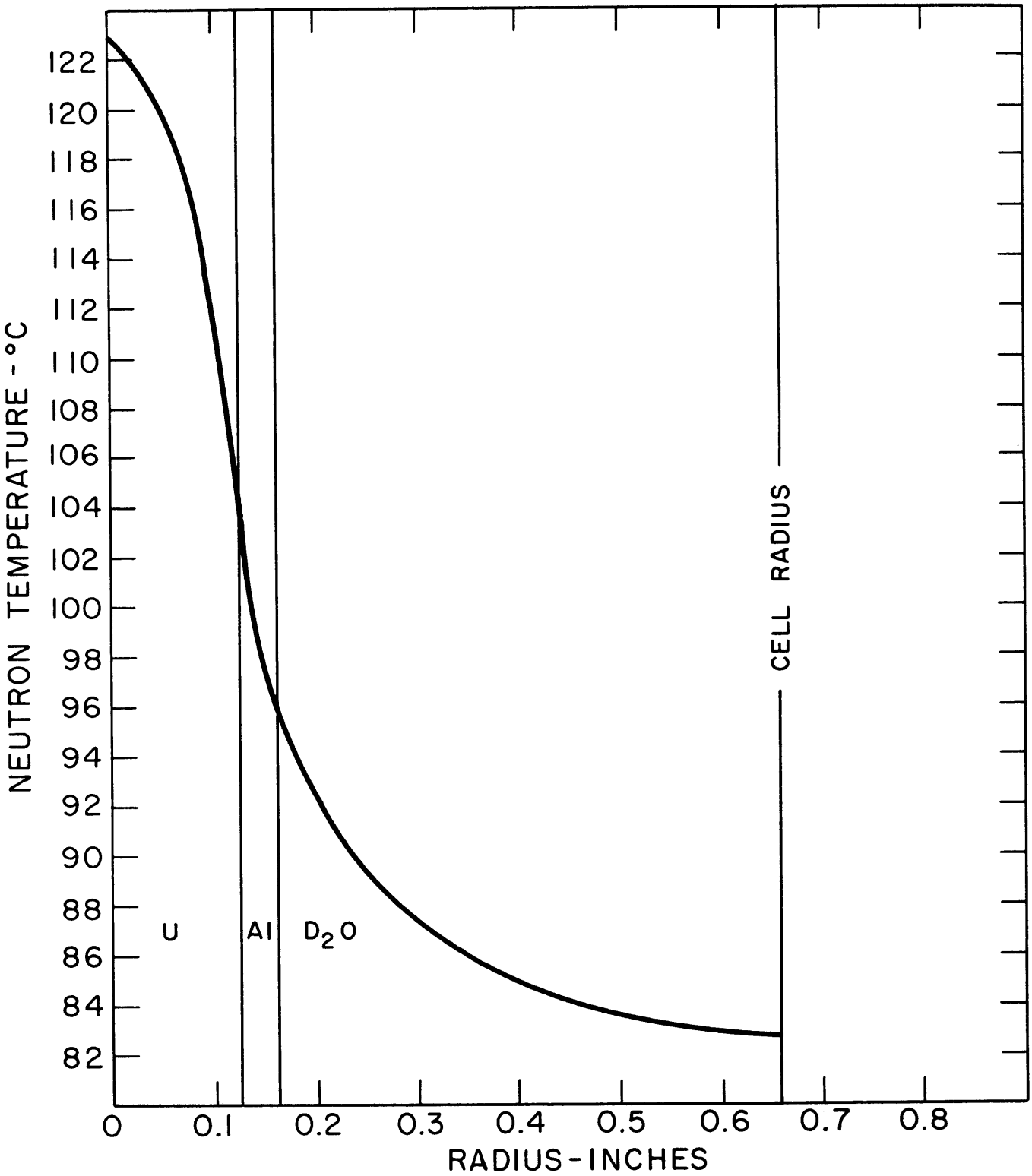

FIG. 4.60 NEUTRON TEMPERATURE DISTRIBUTION, 0.25 - IN. DIA. RODS OF 1.03% U^{235} ON A 1.25 - IN. TRIANGULAR SPACING

sections in this table are based on the latest BNL-325 (H13) cross sections, which are listed in Table 4.15. In Table 4.25 are given europium absorption cross sections which have been averaged over energy up to 0.194 ev and 0.785 ev, corresponding to the two europium cutoffs.

TABLE 4.24

Average Subcadmium Cross Sections (in barns) of Nuclides Commonly Used to Measure Activity Distributions, 1.25-inch Lattice

Au	Lu^{176}	Eu^{151}	Dy^{164}	Pu^{239}	U^{235}	U^{233}
			Fuel			
72.9	7006	5200	582	742	412	386
			Moderator			
76.1	6869	5562	609	750	432	402

TABLE 4.25

Average Absorption Cross Sections (in barns) of Eu^{151} in the 1.25-inch Lattice

0.194 ev Cutoff		0.785 ev Cutoff
	Fuel	
5332		5495
	Moderator	
5716		5807

CHAPTER V

SUMMARY, CONCLUSIONS, AND RECOMMENDATIONS

5.1 NEUTRON DENSITY DISTRIBUTIONS

Thermal neutron density distributions were measured with gold foils in three natural uranium, heavy water lattices of 1.010-inch diameter, aluminum clad rods on triangular spacings of 4.5 inches, 5.0 inches, and 5.75 inches, respectively. The measurements were found to be reproducible within the experimental uncertainties. The measured distributions were compared with distributions computed with the THERMOS code. The agreement between THERMOS and experiment was excellent for the gold activity distributions in the fuel and in the moderator.

Thermal neutron density distributions were measured with three kinds of gold detector foils in a slightly enriched uranium, heavy water lattice of 0.25-inch diameter, 1.03% U^{235}, aluminum clad rods on a triangular spacing of 1.25 inches. The three detectors were: one-sixteenth inch diameter pure gold foils, one-thirty-second inch diameter pure gold foils, and one-sixteenth inch diameter foils of a lead-gold alloy which closely matched the absorption and scattering properties of the fuel. The distributions measured with the three detectors were the same, within the experimental uncertainties. The three detectors were chosen because they vary somewhat in the amount of flux perturbation they cause. Because all three detectors gave the same results, it was concluded that the corrections which were used to account for flux perturbations were adequate. The neutron density distribution in the enriched lattice was compared with the distribution computed with THERMOS. When THERMOS was normalized in the fuel, the distribution computed with THERMOS agreed well with the measured distribution in the fuel, but was considerably higher than the measured distribution in the moderator. With normalization at the cell edge, the distribution computed with THERMOS was 13.2% lower than the measured distribution at the cell center. It is possible that the cause of this discrepancy may be attributed to the

cylindrical cell effect: When the cell spacing is less than a mean free path, as in the 1.25-inch lattice, approximation of the true shape of the cell boundary, such as in the Wigner-Seitz cylindrical cell approximation used by THERMOS, may lead to errors in the computed distribution. These errors may arise in any theoretical method which uses a reflection boundary condition similar to that used by THERMOS at the cell boundary. It is recommended that the measured neutron density distributions be compared with other theoretical methods in which the cylindrical cell effect is not a problem. In particular, computations should be made with a new two-dimensional version of THERMOS which does not approximate the shape of the cell boundary. Since the cylindrical cell effect has been found to decrease as the cell size increases, the agreement between the one-dimensional THERMOS code and experiment should improve when lattices with spacings larger than 1.25 inches are studied.

5.2 SPECTRAL DISTRIBUTIONS

Activity distributions were made with bare and cadmium covered foils of lutetium and europium in the three natural uranium lattices and in the enriched uranium lattice. The measurements were found to be reproducible within the experimental uncertainties. A method was developed for treating the partial absorption by cadmium covers of neutrons at the 0.46 ev resonance of europium, and it was found possible to correct the europium activity distributions to energy cutoffs just above and just below the resonance.

In the natural uranium lattices, the agreement between THERMOS and experiment for the lutetium and europium activity distributions was not quite as good as that for the gold distributions, but good enough to indicate that THERMOS gives a good estimate of the degree of spectral hardening from the moderator to the fuel. Part of the discrepancy between THERMOS and experiment was believed to be due to the lack of sufficiently accurate cross section data. If new data for the lutetium and europium cross sections become available, the THERMOS computations should be repeated.

In the enriched lattice, the agreement between THERMOS and experiment for the lutetium and europium activity distributions was similar to that obtained with gold. The measured ratios of the lutetium

activity to gold activity and of europium activity to gold activity compared favorably with those computed with THERMOS. The agreement in the activity ratios indicates that THERMOS gives a good estimate of the degree of spectral hardening, even though the estimated neutron density distribution may be in error because of the cylindrical cell effect. The lutetium foils used in the enriched lattice were quite small in size and nearly infinitely dilute. As a result, their activation was very low and there was considerable scatter in the lutetium data. Future measurements with lutetium should be made with thicker foils. In thicker foils, self-shielding effects may become significant and will have to be considered.

Neutron temperature changes from the cell edge to the cell center and from the cell edge to the rod surface were calculated from the measured lutetium, europium, and gold activity distributions in the natural and enriched lattices. Westcott effective cross sections were used in these calculations. The temperature changes based on the lutetium distributions agreed well with those based on the europium distributions, within the experimental uncertainties. However, since the Westcott g factor for europium varies much less with temperature than that for lutetium, europium did not prove to be as sensitive a spectral indicator as lutetium; as a result, the temperature changes for europium had much greater uncertainties than those for lutetium. The agreement between the temperature calculations based on the Westcott method and the temperature calculations made with THERMOS was good. This result indicates that the Westcott method may still be a useful tool even though it approximates the actual shape of the spectral distribution and fails to account for spectral hardening in the fuel.

5.3 DISADVANTAGE FACTORS AND THERMAL UTILIZATION

The disadvantage factors measured in the natural uranium lattices were in good agreement with those computed with THERMOS. The Amouyal-Benoist-Horowitz (ABH) method with cross sections derived from THERMOS also gave disadvantage factors that were in excellent agreement with those computed with THERMOS. Consequently, the values of f derived from the three methods were in excellent agreement.

In the enriched lattice, the disadvantage factors computed with THERMOS were in poor agreement with the measured values, because of the cylindrical cell effect. The ABH method, with THERMOS cross sections, gave excellent agreement with experiment for the fuel disadvantage factor, but the agreement was not as good for the moderator disadvantage factor. The discrepancy for the moderator disadvantage factor was attributed to an expected breakdown in the ABH method for small cell spacings. The ABH method uses diffusion theory in the moderator, but diffusion theory is applicable only a few mean free paths away from the fuel. Thus, when the cell radius is less than a mean free path, the ABH method may fail to give accurate results. Even though the disadvantage factors obtained by experiment, by THERMOS, and by the ABH method were in some disagreement, the values of f obtained from the three methods were in close agreement because f is close to unity.

5.4 SPACE AND ENERGY SEPARABILITY

Radial and axial buckling measurements were made with lutetium foils in the 5.75-inch lattice. The results agreed well with similar measurements made with gold. This result indicated that the thermal neutron spectrum was uniform in the lattice tank at points sufficiently far from the source.

Measurements of the intracell gold activity distribution were made in cells centered at two rods and three rods off-center, respectively. These measurements showed that the radial flux distribution was not completely separable into macroscopic J_o and microscopic cell distributions. The observed non-separability was small, however, and had a negligible effect on the disadvantage factors and the values of the thermal utilization. In view of the results of the lutetium buckling measurements and of the off-center intracell distributions, it may be concluded that the activity distributions measured in the central cell of the lattice were representative of the lattice as a whole.

5.5 EFFECTS OF ANISOTROPIC SCATTERING AND OF VARYING THE SCATTERING KERNEL

THERMOS calculations were done with and without a $\bar{\mu}_o$ correction for anisotropic scattering. The use or non-use of such a correction had a small effect on the computed distributions, although its use did give somewhat better agreement with experiment. Little difference was also observed in the computed activity distributions when the scattering kernels were changed. It may be that the measurement of activity distributions is not a sensitive enough method for testing the effect of various kernels on lattice spectra. Further work in these areas is being carried on by Mr. R. Simms.

5.6 EXPERIMENTAL PERTURBATIONS

A number of experiments were done to determine the effects of various perturbations on the measurements. These included studies of the following: foil holder perturbations, flux depression by cadmium pillboxes, cadmium ratios of gold as a function of gold foil thickness, and transmission of neutrons through cadmium filters. Most of these experiments are discussed in the appendix. It was found that all experimental perturbations were small and could be corrected for.

APPENDIX A.
FOIL HOLDER PERBURBATION EXPERIMENT

An experiment was performed to check the relative merits of aluminum and plastic foil holders in D_2O. A special foil wheel was constructed from 0.032-inch thick type 1100 aluminum sheet. Six different foil holders, 1/4-inch wide, were arranged on this wheel as shown in Fig. A.1. The foil holders were made of the following materials: 0.032-inch thick type 1100 aluminum, 0.016-inch thick type 1100 aluminum, 0.0006-inch thick aluminum foil, 0.055-inch thick lucite, 0.030-inch thick lucite, and 0.002-inch thick mylar tape. Five 5.2-mil thick, 1/4-inch diameter, gold foils were taped with mylar to each holder. The foils were matched so that the maximum variation in weight was 2%, and the average weight of the five foils on each holder was the same. The wheel was suspended at the end of a shaft in the lattice tank, which was filled only with heavy water. The shaft was rotated by means of a motor to insure uniform irradiation of all the foils. The gold foils were counted, both front and back, for 90,000 counts in the GM counter described in section 2.3.4. Within statistical uncertainties, all the foils on a given foil holder gave the same activity without correction for weight differences. This absence of dependence of activity on weight was due to the fact that in GM counting, most of the activity comes from the foil surface. The foils at the ends of each holder gave the same activity as those at the center, indicating that there were no edge effects in the experiment. No difference, within experimental uncertainty, was noted between the activities of the front and the back of the foils, so that these activities were averaged.

Gold foil activity is plotted against foil holder thickness in Fig. A.2, for both the plastic and the aluminum foil holders. The results show that the plastic depresses the flux considerably more than does the aluminum and that, in the limit of zero thickness of plastic and aluminum (mylar tape and aluminum foil), the curves

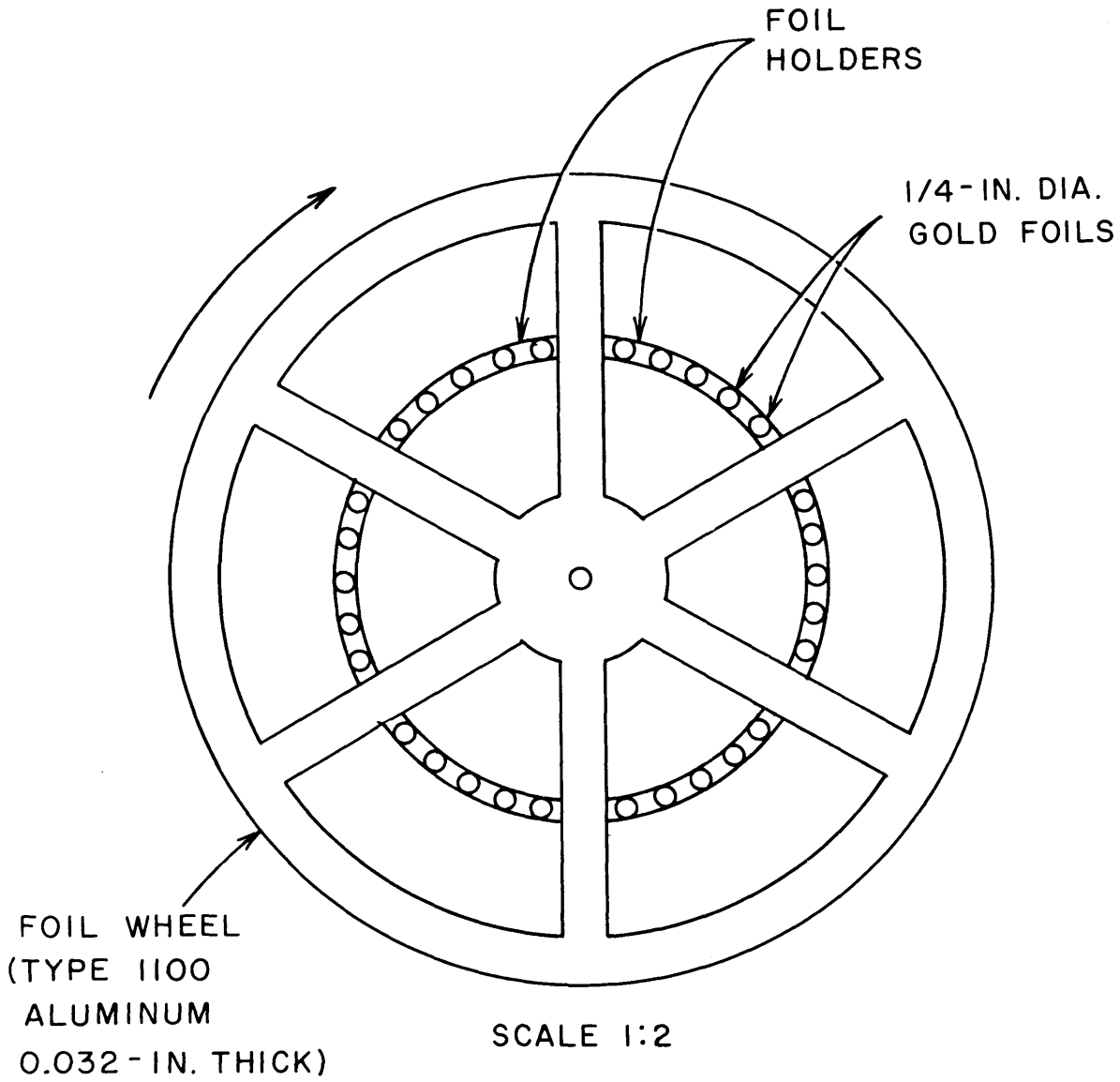

FIG. A.1 ARRANGEMENT USED TO INVESTIGATE FLUX DEPRESSION BY FOIL HOLDERS

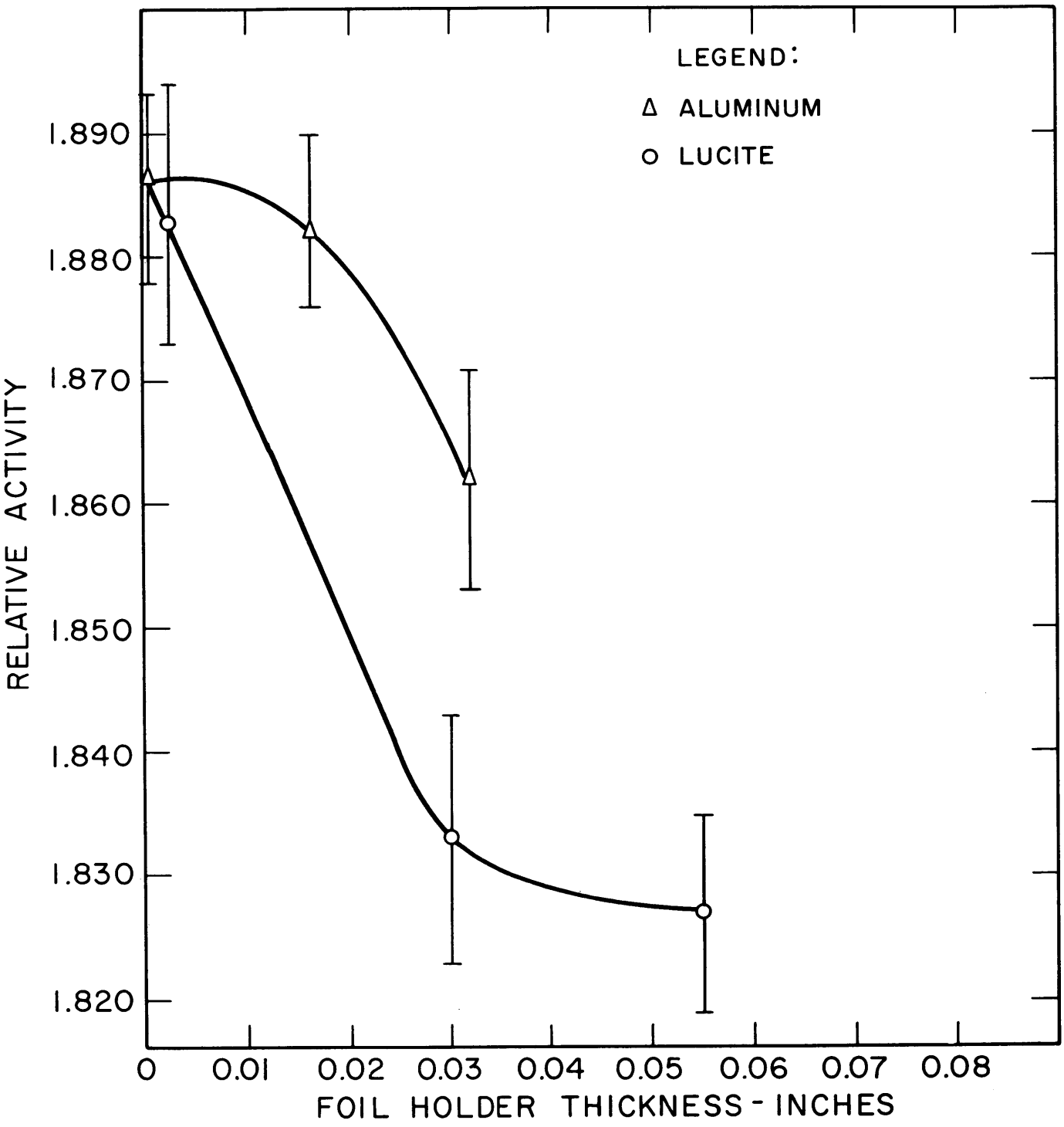

FIG. A.2 FLUX DEPRESSION BY ALUMINUM AND LUCITE FOIL HOLDERS

for the two materials approach the same value. The flux depression effects of the mylar tape used in the lattice experiments thus seem to be negligible. The foil holders used in the natural uranium lattices were 0.032 inches thick. Depressions were milled in these holders to a thickness of 0.016 inches. Figure A.2 shows that the flux depression effect of 0.016 inches of aluminum is 0.64% and a correction was made for this effect in all activity distributions.

The following qualitative explanation is offered for the differences observed between aluminum and plastic holders. The absorption cross sections of the aluminum and the plastic are not very different, so that the depression is probably not due to absorption. The scattering cross section of the plastic, however, is an order of magnitude larger than that of the aluminum; a neutron entering the plastic tends to undergo multiple scattering inside the plastic more than it would in aluminum and has a greater chance of being absorbed. In other words, the diffusion length of thermal neutrons in the plastic is much smaller than that in aluminum. Matching the moderator and foil holder diffusion lengths might help eliminate foil holder perturbations.

APPENDIX B
FLUX DEPRESSION BY CADMIUM

An experiment was performed to determine the flux depression caused by one of the cadmium pillboxes used as foil covers. A cadmium pellet was taped with mylar at the end of an aluminum foil holder of the type used in the natural uranium lattices. Gold foils, 1/8 inch in diameter and 2 mils thick, were taped to the foil holder at varying distances from the cadmium. A gold foil was placed inside the pellet to measure the epicadmium activity. The foil holder was suspended in the lattice tank parallel to the fuel rods and at a point in the moderator equidistant from the three nearest rods. Since the foils were irradiated at different heights along the axis of the tank, the activity of each foil was corrected for the exponential decrease in the flux along the axis. The experiment was done twice.

Subcadmium gold activity is plotted against distance from the center of the cadmium pellet in Fig. B. 1. The results of both experiments are plotted in this figure and are similar. The results show that at a distance of 1-1/2 inches from the cadmium pellet, the flux depression is negligible. As a result, in the measurements of the lattice activity distributions, cadmium covered foils were always placed at least 2 inches away from the bare foils.

The solid line in Fig. B. 1 has been obtained by using simple diffusion theory. The cadmium pillbox has been idealized into sphere of effective radius r_o, where r_o is the point at which the flux extrapolates to zero. The one group diffusion equation in the moderator is:

$$D\nabla^2\phi - \Sigma_a\phi + S = 0 , \qquad \text{(B. 1)}$$

where S is the source and the other terms have their usual meanings. In spherical coordinates, Eq. (B. 1) becomes

$$\frac{d^2\phi}{dr^2} + \frac{2}{r}\frac{d\phi}{dr} - \frac{\Sigma_a}{D}\phi = \frac{-S}{D} . \qquad \text{(B. 2)}$$

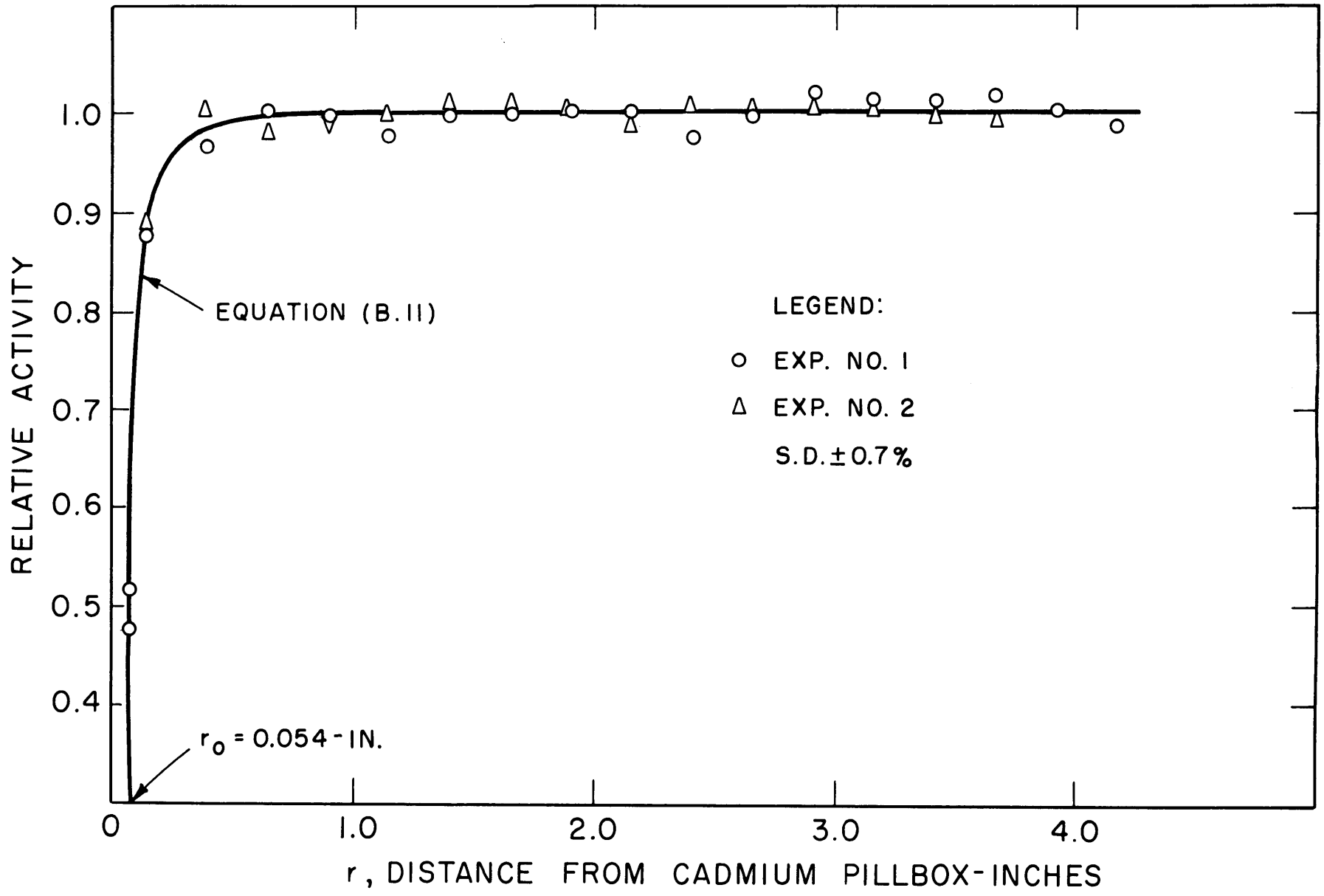

FIG. B.1 THERMAL ACTIVITY OF GOLD FOILS AS A FUNCTION OF DISTANCE FROM A CADMIUM PILLBOX

The homogeneous solution of Eq. (B. 2) is of the form

$$\phi_H = C_1 \frac{I_1(\beta r)}{r} + C_2 \frac{K_1(\beta r)}{r} , \tag{B. 3}$$

where $\beta^2 = -\Sigma_a/D$, and C_1 and C_2 are constants. In an infinite medium of D_2O, or infinitely far away from the cadmium pellet,

$$\frac{d\phi}{dr} = \frac{d^2\phi}{dr^2} = 0 , \quad (\text{at } r = \infty) . \tag{B. 4}$$

The inhomogeneous solution to Eq. (B. 2) is, therefore,

$$\phi_I = \frac{S}{\Sigma_a} . \tag{B. 5}$$

The complete solution to Eq. (B. 2) is then of the form

$$\phi = C_1 \frac{I_1(\beta r)}{r} + C_2 \frac{K_1(\beta r)}{r} + \frac{S}{\Sigma_a} . \tag{B. 6}$$

As $r \to \infty$, $\frac{I_1(\beta r)}{r} \to \infty$, and $\frac{K_1(\beta r)}{r} \to 0$,

so that C_1 must be zero. At $r = r_o$, $\phi = 0$; hence,

$$\frac{S}{\Sigma_a} + C_2 \frac{K_1(\beta r_o)}{r_o} = 0 , \tag{B. 7}$$

and

$$\phi = \frac{S}{\Sigma_a} \left[1 - \frac{r_o}{r} \frac{K_1(\beta r)}{K_1(\beta r_o)} \right] . \tag{B. 8}$$

The values of βr for D_2O are small, with the result that

$$K_1(\beta r) \cong \frac{1}{\beta r} , \tag{B. 9}$$

and Eq. (B. 7) becomes

$$\phi = \frac{S}{\Sigma_a} \left(1 - \frac{r_o^2}{r^2} \right) . \tag{B. 10}$$

Since $\phi_\infty = \frac{S}{\Sigma_a}$,

$$\frac{\phi}{\phi_\infty} = \left(1 - \frac{r_o^2}{r^2}\right). \qquad \text{(B.11)}$$

In Fig. B.1, ϕ_∞ is taken to be unity. The value of r_o that gives the best fit to the experimental data is 0.054 inches. The cadmium pellets were in the shape of cylinders, 3/16 inch in diameter by about 0.080 inches high. The volume of such a cylinder is equivalent to the volume of a sphere of radius 0.08 inches. The effective radius of a spherical cadmium pillbox of radius 0.08 inches would be somewhat smaller (about 0.07 inches), since the flux does not extrapolate to zero at the surface. The errors in a diffusion theory treatment should be greatest near the cadmium pellet; as shown by the disagreement in the effective radii. This disagreement is not bad, however, in view of the necessity to idealize the shape of the pellet into a sphere. As Fig. B.1 shows, diffusion theory does give fairly good results for the flux shape in the moderator.

APPENDIX C
FOIL PERTURBATIONS

The lutetium and europium foils were made close to infinitely dilute so as to eliminate flux perturbations. Since the gold foils were 2 mils thick, they did lead to a small but significant flux perturbation. Many methods have been developed for calculating foil perturbation effects, but the agreement between the results obtained with different methods is often not good. However, with gold foils as thin as 2 mils, and as small as 1/8 inch in diameter, the perturbations are so small, that any errors in estimating them should not be appreciable.

The foil perturbation may be broken down into two parts. The first is the self-shielding by the outer layers of the foil, which leads to a flux depression within the foil itself. The second is a flux depression, by the foil, of the flux in the surrounding medium. For gold foils with a diameter as small as 1/8 inch, in D_2O, the flux depression in the surrounding medium is an order of magnitude smaller than the self-shielding (H1). Calculations based on the method of Tittle (R1) show that the external flux depression for the gold foils used in this report is only about 0.1%; the external flux depression in the fuel should be even less.

The self-shielding effect was calculated with a standard method (R1). It is expressed in terms of the F factor, defined as the ratio of the average flux in the foil to the unperturbed flux. The self-shielding in the foil depends on the difference between the absorption cross sections of the foil and of the surrounding medium. Since the gold absorption cross section is much greater than the absorption cross sections of either the uranium or the heavy water, the flux depression in the gold was practically the same in either of the two media. In the heavy water, the self-shielding effect was less than 1/2% greater than in the fuel, with the result that the F factor was less than 1/2% smaller in the moderator. The uncertainties in calculating the F factor are probably greater than 1/2% because of the assumptions of

isotropic flux and the failure to account for transport effects. Anisotropic flux and transport effects may even change from the fuel to the moderator. Hence, the F factor was assumed to be the same in both the fuel and the moderator, and was calculated to be 0.946. In the 1-1/4-inch lattice, a lead-gold alloy was used whose properties matched the absorption and scattering properties of the fuel. The self-shielding by the lead-gold in the fuel was therefore zero; but since the absorption cross section of the lead-gold was greater than that of the moderator, the lead-gold foils in the moderator were corrected for a small amount of self-shielding. No self-shielding correction was applied to the activity distribution measured with pure gold foils, since the self-shielding correction was assumed to be the same for the foils in the moderator and the fuel. As shown in section 4.3.1, the lead-gold alloy gave the same results as the pure gold. It may be inferred that the self-shielding corrections are very nearly the same for pure gold foils in the fuel and in the moderator.

APPENDIX D
LUTETIUM AND EUROPIUM FOIL FABRICATION

A new method was developed for fabricating Lu_2O_3 and Eu_2O_3 detector foils. It was estimated to save 80% of the total cost of fabrication.

Glyptal varnish and glyptal thinner were first mixed to give 20 cc of a solution dilute enough to be sprayed with a gas-driven spray gun. The desired amount of oxide was mixed with the solution and shaken to give a uniform suspension. The suspension was then sprayed uniformly onto a sheet of 5-mil thick, high purity aluminum foil, 4 inches long by 3-1/2 inches wide. The 20 cc of suspension covered the aluminum sheet completely. When the coating had dried (after about two days), individual 1/8-inch and 1/16-inch diameter foils were punched out of the sprayed sheet. A protective coating of glyptal solution was then sprayed onto the punched foils to protect them from chipping. The amount of lutetium in the foils was estimated to be about 10 mg/cm^2, and the amount of europium about 0.2 mg/cm^2.

For intercalibration, the foils were taped with mylar to an aluminum foil wheel. The wheel was suspended by a motor driven shaft in the lattice tank, which was filled only with heavy water. After irradiation in a uniform flux, the foils were counted on both the GM and scintiallation systems described in section 2.3.4. The relative activity of each foil was proportional to the amount of lutetium or europium in it. The variation in the amount of lutetium or europium in each foil was found to be, on the average, about ± 7%. This variation was corrected for by dividing the activity of each foil irradiated in a lattice measurement by the relative activity obtained with the foil wheel calibration.

APPENDIX E
CADMIUM RATIOS AND RESONANCE INTEGRALS AS A FUNCTION OF GOLD THICKNESS

For the calculations of neutron temperatures and Westcott r factors, gold cadmium ratios at infinite dilution were needed. Gold-cadmium ratios had been measured with 2-mil thick foils in all lattices. To correct these cadmium ratios to values for infinitely thin gold foils, a series of experiments was performed in which the gold-cadmium ratio was measured as a function of the thickness of the gold foils.

Bare and cadmium covered gold foils were taped with mylar to a foil wheel similar to the one described in Appendix D. The gold foils were of five thicknesses, ranging from 2.4×10^{-4} gm/cm^2 (1% by weight gold in aluminum, 3 mils thick) to 0.246 gm/cm^2 (5 mils thick). Three sets of bare and cadmium covered foils were irradiated at each thickness to improve the statistical accuracy of the data. The foils were taped at equal spacing to the outer circumference of the wheel in such a way that every other foil was either bare or cadmium covered. In this way, the cadmium depressed the thermal flux uniformly around the circumference, and all the bare foils were subject to the same perturbation. The central 3-rod cluster of the lattice was removed and was replaced by the rotating foil wheel. The experiment was done in each of the three natural uranium lattices to determine the effect, if any, of the absolute value of the cadmium ratio on the correction factor from the value at 2 mils to that at zero thickness.

Under the assumption that the thermal and the epithermal flux depressions are independent of each other, a plot of $\frac{CR - 1}{CR_o - 1}$ versus foil thickness should be independent of the absolute value of the cadmium ratio, where CR_o is the cadmium ratio of the infinitely thin gold (taken here to be the alloy of 1% gold in aluminum), and CR is the cadmium ratio at an arbitrary thickness of gold. Such a plot is

shown in Fig. E. 1, where the results of the three foil wheel experiments are plotted. The solid line is a smooth curve drawn through the experimental data. The estimated uncertainty in the value of $\frac{CR - 1}{CR_o - 1}$ is about ± 1. 8%. The data have been normalized to unity for the foils of the gold-aluminum alloy. The values of the cadmium ratio, for gold foils 2 mils thick, for the experiments done in the 4. 5-inch, 5. 0-inch, and 5. 75-inch lattices were 6. 53, 8. 18, and 12. 48, respectively. The results for the three runs agree, within the experimental uncertainties, up to a gold thickness of 0. 03 gm/cm^2. At greater thicknesses, the data from the 5. 0-inch lattice lie slightly higher than the data from the 4. 5-inch lattice, and the data from the 5. 75-inch lattice lie slightly higher than the data from the other two lattices. These results indicate that there may be a slight increase in the value of $\frac{CR - 1}{CR_o - 1}$ with an increase in the absolute value of the cadmium ratio. This increase, however, is just outside the experimental uncertainty and may not be significant. The increase may be due to errors in the measured value of CR_o which would affect every point in Fig. E. 1. Cadmium ratios were also measured in the fuel of the natural uranium lattices by Weitzberg (W3) with an alloy of 1% gold in aluminum; he used 1. 010-inch diameter foils. Similar cadmium ratios at infinite dilution were measured with 1/8-inch diameter foils in the fuel of the 5. 75-inch lattice. The values of the cadmium ratio for 2-mil thick foils (0. 096 gm/cm^2) in the fuel were available from the microscopic measurements of the gold activity distributions. The values of the cadmium ratios for the 2-mil thick foils in the fuel were considerably lower than those in the foil wheel experiments. If the values of $\frac{CR - 1}{CR_o - 1}$ really do increase with an increase in the cadmium ratio, the values of $\frac{CR - 1}{CR_o - 1}$ for the 2-mil thick and dilute foils in the fuel should be lower than those in the foil wheel experiments. The ratio $\frac{CR - 1}{CR_o - 1}$ for 2-mil foils is plotted against the cadmium ratio for 2-mil thick foils in Fig. E. 2, which includes both the fuel and the foil wheel data. Fig. E. 2 does not show, within experimental uncertainty, any increase in $\frac{CR - 1}{CR_o - 1}$ with cadmium ratio. Thus, the indication of a trend noted in Fig. E. 1 is probably not significant.

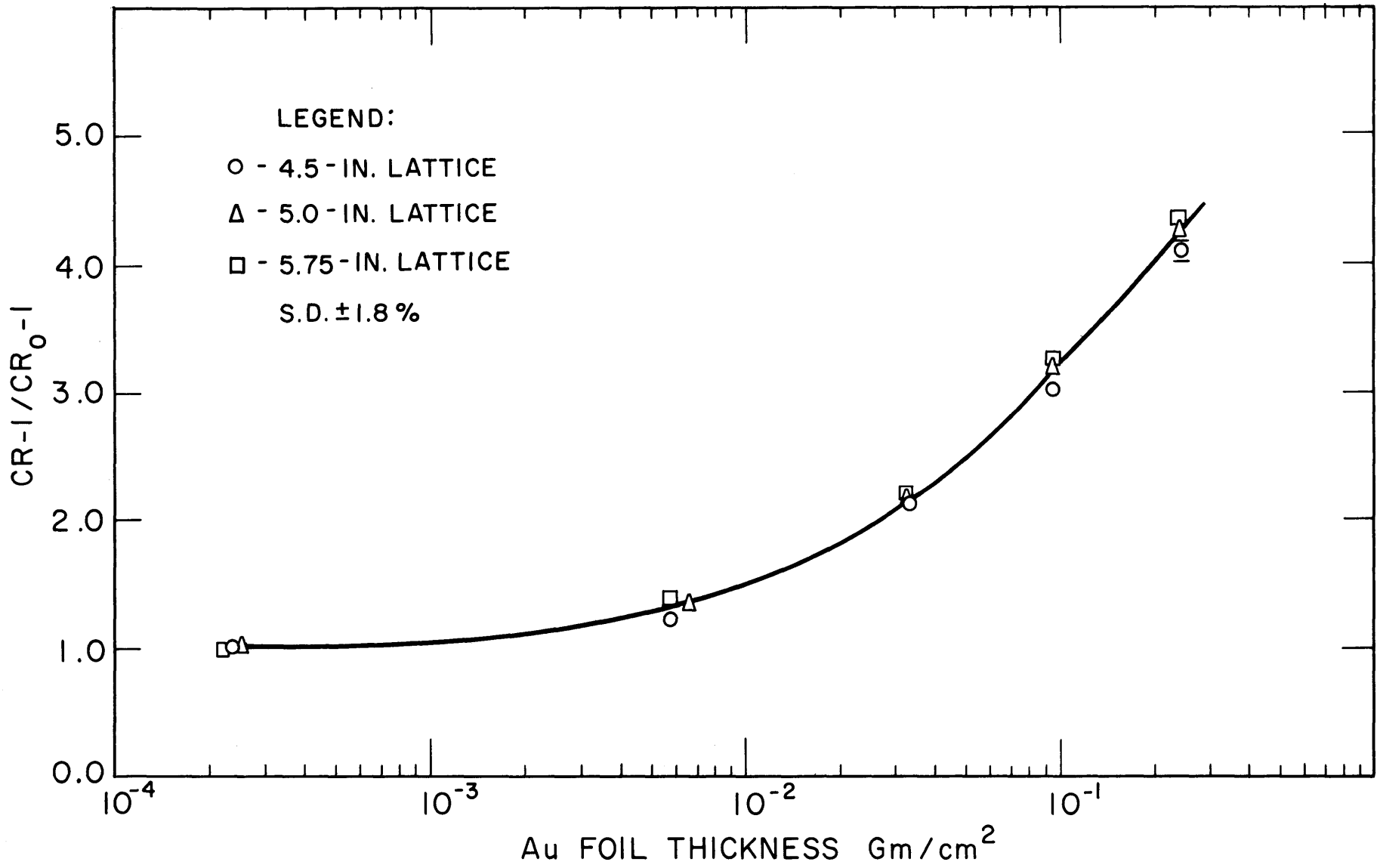

FIG. E. 1 $CR-1/CR_0-1$ OF GOLD AS A FUNCTION OF THICKNESS OF GOLD (FOIL WHEEL MEASUREMENTS IN 4.5-IN., 5.0-IN., AND 5.75-IN. LATTICES)

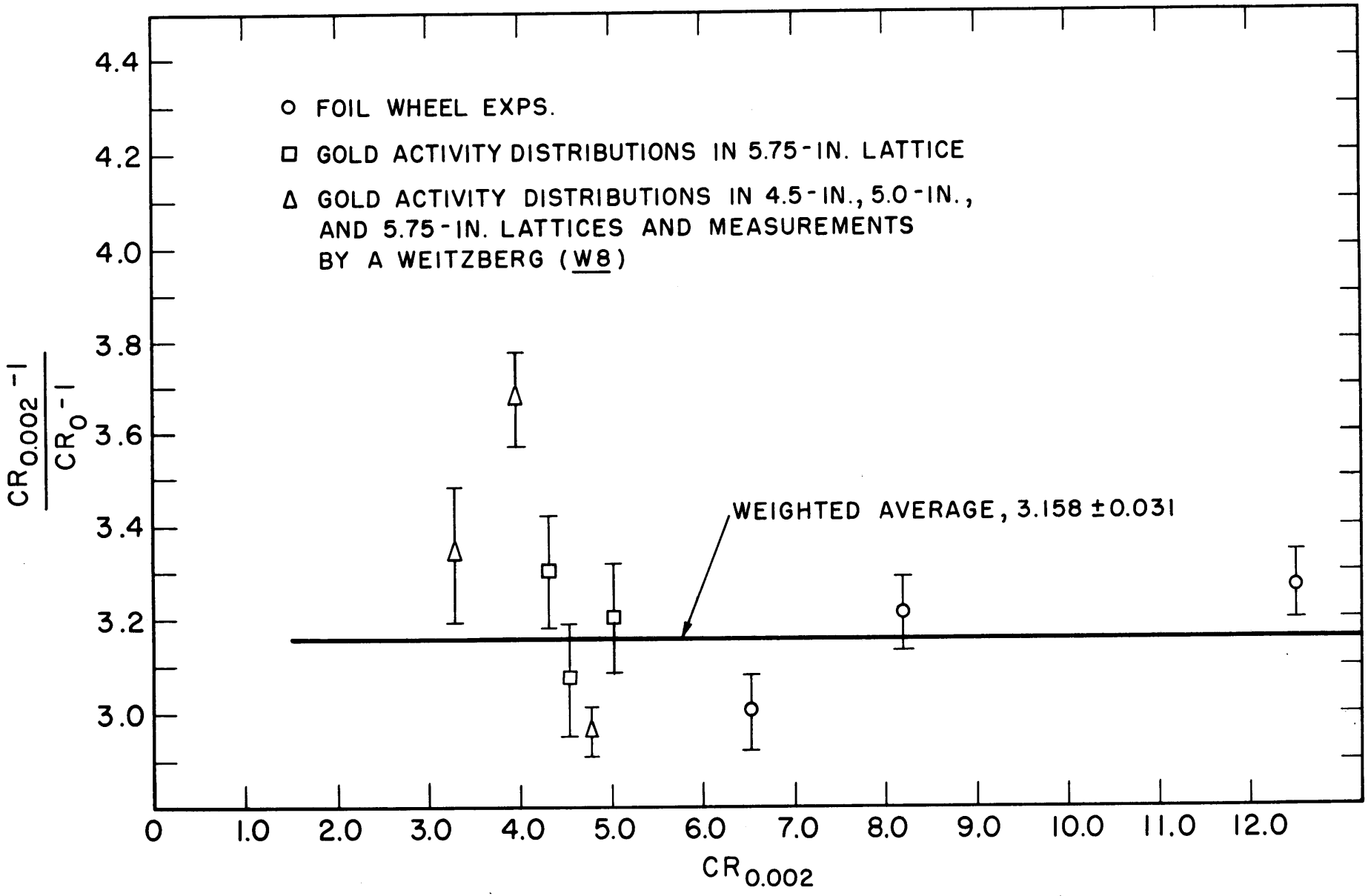

FIG. E.2 $CR-1/CR_0-1$ FOR 2-MIL THICK AU FOILS AS A FUNCTION OF THE CADMIUM RATIO OF 2-MIL THICK AU FOILS

The values of $\frac{CR - 1}{CR_o - 1}$ in Fig. E. 2 were averaged by weighting each point with the inverse square of its experimental uncertainty. The resulting value for $\frac{CR - 1}{CR_o - 1}$ was 3.158 ± 0.031. This value was used to correct all cadmium ratios for 2-mil thick gold foils to cadmium ratios at infinite dilution.

Gold resonance integrals may be calculated from the results of Fig. E. 1. The standard formula for calculating resonance activation integrals from cadmium ratio values is:

$$RI_x = (RI_s) \frac{(CR_s - 1)}{(CR_x - 1)}, \qquad (E.1)$$

where RI denotes a resonance integral, and x and s refer, respectively, to the unknown material and a standard material, the resonance integral of which is known. The standard material was assumed to be the infinitely dilute, gold-aluminum alloy, and 1553 barns was used as the resonance integral for gold at infinite dilution. The value 1553 includes the epicadmium 1/v component of the resonance integral. Since Eq. (E.1) does not account for self-shielding of the thermal flux, the values of CR - 1 had to be divided by the proper values of the self-shielding factor F. The resulting resonance integrals are plotted as the circles in Fig. E. 3. The experimental uncertainty in each point is about ± 2%. The dashed line is a smooth curve drawn through the data. The triangles in Fig. E. 3 are the results of resonance integral measurements made by Bennett (B1). He used 0.040-inch thick cadmium covers, while 0.023-inch thick cadmium covers were used in the present experiments. A correction of 3 barns was thus added to Bennett's data to account for the difference in effective cadmium cutoff energy. Bennett's values lie about 15% lower than those of this report. This result could be caused by too high a value of $CR_s - 1$, which might indicate that the gold-aluminum alloy was not quite infinitely dilute.

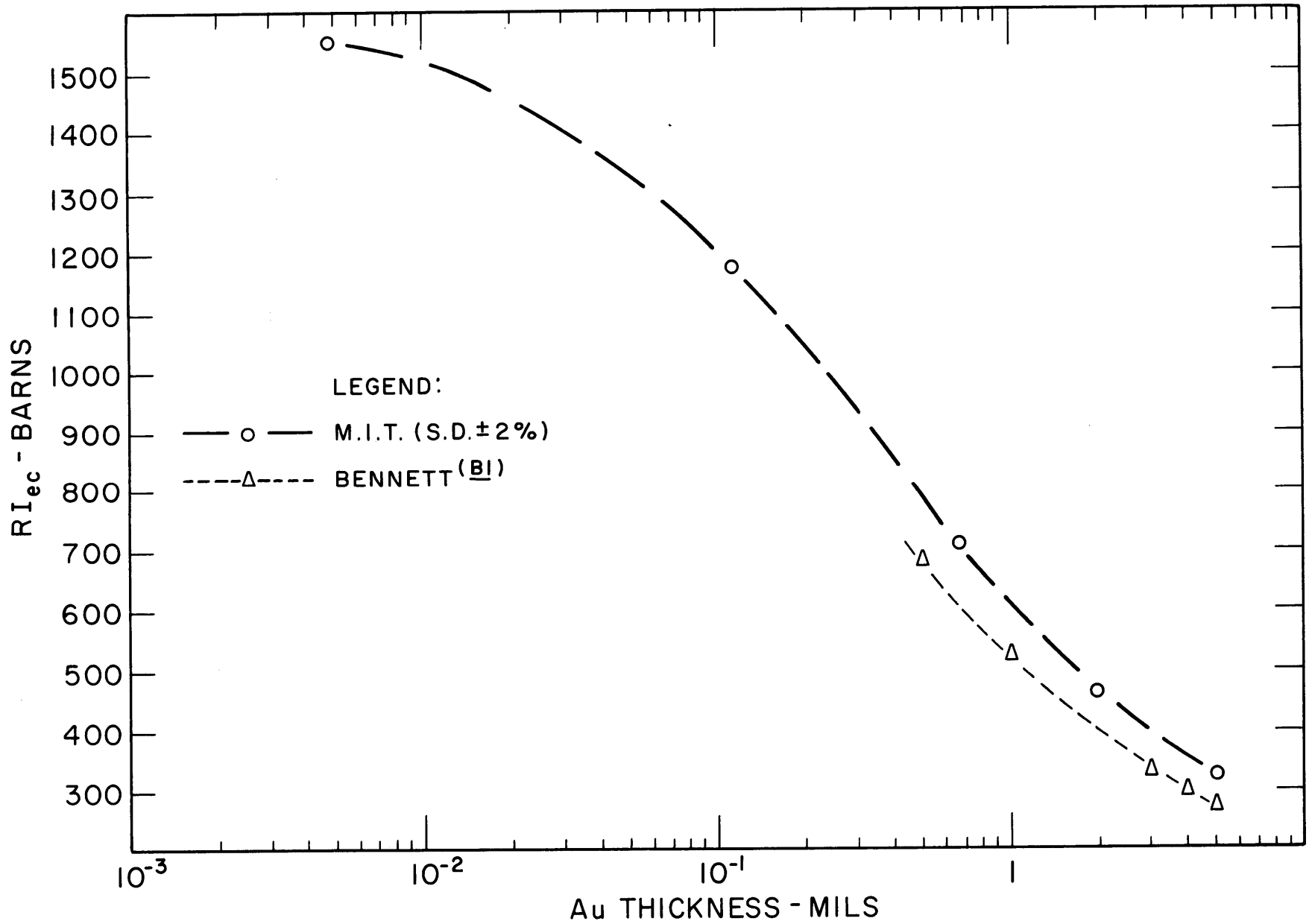

FIG. E.3 EPICADMIUM GOLD RESONANCE INTEGRAL AS A FUNCTION OF THICKNESS OF THE GOLD

APPENDIX F

A TRANSMISSION METHOD FOR MEASURING THERMAL NEUTRON SPECTRA

F.1 THEORY

Workers of the Air Force Cambridge Research Center, through work (B3) at the M.I.T. Reactor, have developed a spectral measurement method based on the transmission of a collimated beam of neutrons through varying thicknesses of an absorber. If the flux in a beam of neutrons incident upon an absorber of thickness x is denoted as $\phi_o(v)$, the flux $\phi(v)$ emerging from the absorber at x can be shown to be:

$$\phi(v) = \phi_o(v)\, e^{-\Sigma(v)\, x} \,. \tag{F.1}$$

The function $\phi_o(v)$ may be written as the product $\phi_o f(v)$, where ϕ_o is the total incident flux, and f(v) is the velocity distribution function of the incident flux. If a detector is placed in front of a neutron beam, and if this detector has an efficiency E(v), the resulting activity A(x) is

$$A(x) = \int_{v=0}^{v=\infty} \phi(v)\, E(v)\, dv = \int_{v=0}^{v=\infty} f(v)\, E(v)\, \phi_o\, e^{-\Sigma(v)x}\, dv \,. \tag{F.2}$$

The activity at x = 0 is

$$A(o) = \int_{v=0}^{v=\infty} \phi_o f(v)\, E(v)\, dv = \overline{K}\phi_o \tag{F.3}$$

where $\overline{K}$ is a constant. Equation (F.2) then becomes

$$\frac{A(x)}{A(o)} = \frac{1}{\overline{K}} \int_{v=0}^{v=\infty} f(v)\, E(v)\, e^{-\Sigma(v)x}\, dv \,. \tag{F.4}$$

If the following identity is used,

$$W(v) = f(v)\, E(v) \tag{F.5}$$

and if the transformation

$$W(v) = -\frac{d\Sigma}{dv}\, \phi(\Sigma) \tag{F.6}$$

is made, then Eq. (F. 4) becomes

$$\frac{A(x)}{A(o)} = \frac{1}{\bar{K}} \int_{\Sigma=0}^{\Sigma=\infty} e^{-\Sigma x} \phi(\Sigma)\, d\Sigma \,. \qquad (F.7)$$

Since $1/\bar{K}$ is just a constant that serves only to multiply the flux distribution f(v) by a constant, without changing its shape, the value of $\bar{K}$ may be taken to be unity. Equation (F. 7) then becomes:

$$T(x) = \frac{A(x)}{A(o)} = \int_0^{\infty} e^{-\Sigma x} \phi(\Sigma)\, d\Sigma \,. \qquad (F.8)$$

Inspection of Eq. (F. 7) shows that T(x) is simply the Laplace transform of $\phi(\Sigma)$. If T(x) is measured and the inverse transform is taken, $\phi(\Sigma)$ may be determined; when $\phi(\Sigma)$ is known, the use of Eqs. (F. 5) and (F. 6) gives f(v), the velocity distribution of the incident flux.

F. 2 EXPERIMENTAL METHOD

The Air Force workers did several experiments using the well thermalized beam of the M. I. T. reactor medical therapy room. With silver as an absorber, and with a BF_3 detector, they obtained a Maxwellian spectrum which agreed very well with spectrometer measurements of the same beam. The apparatus they used was rather large because of the collimators necessary to produce a monodirectional beam, and could not be used conveniently within fuel-moderator lattices. A variation in their technique was consequently developed and is described in the remainder of this appendix. This variation has thus far been applied only to spectra which closely resemble Maxwellian distributions.

Two cadmium tubes were fabricated which were one inch long and had an inside diameter of 1/4 inch and a wall thickness of 0. 020 inches. Inside each tube, at the bottom end, was placed a stack of 5-mil thick gold foils, 1/4-inch in diameter. One tube was capped with 0. 020 inches of cadmium at both ends; the other was capped only at the bottom. The tubes were placed parallel to each other, the open end facing the neutron source. A diagram of the experimental apparatus is shown in Fig. F. 1. The arrangement provides for an approximate beam geometry for thermal neutrons; and calculations show that the approximation is a good one and that appropriate corrections can be made. The gold serves both as the

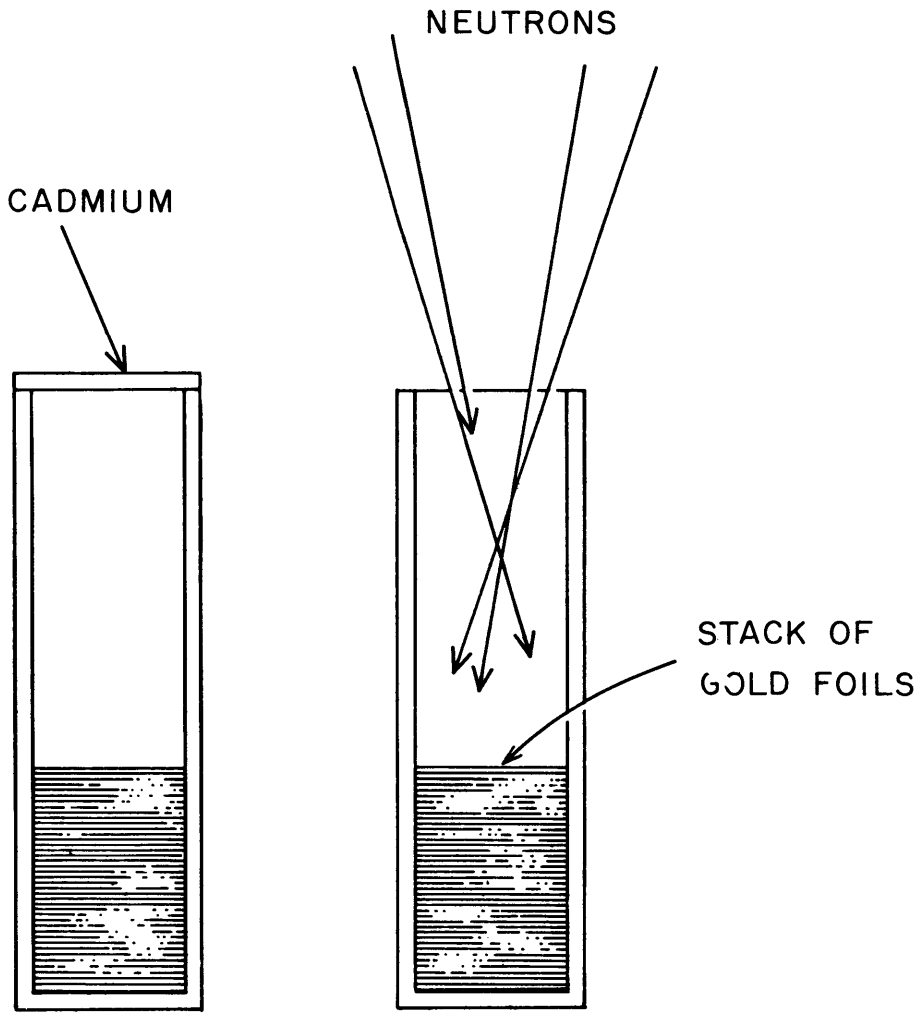

FIG. F.1 TRANSMISSION APPARATUS

absorber and the detector. It should be pointed out that since cadmium is transparent to resonance neutrons, the cadmium tubes do not provide for a beam geometry for these neutrons. For this reason, the method has only been applied to well-thermalized spectra. The completely covered cadmium tube is used to correct the activities for the few epi-cadmium neutrons present, most of which come through the sides of the tube. The following sections describe the corrections necessitated by the approximations to a beam geometry.

F.2.1 GEOMETRIC VIEW FACTOR

Since the neutron source at the open end of the cadmium tube is in most cases isotropic, the neutrons passing down the tube only approximate a beam. The number of neutrons passing through any foil in the detector stack depends on the geometric view factor of each foil relative to the open end. The view factor is identical to that used in the radiative heat transfer between two parallel circular discs. The equation used to calculate the view factor was that derived by Burt (B4). The activity of each foil must be divided by the corresponding view factor to correct the activity to that for a beam geometry.

F.2.2 EFFECTIVE PATH LENGTH OF NEUTRONS THROUGH THE STACK

Because the neutrons do not travel in a parallel beam down the tube axis, some of the neutron path lengths in the stack of foils will be greater than others; the situation is shown in Fig. F.2.

For a beam geometry, the path length at any depth x is just x itself. With the cadmium tubes, however, the path lengths vary in length from y to x, since the neutron source is isotropic and neutrons can enter the stack at angles as great as the angle θ shown in Fig. F.2. An average path length can be computed by weighting each possible path length with its importance. In this case, neutrons are being attenuated as $e^{+\Sigma x}$; thus, $e^{+\Sigma x}$ was used as the importance of each path, and the average path length, $\bar{x}$, was calculated to be

$$\bar{x} = \frac{\int_x^y x' e^{\Sigma x'} dx'}{\int_x^y e^{\Sigma x'} dx'} . \qquad (F.9)$$

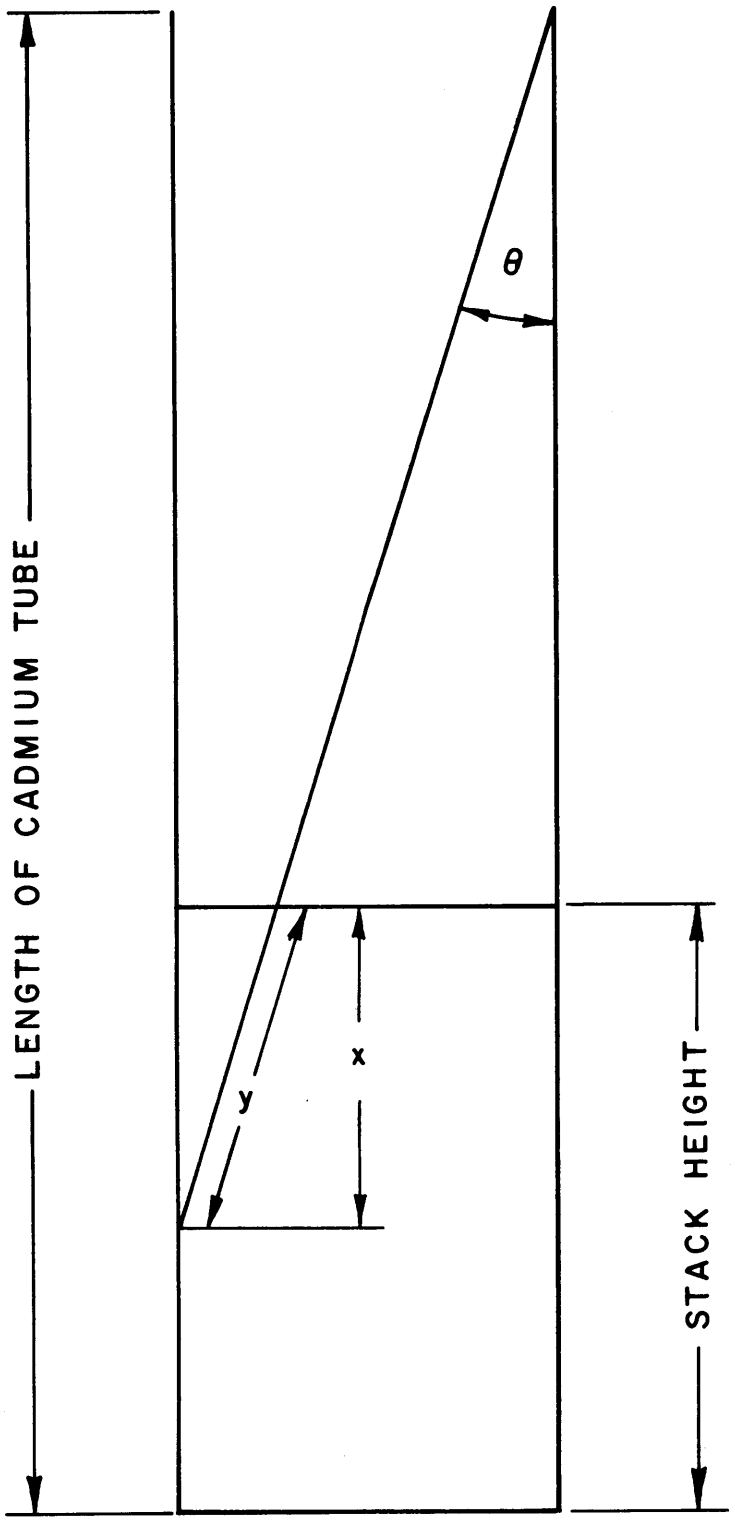

FIGURE F.2 TRANSMISSION GEOMETRY

The value of $\bar{x}$ was found to be, at the most, only 1-1/2% greater than x, so that this type of correction for the deviation from a beam geometry is probably not seriously in error. In plotting neutron transmission curves, the transmission will be given as a function of $\bar{x}$.

F.2.3 DETECTOR EFFICIENCY

The detector efficiency of a foil in a beam of neutrons is just the probability that a neutron passing through it is absorbed, and may be written as

$$E(v) = 1 - e^{-\Sigma(v)t}, \qquad (F.10)$$

where t is the effective thickness of the foil. As t approaches zero, E(v) becomes simply $\Sigma(v)t$. The effective thickness of the foil is calculated in the same way as the effective path length, $\bar{x}$.

F.2.4 BUILDUP FACTOR DUE TO SCATTERING OF NEUTRONS

The quantity Σ in Eq. (F.8) is the total macroscopic cross section and includes the effect of scattering as well as absorption. But neutrons which are scattered are not necessarily removed from the beam. The mean free path for absorption of thermal neutrons in gold is only about 1/16 of an inch. Thus, a neutron which has been scattered in going through the stack, may still be absorbed by one of the detector foils at some other position. This effect might introduce considerable error into the measured transmission curve, since the ratio of scattering to absorption at 0.025 ev is about 10% for gold. Two methods of accounting for this scattering, or buildup, effect have been considered. The first is to assume that the buildup factor is constant with position. Thus, each activity is multiplied by the same amount, which amounts to ignoring the buildup entirely. The second method assumes that each scattered neutron is absorbed at the point of scatter; this leads to a buildup factor of the form:

$$B = 1 + \frac{\bar{\sigma}_s}{\bar{\sigma}_a}, \qquad (F.11)$$

Because the neutron spectrum becomes hardened as the beam passes through the stack, $\bar{\sigma}_a$, the energy-averaged absorption cross section,

will depend upon position in the stack. An incident spectrum is assumed which closely approximates the spectrum to be measured. Equation (F. 1) is then used to calculate the spectral distribution at each point in the stack. The average velocity may be calculated as a function of x, and the value of $\bar{\sigma}_a$ corresponding to the average velocity is then obtained. The buildup correction is applied by dividing the activity at each point by the appropriate value of B from Eq. (F. 11).

A comparison of the results obtained by using the two types of buildup factor will be presented in section F. 3. A method to eliminate entirely the effects of buildup scattering will be given in section F. 4.

F. 3 GOLD TRANSMISSION EXPERIMENT

A transmission experiment was made with gold foils in the graphite-lined cavity of the M. I. T. lattice facility. The spectrum in the cavity was essentially Maxwellian, since the neutron source was the thermal column of the M. I. T. reactor. The activities in the tube capped with cadmium at both ends were subtracted from the activities in the tube open at one end to correct for the small amount of epicadmium activation. The corrections outlined in section F. 2 were made, and the resulting transmission curve as a function of $\bar{x}$ is shown in Fig. F. 3, for constant B. The experimental uncertainties in the results increase with distance through the stack, owing to the increasing statistical uncertainty caused by the rapid decrease in the activity down the stack. Figure F. 4 shows the curve of Fig. F. 3 compared with a similar curve calculated with values of B as given by Eq. (F. 11).

Burke and Lowe (B3) have found that the transmission curve for a Maxwellian spectrum can be fairly well fit by an equation of the form:

$$T(\bar{x}) = \exp[bc^{1/2} - b(\bar{x}+c)^{1/2} - a\bar{x}] \,. \qquad (F.12)$$

The inverse Laplace transform of Eq. (F. 12) is

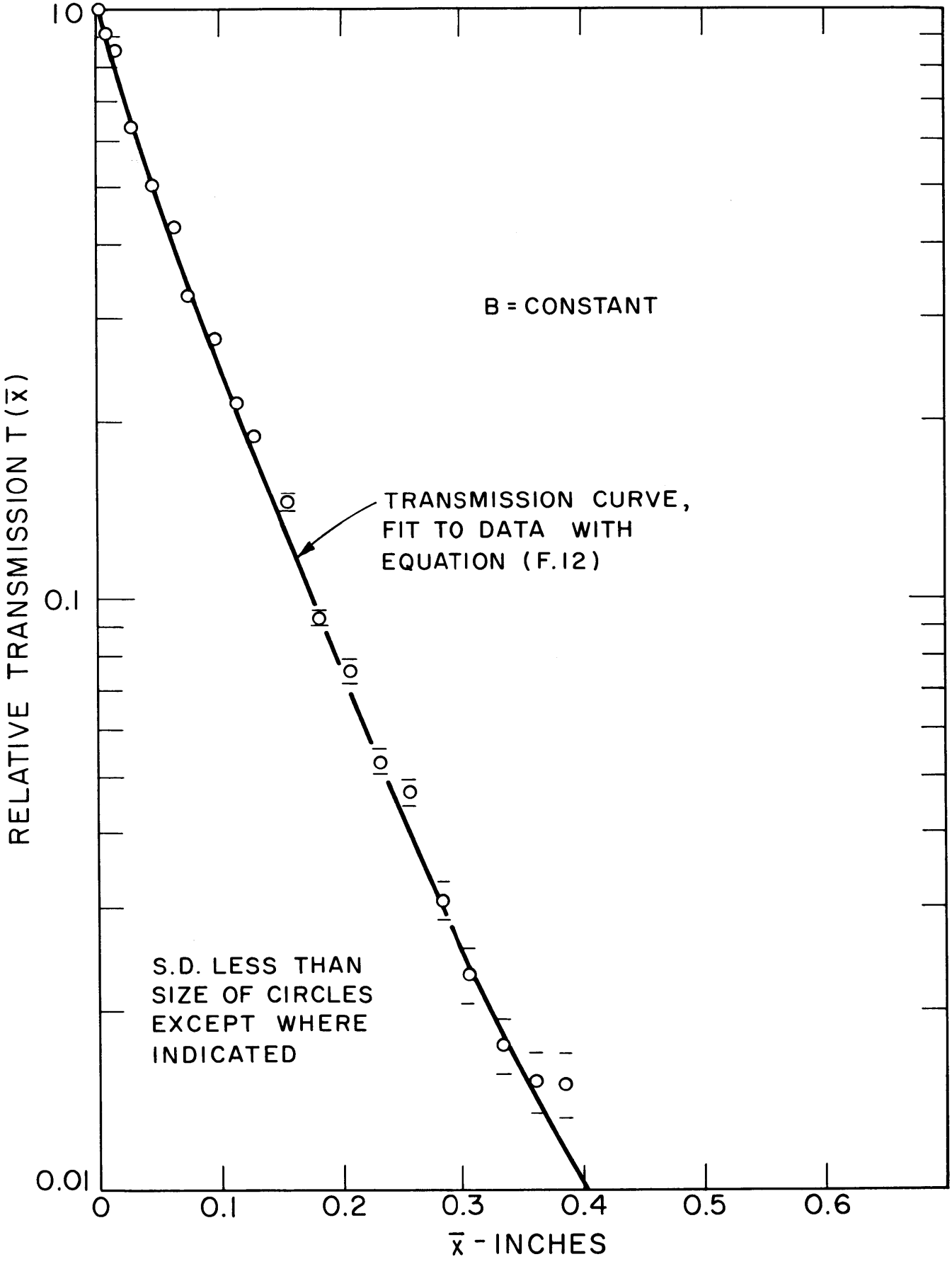

FIG. F.3 TRANSMISSION CURVE, GOLD EXPERIMENT

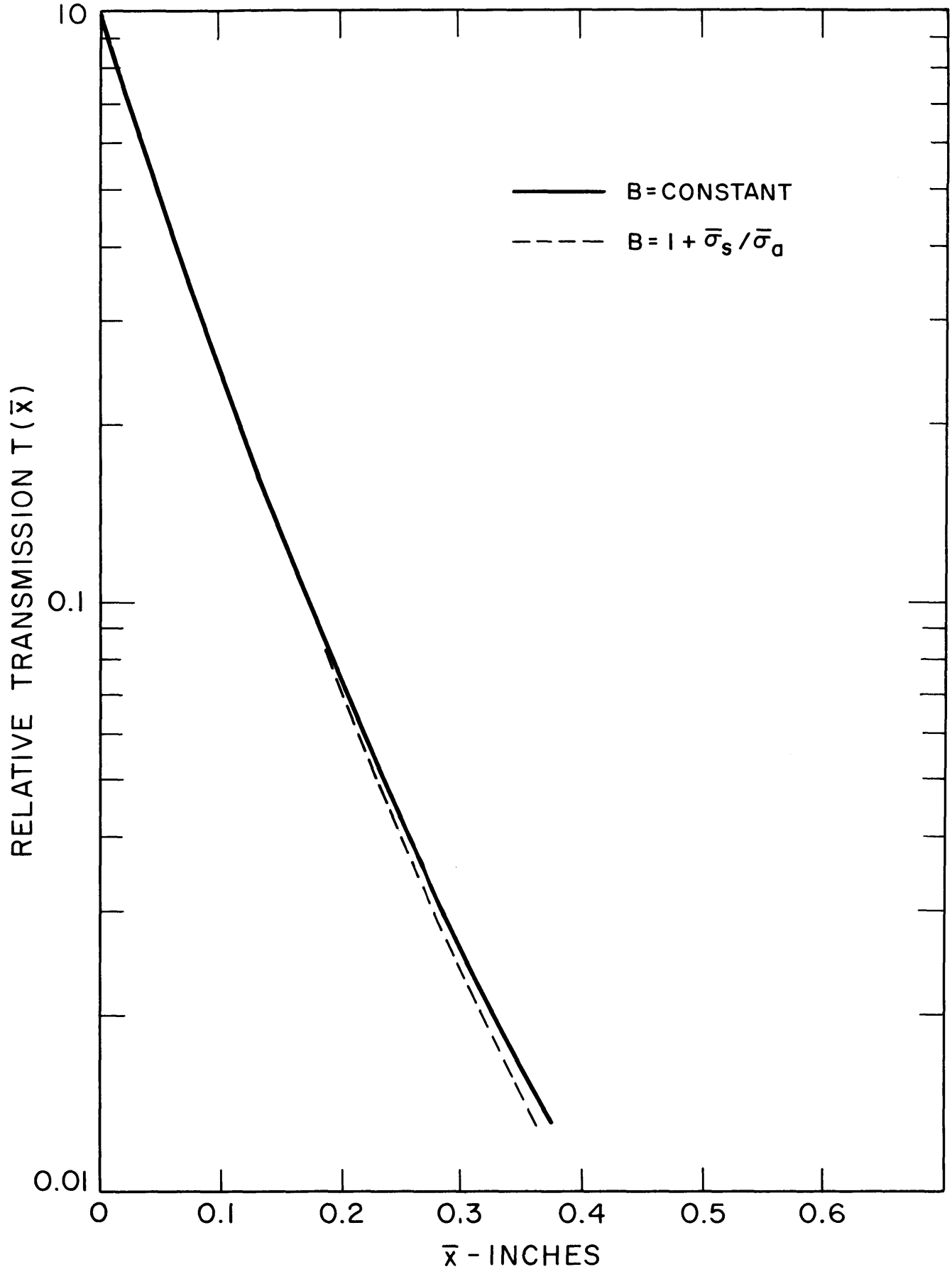

FIG. F.4 COMPARISON OF TRANSMISSION CURVES FOR $B=\text{CONSTANT}$ AND $B=1+\bar{\sigma}_s/\bar{\sigma}_a$, GOLD EXPERIMENT

$$\phi(\Sigma) = \begin{cases} 0, & \text{when } (\Sigma-a) < 0 \\ \frac{1}{2}\pi^{-\frac{1}{2}} b(\Sigma-a)^{-\frac{3}{2}} \exp[bc^{1/2} - c(\Sigma-a) - \frac{1}{4}b^2(\Sigma-a)^{-1}], & \text{when } (\Sigma-a) > 0 \end{cases} \tag{F.13}$$

The function given in Eq. (F. 12) was found to give a very good fit to the curves in Fig. F. 4. The constants a, b, and c were obtained by trial and error. After $\phi(\Sigma)$ had been obtained, Eq. (F. 6) was used to get W(v). The quantity $d\Sigma/dv$ was obtained from the gold cross section curve in BNL-325 (H13). The velocity distribution, f(v), was finally obtained by using Eqs. (F. 5) and (F. 10).

The incident velocity distribution, f(v), is plotted in Fig. F. 5 for the two types of buildup factor. A Maxwellian at 20° C is also plotted in this figure for comparison. The two distributions seem to have shapes close to that of a Maxwellian, and bracket the Maxwellian at 20° C. The curve for a constant buildup factor peaks at a velocity corresponding to a Maxwellian temperature of -21° C. The curve based on Eq. (F. 11) for B corresponds to a temperature of 76° C. Thus, the choice of a buildup factor may make considerable difference in the derived spectrum. Furthermore, as Fig. F. 3 shows, the experimental uncertainty in the second transmission decade is quite large. This uncertainty is estimated to lead to a ± 50° C uncertainty in the computed temperature. The use of a stronger neutron source or a longer irradiation time is essential to decrease this large uncertainty.

F. 4 ELIMINATION OF THE BUILDUP EFFECT

The ratio of σ_s/σ_a in gold is about 0. 1 at 0. 025 ev. It was shown in section F. 3 that appreciable uncertainty may be introduced by such a relatively large ratio of scattering to absorption. Few readily available materials exist that have much lower ratios of scattering to absorption. In B^{10}, the ratio is about 0. 005, but boron cannot be readily fabricated into uniformly thick foils. Uranium-235 has a fairly low scattering to absorption ratio. Uranium foils containing 93. 0% by weight of U^{235} were available; the scattering to absorption ratio of this material is only 0. 015. Hence, a transmission experiment was made with U^{235} as the absorber.

An arrangement similar to that used with the gold was made. Gold detector foils, 2 mils thick, were placed at various positions within the

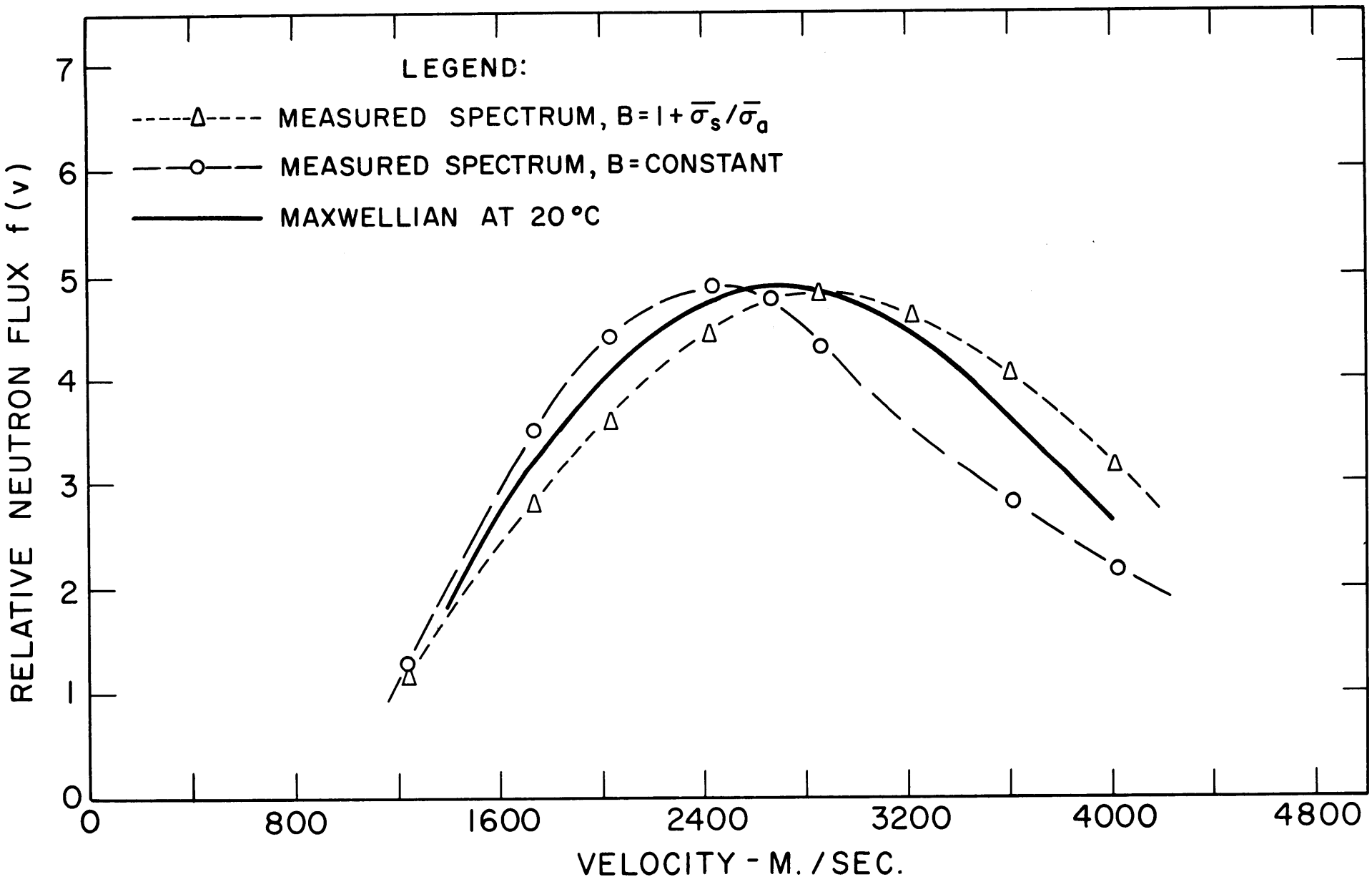

FIG. F.5 SPECTRUM MEASURED IN GOLD TRANSMISSION EXPERIMENT

two stacks of uranium foils. The gold foils were shielded on both sides with 0.6-mil thick aluminum foils to avoid fission product pickup. The two cadmium tubes were placed inside two sealed aluminum cans one inch in diameter by two inches long. The cans were attached to a motor-driven, rotating shaft which was suspended in the lattice tank, filled only with heavy water. The rotating shaft insured that each can would be irradiated in the same flux. The neutrons absorbed in the uranium lead, of course, to the birth of other neutrons from fission. But, since these neutrons have high energy, they escape from the stack without being absorbed, and enter the heavy water. During slowing down, these neutrons may be reflected back into the stack, inducing considerable epithermal activation in the gold detector foils. Hence, indium foil was also wrapped around the sides and bottom of each cadmium covered stack to help reduce the epithermal activation. The ratio of the epithermal to the thermal gold activity ranged from 3-1/2% at the top of the stack to unity at the bottom. This large epithermal correction led to large experimental uncertainties at the stack bottom but, because of the strong neutron source, it was still possible to obtain two decades of accurate transmission data.

The U^{235} transmission curve is shown in Fig. F.6, where transmission is plotted against the number of grams of uranium through which the beam has passed. The gold and aluminum present in the stack have been weighted with their densities and cross sections and have been expressed in equivalent numbers of grams of uranium. The data over the first two decades are fairly accurate and Eq. (F.12) was fitted to the data. The data and the curve agree to within ± 1% up to a uranium thickness of 0.9 grams, and to within ± 2-1/2% at greater thicknesses.

The inverse transform of the curve in Fig. F.6 was taken, and the resulting spectrum is plotted in Fig. F.7. Maxwellians at 27° C (the material temperature of the heavy water in the tank) and 53° C (the temperature corresponding to the peak in the measured distribution) are also shown in Fig. F.7. The Maxwellian at 53° C gives a fairly good fit to the measured spectrum at higher velocities, and the Maxwellian at 27° C gives a fairly good fit at lower velocities. The data may be higher than the 27° C Maxwellian at higher velocities because of the presence of an epithermal tail due to fission neutrons. The assumption that the

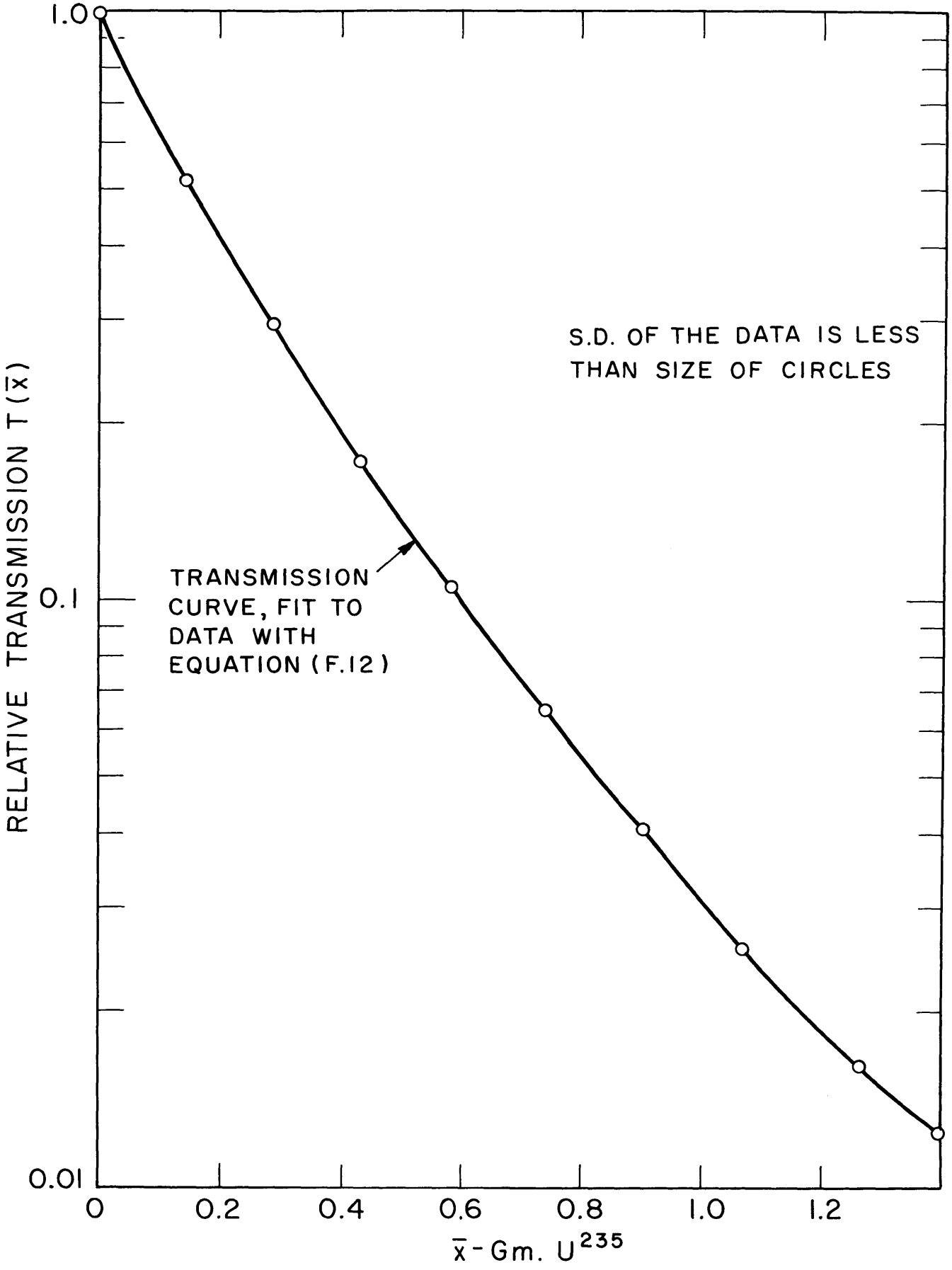

FIG. F.6 TRANSMISSION CURVE, U^{235} EXPERIMENT

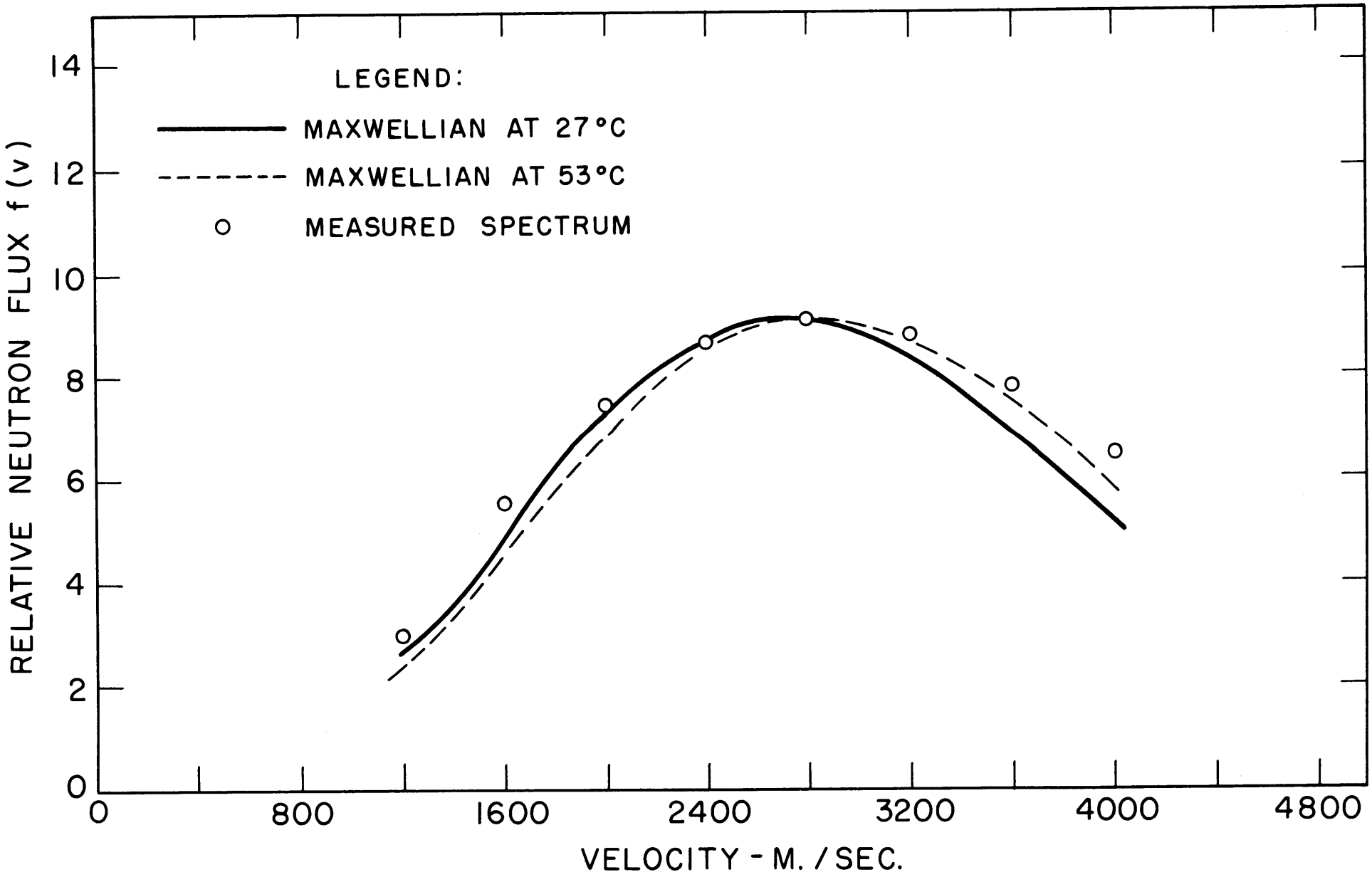

FIG. F.7 SPECTRUM MEASURED IN U^{235} TRANSMISSION EXPERIMET

spectrum is a pure Maxwellian (which led to the subtraction of the epi-cadmium activity) makes possible an integration up to infinite velocity in Eq. (F. 8). If the epithermal contribution is too large, the use of such an assumption may lead to errors. A constant buildup factor was used in computing the spectrum in the U^{235} transmission experiment. A small correction is probably necessary to account for scattering, although the exact type of correction to be used is open to question. The uncertainty in measuring a Maxwellian spectrum with the U^{235} transmission experiment is considerably smaller than that for gold transmission, and is estimated, in this case, to be less than ± 15° C.

F. 5 RECOMMENDATIONS FOR FUTURE WORK

The use of U^{235} eliminated most of the uncertainty due to the scattering present in the gold experiment. However, the U^{235} still scatters neutrons to a small, but possibly significant, extent. The use of B^{10} would eliminate more of the uncertainty due to buildup, if it could be fabricated into foils of uniform thickness. At present, the transmission method is suitable only for the measurement of thermal, nearly Maxwellian spectra. The treatment of neutron transmission in the epithermal region would be greatly complicated by resonances in a material like U^{235}. Boron-10 has no resonances below 0. 4 Mev and should be satisfactory for the measurement of spectra with epithermal components. It is not activated, so that the problem of detection would be difficult. The use of infinitely dilute gold foils, the resonances of which should not perturb the measurement, might solve the detection problem. A very strong neutron source would then be necessary, because of the small expected activities. Furthermore, since cadmium tubes do not provide a beam geometry for resonance neutrons, a transmission tube would also have to be wrapped with a filter that absorbs resonance neutrons, such as gold or indium foil. A transmission experiment could probably be made in a non-Maxwellian spectrum, e. g., in a lattice spectrum, by using two cadmium tubes as was done in the present work. The measurement would then be of the subcadmium spectrum, and Eq. (F. 8) could no longer be integrated to infinite energy, but only to about 0. 4 ev. The Laplace Transform method would no longer be applicable, and a computer would be

needed for the solution of the integral equation. The feasibility of such a lattice measurement is open to question because of the possible disturbance of the lattice spectrum by the cadmium tubes. There were probably such perturbations in the gold and uranium transmission experiments discussed above; but both of those experiments were made in cavities of the media being investigated, so that the perturbations were probably not too large. A transmission experiment could, of course, be done in a cavity in a lattice. Orientation of the transmission tubes might yield valuable information about the angular dependence of the neutron energy spectrum.

Experiments done to date have been exploratory in nature. Refinements in the experimental and analytical methods can be made. It is believed that the transmission method can be developed into a useful technique for measuring near-Maxwellian spectra. Much development work will be required, however, before the method will be suitable for more complicated spectra.

APPENDIX G
THERMOS INPUT DATA

1. Natural Uranium Lattices

Number of velocity groups: 30; a listing of the group energies is given in BNL-5826 (H6).

Number of space points: 5 equally spaced points in the fuel, 1 in the cladding, and 8 equally spaced points in the moderator

Slowing-down source: Spatially flat in fuel and moderator

Effective temperature of moderator: 1.0

High energy scattering cross sections:

Nuclide	Cross section (barns)
U^{238}	8.3
Al^{27}	1.35
D^{2}	2.75

Nuclide concentrations:

Nuclide	Concentration (atoms/barn/cm)
U^{235}	3.4541×10^{-4}
U^{238}	4.7592×10^{-2}
Al^{27}	6.0275×10^{-2}
O^{16}	3.1805×10^{-2}
D^{2}	5.3944×10^{-2}
H^{1}	9.7362×10^{-5}

Cross sections: All thermal cross sections are tabulated in BNL-5826 (H6). Lu^{176} cross sections were obtained from reference (R2).

2. The 1.25-inch Lattice

The input data for the 1.25-inch lattice were the same as for the natural uranium lattices except for the following:

Number of space points: 3 equally spaced points in the fuel, 1 point in the cladding, and 6 equally spaced points in the moderator

Nuclide concentrations:

Nuclide	Concentration (atoms/barn/cm)
U^{235}	4.9752×10^{-4}
U^{238}	4.7340×10^{-2}

APPENDIX H
TRANSMISSION OF NEUTRONS THROUGH CADMIUM

An experiment was made to determine the activity of cadmium-covered europium foils as a function of the thickness of the cadmium. Europium foils covered with several thicknesses of cadmium were irradiated in a uniform flux on a rotating foil wheel. The foil wheel was inserted in the lattice tank in place of the central three-rod cluster of the 5.75-inch lattice. Three foils were irradiated at each thickness to improve the statistical accuracy of the results. The foil activities were measured with the GM counting system described in section 2.3.4. The results of this experiment are discussed in section 4.2.3.

The attentuation of monoenergetic neutrons by cadmium is described in this appendix. Consider monoenergetic neutrons impinging isotropically on an effectively infinite cadmium sheet of thickness x. See Fig. H.1. The absorption cross section of the cadmium for these neutrons is Σ. The angle of incidence of a particular neutron is θ, and cos θ is denoted by μ. The angular dependent incident flux is $\phi_o(\mu)$. The emergent flux for a particular direction μ is then given by

$$\phi_x(\mu) = \phi_o(\mu)\, e^{-\Sigma x \sec \theta}. \qquad \text{(H.1)}$$

Since the incident flux is isotropic, $\phi_o(\mu)$ is a constant,

$$\phi_o(\mu) = Q. \qquad \text{(H.2)}$$

Integration of $\phi_x(\mu)$ over all directions yields the total emergent flux:

$$\phi_x = \int_0^1 \phi_x(\mu)\, d\mu = \int_0^1 \phi_o(\mu)\, e^{-\Sigma x \sec \theta}\, d\mu, \qquad \text{(H.3)}$$

or

$$\phi_x = Q \int_0^1 e^{-\Sigma x \sec \theta}\, d(\cos \theta). \qquad \text{(H.4)}$$

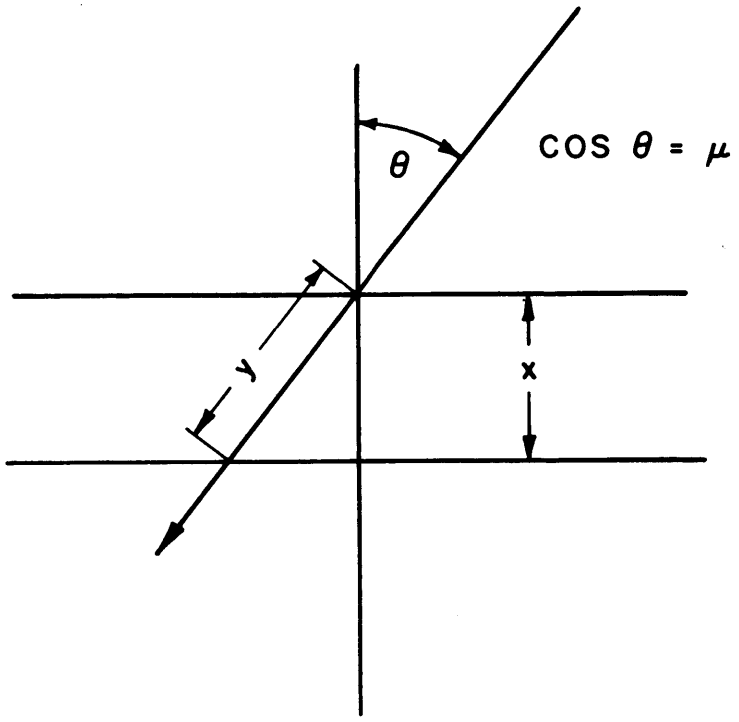

FIG. H.1 GEOMETRY OF TRANSMISSION OF NEUTRONS THROUGH CADMIUM

Since

$$\sec \theta = \frac{y}{x} , \tag{H. 5}$$

and

$$d (\cos \theta) = - \frac{x}{y^2} dy , \tag{H. 6}$$

then

$$\phi_x = - Qx \int_{\infty}^{x} \frac{e^{-\Sigma y}}{y^2} dy , \tag{H. 7}$$

and

$$\phi_x = QE_2(\Sigma x) . \tag{H. 8}$$

Thus, the attentuation of the neutrons by the cadmium sheet may be described by an exponential integral of the second kind. The result for an infinite cadmium sheet should be applicable to circular cadmium foils with a large ratio of diameter to thickness. For the cadmium covers used in the natural uranium lattices, this ratio was 5. 5, and for the 1. 25-inch lattice, it was 3. 0. The errors introduced by the use of Eq. (H. 8) are probably no worse than those due to the assumption of monoenergetic neutrons. The use of the function $E_2(\Sigma x)$ is, indeed, an approximation but, as explained in section 4. 2. 3, it is probably justified by the small size of the correction.

APPENDIX I
NOMENCLATURE

A	Brown-St. John effective mass for D_2O (amu)
A	Activity (when A is used to denote activity, it is subscripted or superscripted)
a	Constant used in Eq. (F. 12)
a_s	Constant used in Eq. (1. 2)
B	Buildup factor
B^2	Buckling (cm^{-2})
b	Constant used in Eq. (F. 12)
b_e	Constant used in Eq. (1. 2)
c	Constant used in Eq. (F. 12)
C_1	Constant used in Eq. (B. 3)
C_2	Constant used in Eq. (B. 3)
CR	Cadmium ratio
CR_o	Cadmium ratio of a zero thickness foil
CR_s	Cadmium ratio of a standard material, Eq. (E. 1)
CR_x	Cadmium ratio of an unknown material, Eq. (E. 1)
D	Thermal diffusion constant (cm)
E	Energy (ev)
E_o	Energy corresponding to the most probable velocity of a Maxwellian (ev)
E_2	Exponential integral function of the second kind
E(v)	Detector efficiency as function of velocity
F	Fuel disadvantage factor; also used in Appendix C to denote a foil self-shielding factor

F_m	Moderator disadvantage factor
FF_m	The product of F and F_m
f	Thermal utilization factor
f(v)	Velocity distribution function of the flux used in Appendix F
g	Westcott g factor
I_1	Modified Bessel function of the first kind of order 1
J_o	Bessel function of the first kind of order 0
K	Constant used in Eq. (4.1)
$\bar{K}$	Constant defined in Eq. (F.3)
K_{Cd}	Constant used in Eq. (3.17)
K_1	Modified Bessel function of the second kind of order 1
k_∞	Infinite multiplication factor
L	Thermal diffusion length (cm)
M(v)	Function defined in Eq. (3.26)
$N(\bar{r}, v)$	Neutron density per unit velocity at position $\bar{r}$ ($n/cm^3/cm/sec$)
$\bar{N}$	Neutron density averaged over space and energy (n/cm^3)
N_i	Density of material i ($atoms/cm^3$)
P_n	Legendre polynomial of degree n
p	Resonance escape probability
Q	Constant used in Eq. (H.8)
r	Westcott r factor; also used to denote radius
r_o	Effective radius of a cadmium pillbox (cm)
$\bar{r}, \bar{r}'$	Symbols used to denote position coordinates
RC	Symbol used to denote the quantity $\frac{(CR-1)_{Pb-Au}}{(CR-1)_{0.002}}$
RI_s	Resonance integral of a standard material (barns)
RI_x	Resonance integral of an unknown material (barns)

S	Neutron source ($n/cm^3/sec$)
S_n	Symbol used to denote Carlson's method, where n is the degree of the approximation
s	Westcott s factor
T	Neutron temperature
T_o	293.6°K
$T(x)$	Transmission as a function of x
t	Foil thickness (cm)
V	Volume (cm^3)
v, v'	Velocity (cm/sec) or (m/sec)
$\bar{v}$	Average velocity (cm/sec) or (m/sec)
v_o	Most probable velocity (2200 m/sec)
v_t	Velocity defined in Eq. (3.26) (cm/sec) or (m/sec)
$W(v)$	Function defined in Eq. (F.5)
x	Thickness or distance (cm)
x'	Dummy variable in Eq. (F.9) (cm)
$\bar{x}$	Effective path length defined in Eq. (F.9) (cm)
y	Distance defined in Figs. F.2 and H.1 (cm)

Greek Symbols

α	Constant used in Eq. (3.15)
β	Constant defined in Eq. (B.3)
ΔT	Change in temperature
∇^2	Laplacian operator
ϵ	Fast fission factor
η	Number of neutrons released per thermal absorption in fuel
θ	Angle used in Figs. F.2 and H.1
μ	Cos θ

μ_o	Cosine of the scattering angle
$\bar{\mu}_o$	Average cosine of the scattering angle
ρ	Ratio of the epicadmium to the subcadmium activity used in the Fermi method
ρ'	Ratio defined in Eq. (1.3)
$\sigma(\bar{r}, v)$	Cross section at velocity v and position $\bar{r}$ (barns)
$\sigma(v)$	Cross section at velocity v (barns)
σ_o, σ_{2200}	Cross section at velocity of 2200 m/sec (barns)
$\hat{\sigma}$	Westcott effective cross section (barns)
$\bar{\sigma}$	Cross section averaged over space and energy (barns)
Σ	Macroscopic cross section (cm^{-1})
$\phi(\bar{r}, v)$	Neutron flux per unit velocity ($n/cm^2/sec/cm/sec$)
$\phi(\Sigma)$	Function defined in Eq. (F.6)
$\bar{\phi}$	Flux averaged over velocity and position ($n/cm^2/sec$)
ϕ_a	Flux at the surface of the fuel ($n/cm^2/sec$)
ϕ_o	Total incident flux in transmission experiment ($n/cm^2/sec$)
$\phi_o(v)$	Velocity dependent incident flux in transmission experiment ($n/cm^2/sec/cm/sec$)
ϕ_∞	Flux infinitely far from a cadmium pillbox

Subscripts and Superscripts

a	Absorption (except in ϕ_a, where a denotes surface of fuel)
clad	Refers to cladding region
epi	Refers to epicadmium activity
f, fuel	Refers to fuel region
fuel surf	Refers to the surface of the fuel
i	Refers to region i
m, mod	Refers to moderator region
s	Scattering
th	Refers to thermal activity
Total	Refers to total activity

APPENDIX J
REFERENCES

A1. Amouyal, A., Benoist, P., and Horowitz, J., "A New Method for the Determination of the Thermal Utilization Factor of a Cell," J. Nuclear Energy, 6, 79-98 (1957).

B1. Bennett, R. A., "Effective Resonance Integrals of Cu and Au," Nuclear Physics Research Quarterly Report, HW-63576 (January, 1960).

B2. Biell, A. T., Cohen, E. R., and Woods, D., "A Measurement of the Neutron Temperature Effect Using Europium Oxide Foils," NAA-SR-148 (1951).

B3. Burke, E. A., and Lowe, L. F., "Derivation of Thermal Neutron Spectra from Transmission Data," Nuclear Instruments and Methods, 7, p. 193 (1960).

B4. Burt, B. P., Nucleonics, 5 (1949).

B5. Brown, H. D., and St. John, D. S., "Neutron Energy Spectrum in D_2O," DP-33 (February, 1954).

C1. Carlson, B. G., "Solutions of the Transport Equation by S_n Approximations," LA-1599 (1953).

C2. Carlson, B. G., "Solutions of the Transport Equation by S_n Approximations," LA-1891 (1955).

C3. Carlvik, I., and Pershagen, B., "Calculation of the Flux at the Surface and the Average Flux (Disadvantage Factor) for a Cylindrical Fuel Element," AEF-68 (Swedish) (October, 1956), AEC-tr -3313 (English).

C4. Cohen, E. R., "Exponential Experiments on D_2O-Uranium Lattices," A/Conf. 8/ P/605.

G1. Galanin, A. P., "The Theory of Thermal Neutron Nuclear Reactors," Part 2, Consultants Bureau, Inc., New York (1953).

G2. Groshev, L. V., et al, "Conference of the Academy of Sciences of the U.S.S.R. on the Peaceful Uses of Atomic Energy," Vol. 1 (July 1955) p. 45, also AEC-tr-2435.

H1. Hanna, G. C., "The Depression of Thermal Neutron Flux and Density by Absorbing Foils," Nucl. Sci. Eng., 3, (November, 1961).

H2. Heath, R. L., "Scintillation Spectrometry Gamma-Ray Spectrum Catalogue," IDO-16408 (July, 1957).

H3. "Heavy Water Lattice Research Project Annual Report," NYO-9658 (September, 1961).

H4. Heinzman, O. W., and Kash, S. W., "Intracell Flux Distributions for an Extensive Series of Heavy Water, Uranium Rod Lattices," NAA-SR-1546 (August, 1956).

H5. Hickman, G. D., and Leng, W. B., "The Calculation of Effective Cutoff Energies for Cadmium and Samarium," Trans. ANS, 4, No. 1 (June, 1961).

H6. Honeck, H. C., "THERMOS, A Thermalization Transport Theory Code for Reactor Lattice Calculations," BNL-5826 (Sept., 1961).

H7. Honeck, H. C., and Kaplan, I., "The Distribution of Thermal Neutrons in Space and Energy in Reactor Lattices, Part I: Theory, and Part II: Comparison of Theory and Experiment," Nucl. Sci. Eng., 8, No. 3 (September, 1960).

H8. Honeck, H. C., "A Method for Computing Thermal Neutron Distributions in Reactor Lattices as Functions of Space and Energy," Ph.D. Thesis, M.I.T. (June, 1959).

H9. Honeck, H. C., "An Incoherent Thermal Scattering Model for Heavy Water," Trans. ANS, 5, No. 1 (June, 1962).

H10. Honeck, H. C., Summary paper presented at the Brookhaven Conference on Neutron Thermalization (1962), to be published in a future BNL report.

H11. Honeck, H. C., "The Calculation of the Thermal Utilization and Disadvantage Factor in Uranium Water Lattices," IAEA Conf. on Light Water Lattices (April, 1962).

H12. Horowitz, J., and Tretiakoff, O., "Effective Cross Sections for Thermal Reactors," European American Nuclear Data Committee, Oak Ridge Meeting EANDC (E) 14 (November, 1960).

H13. Hughes, D. J., and Schwartz, R. B., "Neutron Cross Sections," second edition, BNL-325 (1958); also, 1960 Supplement.

H14. Haefner, R., "A Multigroup P_3 Program for the Neutron Transport Equation," DP-427 (1959).

K1. Kim, H., Research Project, Course 22.42, M.I.T., unpublished (June, 1962).

K2. Kushneriuk, S. A., and McKay, C., "Neutron Density in an Infinite Non-Capturing Medium Surrounding a Long Cylindrical Body which Scatters and Captures Neutrons," AECL-137, Chalk River (1954).

K3. Kushneriuk, S. A., "Neutron Capture by Long Cylindrical Bodies Surrounded by Predominantly Scattering Media," AECL-462 (June, 1957).

K4. Kranz, A. Z., "Measurements of f, p, and ϵ of Water-Moderated Slightly Enriched Lattices," WAPD-134.

M1. Macdougall, J. P., "Application of Scattering Law Data to the Calculation of Thermal Neutron Spectra," paper presented at the Brookhaven Conference on Neutron Thermalization (1962), to be published in a future BNL report.

M2. Madell, J., Thompson, T. J., Profio, A. E., and Kaplan, I., "Spatial Distribution of the Neutron Flux on the Surface of a Graphite-Lined Cavity," NYO-9657 (April, 1962).

N1. Nelkin, M., "Scattering of Slow Neutrons by Water, Phys. Rev., 119, 741 (1960).

P1. Palmedo, P. F., Kaplan, I., and Thompson, T. J., "Measurements of the Material Bucklings of Lattices of Natural Uranium Uranium Rods in D_2O," NYO-9660 (January, 1962).

P2. Peak, J. P., Kaplan, I., and Thompson, T. J., "Theory and Use of Small Subcritical Assemblies for the Measurements of Reactor Parameters," NYO-10204 (April, 1962).

P3. Pershagen, B., and Carlvik, I., "Calculation of the Disadvantage Factor in a Cylindrical Lattice Cell," AEF-69 (Swedish) (November, 1956), AEC-tr-3314 (English).

R1. "Reactor Physics Constants," ANL-5800, 485-487.

R2. Roberge, J. P., and Sailor, V. L., "Parameters of the Lu^{176} Neutron Resonance at 0.142 ev," Nucl. Sci. Eng., 7, p. 502 (June, 1960).

S1. Sefchovich, E., Research Project, Course 22.42, M.I.T., unpublished (June, 1962).

S2. Simms, R., Private communication about calculations done at the M.I.T. Computation Center.

S3. SLO P-1, "A Thermal Multigroup Program for the IBM-704," WAPD-TM-188 (October, 1960).

T1. Tait, J. H., "The Calculation of the Fine Structure of the Thermal Neutron Flux in a Pile by the Spherical Harmonics Method," A/Conf. 8/P/433.

T2. Theys, M. H., "Integral Transport Theory of the Thermal Utilization in Heterogeneous Reactors," M.S. Thesis, M.I.T. (September, 1958).

T3. Thie, J. A., "Failure of Neutron Transport Approximations in Small Cells in Cylindrical Geometry," Nucl. Sci. Eng., 9, (February, 1961).

W1. Weinberg, A. M., and Wigner, E. P., "The Physical Theory of Neutron Chain Reactors," University of Chicago Press, p. 632 (1958).

W2. Ibid, p. 246.

W3. Weitzberg, A., Kaplan, I., and Thompson, T. J., "Measurements of Neutron Capture in U-238 in Lattices of Uranium Rods in Heavy Water," NYO-96591 (January, 1962).

W4. Westcott, C. H., "Effective Cross Section Values for Well-Moderated Thermal Reactor Spectra," 3rd Edition Corrected, AECL-1101 (November, 1960).

W5. Westcott, C. H., "Effective Cross Section Values for Well-Moderated Thermal Reactor Spectra," 1958 Revision, AECL-670 (August, 1958).

W6. Westcott, C. H., Walker, W. H., and Alexander, T. K., "Effective Cross Sections and Cadmium Ratios for the Neutron Spectra of Thermal Reactors," A/Conf. 15/P/202.

W7. Wigner, E. P., and Wilkins, J. E., "Effect of the Temperature of the Moderator on the Velocity Distribution of Neutrons, with Numerical Calculations for H as Moderator," AECD-2275 (September, 1944).

W8. Wikdahl, C., A. B. Atomenergi, Sweden, Private Communication, 1961.

W9. Wolberg, J., Kaplan, I., and Thompson, T. J., "A Study of the Fast Fission Effect in Lattices of Uranium Rods in Heavy Water," NYO-9961 (February, 1962).

W10. Woods, D. C., and Biehl, A. T., "Intra Cell Neutron Densities in Natural Uranium-D_2O Lattices, Part II," NAA-SR-138 (August, 1953).

APPENDIX K
SUPPLEMENTARY LITERATURE SURVEY

In this appendix, a number of papers on the general subject of thermal neutron capture are listed to serve as a guide to future workers in this area. The papers are divided under several sub-headings and, in each group, are listed in chronological order. The list is not complete, but contains most of the more important papers. Occasional cross references are included, and these refer to other references in this section.

CONTENTS

K. 1 General References and Summaries

1. Case, K. M., de Hoffman F., and Placzek G., "Introduction to the Theory of Neutron Diffusion," Vol. I, Los Alamos (1953).

2. Davison, B., Neutron Transport Theory, Oxford University Press, chs. X, XI, XII (1957).

3. Glasstone and Edlund, The Elements of Nuclear Reactor Theory, Van Nostrand, New York (1958).

4. Weinberg, A. M., and Wigner, E. P., The Physical Theory of Neutron Chain Reactors, University of Chicago Press (1958).

5. Meghreblian and Holmes, Reactor Analysis, McGraw-Hill, New York (1960).

6. Kaplan, I., "Measurements of Reactor Parameters in Subcritical and Critical Assemblies: A Review," Trans. ANS, 5, 1 (1962); to be published in more detail in a NYO Report.

K. 2 Theoretical Methods for Obtaining Neutron Distributions, Disadvantage Factors, and Thermal Utilization.

1. Cohen, E. R., "Neutron Flux Distribution in a Lattice Cell," NAA-SR-Memo-58 (July, 1951).

   Diffusion theory calculation of thermal flux distribution in a square cell.

2. Kelley, "Neutron Temperature Increase in Absorbers Caused by Selective Diffusion," NAA-SR-228 (1953).

   Method of calculating spectral hardening in fuel rods by using selective diffusion of neutrons.

3. Galanin, A. P., "The Theory of Thermal Neutron Nuclear Reactors, II," Consultants Bureau, Inc., New York (1953).

   Gives good derivation of the P_3 approximation in cylindrical coordinates.

4. Carlson, B. G., "Solutions of the Transport Equation by the S_n Approximations," LA-1599 (1953).

   Description of a fairly accurate method of solution to the transport equation.

5. Kushneriuk, S. A. and McKay, "Neutron Density in an Infinite Noncapturing Medium Surrounding a Long Cylindrical Body which Scatters and Captures Neutrons," CRT-566 (1954); also AECL-137.

   Calculates disadvantage factors by considering neutron current at rod surface and the rod blackness.

K. 2 (Continued)

6. Groshev, L. V. et al., "Conference of the Academy of Sciences of the U.S.S.R. on the Peaceful Uses of Atomic Energy," 1, p. 4, AEC-tr-2435 (July, 1955).

Application of the Fermi cadmium ratio method of measuring thermal utilization.

7. Amouyal A., and Benoist, P., "Supplement to CEA 571. Interpretation of the Results Obtained by S. A. Kushneriuk and C. Mckay," AEC-tr-3575.

See ref. K. 2. 5.

8. Tait, J. H., "The Calculation of the Fine Structure of the Thermal Neutron Flux in a Pile by the Spherical Harmonics Method," A/Conf. 8/P/433.

Description of the P_3 approximation in cylindrical coordinates.

9. Carlson, B. G., "Solutions of the Transport Equation by S_n Approximations," LA-1891 (1955).

Description of the S_n method (ref. K. 2. 4).

10. Newmarch, D. A., "A Modification to the Diffusion Theory of the Thermal Fine Structure in a Reactor to Account for the Effect of Air Channels," J. Nuclear Energy, 2, 52-58 (1955).

11. Noderer, L. and Goertzel, "Solutions of a Two-Dimensional Neutron Diffusion Problem," MonP-321 (1956).

Analysis of fine structure in square lattices.

12. Carlvik, I. and Pershagen, B., "Calculation of the Flux at the Surface and the Average Flux (Disadvantage Factor) for a Cylindrical Fuel Element," AEF-68 (Swedish) (1956); also, AEC-tr-3313 (English).

Uses diffusion theory in moderator and integral transport theory in the fuel.

13. Carlvik, I. and Pershagen, B., "Calculation of the Disadvantage Factor in a Cylindrical Lattice Cell," AEF-69 (1956) (Swedish); also, AEC-tr-3314 (English).

Application of ref. K. 2. 12 to a cell.

14. Lee, M. T., "Successive Generations Disadvantage Factors," HW-47707 (December, 1956).

Application of the successive generations method to the calculation of disadvantage factors.

K. 2 (Continued)

15. Davison, B., "Spherical Harmonics Method for Neutron Transport Problems in Cylindrical Geometry," Can. J. Phys., 35, 576-93 (May, 1957).

Application of spherical harmonics method to systems with complete cylindrical symmetry.

16. Bailley du Bois, B., "The Influence of Cell Configuration on the Laplacian and Fine Structure of Thermal Flux in a Heterogeneous Reactor," CEA-740 (French) (1957); also, AEC-tr-3559.

Corrections to a diffusion theory calculation for approximations of the Wigner-Seitz cell.

17. Neumann, H., "Thermal Utilization, Thermal Flux, and Lattice Cell Shape," HW-52048 (August, 1957).

The effects of cell cylindricalization on calculated values of f as a function of the cell dimensions.

18. Kushneriuk, S. A., "Neutron Capture by Long Cylindrical Bodies Surrounded by Predominantly Scattering Media," CRT-712 (1957); also, AECL-462.

Calculation of disadvantage factors by considering neutron current at rod surface and the rod blackness.

19. Clancey, W. R., "The Effect of Cladding Material on the Thermal Neutron Flux Shape in a Unit Cell," WAPD-P-550 (September, 1957).

Use of diffusion theory to investigate how ratio of the flux at the outer edge of the clad to the flux at the inner edge depends on clad material and dimensions.

20. Kushneriuk, S. A., "Effective Cross Sections and Neutron Flux Distributions in a Natural Uranium Rod-Application to Rod No. 683," AECL-497 (September, 1957).

Calculations of effective cross sections and neutron fluxes in a natural uranium rod.

21. Stuart, G. W. and Woodruff, R. W., "Method of Successive Generations," Nucl. Sci. Eng. 3, 359 (1958).

Comparison of successive generations calculations of disadvantage factors with experimental results.

22. Amouyal, A., Benoist, P., and Horowitz, J., "New Method of the Determination of the Thermal Utilization Factor of a Cell," J. Nucl. Energy, 6, 79-98 (1958).

A method of obtaining disadvantage factors which uses diffusion theory in the moderator and integral transport theory in the fuel.

K. 2 (Continued)

23. Weinberg, A. M. and Wigner, E. P., The Physical Theory of Neutron Chain Reactors, University of Chicago Press, p. 632 (1958).

Gives theory of the Fermi cadmium ratio method for measuring f.

24. Sato, K., "Thermal Neutron Flux Distribution in the Uranium Rod," BNL Internal Memo, (April, 1958), unpublished.

Gives simple formula which fits the flux distribution inside uranium rods; the formula is independent of the moderator properties and depends only on the properties of the fuel rod; see ref. K. 1. 6 for details of the method.

25. Theys, M. H., "Integral Transport Theory of the Thermal Utilization in Heterogeneous Reactors," M.S. Thesis, M.I.T. (September, 1958).

Comparison and use of methods of refs. K. 2. 22 and K. 2. 13 to calculate disadvantage factors and thermal utilization in graphite, light water, and heavy water lattices; comparison of calculations with experimental results.

26. Asoka, T., "Calculat on of Thermal Utilization in Heterogeneous Nuclear Reactors by the P_3 Spherical Harmonics Approximation," Nucl. Sci. Eng., 5, 57-60 (January, 1959).

Derivation of an approximate P_3 calculation for obtaining values of f in cylindrical cells.

27. Matsumoto, D. and Richey, C., "Program on the IBM-709 Digital Computer of the P_3 Approximation to the Boltzmann Transport Equation in Cylindrical Geometry," HW-60781 (June, 1959).

Good example of a P_3 computer program.

28. Royston, R. J., "One Group Calculations of the Neutron Flux Distribution in a Lattice Cell by Carlson's Method," AERE-M-454 (August, 1959).

Comparison of S_n calculation (see refs. K. 2. 4 and K. 2. 9) with experiment and other calculated results.

29. Murray, R. L., Nuclear Reactor Physics, 3rd edition, Prentice-Hall, ch. 9 (1959).

Derivation of the P_3 approximation in slab geometry.

30. Haefner, R. R., "A Multigroup P_3 Program for the Neutron Transport Equation," DP-427 (1959).

Program uses five energy groups.

K. 2 (Continued)

31. Vaughan, E. U., "Flux Hardening in Fuel Rods," NAA-SR-4780 (March, 1960).

Corrections to diffusion theory to account for spectral hardening in the fuel.

32. Zink, J. W. and Rodeback, G., "The Determination of Lattice Parameters by Means of Measurements on a Single Fuel Element," NAA-SR-5392 (July, 1960).

An equation is derived for f by using a system of current balances at a point in the moderator.

33. Honeck, H. C. and Kaplan, I., "The Distribution of Thermal Neutrons in Space and Energy in Reactor Lattices: Part I, Theory, and Part II, Comparison of Theory and Experiment," Nucl. Sci. Eng., 8, 3 (September, 1960).

Use of a multigroup solution to the integral transport equation; computes neutron distribution as function of space and energy.

34. SLO P-1, "A Thermal Multigroup Program for the IBM-704," WAPD-TM-188 (October, 1960).

Code for calculating neutron distributions as function of space and energy.

35. Kim, Y. S., "Calculations of the Distribution of Thermal Neutrons in Reactor Lattices," M.S. Thesis, M.I.T. (January, 1961).

Comparison of distributions obtained with methods of ref. K. 2. 33 and ref. K. 6. 15.

36. Thie, J. A., "Failure of Neutron Transport Approximation in Small Cells in Cylindrical Geometry," Nucl. Sci. Eng., 9, (February, 1961).

Indicates possible breakdown due to Wigner-Seitz cylindrical cell approximation.

37. Tralli, N. and Agresta, J., "Spherical Harmonics Calculations for a Cylindrical Cell of Finite Height," Nucl. Sci. Eng., 10, 2 (June, 1961).

P_3 method used in a cell of finite length.

38. Seren, L. and Tang, L. H., "Determination of Thermal Utilization by a Method of Images - a Semi-Empirical Method," Trans. ANS, 4, 1, p. 16 (1961).

The thermal utilization is obtained by flux mapping in a single rod and using the results of this single rod and the method of images to get f for a lattice.

K. 2 (Continued)

39. Honeck, H. C., "THERMOS, a Thermalization Transport Theory Code for Reactor Lattice Calculations," BNL-5826 (September, 1961).

Description of the code used in ref. K. 2. 33.

40. Pazy, A. and Goshen, S., "The Thermal Utilization in a Rectangular Cell," Nucl. Sci. Eng., 11, 357-361 (1961).

Discusses errors introduced by cylindricalization of the cell.

41. Mingle, J. O., "Disadvantage Factors in Slab Geometry by the P_2 Calculation," Nucl. Sci. Eng., 11, (September, 1961).

Use of P_2 spherical harmonics approximation.

42. Honeck, H. C., "The Calculation of the Thermal Utilization and Disadvantage Factors in Uranium-Water Lattices," Paper submitted to the IAEA Conf., on Light Water Lattices, Vienna (June, 1962).

Comparison of theoretical calculations and experimental results for light water lattices measured at Brookhaven.

43. Macdougall, J. P., "Application of Scattering Law Data to the Calculation of Thermal Neutron Spectra," Paper submitted to International Conf. on Neutron Thermalization, Brookhaven (April, 1962), to be published as a BNL Report.

This paper contains a description of a multigroup S_n code.

K. 3 Experimental Results: Heavy Water-Moderated Lattices

1. Woods, D. C., Biehl, A. T., "Intracell Neutron Densities in Natural Uranium-D_2O Lattices, Part II," NAA-SR-138 (August, 1953).

Comparison of experimental neutron density distributions with theoretical results.

2. Estabrook, F. B., "Single Rod Exponential Experiments," NAA-SR-925, 13-14 (1954).

Measurements of neutron density distribution in and around a single rod immersed in a tank of D_2O.

3. Laubenstein, R. A., "Reactor Physics Quarterly Progress Report for May-July 1954," NAA-SR-1102 (January, 1954).

Gives experimental verification that the thermal utilization does not depend on position of the cell in the reactor.

K. 3 (Continued)

4. Siegal, S. and Inman, G. M., NAA-SR-1049 (September, 1954).

Measurements of the intracell flux distribution in seven-rod clusters in D_2O.

5. Estabrook, F. B. and Kash, S. W., "Measurement and Analysis of Uranium-D_2O Lattices," TID-2506, (Extracts from Nuclear Science and Technology, 1, Issues 1-3, 1955).

Summary of work on natural uranium-D_2O lattices at North American Aviation, Inc.

6. Cohen, E. R., "Exponential Experiments on D_2O-Uranium Lattices," A/Conf. 8/P/605.

Good summary of work done by North American Aviation, Inc. between 1954 and 1956.

7. Heinzman, O. W. and Kash, S. W., "Intracell Flux Distributions for an Extensive Series of D_2O-U Rod Lattices," NAA-SR-1546, (1956).

Presents many intracell flux traverses measured at North American.

8. Bjørnerud, E. K., "Intracell Flux Distributions and Thermal Disadvantage Factors for Uranium Rods in D_2O Obtained by the S_4 Approximation," GA-166 (July, 1957).

Use of S_4 method to study the effects of varying dimensions and properties of the fuel and moderator.

9. Girard, Y., et al., "Natural Uranium-D_2O Lattices," A/Conf. 15/P/336.

Flux fine structure measurements made at Aquilon.

10. Heineman, R. E., "Experience on the Use of the Physical Constants Testing Reactor," A/Conf. 15, 12, p. 650 (1958).

Measurements of f in D_2O-UO_2 lattices in the PCTR.

11. Hone, D. W., et al., "Natural Uranium-D_2O Lattices," A/Conf. 15/P/212.

Summary of ZEEP (Chalk River) work in rods, clusters, and composite rods in D_2O lattices.

12. Lehman, P. et at., "The Physical Properties of Some Composite Fuel Elements in U-D_2O Type Reactors," A/Conf. 15/P/245.

Measurements of f made in these lattices.

13. Pershagen, B. et al., "Calculation of Lattice Parameters for Uranium Rod Clusters in Heavy Water and Correlation with Experiments," A/Conf. 15/P/151.

Compares measured and calculated disadvantage factors.

K. 3 (Continued)

14. Redman, W. C. and Thie, J. A., "Properties of Exponential and Critical Systems of Thoria-Urania and Heavy Water and their Application to Reactor Design," A/Conf. 15/P/600.

Measurements of intracell traverses.

15. Wikdakl, C. E. and Åkerheim, F., "Measurements of Disadvantage Factors in a Small Mockup," A/Conf. 15/P/162.

Measurements of disadvantage factors of clusters of U and UO_2 rods in a miniature lattice.

16. Hurley, T. J. and O'Neill, G. F., "Measured Nuclear Parameters for Natural Uranium Rod Lattices in D_2O," Trans. ANS, 4, 2, p. 295 (1961).

Presents measured values of f in lattices of U rod clusters in D_2O.

17. Kinard, F. E., "Nuclear Parameters of Massive Uranium Rods in D_2O", DP-649 (November, 1961).

Intracell traverses in lattices of rods three inches in diameter.

18. Peak, J., Kaplan, I., and Thompson, T. J., "Theory and Use of Small Subcritical Assemblies for the Measurement of Reactor Parameters," NYO-10204 (April, 1962).

Measurements of intracell distributions in lattices of slightly enriched U rods in D_2O-H_2O mixtures; measurements done in a miniature lattice.

19. Wittkopf, W. A. and Roach, K. E., "Nuclear Analysis of 4%-Enriched UO_2 Lattices Moderated by D_2O-H_2O Mixtures," Trans. ANS, 4, 2 (1962).

Measurements of disadvantage factors in D_2O-H_2O mixtures.

K. 4 Experimental Results: Light Water-Moderated Lattices

1. Kouts, H., Chernick, J., and Kaplan, I., "Exponential Experiments on Light Water-Moderated, One Per Cent U^{235} Lattices," BNL-2094 (November, 1952).

Presents intracell flux traverses.

2. Kouts, H. et al., "Intracell Flux Traverses and Thermal Utilizations, 1.027% Enrichment Uranium Rods in Light Water," BNL-1796 (March, 1954).

Use of Dy_2O_3 foils in intracell flux measurements.

K. 4 (Continued)

3. Chernick, J., "Results of a Univac Survey of the Thermal Utilization of BNL Experimental Lattices," BNL-1797 (1954).

P_3 calculations for H_2O lattices measured at BNL. Hardening is accounted for by adjusting neutron temperature in the fuel until agreement between P_3 and experiment is obtained.

4. Krasik, S. and Radkowsky, A., "Pressurized Water (PWR) Critical Experiment," A/Conf. 8/P/601.

Describes f measurements made at Bettis on light water lattices.

5. Kouts, H. et al., "Exponential Experiments with Slightly Enriched Uranium Rods in Ordinary Water," A/Conf. 8/P/600.

Summary of Brookhaven work on slightly enriched U, H_2O lattices.

6. Kouts, H. "Intracell Flux Traverses and Thermal Utilizations for 1.15% Enriched Uranium Rods in Ordinary Water," BNL-1987 (October, 1955).

Intracell measurements in uranium-water lattices and in borated uranium-water lattices.

7. Kranz, A. Z., "Measurements of f, p, and ϵ of Water-Moderated, Slightly Enriched Uranium Lattices," WAPD-134 (November 1955).

Reports methods and results of measurements in lattices of 1.3% U^{235} rods in H_2O.

8. Kouts, H., Price, G., and Walsh, V., "Thermal Utilization, 0.387" Diameter, 1.15% Enriched Uranium Rods in Light Water," BNL-2754 (April, 1956).

Reports results of intracell traverses with Dy_2O_3 foils.

9. Kouts, H., Price, G., Walsh, V., "Thermal Utilization of 0.600" Diameter, One Per Cent Enriched Uranium Rod Lattices," BNL-2849 (May, 1956).

Report of earlier intracell measurements.

10. Klein, D., "Measurements of f, p, and ϵ in Enriched Low Density UO_2-Fueled Lattices," WAPD-P-721 (August, 1956).

11. Kouts, H. "Thermal Utilization 1.3% Enriched, 0.600" Diameter Uranium Rods in Light Water," BNL-2840 (February, 1957).

Presents measured intracell distributions. Gives corrections to distributions reported earlier in ref. K.4.5.

K. 4 (Continued)

12. Kouts, H. and Sher, R., "Experimental Studies of Slightly Enriched Uranium, H_2O Moderated Lattices, Part I, 0.600-Inch Diameter Rods," BNL-486 (1957).

Experimental results of f measurements compared with P_3 calculations using adjusted neutron temperatures in the fuel to give agreement between theory and experiment.

13. Amouyal, A., and Benoist, P., "Application of the Formula for f to the Case of Cells with Ordinary Water," SPM-305 (1957).

Use of method of ref. K. 2. 22 in treatment of light water lattices.

14. Klein, D. et al., "Measurements of Thermal Utilization, Resonance Escape Probability, and Fast Effect in Water-Moderated, Slightly Enriched Uranium and Uranium Oxide Lattices," Nucl. Sci. Eng., 3, 403 (1958).

15. Kouts, H. and Sher, R., "Experimental Studies of Slightly Enriched 0.600-Inch Diameter Metallic Uranium, Water Moderated Lattices," Prog. in Nucl. Energy, Series II, Reactors, 2, p. 285, Pergamon Press, London (1958).

Measurements of f in U-H_2O Lattices.

16. Kouts, H. et al., "Physics of Slightly Enriched Normal Water Lattices (Theory and Experiment)," A/Conf. 15/P/1841.

Summary of the work done at BNL.

17. Mills, J. E. C. and Campbell, C. G., "The Fine Structure Thermal Neutron Distribution in Uranium-Natural Water Lattices, Experimental Results," AERE-RP/R-1826 (1958).

Use of manganese wire detectors in intracell measurements. Some lattices contained slightly enriched uranium.

18. Mills, J. E. C and Newmarch, D. A., "The Interpretation of Fine Structure Measurements, Part II: Natural Water-Uranium Lattices," AERE-RP/R-1827 (May, 1958).

Comparison of intracell traverses with diffusion theory calculations.

19. Rotenberg, Lapidus, and Richtmeyer, "A Monte Carlo Calculation of Thermal Utilization," NYO-7976 (1958).

Monte Carlo calculations of f which are in one per cent agreement with experimental results found in Brookhaven and Westinghouse lattices.

K. 4 (Continued)

20. Hill, R. E., "A Measurement of Thermal Utilization in a Non-Uniform UO_2-H_2O Lattice," Nucl. Sci. Eng., 2, No. 1 Suppl., 165-6 (June, 1959).

An integral method used to measure f in the Dresden Critical Assembly Lattice. Relative activities of $MnSO_4$ solutions located in the moderator and fuel regions, respectively, were measured.

21. Vigon, M. A. and Granados, C. E., "Measurements in a Subcritical Assembly of Natural Uranium and Light Water," Anales real soc. espan. fis. y q. (Madrid), Ser. A, 56: 249-256 (1960) (Spanish).

Reports measurements of intracell flux traverses.

22. Finn, H. et al., "Flux Measurements in Superheater Cells," Trans. ANS., 4, 2 (1961).

Compares measured disadvantage factors with results of P_3 calculations.

23. Price, G. A., "Measurements of Reactor Parameters in Subcritical and Critical Assemblies - Lattices of Slightly Enriched Uranium in Water," Trans. ANS., 5, 1 (1962).

Comparison of measured values of f in the Brookhaven miniature lattice and in the Westinghouse critical assembly.

24. Hellens, R. L. and Honeck, H. C., "A Summary and Preliminary Analysis of the BNL Slightly Enriched Uranium, Water Moderated Lattice Measurements," paper submitted to the IAEA Conf. on Light Water Lattices, Vienna (June, 1962).

Summary evaluation of the experimental and theoretical results of the work done at Brookhaven.

K. 5 Experimental Results: Graphite-Moderated Lattices

1. Chernick, J. et al., "An Experimental and Theoretical Study of the Subcritical BNL Reactor," BNL-60 (June, 1950).

Fermi cadmium ratio method used to measure f.

2. Richey, C. R., "Thermal Utilization and Lattice Diffusion Length in Graphite-Uranium Lattices from Exponential Pile Measurements," AECD-3675 (April, 1954).

Use of foils to measure intracell traverses.

3. Clayton, E. D., "Exponential Pile Measurements in Graphite-Uranium Lattices," AECD-3677 (June, 1954).

Reports results of f measurements in 30 uranium-graphite lattices.

K. 5 (Continued)

4. Price, G. A., "Thermal Utilization Measurement," BNL-1992 (August, 1954).

Intracell traverse in the BNL graphite reactor.

5. Mummery, P. W. and Thomas, M. E., "The Interpretation of Fine Structure Measurements, I. Graphite-Uranium Lattices," AERE-RP/P-1589 (February, 1955).

Comparison of fine structure measurements with diffusion theory calculations.

6. Richey, C. R., Clayton, E. D., and Davenport, D. E., "Thermal Utilization and Lattice Diffusion Length in Graphite-Uranium Lattices from Exponential Pile Measurements," HW-31305 (August, 1955).

7. Lloyd, J. M. and Mills, J. E. C., "The Fine Structure Thermal Neutron Distribution in Natural Uranium-Graphite Lattices," AERE-RP/R-1825 (1956).

Use of manganese wires in intracell traverses.

8. Fillmore, F. L., "Buckling of Graphite Moderated Lattices Containing Seven-Rod Fuel Clusters," NAA-SR-1535 (August, 1956).

Intracell flux traverses made in three assemblies of seven-rod clusters in graphite.

9. French-American Conference on Graphite Reactors, Proc., BNL-489 (1957).

Several papers presented at this conference which give experimental results of f measurements in graphite systems.

10. Richey, C. R., "The Calculation of the Thermal Neutron Flux Distribution in a Unit Lattice Cell - Comparison of Theory and Experiment," p. 211-215, ref. K. 5. 9.

Comparison of experimental flux distributions with P_3 calculations.

11. Koechlin, J. C. et al., "French Results on the Natural Uranium-Graphite Lattices," p. 97-126, ref. K. 5. 9.

Measurements of intracell traverses in the French pile, G1.

12. Lanning, D. D., Donahue, D. S., and Bennett, R. A., "The Nuclear Parameters of Some Graphite, Natural Uranium Lattices Measured in the PCTR," p. 85-88, ref. K. 5. 9.

Measurements of f using the PCTR.

K. 5 (Continued)

13. Lanning, D. D., Donahue, D. S., and Bennett, R. A., "The Nuclear Parameters of Some Large Process Tube Lattices Determined from PCTR Measurements," p. 89-94, ref. K. 5. 9.

Measurements of f using the PCTR.

14. Roullier, F. and Schmitt, A. P., "Réacteur G1, Mesure du Facteur d'Utilisation Thermique," Rapport CEA-670(J)(1957).

Measurement of intracell distribution in the French pile G1.

15. Niemuth, W. E. and Nilson, R., "Lattice Parameters Derived from Neutron Distributions," A/Conf. 15/P/591.

Intracell measurements with U^{235} in natural uranium-graphite lattices.

16. Grant, I. S. and Mills, J. E. C., "The Interpretation of Fine Structure Measurements, Part III, Graphite Uranium Lattices," AERE-RP/R-2569 (1958).

Comparison of intracell traverses with results calculated with diffusion theory.

17. Skeen, C. H., "Temperature Dependence of the Thermal Neutron Flux Distribution for a Square Uranium-Graphite Lattice," NAA-SR-Memo-3116 (September, 1958).

Measurements of disadvantage factors and f as a function of the temperature of the system, resulting in a measured temperature coefficient for f.

18. Nilson, R. and Oakes, T. J., "Radial Thermal Flux Traverses in Natural Uranium-Graphite Lattices," HW-59046 (1959).

Measurements of intracell distributions with and without liquid coolants in the cooling channels.

19. Wood, D. E., "The Effects of Neutron Temperature and Epithermal Flux on Lattice Cell Flux Traverses," Trans. ANS., 3, p. 492 (1960).

Analysis of measured intracell distributions in uranium-graphite lattices and comparison with P_3 calculations in which the neutron temperature in the fuel is adjusted to force agreement with experiment.

20. Wood, D. E. et al., "Lattice Parameter Measurements for a Concentric Tube Fuel Element," Trans. ANS., 4, (1961).

Measurement in the PCTR of f for a graphite-uranium lattice with complex fuel geometry.

K. 6 Neutron Thermalization and Calculation of Thermal Neutron Spectra

1. Wigner, E. P. and Wilkins, J. E., "Effect of the Temperature of the Moderator on the Velocity Distribution of Neutrons, with Numerical Calculations for H as a Moderator," AECD-2275 (September, 1944).

Classic treatment of neutron spectra, treating moderator atoms as a free gas; solution is analytically derived.

2. Brown, H. D. and St. John, D., "Neutron Energy Spectra in D_2O," DP-33 (1954).

Derivation of a scattering model for D_2O which accounts for chemical binding effects.

3. Hurwitz, H., Nelkin, M. S., and Habetler, G. J., "Nucl. Sci. Eng., 1, (1956).

Solution of Wigner-Wilkins equations for a heavy gaseous moderator.

4. Brown, H. D., "Neutron Energy Spectra in Water," DP-64 (February, 1956).

Calculates neutron spectra in homogeneous systems of H_2O and D_2O, taking into consideration chemical binding, moderator motion, and neutron absorption.

5. Coveyou, R., Bate, R., and Osborn, R., "J. Nuc. Energy, 2, 153 (1956).

Monte Carlo solution of the Wigner-Wilkins equations.

6. Cohen, E. R., Nucl. Sci. Eng., 2, 227 (1957).

Solution of Wigner-Wilkins equations for heavy gaseous moderators.

7. Amster, H. J., Nucl. Sci. Eng., 2, 394 (1957).

Analysis of Poole's data on spectra in which dependence of spectra on ratios of absorption cross section to scattering cross section is studied.

8. Schofield, P. and Hassitt, A., "The Calculation of Thermal Neutron Spectra," A/Conf. 15/P/18.

Results of neutron spectrum calculations in uranium-graphite systems; account has been made of crystal binding in the graphite.

9. Takahashi, H., "The Thermal Neutron Spectrum in a Heterogeneous Reactor," Nucl. Sci. Eng., 5, 338 (1959).

Presents some calculations of neutron spectra and temperatures in each region of a UO_2-H_2O reactor.

K. 6 (Continued)

10. Högberg, T., "Monte Carlo Calculations of Neutron Thermalization in a Heterogeneous System," AE-6 (June, 1959).

Analysis of spectrum of a uranium-D_2O system in slab geometry.

11. Purica, I. et al., "Sur la Variation Spatiale du Spectre des Neutrons dans un Réacteur Hétérogène Modéré et Refroidi à l'Eau Naturelle," IFA-FR-21 (1959).

Study of variation of neutron temperature in a H_2O-U (10% U^{235}) reactor.

12. Calame, G. P. and Federighi, F. D., "A Variational Procedure for Obtaining Spatially Dependent Thermal Spectra," KAPL-M-GPC-2 (December, 1959).

Comparison of the method with experimental results was found to be excellent.

13. Nelkin, M., "Scattering of Slow Neutrons by Water," Phys. Rev., 119, 741 (1960).

Derivation of a scattering model for H_2O.

14. Nelkin, M. S., "Neutron Thermalization," GA-746 (1961).

Summary discussion of thermalization.

15. L. de Sobrino and M. Clark, "Comparison of Wilkins Equation with Experiments on Water Systems," Nucl. Sci. Eng., 10, 377-83 (August, 1961).

Calculation of neutron spectra in heterogeneous and homogeneous water systems and comparison with experimental measurements.

16. L. de Sobrino and M. Clark, "Comparison of the Wilkins Equation and Higher Order Approximations for Solid Moderators," Nucl. Sci. Eng., 10, 384 (1961).

Calculations of spectra for beryllium and graphite moderators.

17. L. de Sobrino and M. Clark, "A Study of the Wilkins Equation," Nucl. Sci. Eng., 10, 388 (1961).

Study of the Wilkins Equation for 1/v capture with a constant leakage term.

18. Deutsch, R. W., "Spatial Dependence of Thermal Neutron Spectra and the Interpretation of Thermal Utilization Measurements," Nucl. Sci. Eng., 10, 400 (1961).

Discusses importance of considering spectral hardening.

K. 6 (Continued)

19. Meetz et al., "Iteration of the Multigroup Theory and Application to the Calculation of the Neutron Spectrum in Plate Reactors," Nukleonik, 3, 155-163, (German).

Calculation of energy distribution of thermal and epithermal neutrons in homogeneous and heterogeneous media.

20. Sher, R., Kouts, H., and Klein, D. "Spatial Dependence of Thermal-Neutron Spectra and the Interpretation of Thermal Utilization Measurements," Nucl. Sci. Eng., 12, 3 (March, 1962).

Some comments on ref. K. 6. 18.

21. Deutsch, R. W., "Re: Spatial Dependence of Thermal-Neutron Spectra and the Interpretation of Thermal Utilization Measurements," Nucl. Sci. Eng., 12, 3, (March, 1962).

Some comments on ref. K. 6. 20.

22. International Conference on Neutron Thermalization, Brookhaven (April, 1962); all papers presented at the conference will be published in a future BNL Report.

Many papers presented in the area of neutron thermalization, both theoretical and experimental.

23. Honeck, H. C., Summary paper presented at the Brookhaven Conference, ref. K. 6. 22.

Good summary of experimental and theoretical neutron spectra in lattices.

24. Honeck, H. C., "An Incoherent Scattering Model for Heavy Water," Trans. ANS., 5, 1 (June, 1962).

Description of a scattering model for D_2O.

K. 7 Measurements of Thermal Neutron Spectra and Neutron Temperatures

1. Branch, G. M., "Neutron Temperature Measurements in Graphite and in a Uranium-Graphite Reactor," AECD-747 (1946).

Measurements of Oak Ridge X-10 neutron temperature by transmission of thermal neutrons through sandwiches of indium foils between 1/v absorbers.

2. Anderson, F., Fermi, E., Wattenberg, A., Weil, G., and Zinn, W. H., Phys. Rev., 72, (1947).

Measurements of neutron temperature in Argonne's CP-2 Reactor. Method was based on reactivity changes in reactor brought about by insertion of cadmium and 1/v absorbers.

K. 7 (Continued)

3. Biehl, A. T. and Cohen, E. R., "A Measurement of the Neutron Temperature in a Natural Uranium-D_2O Lattice," NAA-SR-140 (1951).

Use of a non-multiplying lattice of Pb-Cd alloy rods in heavy water in comparison with a natural uranium lattice in heavy water to measure the neutron temperature.

4. Biehl, A. T., Cohen, E. R., and Woods, D., "A Measurement of the Neutron Temperature Effect Using Eu_2O_3 Foils," NAA-SR-148 (1951).

Microscopic traverses made with Eu and Au foils in natural U-D_2O lattices.

5. Taylor, B. T., "Measurement of the Neutron Spectrum at the Centre of the Harwell Pile," AERE-N/R-1005 (1952).

Crystal spectrometer measurements of the thermal neutron spectrum.

6. Hughes, D. J., Pile Neutron Research, Addison-Wesley, Cambridge, p. 91 (1953).

Crystal spectrometer measurements of thermal neutron spectra in the Oak Ridge X-10 Reactor.

7. Kouts, H. et al., "A Measurement of Neutron Temperature in a Uranium Rod-Water Moderated Lattice," BNL-1986 (1955).

Use of boron and cadmium in a danger coefficient measurement of neutron temperature.

8. Küchle, M., Nucl. Sci. Eng., 2, 87-95 (1957).

Measurements similar to those made by Branch, ref. K. 7. 1.

9. Gavin, G. B., "A Determination of the Neutron Temperature at the Center of the Thermal Test Reactor," KAPL-1142 (1954); also, Nucl. Sci. Eng., 2, 1-13 (1957).

Neutron temperature measurements made by changes in pile reactivity after insertion of various absorbers.

10. Uthe, P. M., "Attainment of Neutron Flux Spectra from Foil Activations," WADC-TR-57-3 (March, 1957).

Description of several analytical methods for obtaining spectra from foil data.

11. Danzker, "A Proposed Method of Measuring the Thermal Neutron Energy Spectrum Distribution in the Interior of a Reactor," WAPD-RM-60 (March, 1957).

Method is based on differential absorption.

K. 7 (Continued)

12. Trice, J. B., "Preliminary Report of an Analytical Method for Measuring Neutron Spectra," APEX-408 (April, 1957).

Method for unscrambling foil activation data to derive neutron spectra.

13. Poole, M. J., J. Nucl. Energy, 5, 325 (1957).

Time of flight measurements of neutron spectra in H_2O systems poisoned with boric acid.

14. Sturm, W., Phys. Rev., 71, 757 (1957).

Crystal spectrometer measurements of thermal neutron spectrum in D_2O moderated CP-3 Reactor.

15. Brown, F. and Westcott, C. H., "On the Use of Lu^{176} as an Activation Detector for Measuring the Temperature of Thermal Neutrons," TNCC (CAN)-9 (May, 1957).

16. Hartmann, S. R., "A Method for Determining Neutron Flux Spectra from Activation Measurements," WADC-TR-57-375 (June, 1957).

Method involves approximating the flux distribution by a linear combination of the cross sections of various detectors.

17. Campbell, C. G., Freemantle, R. G., and Poole, M. J., "Measurements of Reactor Spectra by Time of Flight and Integral Methods," A/Conf. 15/P/10.

Time of flight and integral measurements of thermal neutron spectra in subcritical, slightly enriched, H_2O moderated, uranium lattices; integral measurements involved measuring ratio of Pu^{239} to U^{235} fission product activity.

18. Mostovoy, V. I., et al., "Measurement of Neutron Spectrum in Uranium Water Lattices," A/Conf. 15/P/2152.

Time of flight measurements.

19. Poole, M. J., Nelkin, M. S., and Stone, R. S., "The Measurement and Theory of Reactor Spectra," Prog. in Nuclear Energy, Series I, (Physics and Mathematics) Vol. 1, pp. 91-164 (1958).

Good summary of reactor spectra, theory and experiment.

20. Poole, M. J., "Neutron Spectra Measurements Using a Pulsed Neutron Source," UCRL-5665 (December, 1958).

Description of the pulsed source method.

K. 7 (Continued)

21. Price, G. A., "Neutron Temperature Measurements with Lu^{176}," Reactor Sci., 10, 157 (1959).

Use of lutetium to measure neutron temperatures.

22. Donnert, H. J., "A Method for Analysis of Activation Foil Data," Radiological Laboratory, Army Chemical Center, Md. (September, 1959).

Method involves expanding the flux distribution in terms of the cross sections of various detectors.

23. Walker, Westcott, and Alexander, "Measurement of Radiative Capture Resonance Integrals in a Thermal Reactor Spectrum," Can. Jnl. Phys., 38, 1 (January, 1960).

Measurement of neutron temperature by means of transmission of neutrons through a 1/v filter.

24. Schmid, L. C. and Stinson, W. P., "Lutetium as a Spectral Index Indicator," HW-64866 (March, 1960).

Discusses use of lutetium as a spectral index indicator.

25. Schmid, L. C. and Stinson, W. P., "Calibration of Lutetium for Measurements of Effective Neutron Temperatures," Nucl. Sci. Eng., 7, 5 (May, 1960).

Measurement of ratio of Lu^{177} to Lu^{176m} activities in graphite as a function of the temperature of the medium.

26. Stinson, W. P., Schmid, L. C., and Heineman, R. E., "An Investigation of Effective Neutron Temperature," Nucl. Sci. Eng., 7, (May, 1960).

Measurement of neutron temperature by measuring the ratio of Pu^{239} to U^{235} fission product activities.

27. Nisle, R. G., "An Integral Method for Identifying Neutron Flux Spectra," Trans. ANS, 3, 1 (1960).

Method depends on activation of foils like gold, lutetium, and manganese.

28. Burke, E. A. and Lowe, L. F., "Derivation of Thermal Neutron Spectra from Transmission Data," Nucl. Instr. and Methods, 7, p. 193 (1960).

A transmission method for measuring thermal neutron spectra.

29. Schmid, L. C. "Lutetium as a Spectral Index Detector - Part II, Resonance Integrals," HW-69475 (April, 1961).

Calculations and measurements of Lu^{175} and Lu^{176} resonance integrals.

K. 7 (Continued)

30. Glazkov et al., "Use of a Monochromater to Measure the Thermal Neutron Spectrum of a Research Reactor," Atomnaya Energ., 10, (April, 1961) (Russian).

    Measurement of thermal spectra in slightly enriched uranium-graphite lattices.

31. Doil'nitsyn, E. Ya, and Novikov, A. G., "The Spectrum and Temperature of the Neutron Gas in a Graphite-Water Reactor," Atomnaya Energ., 10, (May, 1961).

    Use of a mechanical neutron selector to measure spectra at temperatures from 300°K to 800°K.

32. Young, J. C. et al., "Measurements of Neutron Spectra and Decay Constants in a Water Moderated Multiplying Assembly," Trans. ANS, 4, 2 (1961).

    Use of pulsed source method in measurement of spectra.

33. Parkinson, T. F. and Salah, S., "Integral Spectrum Measurements with Lutetium," Trans. ANS, 4, 2 (1961).

    Measurements of neutron temperature in heterogeneous cells.

34. Chidley, B. G. et al., "Experimental Effective Cross Sections and Neutron Spectra in a Uranium Fuel Rod," Trans. ANS, 4, 1 (1961).

    Use of Pu^{239}, U^{235}, Lu^{176}, and Mn foils to get neutron temperatures in a fuel rod.

35. Barclay, F. R. et al., "Low Energy Neutron Spectra in the Zenith Heated Graphite Moderated Reactor," ref. K. 6. 22.

    Comparison of measured and computed spectra.

36. Gelbard, E. M. et al., "A Comparison of the Nelkin and Radkowsky Thermal Neutron Scattering Kernels for Water," ref. K. 6. 22.

    Presents measurements on slabs of water. Little sensitivity of flux shapes and decay constants were found in varying the type kernel used in the calculations.

37. Parkinson, T. F. and Salah, S., "Integral Spectrum Measurements in Heterogeneous Media," ref. K. 6. 22.

    Measurements of neutron temperature with lutetium.

38. Anderson, C. A. and Thompson, T. J., "Measurement of Neutron Energy Spectra with the Massachusetts Institute of Technology Fast Chopper," Trans. ANS, 5, 1 (1962).

    Leakage spectrum measurements in an enriched U-D_2O reactor.

K. 8 Cross Section Data

1. Westcott, C. H., "Effective Cross Sections and Cadmium Ratios for the Neutron Spectra of Thermal Reactors," A/Conf. 15/P/202.

2. Hughes, D. J. and Schwartz, R. B., "Neutron Cross Sections," BNL-325 (1958); also, 1960 Supplement.

3. Roberge, J. P. and Sailor, V. L., "Parameters of the Lu^{176} Neutron Resonance at 0.142 ev," Nucl. Sci. Eng., 7, 502 (June, 1960).

4. Westcott, C. H., "Effective Fission and Capture Cross Sections for Hardened Maxwellian Spectra," Reactor Sci., 2, No. 3 (June, 1960).

   Gives effective cross sections as function of position in plates for isotropic and beam sources on the plates.

5. Baston, A. H. et al., "Thermal Neutron Cross Section Measurements on Lu^{175} and Lu^{176}," J. Nucl. En., Pt. A., Reactor Sci., 13, 5-6 (October, 1960).

6. Horowitz, J. and Tretiakoff, O., "Effective Cross Sections for Thermal Reactors," EANDC(E) 14 (November, 1960).

   A method for representing effective cross sections.

7. Westcott, C. H., "Effective Cross Section Values for Well-Moderated Reactor Spectra," 3rd. ed. corrected, AECL-1101 (November, 1960).

8. Tassan, S., Hellsten, A., and Sailor, V. L., "Low Energy Neutron Resonances in Eu^{151}," Nucl. Sci. Eng., 10, 169 (June, 1961).

9. Safford, G. J. and Havens, W. W., "A Precision Measurement of the Total Cross Section of Pu^{239} between 0.00291 and 0.1 ev," Nucl. Sci. Eng., 11, 65 (September, 1961).

DISTRIBUTION

NYO-10205

AEC Research and Development Report

UC-34 Physics

(TID-4500, 17th Edition)

1. USAEC, New York Operations Office (D. Richtmann)
2. USAEC, Division of Reactor Development (P. Hemmig)
3. USAEC, New York Patents Office (H. Potter)
4. USAEC, New York Operations Office (S. Strauch)
5. USAEC, Division of Reactor Development, Reports and Statistics Brach
6. USAEC, Maritime Reactors Branch
7. USAEC, Civilian Reactors Branch
8. USAEC, Army Reactors Branch
9. USAEC, Naval Reactors Branch
10. Advisory Committee on Reactor Physics (E. R. Cohen)
11. ACRP (G. Dessauer)
12. ACRP (D. de Bloisblanc)
13. ACRP (M. Edlund)
14. ACRP (R. Ehrlich)
15. ACRP (I. Kaplan)
16. ACRP (H. Kouts)
17. ACRP (F. C. Maienschein)
18. ACRP (J. W. Morfitt)
19. ACRP (B. I. Spinrad)
20. ACRP (P. F. Zweifel)
21. ACRP (P. Gast)
22. ACRP (G. Hansen)
23. ACRP (S. Krasik)
24. ACRP (T. Merkle)
25. ACRP (T. M. Snyder)
26. ACRP (J. J. Taylor)
27. - 29. O.T.I.E., Oak Ridge, for Standard Distribution, UC-34, TID-4500 (17th Edition)
30. - 49. P. S. Brown
50. - 100. Internal Distribution